Note to reader

This draft version of Chapter 1 in the Technical Background Report to the Global Mercury Assessment 2018 is made available for review by national representatives and experts. The draft version contains material that will be further refined and elaborated after the review process. Specific items where the content of this draft chapter will be further improved and modified are:

1. All graphics will be redrawn to a common appearance from the originals presented here, with their sources cited in the captions.
2. References will be completed and presented in a uniform style.
3. Conclusions and main messages will be formulated

GMA 2018 Draft Chapter 1 Introduction. Peter Outridge, Robert Mason, Feiyue Wang, Lars-Eric Heimburger, Milena Horvat, Xinbin Feng, Simon Wilson

18

19 # Contents

29

30

31

32

33

Chapter 1 Introduction

1.1 Background and Mandate

This report constitutes the Technical Background Material to the Global Mercury Assessment 2018 (GMA 2018). The GMA 2018 has been prepared in response to a request issued by UNEP's Governing Council (now UN Environment Assembly) that UN Environment should update its 2013 Global Mercury Assessment (GMA 2013) within a period of 6 years, i.e. for delivery no later than 2019. This Technical Background report is developed as a joint project by UN Environment and the Arctic Monitoring and Assessment Programme (AMAP).

The GMA 2018 provides a scientific assessment of Hg emissions and releases, and its transport of fate in the global environment. The report reflects progress made by the scientific community, national authorities and organisations in better understanding atmospheric Hg emissions (Chapter 2), Hg levels in air (Chapter 3), atmospheric transport and fate (Chapter 4), releases to water (chapter 5), and the cycling and methylation of Hg in the aquatic environment (Chapter 6). In addition to updating the GMA 2013, this report includes additional, new sections on observed levels of Hg in biota (Chapter 7), and observed levels and effects of Hg in humans (Chapter 8).

1.2 Recent advances in understanding of global mercury cycling

1.2.1 A General Overview

Owing to the scale and chemical complexity of Hg in the global environment, and the lack of detailed information for many parts of the Hg cycle, the planetary Hg cycle is best described and communicated in a quantitative manner by using the outputs from global-scale models, the subject of this section. In general, Hg is released into the global environment from natural sources and processes such as volcanoes and rock weathering, and as a result of human activities. Once it has entered the environment, Hg cycles between the major environmental compartments – air, soils and waters – until it is eventually removed from the system through burial in deep ocean sediments and mineral soils (Fig. 1.2.1). Only a minute fraction of the Hg present in the environment is in the most toxic and bioavailable form - monomethylmercury (MeHg). Monomethylmercury is produced from inorganic Hg mainly in aquatic ecosystems through natural microbiological processes. The natural processes responsible for the formation and destruction of MeHg are only partly understood, which contributes to the difficulties in predicting the direct positive effects of regulatory action on biological Hg concentrations and human

exposure. However, regulatory action can only work to reduce anthropogenic Hg inputs into the environment. Recent findings on the methylation/ demethylation part of the Hg cycle are presented in Chapter 6.2.

In the 2013 Global Mercury Technical Assessment (AMAP/UNEP, 2013), based on a global model and budget developed by Mason et al. (2012), it was estimated that over the past century anthropogenic activities cumulatively have increased atmospheric Hg concentrations by 300-500%, whereas Hg in surface ocean waters less than 200 metres deep has increased on average by ~200%. Deeper waters exhibit smaller increases (11-25%) because of limited exposure to atmospheric and riverine anthropogenic Hg inputs, and the century- to millennium-scale residence times of these slowly over-turning, isolated water masses. Because of the naturally large Hg mass present in soils, the average Hg increase is only ~20% in surface organic soils and is negligible in mineral soils.

As with almost all modelled global budgets of trace elements and chemical substances, large uncertainties exist regarding the amounts of Hg 'stored' in different environmental compartments, the fluxes of Hg between them, and the rates of removal of Hg from the biologically active parts of the global environment (AMAP/UNEP, 2013). These uncertainties limit confidence in our understanding of the Hg cycle and in our ability to predict the responses of ecosystem Hg concentrations to changes in emissions due to international regulatory actions. Therefore, major on-going efforts have been mounted to reduce these uncertainties and derive a more robust, accurate global model.

Since 2012, additional measurements of Hg concentrations and fluxes in oceans, atmosphere and soils have led to suggested refinements of global budgets and models by several research groups (Table 1.2.1), but major uncertainties persist. In general, the new estimates of Hg in the atmosphere mostly agree within the limits of uncertainty with the AMAP/UNEP (2013) budget. However, two of the recent studies (Amos et al., 2013; Zhang et al., 2014) suggest that the terrestrial system contains a larger fraction of anthropogenic Hg compared to the oceans than was previously believed. This revision is supported by new modelling of the global transport and fate of atmospheric gaseous elemental mercury (GEM) (Song et al., 2015). Also, recent work on atmospheric Hg dynamics under forest canopies suggests that the uptake of GEM through leaf stomata at night-time has previously been significantly underestimated, and that GEM-containing litterfall and throughfall in global vegetation, and not wet and dry deposition of Hg^{II} species, may represent the largest net flux of atmospheric Hg to terrestrial ecosystems (Fu et al., 2016; Wang et al., 2016; Obrist et al., 2017).

With respect to the world's oceans, there are significant differences between the new models concerning the quantity of anthropogenic Hg presently circulating in seawater (c.f. Amos et al., 2013, 2015; Zhang et al., 2014; Lamborg et al., 2014). Because much of the current risk from Hg to human and wildlife is derived from marine food-webs, the questions of how much anthropogenic Hg is present in the oceans, its distribution, and its rate of clearance from seawater, are of fundamental importance and so are the main focus of section 1.2.

The observed differences between models concerning these questions are primarily due to varying estimates of the amount and environmental fate of atmospheric emissions from historical mining in the Americas between the 15thand late 19thcenturies, and to differences in the estimated amount of natural Hg originally present in the oceans (see Table 1.2.1). Overall, the different chemical rate constants used for modelling circulation processes within and between oceanic, atmospheric and terrestrial compartments are a secondary factor in uncertainty. Substantial Hg releases to land, freshwaters and air occurred from primary Hg mineral mining, and gold (Au) and silver (Ag) mining and amalgamation, in South/Central America during the Spanish colonial period (ca. 1450-1850 AD), and later from North American artisanal and small-scale Au and Ag mining during the "Gold Rush" era (ca. 1850-1920) (Nriagu, 1993; Strode et al., 2009). It is generally agreed that some fraction of the Hg from these historical emissions is still circulating within the global environment, and that this has had an effect on present-day environmental Hg levels, especially in the oceans. But quantification of that effect is currently uncertain.

Table 1.2.1. Recent estimates of total, anthropogenic and "natural"[a] Hg in global air, soils and oceans (units in kilotonnes (1 kt = 1,000 t)).

	Amos et al. (2013)	Zhang et al. (2014)	Lamborg et al. (2014)	Mason et al. (2012); AMAP/UNEP (2013)
Atmospheric Hg				
Total	5.3	4.4	n/a	5.1
Anthropogenic	4.6	3.6		3.4-4.1[b]
Natural	0.7	0.8		1.0-1.7
Soil Hg				
Total	271	--	n/a	201
Anthropogenic	89	92		40
Natural	182	--		161
Oceanic Hg				
Total	343	257	316	358
Anthropogenic	222	66 (38-106)[c]	58±16[d]	53
Natural	122	191	258[e]	305

[a] – The time point for designation of the "natural" Hg states, and therefore the quantification of "natural" and "anthropogenic" Hg masses, differed between studies: specified at 2000 BC in the "pre-anthropogenic period" by Amos et al. (2013), at 1450 AD by Zhang et al. (2014) which was prior to major historical mining, and *ca.* 1840 AD by Lamborg et al. (2014) which was prior to the North American "Gold Rush" and the expansion of coal-fired combustion sources. The anthropogenic Hg values from Mason et al. (2012) are based on increases over the last century, and thus their "natural" Hg mass may be over-estimated and the anthropogenic mass under-estimated compared with the other studies.

[b] – Ranges for anthropogenic and "natural" Hg calculated assuming an estimated 300-500% increase in total Hg due to anthropogenic activities over past century (Mason et al. 2012).

[c] - the Zhang et al. (2014) best estimate for oceanic anthropogenic Hg is followed by its uncertainty range in brackets.

[d] - based on an oceanic anthropogenic Hg:anthropogenic CO_2 ratio for 1994; a more recent (higher) oceanic CO_2 estimate gave an Hg_{anthr} estimate of 76 kt Hg (Lamborg et al., 2014).

[e] – calculated by subtraction.

1.2.2 How much anthropogenic Hg is in the world's oceans, and what was its source?

The total amount of Hg currently in oceans reflects a mixture of sources: historical anthropogenic inputs to air, land and oceans; historical natural emissions; and current year anthropogenic and natural releases. Consequently, global models need to estimate these quantities and how they have been cycled, transported and transformed over long (decadal to century) time-scales.

Up until 2012, the published estimates of oceanic anthropogenic Hg exhibited more than an order of magnitude range, from 7.2 to 263 kt (Mason et al., 1994; Lamborg et al., 2002; Sunderland and Mason, 2007; Selin et al., 2008; Strode et al., 2010; Soerensen et al., 2010; Streets et al., 2011; Mason et al. 2012). Since then, another estimate (222 kt) near the upper end of this range was derived by Amos et al. (2013) based on Streets et al. (2011) putative history of major emissions from historical Ag and Au mining activities. Subsequently, however, Zhang, Streets and colleagues (Zhang et al., 2014) revised the historical mining emissions downwards by three-fold to make the trends in global Hg emissions more compatible with the Hg deposition histories recorded in 120 lake sediments world-wide (Figure 1.2.2).

The revision was stimulated in part by a historical analysis of documented liquid elemental Hg importation and consumption during Ag mining operations in the 15-17th centuries in what is today Mexico, Peru and Bolivia (Guerrero, 2012). In the AMAP/UNEP 2013 report, it was estimated that 45% of the Hg used in artisanal gold mining and amalgamation in the present-day was volatilized into the atmosphere. By comparison, Guerrero (2012) suggested that only 7-34% was volatilized during historical Ag production, with 66-93% of the consumed Hg forming solid calomel (Hg_2Cl_2) that was trapped in mining waste and deposited locally into streams or landfills. This new study of historical Ag production is a potentially important advance in understanding of the global Hg cycle, because another recent estimate of cumulative global atmospheric Hg emissions from all man-made sources up to 2010 suggested that Ag production was the largest single source of Hg, contributing several-times more Hg to air throughout history (146 kt, 31% of total) than large-scale and artisanal gold production combined (55.4 kt; Streets et al. 2017). Emissions from Ag production are thought to have peaked during the late 19th century, coincident with North American mining, however, there are relatively large uncertainties of up to 100% (represented in terms of 80% confidence intervals) around the total emissions for the period 1870-1910 (Streets et al. 2017).

After assuming that historical Ag and Au mining and amalgamation had the same loss rate to the atmosphere (17%), Zhang et al.'s (2014) revised anthropogenic emission inventory (see Fig. 1.2.2) was

markedly smaller than that of Streets et al. (2011) (cumulative totals of 190 kt versus 351 kt, respectively). Using this revised inventory with the GEOS-Chem model, Zhang et al. (2014) found a 3-fold lower current oceanic anthropogenic Hg mass than that derived by Amos et al. (2013) using the same model but a larger emission from historical mining (see Table 1.2.1).

Corroborative data supporting the lower historical mining emissions proposed by Zhang et al. (2014) came from an independent analysis of another large global set of lake sediment Hg profiles (Engstrom et al. 2014). Atmospheric Hg deposition was substantially increased during the Spanish colonial period in one South American lake (Negrita) close to the sites of historical mining and amalgamation activities, with less impact in another regional lake (El Junco) further away (Fig. 1.2.3). But no evidence of increased deposition at this time was found in sediment cores from remote North American or African lakes (see Fig. 1.2.3), suggesting that the historical contamination from Spanish colonial mining was geographically limited to surrounding terrestrial and freshwater ecosystems. Thus, the world-wide lake sediment record indicates a large local, but negligible global, impact from Spanish era Au and Ag mining and production during the 15^{th} to 17^{th} centuries.

Amos et al. (2015) discounted this evidence by arguing that lake sediments in general respond relatively slowly and insensitively to changes in atmospheric Hg deposition. Recent evidence of significant GEM uptake by plant leaves, and of high Hg fluxes to soils in leaf litterfall and throughfall (Fu et al., 2016; Obrist et al., 2017), raises another complicating possibility - that sediment archives ultimately may be more reflective of trends in GEM concentrations, through transfer from watersheds via litterfall and throughfall, rather than of wet and dry deposition. Amos et al. (2015) also proposed that the Guerrero (2012) volatilization estimate was unrealistically low because it omitted Hg losses during amalgamation, reprocessing of Hg-containing Ag and Au products, and revolatilization from historic solid mining wastes. Evaluation of alternative GEOS-Chem model scenarios by Amos et al. (2015) suggested that the “mining reduced 3x” history of Zhang et al. (2014) was inconsistent with Hg measurements in present-day environmental reservoirs, as well as with the magnitude of Hg enrichment in peat and some lake sediment archives. However, examination of the published model outputs shows that the reduced mining scenario gave markedly closer agreement with observed upper ocean total Hg concentrations and net oceanic evasion rates than the original mining emission history of Streets et al. (2011), with almost identical present-day soil Hg concentrations and net terrestrial flux (see Amos et al. (2015), c.f. Figs. 3d, 3g, 3f, 3h, respectively).

Independent evidence supporting the revised (lower) Zhang et al. (2014) emission history, and the lake sediment records of Engstrom et al. (2014), was recently provided by three remote glacier ice core records from the Yukon, Greenland, and Tibetan Plateau (Fig. 1.2.4). Streets et al. (2011) estimated there to have been an average ~500% increase in primary anthropogenic emissions globally between 1850 and the late 1800s that was attributable to the North American Gold Rush. However, the two Arctic or sub-Arctic glacier records (Mount Logan, Yukon (Beal et al., 2015), and the NEEM site, Greenland (Zheng, 2015)) reported increases in mean Hg accumulation rate of only 120% and 30%, respectively, between 1748-1850 and 1851-1900. The ice core from Tibetan Plateau (Mount Gelaidandong, ~6620 m.a.s.l.; Kang et al., 2016) did not display any marked increase in Hg accumulation in the late 1800s that could be due to large, globally-distributed emissions from the North American Gold Rush (see Fig. 1.2.4). Furthermore, neither the Mt. Logan core, which extended back to ~1400 AD, nor the Mt. Gelaidandong core, which extended back to 1477 AD, revealed elevated Hg accumulation during the 15th to 17th centuries that could be attributed to the Spanish Colonial Ag and Au mining operations in Central America and Mexico. In both glacier cores, by far the highest Hg accumulation rates over the last ~600 years occurred after the 1920s (Beal et al., 2015; Kang et al., 2016). In summary, all three ice core records are in closer agreement with the downwards-revised historical emissions budget of Zhang et al. (2014) than with the earlier estimate by Streets et al. (2011) which underpinned Amos et al.'s (2013) global model.

Thus, the weight of evidence at present supports the Zhang et al. (2014) emission history, and suggests that the atmospheric Hg emissions produced by historical mining and amalgamation techniques were geographically restricted, with dispersion confined mostly to local and regional terrestrial and freshwater environments. That these historical emissions had significant effects on Hg levels in areas around the mining operations is not in dispute. Other studies have shown marked local or regional contamination of lake sediment and glacial ice archives by historical Ag/Au mining (e.g., Schuster et al., 2002; Cooke et al., 2009; Correla et al., 2017). However, current evidence supports the interpretation that historical mining had less impact on globally-distributed atmospheric emissions and deposition than coal combustion and other high temperature industrial emissions had in the 20th century. Commercial Hg-containing products have also been suggested to be significant contributors to global Hg releases to air, soil and water from the late 1800s onwards (Horowitz et al., 2014). Overall, the recent revised emissions estimates, and archival records of deposition, support the prevailing paradigm that present-

day atmospheric deposition rates are 3- to 5-fold higher than during the pre-industrial period (i.e. from 1450 to 1850) (Engstrom et al., 2014; Lamborg et al., 2014; Zhang et al., 2014).

Nonetheless, the cumulative impacts of historical mining over four centuries on the current oceanic (and terrestrial) anthropogenic Hg inventory have been substantial. Zhang et al. (2014) calculated that about 67% of the cumulative anthropogenic Hg emissions to air throughout history (130 out of 190 kt) was due to precious metal mining, with 21% (40 kt) due to coal combustion and 11% (20 kt) from other industrial activities. Zhang et al. (2014) also calculated that most of the anthropogenic Hg mass in today's oceans (44 kt out of 66 kt) was deposited between 1450 and 1920 due to the emissions from historical Ag/Au mining, with the remaining one-third coming from predominantly coal-based emissions since 1920. The total anthropogenic mass in today's oceans (66 kt) estimated by Zhang et al. (2014) is in good agreement with another recent estimate of oceanic anthropogenic Hg (58±16 kt; Lamborg et al., 2014) derived using a completely different methodology based on seawater Hg concentration profiles combined with anthropogenic CO_2 and remineralized phosphate as proxies for oceanic Hg distribution. That two studies, using different approaches, arrived at similar estimates increases confidence in the robustness of their conclusions. Both of these recent estimates fall within the lower half of the previous range of values and are close to the Mason et al. (2012) estimate of 53 kt used in AMAP/UNEP (2013) (see Table 1.2.1).

Inconsistencies remain in the evidence pertaining to the actual rates of atmospheric historical mining emissions that impacted the global atmosphere and oceans. Although the 3-fold reduction in mining emissions by Zhang et al. (2014) brought their modelled emission history during the late 19th and early 20th centuries closer to global lake sediment flux patterns, compared with the Streets et al. (2011) inventory, the emissions pattern remained elevated compared to lake sediment trends during the same period (see Fig. 1.2.2). Also, the estimate for cumulative pre-1920 anthropogenic emissions by Zhang et al. (2014; i.e., 67% of the total) is several times larger than the Mt. Logan ice core results reported by Beal et al. (2015; in which only 22% of total accumulated Hg was deposited prior to 1900), and the Mt. Gelaidandong study by Kang et al. (2016; see above). It may be that a further reduction in the assumed proportion of volatilized Hg from historical mining/amalgamation would bring the emission history and the remote lake sediment and ice core records into even closer agreement.

1.2.3 Where is anthropogenic Hg distributed in the environment, especially the oceans?

The Zhang et al. (2014) global model projected that in the current global environment, 2% (3.6 kt) of the all-time cumulative anthropogenic emissions remains in the atmosphere, 48% (92 kt) is held in soils, and 50% (94 kt) in the oceans - 35% (66 kt) in seawater, and 15% (28 kt) buried in ocean sediments. For the oceans, atmospheric deposition from current primary emissions as well as revolatilization of legacy emissions contributes over 90% of the total (atmosphere + rivers) Hg inputs (4.0 out of 4.3 kt/yr; Fig. 1.2.5), with riverine inputs that reach the open ocean comprising a minor fraction (6%, 0.3 kt/yr.). Amos et al. (2014) estimated a substantially higher riverine contribution (1.5±0.8 kt/yr.; 30% of total 5.2 kt/yr. inputs) to the open ocean based on an observational database of riverwater Hg concentrations and consideration of river-offshore transport efficiencies for different estuary types. Most (72%) of the riverine Hg entering into estuaries was scavenged and deposited into coastal marine sediments (Amos et al., 2014). By comparison, Mason et al. (2012) arrived at an estimate of 0.38 kt/yr. from rivers, which comprised ~10% of total ocean inputs. Recent data from Chinese rivers (Liu et al., 2016) support the lower estimates of Mason et al. (2012) and Zhang et al. (2014).

Significant differences exist between recent models in their portrayal of the vertical distribution of oceanic anthropogenic Hg because of the above-mentioned variance in historical emission estimates and different assumptions about the penetration rate of anthropogenic Hg into deep ocean waters. Zhang et al. (2014) and Lamborg et al. (2014) largely agreed in their relative distribution, except that the deep ocean (below 1000 m depth) contained proportionally more anthropogenic Hg in Zhang et al.'s (2014) simulation (45% of total oceanic anthropogenic Hg, vs 35% in Lamborg et al. (2014)). Compared to Zhang et al. (2014), Streets et al. (2011) and Amos et al. (2013) calculated similar increases in the anthropogenic Hg content of the surface ocean (4.4 times natural concentrations, vs. 3.6-5.9 times, respectively), but larger increases in the thermocline/intermediate depths (1.2 times, vs 2.7-5.3 times) and deep ocean (1.2 times, vs. 1.5-2.1 times). In addition to their adoption of larger historical mining emission estimates, Streets et al. (2011) and Amos et al. (2013) assumed faster vertical mixing rates compared with the other two studies.

Large inter-basin differences in the distribution of anthropogenic Hg were also apparent in intermediate and deep ocean waters, but were relatively uniform in surface waters, in the modelling of Zhang et al. (2014) (Fig. 1.2.6). Vertical and horizontal advection of Hg inputs to the ocean which reflect ocean currents and areas of deep water formation, and high biological productivity and rapid particle scavenging of dissolved Hg in some tropical seas, account for the inter-basin patterns.

1.2.4 What are the implications of different models for the rate of clearance of anthropogenic Hg from the world's oceans?

The differences between models and their underpinning historical mining emission estimates are associated with significant differences in implied response times of the oceans to emission reduction scenarios. All global ocean-atmosphere models predict that Hg clearance rates from most ocean basins will be slow relative to the rate of anthropogenic emission reductions in future, such that removal of anthropogenic Hg from the world's oceans will take many decades to centuries depending on the ocean basin and depth interval of the water mass in question, as well as the trajectory of emission controls (Mason et al., 2012; Lamborg et al., 2014; Zhang et al., 2014; Amos et al., 2015). But according to Selin (2013) and Engstrom et al. (2014), the "high emission" scenario of Streets et al. (2011) and Amos et al. (2013, 2015) suggests much slower and delayed reductions in environmental Hg levels than other models, especially in the oceans, following emission curbs. Even at current global emission levels, there exists a general scientific consensus that seawater and marine food chain Hg levels are likely to substantially increase, because of the slow clearance rate of legacy Hg from the world's oceans coupled with additional legacy anthropogenic Hg released from soil profiles into rivers and revolatilized into the air (Sunderland and Selin, 2013).

Until current significant deficiencies in our understanding of marine Hg cycling, and the rates of transformation between species that influence the major sinks for ocean Hg (evasion to the atmosphere and burial in sediments) are resolved, and greater consistency is achieved in the interpretation of various natural archive recorders of Hg deposition from the atmosphere, the prediction of the timeline and effects of global emission reductions will remain uncertain. It is clear, however, that irrespective of these scientific uncertainties, emissions reductions are required as soon as possible to reverse the trend in oceanic anthropogenic Hg back towards natural levels because of the long response time of the ocean to changes in inputs (Selin 2013; Sunderland and Selin, 2013; Engstrom et al., 2014).

1.2.5 What are the main uncertainties in global Hg models and budgets?

Here we summarize the knowledge gaps and recommendations for further research from a number of recent papers (Amos et al., 2013; Engstrom et al., 2014; Zhang et al., 2014, 2016; Lamborg et al., 2014, 2016; Song et al., 2015). Scientific uncertainties can be grouped under two headings: natural inputs and processes, and anthropogenic emissions. Under the former category can be listed:

- Removal rates of anthropogenic Hg from the surface ocean are the net result of competition between three simultaneously occurring natural processes: particulate flux from the surface to the deep ocean (the "biological pump", involving particle scavenging and settling); the mixing of surface and deep-ocean waters; and the reduction of inorganic Hg^{II} and subsequent evasion of Hg^0 back into the atmosphere. Further coupled ocean-atmosphere measurement studies are needed to comprehensively measure the concentrations of various Hg species spatially and temporally, and to better understand the transport and transformation rates of these processes. The need is particularly acute in the Southern Hemisphere open oceans, as well as in regions where elevated anthropogenic Hg concentrations can be expected, such as the eastern equatorial Atlantic, eastern equatorial and high latitude Pacific, and northern Indian Oceans.
- Related to the latter effort, uncertainties in the robustness of measurements of atmospheric and seawater Hg concentrations are exacerbated by relatively large inter-laboratory comparison errors. Few inter-comparison efforts have been mounted (e.g. Gustin et al., 2013 for atmospheric Hg^0 determinations); there is a particular need improve the overall reliability of seawater Hg measurements. Past intercalibration exercises have only addressed total Hg and total methylated Hg in seawater, and the results indicated significant discrepancies amongst the participating laboratories. Future intercalibration exercises should continue the effort of attaining reliable total Hg and MeHg measurements, and be extended to all Hg species including unstable species such as dimethyl Hg and dissolved Hg^0. The development of suitable seawater reference materials is encouraged.
- The role of natural inputs in the global Hg budget is poorly constrained but potentially is of primary importance. If the actual rate of emissions from natural sources is markedly higher than currently believed, it would undermine current assumptions about the absolute amounts of, relative balance between, natural and anthropogenic sources which are fundamental to modelling efforts and to our understanding of the global Hg cycle.

Present estimates of global volcanic Hg emissions to air range over three orders of magnitude (0.1 – 1000 t/yr.) (Nriagu, 1989; Ferrara et al., 2000; Pyle and Mather, 2003; Nriagu and Becker, 2003; Bagnato et al., 2014). For oceans, the AMAP/UNEP (2013) report assigned a value of <600 t/yr. total Hg input from hydrothermal vents, which was based on few data and no systematic studies. Two recent Geotraces cruises sampled waters around hydrothermal vents in the North Atlantic and

equatorial Pacific Oceans (Bowman et al., 2015; 2016). In the North Atlantic, the plume of elevated Hg concentration around the vent was highly developed and extended vertically over a depth of around 1000 m and for 1000 km away from the ridge crest (Bowman et al. 2015). In contrast, there was no strong evidence for a plume over the East Pacific Rise in the equatorial Pacific (Bowman et al., 2016). These results further indicate that there is a substantial difference in the extent of Hg inputs from different hydrothermal sources. Overall, there is not sufficient new information to update the estimate of hydrothermal inputs made in 2013, although this may be the single most important primary natural Hg source to the global Hg cycle (Sonke et al. 2013). In order to make direct estimations for global hydrothermal Hg fluxes, more observations of (focused and diffuse-flow) vent fluids and hydrothermal plumes are needed to better constrain the Hg flux, and its contribution to the global Hg cycle (German et al. 2016). In addition, submarine groundwater discharges are likely to bring important amounts of Hg into the ocean, which global models do not account for. Several recent papers indicate that Hg inputs *via* submarine groundwater are as large as atmospheric inputs, at least in coastal environments (Bone et al. 2007, Laurier et al. 2007, Black et al. 2009, Lee et al. 2011, Ganguli et al. 2012).

- Given the importance of terrestrial soils as possibly the largest repository of legacy anthropogenic Hg, global budget calculations will benefit from better understanding of terrestrial Hg cycling including measurements of the evasion rates of deposited Hg from soils, and release rates of Hg to water following degradation of soil organic matter.

In terms of anthropogenic emissions, the absolute amounts of historical emission inventories, especially the role of precious metal mining, has been called into question by recent work comparing model outputs with past Hg deposition rates reconstructed from natural archives of atmospheric deposition (see Zhang et al. 2014, c.f. Amos et al., 2015). Some of the uncertainty lies with the natural archives. For example, a recent paper has shown that the Hg accumulation rates in a Tibetan Plateau glacier ice core were 1 to 2 orders of magnitude lower than in a nearby lake sediment, yet the two archives yielded remarkably similar trends (Kang et al., 2016). While the agreement in trends is encouraging, the difference in absolute values begs the question of what is the most reliable quantitative estimate of past atmospheric deposition. Amos et al. (2015) concluded that peat bog cores gave more accurate reconstructions than most lake sediment cores. Given the now-apparent importance of historical emissions to current world Hg budgets and to future emission reduction scenarios, and the significant

differences in the natural archive records of those emissions, a concerted effort to understand the reasons for the different conclusions from peat, lake sediment and glacial ice archives is called for. Arriving at an agreed historical emission figure from precious metal mining would eliminate a large degree of the uncertainty surrounding current anthropogenic Hg inventories in soils and the oceans.

The accuracy of the recent global emission inventories, including that in AMAP/UNEP (2013), has been questioned in part because of the inconsistency between the recent trends in emission inventories, which are flat or increasing, and the large (~30-40%) decreases in atmospheric GEM and wet deposition since 1990 at background Northern Hemisphere monitoring stations (Zhang et al., 2016). The latter authors found that the emissions and GEM trends could be brought into closer agreement by accounting for the decline in Hg release from commercial products over this period, by reducing the atmospheric revolatilization rate of Hg from present-day artisanal and small-scale gold mining, and by accounting for the shift in Hg^0/Hg^{II} speciation of emissions from coal-fired utilities after implementation of gaseous pollutant control measures. Because the emission inventories are the basis of global modelling efforts, resolving this discrepancy will improve the accuracy of global budgets and future trend scenarios. ASGM emissions were the largest single anthropogenic source of atmospheric Hg in AMAP/UNEP (2013), but this finding has been disputed (Engstrom et al., 2014; Zhang et al., 2016). Verifiable and higher quality emission data from ASGM operations are therefore a priority need.

The global models and an improved understanding of the global Hg cycle are important for our capacity to predict how regulatory efforts to reduce current emissions to air, water and land will affect concentrations in environmental compartments, biota and human exposure. The large uncertainties and identified knowledge gaps described above should not be taken as a sign that regulatory action is not needed or can be delayed until the large research efforts have led to a reduction of these uncertainties. All models and evaluations based on field measurements are in agreement that current anthropogenic emissions of Hg lead to increased environmental exposure of wildlife and humans (albeit of varying magnitude) and that reducing these emissions is a necessity for reducing the negative environmental impacts of Hg. The uncertainties and knowledge gaps are mainly affecting our capability to predict where and when the environment will respond to reduced emissions, not if it will.

392

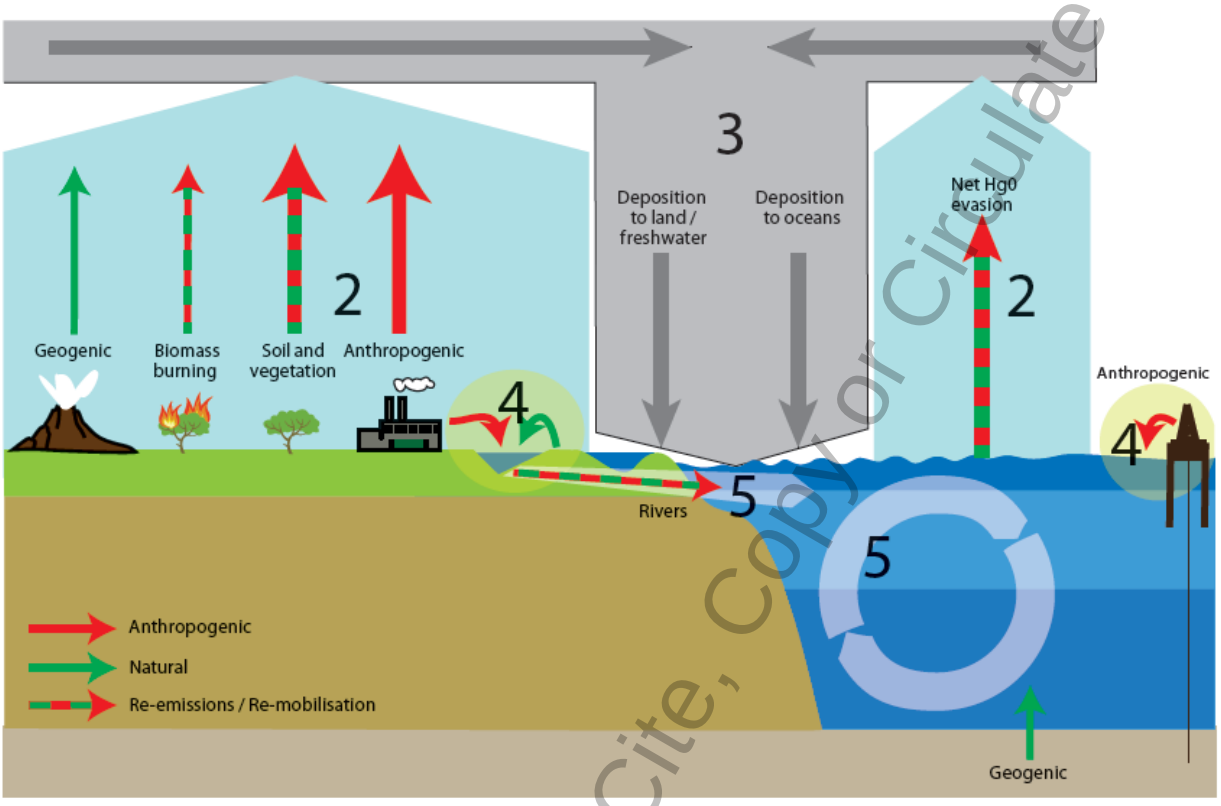

393

394 Figure 1.2.1 Summary diagram of global movements of total mercury between air, soils and oceans
395 (source: AMP/UNEP 2013). Figure to be redrafted (remove chapter numbers, add deposition into
396 mineral soils and deep ocean sediments, deposition arrows to land and oceans need to be mixed
397 red/green colour, remove marine oil well symbol).

398

399

400

401

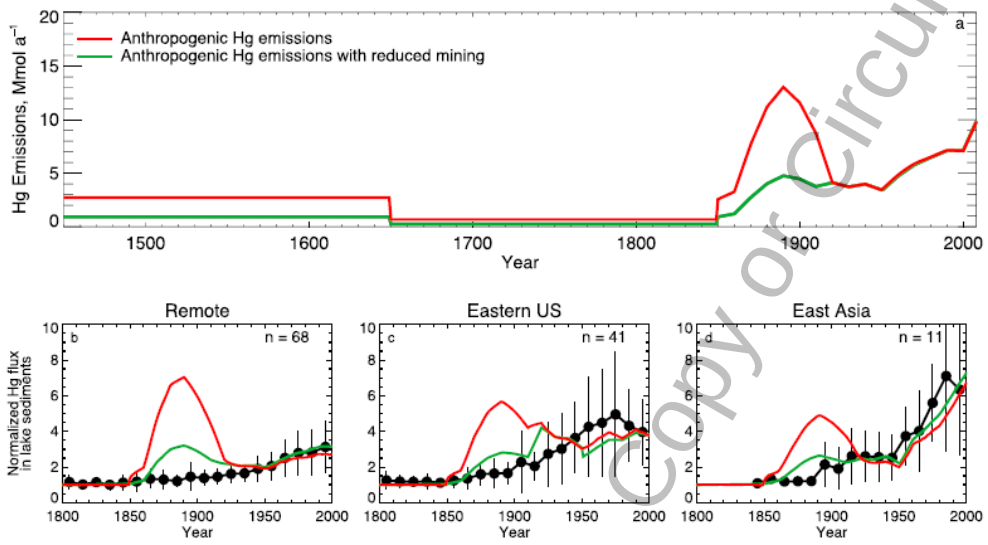

Figure 1. Historical trends in anthropogenic Hg emissions and Hg accumulation flux to lake sediments. (a) Global anthropogenic Hg emissions between 1450 and 2008. The emission inventory from Streets et al. (3) is shown in red, while the emission inventory with mining emissions reduced by a factor of 3 is shown in green. Mean historical Hg flux inferred from sediment cores in (b) 68 remote lakes, (c) 41 lakes in the eastern U.S., and (d) 11 lakes in East Asia. All the fluxes are normalized to 1800–1850 levels. Observations (black filled circles with vertical line showing 1σ) are compared against model results (red and green lines correspond to the original and reduced mining inventories, respectively).

402

403 Figure 1.2.2. Revision of global anthropogenic Hg emission history based on a three-fold reduction in

404 mining emissions from 1450 to ~1920 AD. (Source: Zhang et al. 2014).

405 [figure to be redrawn, and caption revised using Zhang's caption, if this fig is used)

406

407

408

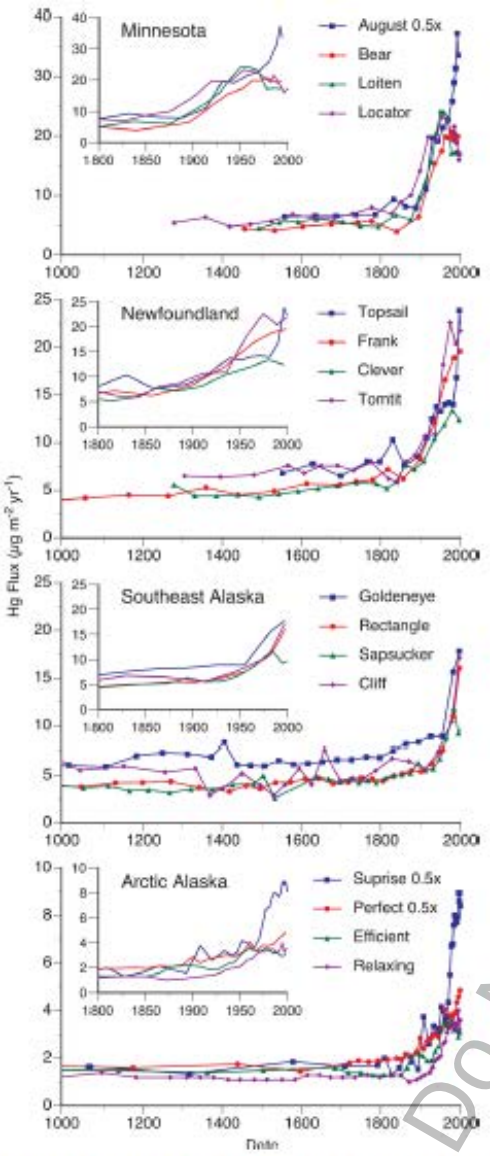

Figure 1. Hg accumulation trends in sediment cores from remote North American lakes. Fluxes scaled by 0.5× for August, Surprise, and Relaxing lakes. Insets show detail for most recent 200 years.

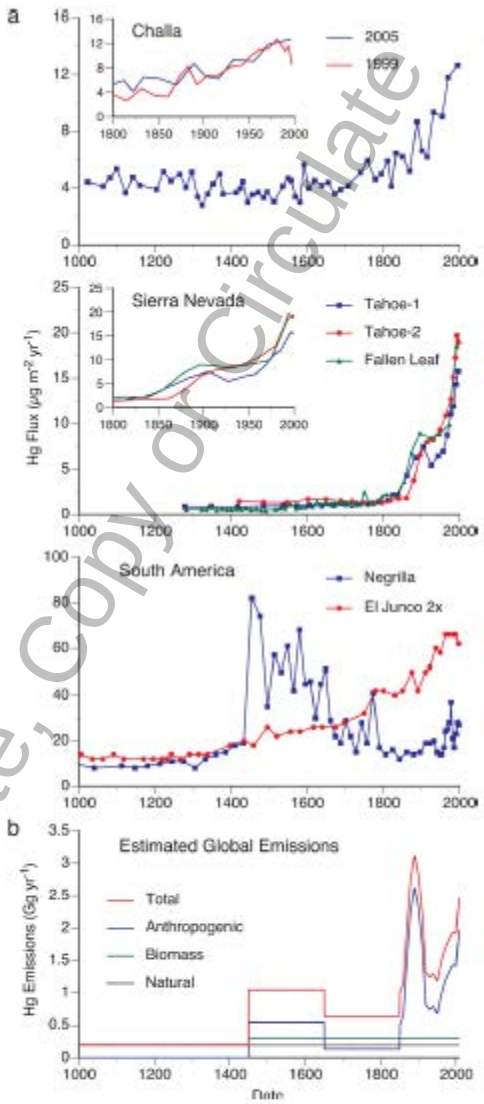

Figure 2. (a) Hg accumulation trends in sediment cores from Lake Challa (Kenya/Tanzania), El Junco and Negrilla (S. America), and Tahoe and Fallen Leaf (Sierra Nevada). Insets show detail for most recent 200 years. The two cores shown for Lake Challa were collected in 1999 and 2005 from nearby locations,[16] while the two cores from Lake Tahoe were collected from different parts of the basin.[33] (b) Primary Hg emissions as estimated by Streets et al.[15]

Figure 1.2.3 Historical Hg fluxes in global lake sediments. From Engstrom et al. 2014 ES&T. [figure to be redrawn, and caption revised using Engstrom's caption, if this fig is used)

418

419

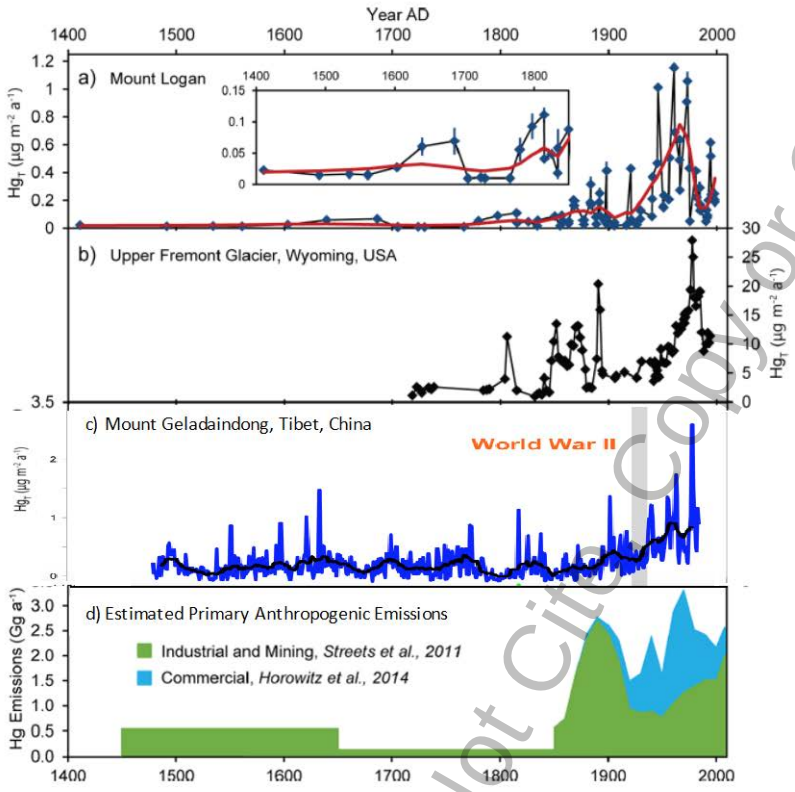

Figure 3. Multicentury Hg_T records from ice cores compared with estimates of primary anthropogenic emissions used in recent global Hg models. (a) Mount Logan Hg_T fluxes (blue points) with 1σ error bars, LOESS smoother (red line), and inset with adjusted *y*-axis for the Preindustrial Period. (b) Hg_T fluxes in the Upper Fremont Glacier ice core calculated using an assumed constant accumulation rate of 800 kg m^{-2} a^{-1} modified from Schuster et al.[1] (c) Geladaindong Glacier HgT fluxes (bars) with the 15-year running average (blue line) (Kang et al., 2016). (d) Estimated primary anthropogenic Hg emissions from industrial and mining sources modified from Streets et al.,[7] and additional

420

421 Figure 1.2.4. Glacial ice core records of atmospheric Hg deposition from Mount Logan, Yukon (source:
422 Beal et al., 2016), the Upper Fremont Glacier, Wyoming, USA (source : Beal et al. 2015) and Mount
423 Geladaindong, Tibetan Plateau, China (source: Kang et al., 2016), compared with the suggested global
424 atmospheric emission since 1450 AD by Streets et al. (2011).

425 [figure source from Beal et al 2016, to be redrawn, and caption revised using Beal's caption, if this fig is
426 used]

427

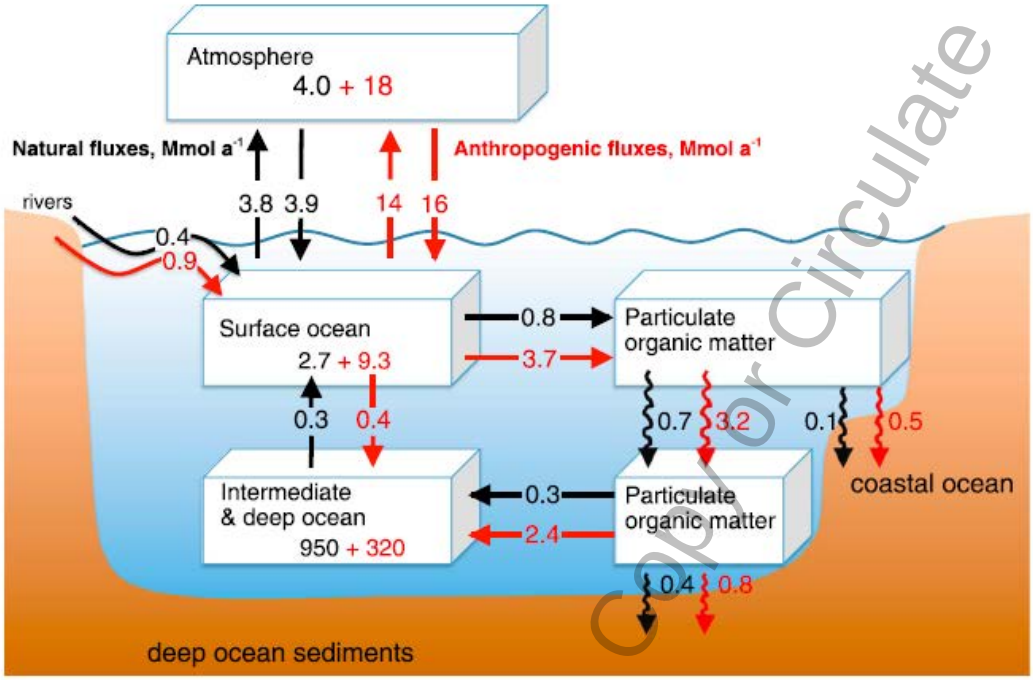

Figure 5. Human influence on the marine Hg cycle. The numbers in the boxes correspond to the mass of Hg in each reservoir (in units of Mmol), while the arrows indicate fluxes in Mmol a^{-1}. The preanthropogenic conditions are in black arrows and numbers, while the human perturbation is shown in red.

428

429 Figure 1.2.5. Natural and anthropogenic Hg inputs and masses in the world's oceans. from Zhang et al.

430 2014 GBC (to be redrawn, and Mmol units converted into kilotonnes).

431

432

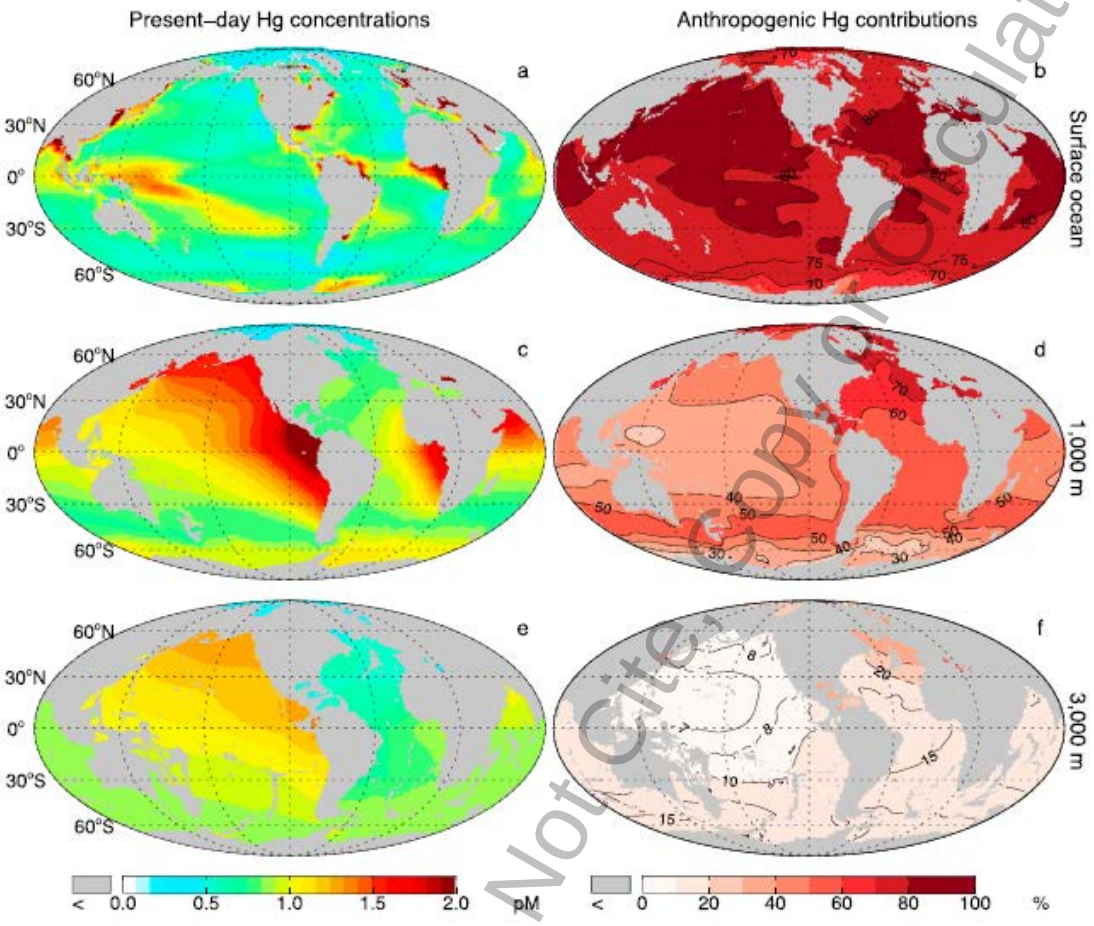

Figure 3. Spatial distribution of Hg concentrations in the present-day ocean. Annual mean concentrations of total Hg (in pM) for (a) the mixed layer, (c) 1000 m depth, and (e) 3000 m depth. (b, d, and f) Contributions of anthropogenic Hg to the present-day concentrations, expressed in percentage.

433

434 Figure 1.2.6. Inter-basin and vertical distribution of total Hg concentrations, and the fraction of
435 anthropogenic Hg, in today's oceans. Use caption shown, but figure will be redrawn. from Zhang et al.
436 2014 GBC.

437

1.3 References

AMAP/UNEP 2013. Technical Background Report for the Global Mercury Assessment 2013. Arctic Monitoring and Assessment Programme, Oslo, Norway / UNEP Chemicals Branch, Geneva, Switzerland. 263 p.

Amos, H. M.; Jacob, D. J.; Kocman, D.; Horowitz, H. M.; Zhang, Y.; Dutkiewicz, S.; Horvat, M.; Corbitt, E. S.; Krabbenhoft, D. P.; Sunderland, E. M. 2014. Global biogeochemical implications of mercury discharges from rivers and sediment burial. Environ. Sci. Technol. 48: 9514–9522.

Amos, H. M.; Jacob, D. J.; Streets, D. G.; Sunderland, E. M. 2013. Legacy impacts of all-time anthropogenic emissions on the global mercury cycle. Global Biogeochem. Cycles 27: 410−421.

Amos HM, Sonke JE, Obrist D, Robins N, Hagan N, Horowitz HM, Mason RP, Witt M, Hedgecock IM, Corbitt ES, Sunderland EM. 2015. Observational and modeling constraints on global anthropogenic enrichment of mercury. Environ. Sci. Technol. 49:4036-4047. doi:10.1021/es5058665.

Bagnato E, Tamburello G, Avard G, Martinez-Cruz M, Enrico M, Fu X, et al. 2014. Mercury fluxes from volcanic and geothermal sources: an update. In: Zellmer GF, Edmonds M, Straub SM, editors. The Role of Volatiles in the Genesis, Evolution and Eruption of Arc Magmas. Special Publications, 410. Geological Society, London.

Beal SA, Osterberg EC, Zdanowicz CM, Fisher DA. 2015. Ice core perspective on mercury pollution during the past 600 years. Environ. Sci. Technol. 49, 7641−7647, doi: 10.1021/acs.est.5b01033.

Black, F. J., A. Paytan, K. L. Knee, N. R. De Sieyes, P. M. Ganguli, E. Gary and A. R. Flegal (2009). Submarine Groundwater Discharge of Total Mercury and Monomethylmercury to Central California Coastal Waters. Environmental Science & Technology **43**: 5652-5659.

Bone, S. E., M. A. Charette, C. H. Lamborg and M. E. Gonneea (2007). Has Submarine Groundwater Discharge Been Overlooked as a Source of Mercury to Coastal Waters? Environmental Science & Technology **41**: 3090-3095.

Bowman KL, Hammerschmidt CR, Lamborg CH, Swarr G. 2015. Mercury in the North Atlantic Ocean: The U.S. GEOTRACES zonal and meridional sections. *Deep-Sea Res. II* **116**: 251-261.

Bowman KL, Hammerschmidt CR, Lamborg CH, Swarr GJ, Agather AM. 2016. Distribution of mercury species across a zonal section of the eastern tropical South Pacific Ocean (U.S. GEOTRACES GP16). *Mar.Chem.* **186**: 156-166.

Cooke, C. A.; Hintelmann, H.; Ague, J. J.; Burger, R.; Biester, H.; Sachs, J. P.; Engstrom, D. R. Use and Legacy of mercury in the Andes. Environ. Sci. Technol. 2013, 47 (9), 4181−4188.

Correla J.P., Valero-Garces, BL, Wang F, Martínez-Cortizas A, Cuevas CA, and Saiz-Lopez, A. 2017. 700 years reconstruction of mercury and lead atmospheric deposition in the Pyrenees (NE Spain). Atmospheric Environment 155: 97-107.

Engstrom, D. R.; Fitzgerald, W. F.; Cooke, C. A.; Lamborg, C. H.; Drevnick, P. E.; Swain, E. B.; Balogh, S. J.; Balcom, P. H. 2014. Atmospheric Hg emissions from preindustrial gold and silver extraction in the Americas: A reevaluation from lake-sediment archives. Environ. Sci. Technol. 48: 6533−6543.

Ferrara R, Mazzolai B, Lanzillotta E, Nucaro E, Pirrone N. Volcanoes as emission sources of atmospheric mercury in the Mediterranean basin. Sci. Total Environ. 2000; 259: 115–121.

Fu X, Zhu W, Zhang H, Sommar J, Yu B, Yang X, Wang X, Lin C-J, and Feng X. 2016. Depletion of atmospheric gaseous elemental mercury by plant uptake at Mt. Changbai, Northeast China. Atmos Chem Phys 16: 12861–12873. doi:10.5194/acp-16-12861-2016

Ganguli, P. M., C. H. Conaway, P. W. Swarzenski, J. A. Izbicki and A. R. Flegal (2012). Mercury Speciation and Transport via Submarine Groundwater Discharge at a Southern California Coastal Lagoon System. Environmental Science & Technology **46**: 1480-1488.

German, C. R., K. A. Casciotti, J.-C. Dutay, L. E. Heimbürger, W. J. Jenkins, C. I. Measures, R. A. Mills, H. Obata, R. Schlitzer, A. Tagliabue, D. R. Turner and H. Whitby (2016). Hydrothermal impacts on trace element and isotope ocean biogeochemistry. Philosophical Transactions of the Royal Society A: Mathematical, Physical and Engineering Sciences **374**(2081).

Guerrero, S. 2012. Chemistry as a tool for historical research: Identifying paths of historical mercury pollution in the Hispanic New World. Bull. Hist. Chem. 37: 61−70.

Horowitz, H. M.; Jacob, D. J.; Amos, H. M.; Streets, D. G.; Sunderland, E. M. 2014. Historical mercury releases from commercial products: Global environmental implications. Environ. Sci. Technol. 48: 10242−10250.

Kang S., Huang J., Wang F., Zhang Q., Zhang Y., Li C., Wang L., Chen P., Sharma C., Li Q., Sillanpää M., Hou J., Xu B., and Guo J., 2016. Atmospheric mercury depositional chronology reconstructed from lake sediment and ice cores in the Himalayas and Tibetan Plateau. Environ. Sci. Technol., 50, 2859–2869

Lamborg, C. H., C. R. Hammerschmidt and K. L. Bowman (2016). An examination of the role of particles in oceanic mercury cycling. Philosophical Transactions of the Royal Society A: Mathematical, Physical and Engineering Sciences 374 (2081), doi: 10.1098/rsta.2015.0297

Lamborg, C. H., Fitzgerald, W. F., O'Donnell, J. & Torgersen, T. A non-steady-state compartmental model of global-scale mercury biogeochemistry with interhemispheric atmospheric gradients. Geochim. Cosmochim. Acta 66: 1105–1118 (2002).

Lamborg, C. H.; Hammerschmidt, C. R.; Bowman, K. L.; Swarr, G. J.; Munson, K. M.; Ohnemus, D. C.; Lam, P. J.; Heimbürger, L. E.; Rijkenberg, M. J. A.; Saito, M. A. 2014. A global ocean inventory of anthropogenic mercury based on water column measurements. Nature 512: 65−68.

Lamborg, C. H., K. L. Von Damm, W. F. Fitzgerald, C. R. Hammerschmidt and R. Zierenberg (2006). Mercury and monomethylmercury in fluids from Sea Cliff submarine hydrothermal field, Gorda Ridge. Geophys. Res. Lett. **33**(17): L17606.

Laurier, F. J. G., D. Cossa, C. Beucher and E. Breviere (2007). The impact of groundwater discharges on mercury partitioning, speciation and bioavailability to mussels in a coastal zone. Marine Chemistry 104: 143-155.

Lee, Y.-G., M. D. M. Rahman, G. Kim and S. Han (2011). Mass Balance of Total Mercury and Monomethylmercury in Coastal Embayments of a Volcanic Island: Significance of Submarine Groundwater Discharge. Environmental Science & Technology 45: 9891-9900.

Liu M, Zhang W, Wang X, Chen L, Wang H, Luo Y, Zhang H, Shen H, Tong Y, Ou L, Xie H, Ye X, and Deng C. 2016. Mercury Release to Aquatic Environments from Anthropogenic Sources in China from 2001 to 2012.Environ Sci Technol *50*: 8169–8177. doi: 10.1021/acs.est.6b01386

Mason, R. P., A. L. Choi, W. F. Fitzgerald, C. R. Hammerschmidt, C. H. Lamborg, A. L. Soerensen, and E. M. Sunderland. (2012) Mercury biogeochemical cycling in the ocean and policy implications. Environ. Res., 119: 101–117. doi:10.1016/j.envres.2012.03.013.

Mason, R. P.; Fitzgerald, W. F.; Morel, F. M. M. 1994. The biogeochemical cycling of element mercury - Anthropogenic influences. Geochim. Cosmochim. Acta 58: 3191−3198.

Melitza Crespo-Medina, A. D. Chatziefthimiou and N. S. Bloom (2009). Adaptation of chemosynthetic microorganisms to elevated mercury concentrations in deep-sea hydrothermal vents. Limnology and Oceanography **54**: 41-49.

Nriagu J, Becker C. 2003. Volcanic emissions of mercury to the atmosphere: global and regional inventories. Sci. Total Environ. 304: 3–12.

Nriagu JO. 1989. A global assessment of natural sources of atmospheric trace metals. Nature 338: 47-49.

Nriagu, J. O. (1993). Legacy of mercury pollution. Nature 363, 589.

Obrist D, Agnan Y, Jiskra M, Olson CL, Colegrove DP, Hueber J, Moore CW, Sonke JE, and Helmig D. 2017. Tundra uptake of atmospheric elemental mercury drives Arctic mercury pollution. Nature 547: 201-204.

Pyle, D. M., and T. A. Mather. 2003. The importance of volcanic emissions for the global atmospheric mercury cycle. Atmos. Env. 37, 5115-5124.

Schuster, P. F.; Krabbenhoft, D. P.; Naftz, D. L.; Cecil, L. D.; Olson, M. L.; Dewild, J. F.; Susong, D. D.; Green, J. R.; Abbott, M. L. Atmospheric mercury deposition during the last 270 years: A glacial ice core record of natural and anthropogenic sources. Environ. Sci. Technol. 2002, 36 (11), 2303−2310.

Selin, N. E. et al. 2008. Global 3-D land-ocean-atmosphere model for mercury: present day versus preindustrial cycles and anthropogenic enrichment factors for deposition. Glob. Biogeochem. Cycles 22, GB2011.

Selin, N. E. Global change and mercury cycling: Challenges for implementing a global mercury treaty. Environ. Toxicol. Chem. 2013, DOI: 10.1002etc.237.

Sherman, L. S., J. D. Blum, D. K. Nordstrom, R. B. McCleskey, T. Barkay and C. Vetriani (2009). Mercury isotopic composition of hydrothermal systems in the Yellowstone Plateau volcanic field and Guaymas Basin sea-floor rift." Earth and Planetary Science Letters 279: 86-96.

Sonke, J. E., L.-E. Heimbürger and A. Dommergue (2013). Mercury biogeochemistry: Paradigm shifts, outstanding issues and research needs. Comptes Rendus Geoscience 345: 213-224

Soerensen, A. L. et al. 2010. An improved global model for air-sea exchange of mercury: high concentrations over the North Atlantic. Environ. Sci. Technol. 44, 8574–8580.

Song S, Selin NE, Soerensen AL, Angot H, Artz R, et al 2015. Top-down constraints on atmospheric mercury emissions and implications for global biogeochemical cycling. Atmos. Chem Phys. 15: 7103-7125.

Streets DG, Horowitz HM, Jacob DJ, Lu Z, Levin L, ter Schure AFH, and Sunderland EM. 2017. Total mercury released to the environment by human activities. Environ. Sci Technol. doi: 10.1021/acs.est.7b00451.

Streets, D. G.; Devane, M. K.; Lu, Z. F.; Bond, T. C.; Sunderland, E. M.; Jacob, D. J. 2011. All-time releases of mercury to the atmosphere from human activities. Environ. Sci. Technol. 45: 10485−10491.

Strode, S., Jaegle, L. & Emerson, S. Vertical transport of anthropogenic mercury in the ocean. Glob. Biogeochem. Cycles 24, GB4014 (2010).

Strode, S., L. Jaeglé, and N. E. Selin (2009), Impact of mercury emissions from historic gold and silver mining: Global modeling, Atmos. Environ., 43, 2012–2017.

Sunderland EM, and Selin NE. 2013. Future trends in environmental mercury concentrations: implications for prevention strategies. *Environmental Health* **12**, doi**:** 10.1186/1476-069X-12-2.

Sunderland, E. M.; Mason, R. P. 2007. Human impacts on open ocean mercury concentrations. Global Biogeochem. Cycles 21 (4), No. GB4022.

Wang X, Bao **Z**, Lin C-J, Yuan W, and Feng X. 2016. Assessment of Global Mercury Deposition through Litterfall. *Environ. Sci. Technol. 50*: 8548–8557. doi: 10.1021/acs.est.5b06351.

Zhang, Y., Jacob, D.J., Horowitz, H.M., Chen, L., Amos, H.M., Krabbenhoft, D.P. Slemr, F., St. Louis, V.L., and Sunderland, E.M. 2016. Observed decrease in atmospheric mercury explained by global decline in atmospheric emissions. Proc. Nat. Acad. Sci., doi:10.1073/pnas.1516312113.

Zhang, Y.; Jaeglé, L.; Thompson, L.; Streets, D. 2014. Six centuries of changing oceanic mercury. Global Biogeochem. Cycles No. 2014GB004939.

Zheng, J. 2015. Archives of total mercury reconstructed with ice and snow from Greenland and the Canadian High Arctic. Sci. Total Environ. 509–510: 133–144.

Note to reader

This draft version of Chapter 2 in the Technical Background Report to the Global Mercury Assessment 2018 is made available for review by national representatives and experts. The draft version contains material that will be further refined and elaborated after the review process. Specific items where the content of this draft chapter will be further improved and modified are:

1. Key findings/messages
2. Figures will be updated/redrawn.
3. Redundant significant figures in tables and quoted values will be rounded.
4. Section on *Emission Factors and Technology Profiles (2.2.1.2).*
5. Uncertainty ranges to be double-checked and/or added
6. Comparisons between GMA 2018 inventory estimates for the nominal year 2015 and national estimates. Will be compiled in Annex 7
7. Comparing 2010 and 2015 global inventory estimates (Chapter 2.4)
8. Conclusions (chapter 2.5)

2016 # Contents

2048

2049

Chapter 2. Global Emissions of Mercury to the Atmosphere from anthropogenic sources

Key Findings/Messages:

Anthropogenic emissions of mercury to the atmosphere currently amount to more than 2000 tonnes per year, accounting for about 30% of mercury emitted annually to the atmosphere, the remainder coming from natural processes (60%) that result in re-emission of mercury previously deposited to soils and water (much of which is itself derived from earlier anthropogenic emissions and releases), and natural sources (ca. 10%).

A new global inventory of mercury emissions to air from anthropogenic sources in 2015 (primarily utilising activity data from 2014) quantifies emissions from 20 key sectors at ca. 2150 (1960 – 2745) tonnes. Additional emissions of the order of tens to hundreds of tonnes per year may arise from smaller anthropogenic sources not currently detailed in the global inventory work.

Inventory methodologies are constantly improved as new information and data becomes available. Changes in emissions estimates for different periods therefore reflect both real-world trends and artefacts of improvements in inventory methods and data availability. Simple comparisons between the new inventory and previous inventories can result in misinterpretation and should therefore be avoided.

Global emissions of mercury to the atmosphere in 2015 are approximately 12% higher than they were in 2010. Continuing action to reduce emissions has resulted in modest decreases in emissions in some regions (North America and EU) but emissions have increased in most other regions. Increased economic activity in these regions (including recovery following the economic down-turn that may have influenced global emissions in 2010) therefore appears to have more than offset any efforts to reduce mercury emissions.

Regional and sectoral attribution of the 2015 global emissions inventory indicates that emissions patterns in 2015 are very similar to those in 2010. The majority of the 2015 emissions occur in Asia (52%; primarily East and South-east Asia) followed by Sub-Saharan Africa (17%) and South America (13%). In the latter two regions, ASGM-associated emissions account for about 70-75% of the emissions. ASGM also account for a significant part of emissions in Central America and the Caribbean (40%) and East and South-east Asia (25%), and constitute almost 34% of the global total. In

other regions, emissions associated with energy production and industrial emissions predominate.

Stationary combustion of fossil fuels and biomass is responsible for about 25% of the estimated global emissions, primarily from coal burning (22%). Emissions from combustion of biomass for energy production are quantified for the first time in the 2015 inventory work and comprise about 2.5% of the global inventory. Main industrial sectors remain non-ferrous metal production (15% of the global inventory), cement production (11%) and ferrous metal production (3.5%). Emissions from wastes from mercury-containing products comprise ca. 7.5% of the global inventory estimate in 2015.

2.1 Sources of anthropogenic mercury emissions to the atmosphere: Introduction

Previous assessments (UNEP, 2013; AMAP/UNEP, 2013) have described how industrial activities to produce power and other commodities, together with a range of intentional uses of mercury in processes and products result in anthropogenic emissions of mercury to the atmosphere. Such emissions currently amount to more than 2000 tonnes per year, accounting for about 30% of mercury emitted annually to the atmosphere, the remainder coming from natural processes (60%) that result in re-emission of mercury previously deposited to soils and water (much of which is itself derived from earlier anthropogenic emissions and releases) and natural sources such as volcanoes (ca. 10%).

Mercury emissions to air are associated with a number of anthropogenic activities that can be characterized as 'by-product' or 'intentional-use' sectors (AMAP/UNEP, 2013). Stationary combustion of fossil fuels (coal in particular), and high temperature processes involved in industrial activities such as primary metal smelting and cement production give rise to 'unintentional' mercury emissions (i.e., the mercury emissions are a 'by-product' of their presence in trace quantities in fuels and raw materials). Intentional-use sectors include the use of mercury-containing products (e.g. lamps, batteries, instrumentation) or dentistry (dental amalgam), where much of the mercury emissions to air (and releases to water) are associated with waste disposal. A further intentional use of mercury is in artisanal and small-scale gold mining (ASGM) where mercury is used to extract gold from gold bearing sediments and rocks. Of these sources, stationary combustion of coal (for power, industry and domestic/residential heating) and artisanal gold mining were estimated to be responsible for over 60% of emissions to air in 2010.

Mercury emissions to air have changed over time. Historically gold and silver mining has been a major source of mercury emissions and releases. These emissions/releases have had local and regional impacts that can be traced today in sedimentary records. With the advent of the industrial revolution (ca. 1850s) and the subsequent rise of fossil fuel economies, mercury emissions increased, likely reaching a maximum in the latter decades of the 20th century, coincident with peak coal use. Emissions have declined since then but remain high, estimated at around 2000 tonnes per year during the first decades of the 21st century. These emissions give rise to global pollution; including long-range transport to remote regions (see Chapter 4), with associated concerns for impact on health of wildlife and human populations (see Chapters 7 and 8).

The GMA2013 (UNEP, 2013, AMAP/UNEP, 2013) included a first global inventory of anthropogenic mercury emissions to air for 2010 prepared according to a new core methodology, an extension of methods employed to produce earlier global inventories for the years 1995-2005 (Pacyna et al. ref). As part of the work to update the GMA2013, a new global inventory of anthropogenic mercury emissions to air has been produced, for the target year 2015. This inventory addresses emissions from the source sectors and activities identified in Table X1; these include 3 new sectors not previously quantified, namely biomass combustion (for energy production), secondary steel production and mercury emitted during production of vinyl chloride monomer (VCM), a raw material for plastics including polymer polyvinyl chloride (PVC). The table also identifies additional sectors not yet fully quantified in global emission inventory work.

2.2 Estimating 2015 global anthropogenic mercury emissions to air: Methodology and important considerations

2.2.1 General methodology

The methodology employed to produce the 2015 global inventory of anthropogenic emissions to air is essentially the same as that applied in developing the 2010 inventory reported in the GMA 2013 (AMAP/UNEP, 2013). The methodology applies a mass-balance approach (see Figure M1) to derive emissions estimates that considers:

- the amounts of fuels and raw materials used, or commodities produced (activity data);
- the associated mercury content of fuels and raw materials and the types of process involved (reflected in 'unabated' emissions factors); and
- technology applied to reduce (abate) emissions to air (through technology profiles that reflect the degree of application and the degree of effectiveness of air pollution controls)

The ASGM and mercury-added product sectors employ variations on this approach.

2107

2108

2109 *Figure M1. General methodology*

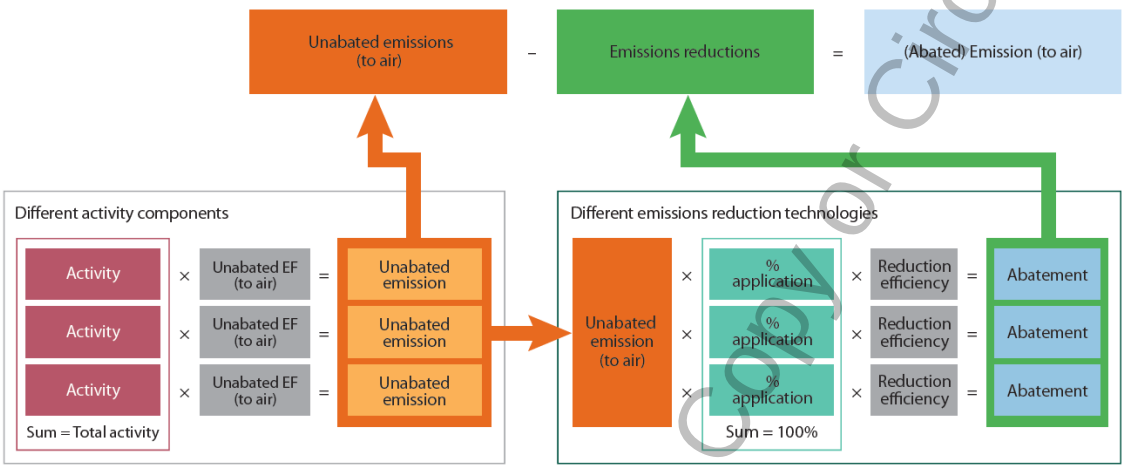

2110

2111 The general methodological approach and its development from earlier methods that were used to
2112 produce the original (1995, 2000 and 2005) global inventories of emissions to air is described in the
2113 GMA2013 report (AMAP/UNEP, 2013 - Section 2.2) and not repeated here. However, a key element
2114 in the delivery of the GMA is transparency. Consequently, the following documentation includes a
2115 discussion of some of the more significant changes that have been applied in the methodology
2116 and/or to key parameters that influence calculated emissions estimates for particular sectors.
2117 Generally this reflects improvements in available information. The current report therefore also
2118 includes a comprehensive set of annexes (Annexes 1-8) that present the (updated) factors and
2119 assumptions applied in calculating the 2015 emissions estimates, together with the activity data used
2120 and the resulting emission estimates on a country/sector basis.

2121 In addition to improving the methods used to estimate global emissions by incorporating new
2122 information, the method used to geospatially distribute the global inventory has also been upgraded
2123 as part of the GMA2018 work. These new developments allow national estimates to be mapped
2124 (gridded) at a finer resolution for use in modelling work.

2125 ***2.2.1.1 Activity data***

2126 Information on amounts of fuel or raw materials used in different applications or amounts of
2127 products or commodities produced is the basis for estimating emissions of mercury to air. This
2128 activity data is available from various sources, such as national statistics agencies, international
2129 organisations and industry associations.

2130 Sectors and sources of activity data used in preparing the 2015 global estimates are presented in
2131 Table X1. Activity data applied to national emission estimates are presented in Appendix 5.

2132 Whenever available, statistics for the target year 2015 have been used for this emission inventory. In
2133 many cases, information for 2015 was not available at the time of preparing the inventory; therefore,
2134 data from 2014 (and in some cases earlier) were used.

2135 *Table X1 – LIST OF SECTORS / CODES – SOURCES OF ACTIVITY DATA USED*

Sector Code	Sector description	Activity Code	Activity description	Sources of Activity data.	Year of activity data
ASGM	Artisanal and small-scale gold mining	ASGM	Artisanal and small-scale gold mining	AGC, 2017	2014 (and earlier)
BIO	Biomass burning (domestic, industrial and power plant)	PSB - DR	domestic residential burning	IEA 2016	2014
		PSB - IND	industry	IEA 2016	2014
		PSB - PP	power plants	IEA 2016	2014
CEM	Cement production (raw materials and fuel, excluding coal)	CEM	cement (fuels excl.)		
		PC- CEM	pet coke	IEA 2016	2014
		See also BC–IND-CEM and HC-IND-CEM			
CREM	Cremation emissions	CREM	Cremation emissions	National reports and International Cremation Statistics	2014
CSP	Chlor-alkali production (mercury process)	CSP-C	capacity based		
		CSP-P	production based		
NFMP	Non-ferrous metal production (primary Al, Cu, Pb, Zn)	AL-P	aluminium (primary production)	USGS 2016	2013/2014
		CU-P	copper (primary production)	USGS 2016	2013/2014
		CU-T	copper (total production)	USGS 2016	2013/2014
		PB-P	lead (primary production)	USGS 2016	2013/2014
		PB-T	lead (total production)	USGS 2016	2013/2014
		ZN-P	zinc (primary production)	USGS 2016	2013/2014
		ZN-T	zinc (total production)	USGS 2016	2013/2014
		See also BC–IND-NFM and HC-IND-NFM			
NFMP-AU	Large-scale gold production	GP-L	gold production	USGS 2016	2013/2014

NFMP-HG	Mercury production	HG-P	mercury production	USGS 2016	2013/2014
OR	Oil refining	CO-OR	oil refining		
PISP	Pig iron and steel production (primary)	PIP	iron and steel (primary production)	USGS 2016	2013/2014
		See also BC–IND-PIP and HC-IND-PIP			
SC-DR-coal	Stationary combustion of coal (domestic/residential, transportation)	BC-DR	brown coal	IEA 2016	2014
		HC-DR	hard coal	IEA 2016	2014
SC-DR-gas	Stationary combustion of gas (domestic/residential, transportation)	NG-DR	natural gas	IEA 2016	2014
SC-DR-oil	Stationary combustion of oil (domestic/residential, transportation)	CO-HF-IND	heavy fuel oil	IEA 2016	2014
		CO-IND	crude oil	IEA 2016	2014
		CO-LF-IND	light fuel oil	IEA 2016	2014
SC-IND-coal	Stationary combustion of coal (industrial)	BC-IND-CEM	brown coal (cement industry)	IEA 2016	2014
		BC-IND-NFM	brown coal (NFM industry)		2014
		BC-IND-OTH	brown coal (other industry)		2014
		BC-IND-PIP	brown coal (ferrous metal industry)		2014
		HC-IND-CEM	hard coal (cement industry)	IEA 2016	2014
		HC-IND-NFM	hard coal (NFM industry)		2014
		HC-IND-OTH	hard coal (other industry)		2014
		HC-IND-PIP	hard coal (ferrous metal industry)		2014
SC-IND-gas	Stationary combustion of gas (industrial)	NG-IND	natural gas	IEA 2016	2014
SC-IND-oil	Stationary combustion of oil (industrial)	CO-HF-IND	heavy fuel oil	IEA 2016	2014
		CO-IND	crude oil	IEA 2016	2014
		CO-LF-IND	light fuel oil	IEA 2016	2014
SC-PP-coal	Stationary combustion of coal (power plants)	BC-L-PP	brown coal (lignite)	IEA 2016	2014
		BC-S-PP	brown coal (sub-bituminous)	IEA 2016	2014
		HC-A-PP	hard coal (anthracite)	IEA 2016	2014
		HC-B-PP	hard coal (bituminous)	IEA 2016	2014

SC-PP-gas	Stationary combustion of gas (power plants)	NG-PP	natural gas	IEA 2016	2014
SC-PP-oil	Stationary combustion of oil (power plants)	CO-HF-PP	heavy fuel oil	IEA 2016	2014
		CO-LF-PP	light fuel oil	IEA 2016	2014
		CO-PP	crude oil	IEA 2016	2014
SSC	Secondary steel production	SP-S	secondary steel production	Steel statistical yearbook 2015, World Steel Association 2015	2014
VCM	Vinyl-chloride monomer (mercury catalyst)	VCM	Vinyl-chloride monomer	National and literature information combined with Hg consumption data for VCM production by world region from P. Maxson	2015
WASOTH	Waste (other waste)	WASOTH	other waste	Estimated consumption of Hg in mercury added products in 2015 by world region (P. Maxson)	2015
WI	Waste incineration (controlled burning)	WI	waste incineration	Estimated consumption of Hg in mercury added products in 2015 by world region (P. Maxson)	2015
Other (sectors not yet fully characterized in the global inventory)	Contaminated sites				2010 GMA
	Oil and gas extraction (upstream of refineries)			IPIECA estimate (R. Cox, pers. comm.)	
	Other (including pulp and paper, secondary non-ferrous metals, food industry)			Residual totals from national PRT inventories covering primarily North America, Europe and Australia	
	Incineration of industrial and sewage sludge and some hazardous wastes				

2136

2137 ***2.2.1.2 Emission Factors and Technology Profiles***

2138 Information on (unabated and abated) emissions factors and technological profiles (reflecting degree

2139 of application and effectiveness of air pollution control (APC) technologies to reduce emissions of

mercury; see AMAP/UNEP, 2013) are detailed in Annex 6. These factors are defined for individual countries where data are available; where national data are lacking, default factors are applied to groups of countries based on assumptions regarding their level of technological development. For ASGM associated emissions an alternative approach is employed (see Annex 2). The assignment of (emission and APC technology) factors for particular countries/sectors builds on work described in the GMA 2013, and utilises a considerable amount of new information that has become available since that time from published literature, in particular concerning China, as well as information acquired from national experts from more than 25 countries from all world regions during inventory workshops and meetings organized as part of the 2015 inventory compilation activity.

Revision to applied emission factors and assumptions regarding application and effectiveness of APC technologies can significantly affect derived (national-sector) emission estimates; some revisions reflect developments (e.g., in applied APC measures, or changes in sources of fuels or raw materials used nationally) since 2010; others reflect improved information on, e.g. mercury content of fuels and raw materials that would also apply in relation to revised 2010 emissions estimates. Revisions to factors applied in the 2015 inventory work are – for the most part – not yet reflected in the UNEP Toolkit that is been used as the basis for most national Minamata Initial Assessments (MIAs), etc.; see section 2.3.4. The following section discusses some of the more significant changes introduced for individual sectors.

[Additional text will be added. See Annex 6.]

2.2.2 Sector specific methodologies - significant changes and improvements

For the sectors: Stationary Combustion – oil burning; Stationary Combustion – gas burning; Primary production of non-ferrous metals – mercury from cinnabar ore, and; Chlor-alkali production, methods employed are essentially identical to those applied in the GMA2013 (AMAP/UNEP, 2013). Updated information on the basis for calculations applied in the 2015 inventory can be found in Annex 6.

The following sections describe substantive methodological changes that have been introduced in relations to some specific sectors. These changes can have implications for calculated estimates that need to be appreciated when comparing 2015 inventory estimates with previous estimates (including 2010 inventory estimates presented in GMA 2013). For a more detailed discussion of the results regarding emission estimates for selected emission source sectors see section 2.3.3.

1. Methodology update: Stationary Combustion – coal burning

The methods are essentially the same as those applied in the GMA 2013 (AMAP/UNEP, 2013).

For stationary combustion of coal in power plants (SC-coal-PP) and in industry (SC-coal-IND) technology profiles for several countries have been updated. The updates are based on new information concerning application of advanced APCDs in some countries, and better information regarding their effectiveness at reducing emissions of mercury to the atmosphere.

For hard coal and brown (HC and BC) coal combustion, activity data for coal used in industry are now separated between cement (-CEM) iron and steel (-PIP) non-ferrous metal (-NFM) and other industrial uses (-OTH). This allows attribution of industrial coal burning emissions to specific industrial sectors. Unabated Emission Factors (UEFs) applied are equivalent to those defined for the coal-IND activities in the GMA 2013.

For more details see Annex 6.

2. Methodology: Stationary Combustion – biomass burning

Mercury is a trace contaminant present in varying concentrations in biomass fuel and mercury emissions to air arise when biomass is combusted in power plants, in industry and in domestic/residential use. This source was not addressed in the 2010 global emission inventory.

Emission estimates for 2015 have been developed following the general inventory methodology and using activity data from IEA on amounts of biomass combusted as fuel in power plants, industry, and domestic/residential use. IEA data only cover solid biomass used as fuel for energy production, therefore the 2015 emission estimates presented do not include wildfires (a natural source) or agricultural burning, an anthropogenic (or at least anthropogenically enhanced) source that can be a significant activity in some countries. Emission factors were derived using the heat value for air dried wood of 16 MJ/kg (IEA Energy Statistics manual, OECD/IEA, 2005) and literature discussing mercury content in biomass. Detailed information on the factors used in estimating emissions from biomass burning is presented in Annex 6.

3. Methodology update: Cement production

Mercury emissions associated with cement production originate from use of mercury-containing fuels (including conventional, mainly fossil fuels and co-incinerated wastes) and raw materials (limestone, iron oxides, fly ash, clay, silica, etc.). The majority of the emissions occur during clinker production (calcination) in high temperature kilns. Emissions can also occur during drying and preheating processes, but these are assumed to be much lower than those from calcination. Very small amounts of mercury are bound in the clinker itself, therefore subsequent stages of

2202 cement production (blending clinker with other materials, such as gypsum to form cement) are
2203 assumed to be a negligible source of mercury emissions (UNEP, 2015).

2204 The main conventional fuels used in the cement industry are coal and petroleum coke. Allocation
2205 of mercury emissions from these fuels in emission inventories and studies can vary – they are
2206 often aggregated with other fossil fuel combustion or included in the emission factors for cement
2207 production. For example, coal combustion in the cement industry was included under the
2208 category 'stationary combustion of fuel in industry' in the 2010 inventory.

2209 A new development in the methodology applied to prepare the 2015 inventory estimates
2210 concerns the way in which emissions associated with fuels and raw materials used in the cement
2211 industry are derived. In the 2015 global inventory (i.e. the work reported here), emissions
2212 associated with (conventional) fuel combustion in the cement sector are now allocated to new
2213 (sub-)activities under the sectors concerned with stationary combustion of coal, and in the case
2214 of petroleum coke a sub-activity under cement itself. The annexes to this report therefore
2215 separately present information on emission factors, activity data and mercury emissions for coal
2216 and petroleum coke combusted in the cement industry. This modification to the methodology
2217 also allows separate assignment of technology profiles for this sector facilitating better
2218 comparison of emission estimates and emission factors with other data sources.

2219 These changes have been implemented to allow better attribution of emissions between
2220 contributions from fuel and cement raw materials. This is done for all fuels, except for co-
2221 incinerated waste. The contribution from alternative fuels (mainly consisting of waste) varies
2222 considerably between the countries and this is considered in the emission factors applied in the
2223 current inventory (see Annex 6).

Key modifications to cement sector emission factors and technology profiles
The methodology used to estimate cement sector emissions is similar to that applied in the GMA 2013, but with the following changes: • Unabated emission factors (UEFs) are first calculated per tonne clinker and then adjusted with respect to country- or region-specific clinker/cement ratios. • Mercury emissions from combustion of petroleum coke, previously included in UEF for cement, are allocated to a separate sector – fossil fuel combustion in cement sector. • Region-specific default UEF values are developed for all countries based on data on clinker/cement ratios, energy demand and co-incineration of waste as alternative fuel obtained from the GNR database (GNR, 2014). This means that a global-average default UEF is no longer applied for cement emission calculations, only country-specific or region-specific UEFs. • Values of Hg content in raw materials and co-incinerated waste are adjusted in accordance with data presented in recent articles and reports and provided by national experts. The default Hg

content of total raw mix is estimated assuming variable additions of Hg-rich materials such as fly ash and iron oxides and is thus higher than Hg content of limestone alone.

- A distribution factor to air of 0.95 is used (as opposed to a value of 0.8 based on the default UNEP 2011 value that was applied in the 2010 global inventory calculations). This revision is based on the information in BAT/BEP and Wang 2014 indicating that only about 1-5 % of the total mercury input is bound in clinker.
- All technology profiles associated with the cement sector (cement production and related fuel combustion) have been harmonized since process-related emissions (originating in raw materials) and energy-related emissions (originating in fuels) are usually treated in the same abatement system at cement facilities.

For further details see Annex 6.

4. Methodology update: Primary iron and steel production

Primary pig iron and steel is typically produced at integrated facilities where raw materials (iron ore, limestone, lime, dolomite, and metal scrap) undergo several processes. Mercury emissions originate from mercury in these raw materials and fuels used (mainly coal/coke). Virtually all mercury emissions occur during thermal processes – sintering/pelletizing, pig iron production in blast furnaces, and steel-making in basic oxygen furnaces (UNEP, 2015).

Key modifications to pig iron and steel sector emission factors and technology profiles

The methodology used to estimate pig iron and steel sector emissions is similar to that applied in the GMA 2013, but with the following changes:

- The steel-making stage in basic oxygen furnaces is included.
- Hg input from dolomite is included.
- Values of Hg content in raw materials are adjusted with respect to data presented in recent articles and reports and provided by national experts.
- Combustion of coal in production of pig iron and steel is now identified as a separate (sub-) activity under 'industrial stationary combustion emissions'

For further details see Annex 6.

5. Methodology: Secondary steel production

Most secondary steel production is based on an Electric Arc Furnace (EAF) process using steel scrap as the input material. Mercury may be present as a contaminant in the scrap steel, in amounts that are highly variable depending on the type of scrap. In some countries, mercury-containing scrap may be sorted and removed before the scrap enters the EAF. Mercury contained in scrap that is not removed in this way is released during the EAF smelting process. This source was not addressed in the 2010 global emission inventory.

Emission estimates for 2015 have been developed following the general inventory methodology using activity data on annual steel production by EAF from the World Steel Association. Default UEFs were derived from Wang 2016b, Roseborough et al 2008, Burger Chakrabortry 2013, Ocio et al 2012, Kim et al 2010, and BREF_IS (table 8.1) and a default technology profile was developed based mainly on national information in Kim et al 2010 and Roseborough et al 2008. For further details see Annex 6.

6. Methodology update: Primary production of non-ferrous metals (copper, lead and zinc)

Primary production of the non-ferrous metals copper, lead and zinc are a significant source of mercury emissions and releases from both raw materials (metal ores) and fuels used in the process. Metal ores are mined and concentrated; concentrates are further pre-treated, roasted, smelted and refined. Most of the mercury present in metal concentrates evaporate during high-temperature roasting (or sintering) and smelting stages (UNEP, 2017). Releases from ore mining operations are not included in the scope of this inventory.

Most large smelters include acid plants that remove a substantial part of the mercury emitted from the off-gas during the smelting stage. This mercury is either treated as waste (if removed prior to acid production) or contained in the acid (BAT/BEP, 2017). Acid plants are considered a form of (air) pollution control device in the applied methodology.

Key modifications to primary non-ferrous (copper, lead, zinc) sector emission factors and technology profiles
The methodology used to estimate non-ferrous copper, lead and zinc sector emissions is similar to that applied in the GMA 2013, but with the following changes: • Concentrate/metal ratios and values of Hg content in concentrates have been adjusted to reflect new information and data presented in recent articles and reports and provided by national experts. Assumptions on metal content in concentrates are also revised based on concentrate/metal ratios provided in recent literature. • A distribution factor to air of 1 was applied in the 2010 global inventory based on the default UNEP Toolkit value (UNEP 2011). This value has now been adjusted to take account of information in Hui 2016 indicating that about 3-10% of the total mercury input is bound in smelting slag. The proportion of mercury bound in smelting slag is assumed to be 0.9 for Zn (a weighted average over two main production processes, assuming that hydrometallurgical process is used more widely than pyrometallurgical), 0.96 for Cu and 0.97 for Pb. • Default technology profiles of country groups 1 and 2 are revised and imply higher abatement levels in the current inventory than in 2010. • Combustion of coal in production of non-ferrous metals is now identified as a separate (sub-) activity under 'industrial stationary combustion emissions' For further details see Annex 6.

7. Methodology update: Primary production of non-ferrous metals – aluminium

The methodology used to estimate NFM-aluminium production sector emissions is similar to that applied in the GMA 2013, but with a small adjustment to the applied bauxite/alumina ratio based on BREF data. For a group of countries producing alumina for export only, a new emission factor has been developed, see details in Annex 6.

8. Methodology update: Primary production of non-ferrous metals – large-scale gold production

The methodology used to estimate NFM-large-scale gold production sector emissions is similar to that applied in the GMA 2013; however, the default technology profile for group 1 countries has been revised and implies higher abatement levels in the current inventory than in the 2010 inventory. See Annex 6.

Activity data on large-scale gold production from the USGS includes a number of footnotes concerning difficulties distinguishing ASGM and large-scale gold production in some countries. Where possible these notes have been considered in the light of other published information and or discussions with national experts to correctly characterize gold production; however, the possibility of that (some) ASGM produced gold is included in activity data for large-scale gold production remains for some countries.

9. Methodology update: Oil refining

The methodology used to estimate emissions from oil refineries is similar to that applied in the GMA 2013; with some minor adjustments to the assumptions (weighting) applied when calculating mercury content of oils refined in different countries. These adjustments result in a small decrease in total emissions from this sector if 2010 calculations are repeated, but may significantly influence estimates for individual countries. Although industry sources have delivered new information on mercury content of oil from different regions (IPIECA, 2012), for reasons of commercial confidentiality they are unable to specify the exact sources of these oils (i.e., the countries/fields of origin). This means that lack of reliable information on mercury-content of refined oils remains an important limitation in estimating national emissions and releases from oil refineries. Other knowledge gaps include information to resolve different assumptions regarding fate of mercury emitted/released during refinery operations (see section 2.3.3(8), below). See also Annex 6.

10. Methodology: Vinyl Chloride Monomer (VCM) production with mercury-dichloride ($HgCl_2$) as catalyst

Two processes are used in the manufacture vinyl chloride monomer: the acetylene process that uses mercuric chloride on carbon pellets as a catalyst, and a process based on the oxychlorination of ethylene that does not use mercury. Production of VCM with mercury-containing catalyst occurs only in a few countries (China, India and the Russian Federation). Mercury can be emitted during the production of VCM but a large part of the mercury remains in the used catalyst. Recycling of used catalyst is, however, an additional substantial source of mercury emissions. The 2015 estimates of mercury emissions to air from VCM production and from recycling of mercury-containing catalyst are based on national information, in combination with literature information; for further information see Annex 6.

This source was not addressed in the 2010 global emission inventory.

11. Methodology update: Waste and waste incineration

Mercury emissions from waste originating from mercury-added products (lamps, batteries, measuring devices, etc.) have been estimates based on assumptions regarding their entry into different waste streams. The majority of wastes associated with mercury-added products end up in landfill or (controlled/uncontrolled) incinerated waste. Mercury 'consumption' in these mercury-added products is defined in terms of final regional consumption of mercury products to take account of the fact that, for example, although most measuring and control devices are produced in China, many of them are exported, 'consumed' and disposed of in other countries.

It is important to recognize that estimates for mercury emitted from the waste sector do not currently include emissions due to incineration of industrial waste and sewage sludge, or (in most cases) hazardous waste. This is because it is not currently possible to obtain reliable information on the amounts of such wastes incinerated, and more importantly the mercury content of such wastes, which can be highly variable. This subject is further discussed below in relation to national comparisons, chapter 2.3.4.

Key modifications to (mercury-added product) waste and waste incineration sector emission factors and technology profiles
The basic methodology applied to estimate mercury emissions from waste originating from mercury-added products is the same as that applied for the 2010 inventory. • In the 2010 global inventory (GMA 2013) about 30% of the Hg was assumed to remain in products in society and not be emitted until later. In the 2015 global inventory this component is set to zero, to (to some extent) take account of the continuous release of materials in societal use. Consequently, all Hg consumed in one year (2015) is now distributed on pathways of safe storage, breakage or flow into the waste stream.

- Mercury consumed in mercury-added products is distributed on different pathways using distribution factors with emission factors applied to estimate emissions; some distribution factors have been revised based on information from national experts.
- A new technology group was added, covering the least developed level of technology for waste handling. Most countries in Sub-Saharan Africa were assigned to this technology level based on information from experts responsible for coordinating regional MIAs; some additional reclassifications of countries between technology groups, relative to assignments used in the 2010 global inventory, were also applied.

For further details see Annex 3.

12. Methodology update: Crematoria emissions

Methods employed were essentially identical to those applied in the GMA2013. Updated information on regional mercury consumption in dental uses in 2015 was obtained from Maxson (2017) and, where available, cremation statistics updated based on national information and data from the Cremation Society of Great Britain (CSGB, 2017). The methodology is considered sub-optimal in that it does not take account of, e.g. the relationship between time of application of amalgam fillings and life-expectancy, and other factors that will determine cremation emissions following use of mercury in dental amalgam. However it provides a first-level estimate of emissions from this use of mercury that can be compared with other such estimates (e.g., those derived in national inventories or MIAs, see section 2.5). See also Annex 4.

13. Methodology update: Artisanal and small-scale gold production (to be completed)

The information base that underpins the assumptions applied regarding use of mercury in artisanal and small-scale gold mining has been significantly updated and improved for a number of countries. Improved knowledge also resulted in an adjustment to the factors applied in assigning ASGM emissions associated with use of whole ore amalgamation and concentrate amalgamation. This results in a small decrease in the estimate of emissions to air per unit of mercury consumed in ASGM that is reflected in both retrospectively updated (national) estimates for 2010, as well as for 2015. See Annex 2.

2.2.3 Uncertainties

In the GMA2013 a simplistic approach was applied to calculate uncertainties associated with the 2010 inventory estimates. Essentially, this involved calculating high- and low-range estimates for individual country-sector emissions based on assumptions regarding reliability of activity data and (unabated) emission factors. Uncertainties associated with assumptions about applied technologies were ignored. It was noted that this approach would result in over-estimation of uncertainties associated with aggregated emissions estimates such as regional, sectoral or global totals. However,

2338 the method did provide a reminder that inventory estimates – whatever their source or basis – have
2339 large associated uncertainties and need to be regarded in this light.

2340 In the 2015 inventory work, a more detailed evaluation of uncertainties has been applied considering
2341 three different approaches: (i) calculating uncertainties using the approach applied in the GMA,
2342 2013; (ii) applying a modification of this whereby uncertainties associated with technology
2343 assumptions were also introduced, and (iii) employing the propagation of errors method (Frey, et al.,
2344 2006) to evaluate uncertainties associated with aggregated estimates. The latter method was
2345 adapted to apply a cut-off in extreme situations, e.g. so that removal efficiency could not exceed
2346 100%. Further assumption were applied in relation to other factors; for example, unabated emissions
2347 factors used in range estimates were based on assumptions regarding skewed (log-normal)
2348 distribution of mercury-content of fuels and raw materials.

2349 Further details of these three approaches are described in Appendix A. Results of the modified
2350 approach to individual country-sector estimates are reflected in the values tabulated in Annex 8.
2351 Uncertainty estimates associated with aggregated emission estimates using the propagation of errors
2352 approach are included in the values presented in section 2.3, below.

2353 At the global level, uncertainties calculated using approach (i) are -54% / +150%, using method (ii) -
2354 63% / +206%, and using method (iii) -8.4% / +30%.

2355 2.3 Estimating 2015 global anthropogenic mercury emissions to 2356 air: Results

2357 In this section, results for the 2015 global inventory estimates are reviewed from the perspective of
2358 region- and sector-based summaries followed by commentaries on comparisons with national
2359 inventories and air emissions on a sector by sector basis, and an evaluation of apparent trends in
2360 emissions between 2010 and 2015.

2361 The global inventory of mercury emissions to the atmosphere from anthropogenic sources in 2015 is
2362 2150 tonnes (range ca. 1965 – 2743 tonnes).

2363 This global inventory total for 2015 does not include sectors that are not yet addressed discretely in
2364 the inventory work; for example it does not include the ca. 80 tonnes that, in the GMA2013 work was
2365 attributed to emissions to air from 'contaminated sites'. In the case of contaminated sites, emissions
2366 from 'contaminated sites' can be assumed to be similar in 2010 and 2015.

2367 Some key observations are as follows:

- The 2015 inventory total of 2150 tonnes aligns with the GMA2013 statement that global emissions to air in the first part of the 21 century from principle anthropogenic sectors are of the order of 2000 tonnes per year.
- Uncertainties associated with the current global inventory total of 2150 tonnes are of the order of -10% and +30% (i.e., an approximate range of 1930-2800 tonnes).
- Estimated global mercury emissions to air from anthropogenic sources in 2015 are approximately 12% higher than the inventory for 2010, when 2010 estimates are retrospectively updated for comparable methodology and sectors not addressed in the original 2010 inventory. This increase appears to be mainly associated with increased economic activity in certain regions. Possible reasons for the increase are discussed in more detail in sections 2.3.3 and 2.4.
- Sectors not yet addressed in the national-sector estimated inventory may contribute additional emissions to air of the order of some tens-to-hundreds of tonnes per year. These include, for example, ca. 70-95 tonnes of emissions from contaminated sites and XXX from other sectors noted in this report (see section xxx). For example, the global inventory total rises to 2230 tonnes if estimated emissions from contaminated sites are included.

2.3.1 Summary of results by region

The regional (sub-continental) contributions to the global inventory in 2015 are illustrated in Figure R1. The emissions pattern is very similar to that in 2010, with the majority of the emissions occurring in Asia (52%, of which 42% in East and South-east Asia) followed by Sub-Saharan Africa (17%) and South America (13%) (see also Table R1). The consistency in the regional distribution of emissions illustrated in Figure T1 (above) between the 2010 (GMA 2013), 2010 updated and 2015 datasets discussed in this report indicates that these patterns are robust and not influenced to any undue extent by artefacts resulting from changes in methodology and additional sectors introduced since the GMA2013 work.

ASGM-associated emissions account for about 70-75% of the emissions that occur in South America and Sub-Saharan Africa.

If ASGM-associated emissions are discounted, the East and South-east Asian region remains the region responsible for the majority of emissions (48% on the non-ASGM total), with South Asia responsible for a further 15%. The non-ferrous metals industry is the main source of emissions in Sub-Saharan Africa and the 'CIS and other European countries' region; thus these two regions, between them, contribute a further 15% of the total non-ASGM emissions. In the remaining regions, coal combustion still accounts for the major part of the emissions in North America (over 60%), the EU (over 50%) and Australia, New Zealand and Oceania (36%). In the Middle Eastern States and North Africa, the cement industry is the principle source of emissions (43% and 52% of the regional totals, respectively). Sources associated with wastes from mercury-containing products account for

approximately 10-20% of emissions in most regions, somewhat higher in North Africa (27%) and lower in the EU and East and South-east Asian regions.

All percentage contributions need to be considered in relation to the total (absolute) amounts of mercury emitted in each sub-region. The sector-based emission discussion (section 2.3.3) provides additional insights into the relative amounts of emissions from different source sectors.

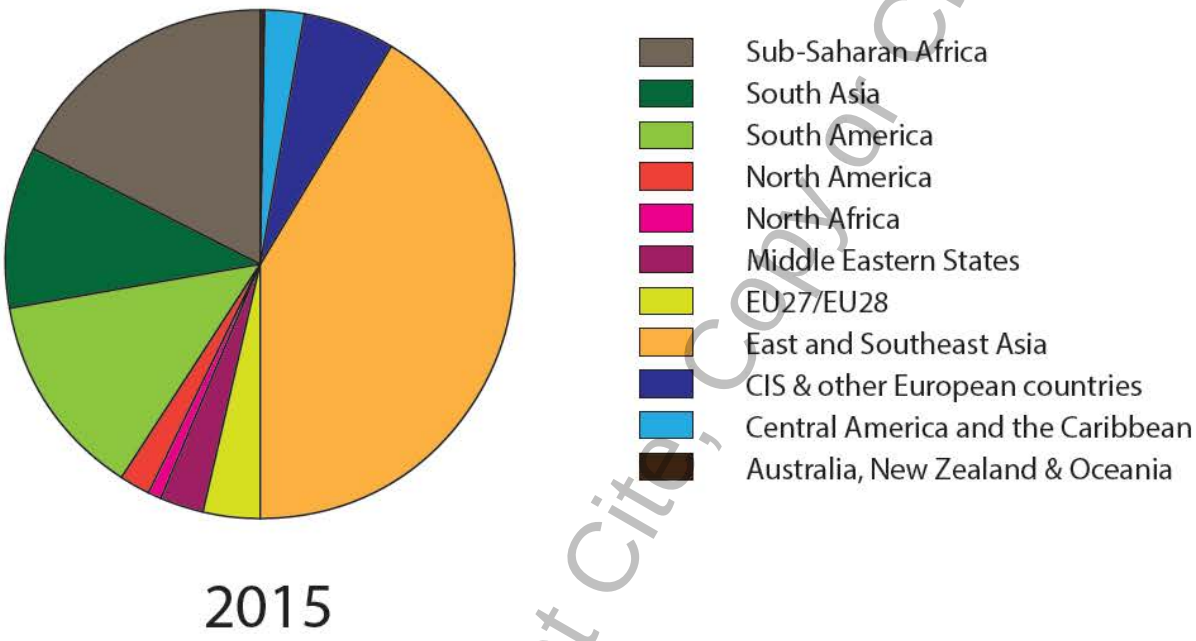

Figure R1: Regional breakdown of global emissions of mercury to air from anthropogenic sources in 2015.

Table R1: Regional breakdown of global emissions of mercury to air from anthropogenic sources in 2015 (and 2010). (Greyed out numbers should not be used for comparative purposes Regional total rounded to 3 significant figures).

(Preliminary) Estimates and Comparsions (Version 13 June 2017)

Subregion		***2015*****	***2010*** (AMAP/UNEP, 2013)
Australia, New Zealand & Oceania	2010 by-product sectors	7.53	21.46
	Mercury in products (waste) (CREM / WASOTH / WI)	1.15	0.81*

	ASGM	-	-
	Regional total	**8.68** **(6.77 - 13.5)**	**22.3**
Central America and the Caribbean	2010 by-product sectors	26.83	20.50
	Mercury in products (waste) (CREM / WASOTH / WI)	6.06	3.60*
	ASGM	23.74	23.63
	Regional total	**56.6** **(xxx - xxx)**	**47.7**
CIS & other European countries	2010 by-product sectors	95.54	95.60
	Mercury in products (waste) (CREM / WASOTH / WI)	15.18	7.15*
	ASGM	12.69	12.48
	Regional total	**123** **(105– 167)**	**115**
East and Southeast Asia	2010 by-product sectors	628.27	467.15
	Mercury in products (waste) (CREM / WASOTH / WI)	50.92	38.20*
	ASGM	210.80	271.87
	Regional total	**890** **(725 – 1470)**	**777**
EU27/EU28	2010 by-product sectors	72.02	81.20
	Mercury in products (waste) (CREM / WASOTH / WI)	7.13	7.42*
	ASGM		
	Regional total	**79.2** **(68 – 108)**	**88.6**
Middle Eastern States	2010 by-product sectors	43.65	32.46
	Mercury in products (waste) (CREM / WASOTH / WI)	9.98	4.55*
	ASGM	0.26	-

	Regional total	**53.9 (41.5 – 95.5)**	**37.0**
North Africa	2010 by-product sectors	15.28	10.99
	Mercury in products (waste) (CREM / WASOTH / WI)	5.55	2.38*
	ASGM		
	Regional total	**20.8 (13.4 – 45.7)**	**13.4**
North America	2010 by-product sectors	38.07	53.99
	Mercury in products (waste) (CREM / WASOTH / WI)	5.59	6.76*
	ASGM	-	-
	Regional total	**43.7 (36.0 – 62.7)**	**60.8**
South America	2010 by-product sectors	55.70	52.21
	Mercury in products (waste) (CREM / WASOTH / WI)	11.28	7.82*
	ASGM	211.41	184.73
	Regional total	**278 (220 – 328)**	**245**
South Asia	2010 by-product sectors	182.15	135.29
	Mercury in products (waste) (CREM / WASOTH / WI)	36.35	17.30*
	ASGM	4.50	1.13
	Regional total	**223 (187 – 293)**	**154**
Sub-Saharan Africa	2010 by-product sectors	91.82	78.60
	Mercury in products (waste) (CREM / WASOTH / WI)	17.02	4.28*
	ASGM	262.39	232.99
	Regional total	**371 (330 – 417)**	**316**

Global inventory	2010 by-product sectors	1141.26	1049.46
	New by-product sectors (BIO / VCM / SSC)	115.60	n/a
	Mercury in products (WI / WASOTH / CREM) (waste/cremation)	166.21 (162.44/3.77)	100.28* (95.51/4.78)
	ASGM	725.74	726.77
	Global inventory total (sum of national sector-based estimates)	**2149** **(1964 – 2743)**	**1876**

*In 2010 ca. 30% of mercury consumed in products was allocated as 'remaining in society'; in the 2015 and updated 2015 values this amount is incorporated in the waste-stream estimates. For valid comparison the 2010 value would be multiplied by 1.3 (i.e. WASTE category total would be ca. 124.16 rather than ca 95.51
** The indicated uncertainties are based on the propagation of errors approach; for by-product sectors, individual country-sector estimates were assigned uncertainties based on the modified GMA2013 approach (including uncertainties associated with APC technology); for ASGM and sectors concerning waste from mercury-containing products, the basic GMA2013 approach was used for country-estimates.

2.3.2 Summary of results by sector

As with the regional breakdown, the relative breakdown of anthropogenic mercury emissions in 2015 between sectors is, in most respects, very similar to that in 2010. The predominant source sector is ASGM (ca. 33.8%) followed by stationary combustion of coal (ca. 22.4%; of which 13.9%, 6% and 2.6% in, respectively, power plants, industrial uses and domestic/residential burning). These are followed by emissions from non-ferrous metal production (ca. 15.1%, of which 3.8% in large-scale gold production and 1% from production of mercury), and cement production (ca. 10.8%). Emissions associated with disposal of mercury-containing product waste (7.6%), ferrous-metal production (3.4%, of which 0.5% from secondary steel production), stationary combustion of other fuels (3%, from combustion of oil, gas and biomass – the latter a newly included component contributing 2.6%) and other (2.9%, with another newly included sector – VCM – responsible for 2.3% of this) make up the rest. See Figure S1 and Table S1.

More detailed discussions are presented in 2.3.3 and other sections – for changes from 2010-2015 see section (2.4).

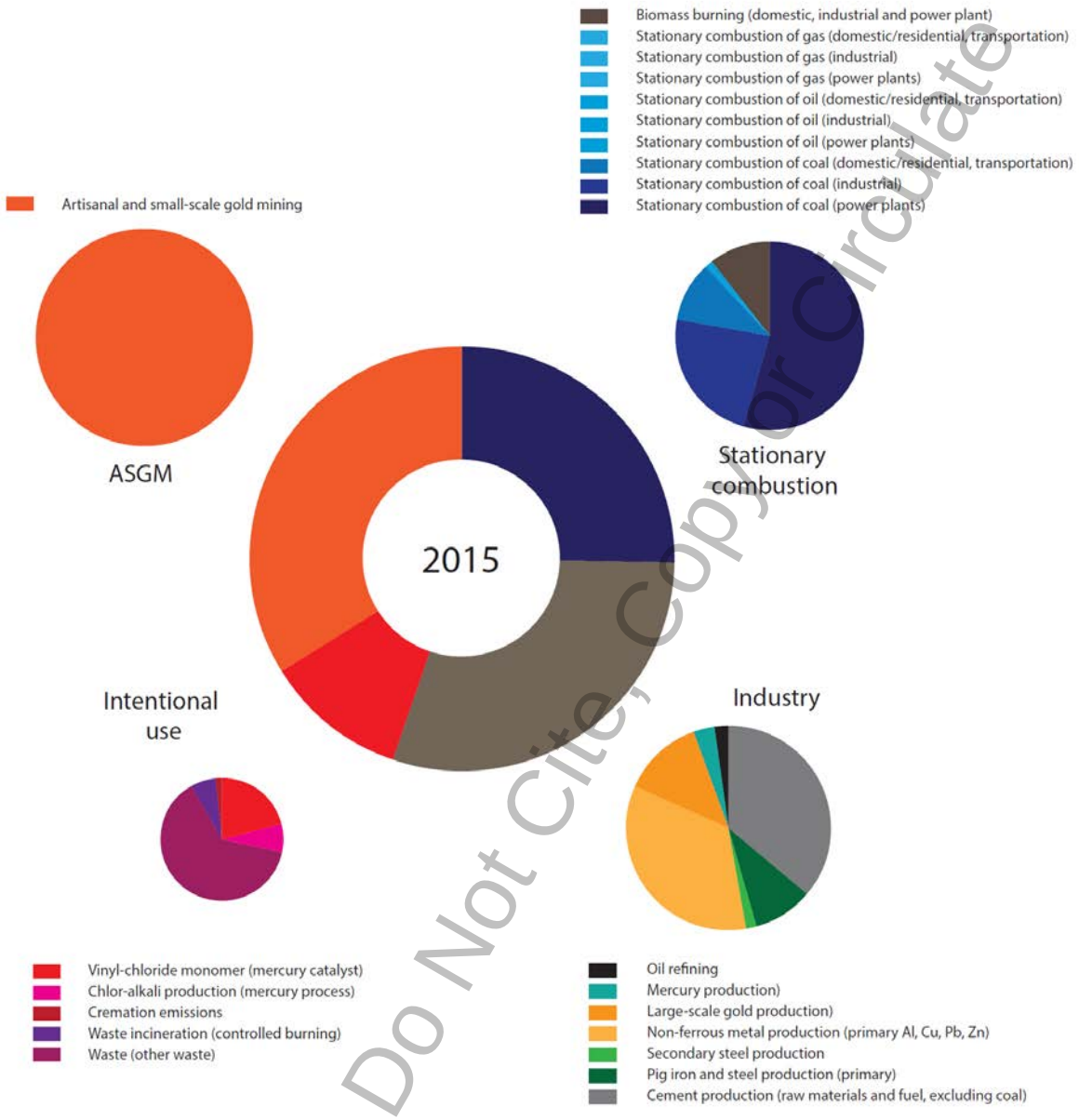

Figure S1: Proportions of global emissions of mercury to air from different anthropogenic source sectors in 2015.

2448 *Table S1: Global emissions of mercury to air from different anthropogenic source sectors in 2015 (and*

2449 *2010) [uncertainty ranges to be added when available for complete dataset]*

2450 (Preliminary) Estimates and Comparsions (Version 13 June 2017)

Sector Code	Description	Activity Code	Description	***2015*****	***2010 GMA***
ASGM	Artisanal and small-scale gold mining	ASGM	Artisanal and small-scale gold mining	725.75	726.77
BIO	Biomass burning (domestic, industrial and power plant)	PSB - DR	domestic residential burning	43.57	n.e.
		PSB - IND	industry	7.98	n.e.
		PSB - PP	power plants	5.37	n.e.
CEM	Cement production (raw materials and fuel, excluding coal)	CEM	cement (fuels excl.)	232.03	173.05
		PC- CEM	pet coke	0.99	n.e.
		See also BC–IND-CEM and HC-IND-CEM			
CREM	Cremation emissions	CREM	Cremation emissions	3.77	4.78
CSP	Chlor-alkali production (mercury process)	CSP-C	capacity based	15.78	26.46
		CSP-P	production based	1.61	1.89
NFMP	Non-ferrous metal production (primary Al, Cu, Pb, Zn)	AL-P	aluminium (primary production)	7.28	4.91
		CU-P	copper (primary production)	42.87	83.99
		CU-T	copper (total production)	4.03	9.90
		PB-P	lead (primary production)	32.70	4.40
		PB-T	lead (total production)	2.89	0.37
		ZN-P	zinc (primary production)	17.11	19.44
		ZN-T	zinc (total production)	115.69	70.32
		See also BC–IND-NFM and HC-IND-NFM			
NFMP-AU	Large-scale gold production)	GP-L	gold production	81.16	97.33
NFMP-HG	Mercury production)	HG-P	mercury production	21.60	11.75
OR	Oil refining	CO-OR	oil refining	14.02	15.99
PISP	Pig iron and steel production (primary)	PIP	iron and steel (primary production)	61.92	45.47
		See also BC–IND-PIP and HC-IND-PIP			

SC-DR-coal	Stationary combustion of coal (domestic/residential, transportation)	BC-DR	brown coal	1.99	2.71
		HC-DR	hard coal	54.00	53.25
SC-DR-gas	Stationary combustion of gas (domestic/residential, transportation)	NG-DR	natural gas	0.17	0.16
SC-DR-oil	Stationary combustion of oil (domestic/residential, transportation)	CO-DR	crude oil	0.00	0.00
		CO-HF-DR	heavy fuel oil	0.57	0.71
		CO-LF-DR	light fuel oil	2.16	1.85
SC-IND-coal	Stationary combustion of coal (industrial)	BC-IND-CEM	brown coal (cement industry)	2.59	8.10
		BC-IND-NFM	brown coal (NFM industry)	0.11	
		BC-IND-OTH	brown coal (other industry)	4.73	
		BC-IND-PIP	brown coal (ferrous metal industry)	0.14	
		HC-IND-CEM	hard coal (cement industry)	43.20	94.14
		HC-IND-NFM	hard coal (NFM industry)	3.35	
		HC-IND-OTH	hard coal (other industry)	43.11	
		HC-IND-PIP	hard coal (ferrous metal industry)	31.00	
SC-IND-gas	Stationary combustion of gas (industrial)	NG-IND	natural gas	0.13	0.10
SC-IND-oil	Stationary combustion of oil (industrial)	CO-HF-IND	heavy fuel oil	1.15	2.71
		CO-IND	crude oil	0.06	0.08
		CO-LF-IND	light fuel oil	0.21	0.24
SC-PP-coal	Stationary combustion of coal (power plants)	BC-L-PP	brown coal (lignite)	59.81	61.39
		BC-S-PP	brown coal (sub-bituminous)	41.22	27.39
		HC-A-PP	hard coal (anthracite)	2.58	2.00
		HC-B-PP	hard coal (bituminous)	194.42	225.36
SC-PP-gas	Stationary combustion of gas (power plants)	NG-PP	natural gas	0.34	0.29
SC-PP-oil	Stationary combustion of oil (power plants)	CO-HF-PP	heavy fuel oil	2.06	3.22

		CO-LF-PP	light fuel oil	0.17	0.14
		CO-PP	crude oil	0.31	0.36
SSC	Secondary steel production	SP-S	secondary steel production	10.14	n.e.
VCM	Vinyl-chloride monomer (mercury catalyst)	VCM-P	Vinyl-chloride monomer production	2.58	n.e.
		VCM-R	Vinyl-chloride monomer recycling	45.95	n.e.
WASOTH	Waste (other waste)	WASOTH	other waste	147.50	89.36*
WI	Waste incineration (controlled burning)	WI	waste incineration	14.94	6.15*
Total				**2149**	**1876**

2451

Other potential emissions (sectors quantified only as global totals)			
	contaminated sites	82 (70 – 95)	82 (70 – 95)
	misc. industrial, manufacturing activities (pulp and paper, food industry, chemical industry, lime production, etc.)	To be inserted	To be inserted
	oil and gas extraction	To be inserted	To be inserted
	industrial/sewage sludge	To be inserted	To be inserted
	Potential Global Inventory including possible additional sectors	**2230**	**1960**

2452

2453 * In 2010 ca. 30% of mercury consumed in products was allocated as 'remaining in society'; in the 2015 values
2454 this amount is incorporated in the waste-stream estimates. For valid comparison the 2010 value would be
2455 multiplied by 1.3 (i.e. WASOTH category total would be ca. 115.46 rather than ca 89.36, and the WI category
2456 total would be 15.40 rather than 6.15.

2457 ** The indicated uncertainties are based on the propagation of errors approach; for by-product sectors,
2458 individual country-sector estimates were assigned uncertainties based on the modified GMA2013 approach
2459 (including uncertainties associated with APC technology); for ASGM and sectors concerning waste from
2460 mercury-containing products, the basic GMA2013 approach was used for country-estimates.

2461 n.e. - not estimated in the 2010 GMA inventory

2462

2463 2.3.3 Sector-based observations

2464 Observations made below include comparisons between 2015 inventory estimates and updated 2010

2465 inventory estimates (see section 2.4).

1. Stationary Combustion – coal, oil and gas burning

Mercury emissions from stationary combustion of fossil fuels are estimated to account for ca. 490 tonnes of mercury emissions to air in 2015, with coal-burning responsible for by far the largest amount (482 tonnes) followed by oil (7 tonnes) and gas (1 tonne). Of these emissions, about 300 tonnes are associated with burning of fossil fuels in power plants, 130 tonnes in industrial uses and the remaining 60 in other, primarily domestic and residential uses. Coal burning is therefore the second largest contributor to global mercury emissions after ASGM.

The 2015 inventory estimate (based largely on IEA 2014 activity data) is 298 (260-355) tonnes from coal burning in power plants (an increase of 13% on a revised estimate for 2010) and 128 (107-150) tonnes in in industry (close to the estimate for 2010). Mercury emissions from coal burning in other (mainly domestic and residential uses) are also relatively stable between 2010 and 2015 at around 55 (37-70) tonnes.

Considering the increase in emissions from coal burning in power plants in more detail, these are almost entirely due to increased emissions in the East and South-east Asian and South Asia regions. Increased mercury emissions of ca. 19 tonnes in each of these regions, constitute a rise of ca. 21% in East and South-east Asia and 42% in South Asia. Decreasing mercury emissions from coal burning in power plants were observed in Australia, New Zealand & Oceania (-15%), CIS & other European countries (-4%), the EU region (-2%) and North America (-13%).

A new feature of the 2015 inventory is the differentiation of emissions from coal burning in industry between some major component activities. Of the total emissions from coal burning in industry of 128 tonnes, ca. 46 tonnes of this was associated with the cement industry, 31 tonnes with ferrous metal production, 3.5 tonnes with non-ferrous metal production, and 48 tonnes with other industrial uses. These emissions are accounted in the 2015 inventory under coal combustion but may also be taken into account as additional emissions when considering the cement, ferrous and non-ferrous metal sectors (see below).

2. Stationary Combustion – biomass burning

Biomass burning constitutes a new sector introduced in the 2015 inventory. Estimated emissions are based on IEA activity data and concern only biomass burning of primary solid biofuels for energy production (in power, industrial, and domestic/residential situation). Thus, they do not include biomass burning from, for example, agricultural burning or land clearance practises that take place in many countries.

2497 The estimated mercury emissions from primary solid biofuel burning in 2015 are 57 tonnes (47-
2498 70 tonnes; ca. 2.5% of the global inventory). A comparable value of ca. 51 tonnes was calculated
2499 retrospectively for 2010.

2500 The main emissions from biomass burning are associated with East and South-east Asia, South
2501 Asia and Sub-Saharan Africa (ca. 29%, 22% and 25% of the biomass emissions total, respectively).

2502 **3. Cement production**

2503 Estimated total global mercury emissions to air from the cement sector are 233 (116-781) tonnes
2504 in 2015. However, the updated methodology allows an improved differentiation of the
2505 contribution to mercury emissions associated with fuels burned in cement-clinker production
2506 and the non-fuel raw materials. In the 2015 inventory, therefore, a part of the emissions
2507 accounted under 'industrial coal combustion' are identified with use of coal as fuel in the cement
2508 industry. If this additional 46 tonnes of emissions is accounted under cement production, the
2509 contribution of the cement sector in the global inventory rises from ca. 10.8% to ca. 13% making
2510 the cement sector the third largest contributor after ASGM and coal burning.

2511 The total mercury emissions in 2015 directly associated with the cement sector (233 tonnes) is
2512 considerably higher than the ca. 172 tonnes associated with this sector in 2010, an increase of
2513 35%. Only in the EU region do the estimated emissions from the cement sector decrease
2514 between 2010 and 2015 (by ca. 25%); in all other regions increases are observed, of between ca.
2515 6% in the Australia, New Zealand, Oceania region, up to 108% in Sub-Saharan Africa. These
2516 emission trends closely mirror the trends in cement production in the different regions, i.e. the
2517 primary activity data used in calculating emissions for the cement sector (see Figure S3).

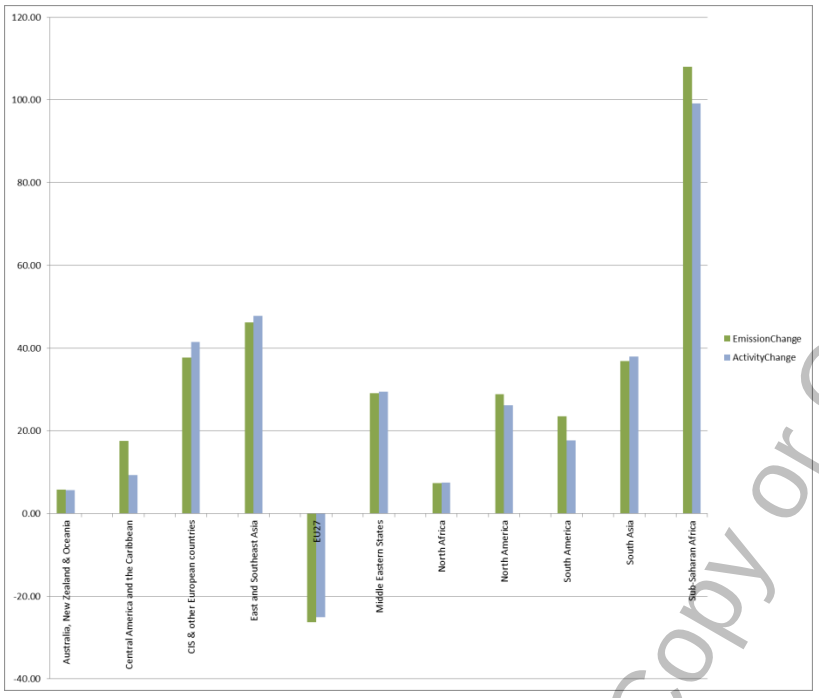

Figure S3: Relative (%) changes from 2010 to 2015 in activity data (cement production) and mercury emissions associated with cement production in different regions.

4. Ferrous metal production (pig iron and steel and secondary steel)

Mercury emissions from primary ferrous metal (pig iron and steel) production are estimated at about 62 tonnes in 2015, with a relatively large uncertainty range (20-226 tonnes) which is somewhat higher than the 45 tonnes in the 2010 inventory presented in the GMA2013 or updated 2010 estimate of 53 tonnes).

Of the increase in mercury emissions between 2010 (updated) and 2015, 7.4 tonnes of this amount is from increased emission in East and South-East Asia, 1.2 tonnes in South Asia and 0.3 tonnes in the CIS and other European region. These three regions are responsible for, respectively 71%, 6.5% and 11% of emissions from primary non-ferrous metal production. Emissions from this sector in South America (responsible for about 3% of the sector emissions) decreased by 0.4 tonnes.

In the previous work (GMA2013) secondary steel production was not included but this sector has been added in the present work.

The resulting estimated emissions from secondary steel production in 2015 are 10 (7.5-18) tonnes of mercury (ca. 0.5% of the global inventory), with a (retrospectively calculated estimate of 9.7 tonnes in 2010). These totals are higher than might be expected and the reason for this

level of emission is unclear at present; assumptions applied in the calculation of the estimated emissions are presented in Section 2.2.2(5) and Annex 6.

5. (Primary) non-ferrous metal production (Al, Cu, Pb, Zn)

Primary production of copper, lead and zinc, and aluminium, were together estimated to be responsible for some 226 tonnes of mercury emissions in 2015 i.e. an increased in comparison to the ca. 200 tonnes estimated for 2010. It should be noted that the estimates for emissions from this sector have relatively large associated uncertainties (range 153-326 tonnes in 2015).

For aluminium, increased emissions in percentage terms are highest in the EU region, but in absolute terms the Asian regions and Central America are responsible for 2.7 tonnes of increased emissions, partly offset by decreased emissions in other regions, resulting in an overall increase in global emissions from this sector of 2.6 tonnes (from to 4.6 to 7.3 tonnes).

Primary production of copper, lead and zinc make a significantly greater contribution to global mercury emissions, 215 tonnes in 2015 (from 194 tonnes in 2010). Here again, increased emissions in the East and South-east Asian and South Asia regions (29 and 2 tonnes, respectively) offset decreases in emissions in most other regions.

Secondary production of non-ferrous metals is not yet addressed as a separate activity in the global emissions inventory activity (see section xxxx).

6. (Primary) non-ferrous metal production (Hg)

Estimated mercury emissions to air associated with production of mercury increased considerably between 2010 (11.7 tonnes) and 2015 (21.6 tonnes). With small decreases in estimated emissions from mercury production in the CIS and other European countries region and North Africa, the increased emissions are mainly from a doubling of the estimates for emissions in East and South-east Asia (from 9.5 to 18.9 tonnes from mercury production in China) and new emissions in the Central American region (2 tonnes of emissions resulting from 300 tonnes of mercury production in Mexico), with a small contribution from South America (0.2 tonnes emissions in Argentina)

7. (Primary) non-ferrous metal production (large scale-gold production)

Mercury emissions from large-scale gold production in 2015 are estimated at ca. 81 (69-94) tonnes which is lower than the 2010 estimates of 97 tonnes. Some of this reduction can be explained by revisions in both activity data and emission factors to better reflect the current situation in e.g. East and South-east Asia and Sub-Saharan Africa. In other regions, in particular

Australia, New Zealand and Oceania (where Australian emissions predominate) and North America, slightly decreased emissions (10.7 and 0.9 tonnes, respectively) are also partly caused by revisions to technology profiles that imply higher abatement levels associated with technology improvements introduced in the period between 2010 and 2015.

Again, the large uncertainties associated with these emission estimates need to be borne-in-mind.

8. Oil refining

Mercury is a trace contaminant present in varying concentrations in produced oil and gas. Mercury emissions associated with oil and gas production arise during different phases of operations. Emissions associated with the production (well-head) activities (including emissions from flaring) are currently not quantified in the global emission inventory due to lack of relevant information. Mercury is removed from oil and gas prior to its transport, in particular by pipelines, to avoid corrosion and damage to distribution systems. A significant part of the removal is done in connection with oil refining operations. Following the 2010 inventory, IPIECA released a commentary on the GMA results [IPIECA Fact Sheet to INC5], concluding that the GMA estimates for emissions to air were significantly over-estimated; they reported estimates of emissions to air of ca. 1.35 tonne as opposed to the ca. 13 tonnes. Total inputs (i.e. amounts of oil refined multiplied by mercury content of the oil) associated with the refinery sector do not differ greatly between the approaches employed in the GMA and the IPECA calculations. The main differences between the GMA and IPIECA estimates for emissions to air (and releases to water) appear to be associated with the assumptions regarding the fate of mercury at refineries. In the IPIECA approach, for example, 5% emissions to air are assumed, based on studies at US refineries [WSPA, 2009 REF in IPIECA note] (with the major part of the mercury – 87% - associated with solid waste). The GMA (and UNEP Toolkit) methodology assumes higher emissions to air (ca. 25%) based on other industry reported studies [e.g. IKIMP, 2012 and references cited therein], with less of the mercury input being distributed to other media. No new information was identified that allowed this discrepancy regarding fate of mercury from oil refineries to be resolved.

9. Chlor-alkali production

Emissions from intentional use of mercury in the chlor-alkali industry have been decreasing for some time in most parts of the world. In part this is due to increased attention to best practices to reduce emissions, but primarily it is due to the shift from production based on the mercury-process to membrane production technology.

Emission estimates for this sector decreased from ca. 25 tonnes in 2010 to around 17.4 tonnes in 2015.

It should be noted that for many parts of the world, updated activity data relevant to the 2015 inventory period are lacking; consequently emission trends can only be described reliably in relation to the EU, North America and South Asia regions, where emissions decreased by ca. 2.8 tonnes (40%), 0.9 tonnes (83%) and 1.9 tonnes (74%) between 2010 and 2015, respectively. In the case of South Asia, the reductions are largely associated with reported phase-out of mercury-process chlor-alkali production in India.

Although a relatively small component in the total global inventory, the continuing decrease in global mercury emissions from the chlor-alkali sector between 2010 and 2015 is a positive development that is not considered to be related to changes in inventory methodology.

10. Waste and waste incineration

Mercury emissions to air from disposal of waste from mercury-containing products are estimated at 162 tonnes in 2015; 147 (120-225 tonnes) from uncontrolled burning and landfill, and 15 (9-32) tonnes from controlled incineration.

The 2015 estimated emissions from these sectors are considerably higher in comparison to the 2010 estimate of 96 tonnes. This is to a large extent due to a change in methodology where previously ca. 30% of mercury in mercury-containing products was assumed to be 'retained in society'. In the 2015 updated methodology, this amount is now accounted as part of the waste-stream. If the 2010 GMA estimates are updated with this new methodology only, the emissions for 2010 would be 131 tonnes.

Based on updated 2010 estimates, emissions from waste sectors declined in the EU and North America regions (by 33% and 45%, respectively; equivalent to 3-4 tonnes of mercury emitted in these regions). In all other regions, waste-associated mercury emissions increased by more than 10 tonnes in South Asia and Sub-Saharan Africa, and around 3-5 tonnes in the Middle East, CIS and other European countries and East and South-east Asia. Increases in Australia, New Zealand and Oceania and South America regions were minor.

Emissions from the waste sector have large associated uncertainties; quoted ranges only reflect uncertainties attributed to activity data (i.e. estimates of regional consumption of mercury in mercury-containing products).

In general, the estimates addressed in the global inventory do not include industrial wastes and only partially include waste that may be classified as hazardous or medical waste, some of which may also be incorporated in fuels used in, e.g. the cement industry.

Emissions associated with waste from mercury-containing products is also an area where large discrepancies have been identified between estimates made in the GMA inventory and those included in some national inventories as part of (preliminary) Minamata Initial Assessments (see section 2.3.4).

11. Crematoria emissions

Human cremation represents a relatively small but important source of emissions associated with intentional use of mercury – specifically mercury use in dental amalgam fillings. Estimated global mercury emissions to air from cremations are highly uncertain, but evaluated to be less than 5 tonnes per year (in 2015 and 2010) (ca. 0.25% of the global inventory). The proportion of regional emissions associated with cremation is slightly greater (around 1%) in the Australia, New Zealand and Oceania region and the EU and North America, likely reflecting comprehensive access to dental care that – in past decades at least – included widespread use of mercury amalgam fillings. Cultural and religious practises associated with burial and cremation also play a role in determining whether cremation emissions are a significant part of the national air emission profile.

Cremation emissions are only part of the emissions associated with use of mercury in dental applications. The 2015 global inventory does not yet quantify emissions that can occur during preparation and routine disposal of mercury fillings. Other work has estimated emissions to air from these activities at XXX [REF]; they are also expected to contribute to mercury releases in waste waters.

12. Artisanal and small-scale gold production

Intentional use of mercury in ASGM is the predominant source of mercury emissions to air at the global level in the 2015 inventory, as was also the case in 2010. There remain, however, large uncertainties associated with emission from ASGM.

ASGM activities take place in 7 of the 11 sub-regions considered in the current work. Of the estimated total global emissions from ASGM, of ca. 725 tonnes in 2015, ca. 36% of this amount (262 tonnes) is from Sub-Saharan Africa, and 29% (ca. 210 tonnes) from each of South America and East and South-east Asia. Mercury emissions from ASGM activities in Central America and

the Caribbean, the CIS region and South Asia are considerably lower (4.5 – 24 tonnes in 2015) with a very minor contribution also from Middle Eastern States.

ASGM-associated emissions are thus the predominant source of mercury emissions in some regions, accounting for about 70-75% of the emissions that occur in South America and Sub-Saharan Africa, about 40% of emissions in Central America and the Caribbean and about 25% of the emissions occurring in East and South-east Asia.

The estimated emissions from ASGM in 2015 (725 tonnes) are very close to the value reported for 2010 in the GMA2013. However, this masks some important differences. Firstly, a recalculation of the 2010 emissions using the improved information base on ASGM-related activities, and revised emission factor assumptions results in a reduction in the emissions estimate for 2010 to ca. 680 tonnes. This implies that, rather than remaining constant, ASGM emissions increased by ca. 7% between 2010 and 2015. Furthermore, there are differing trends in emissions between 2010 and 2015 in different regions. The most significant increases are for South America (mercury emissions increasing from ca. 165 in 2010 to 210 tonnes in 2015) and Sub-Saharan Africa (from ca. 230 to 260 tonnes); conversely, ASGM emissions from East and South-east Asia declined from an estimated 245 tonnes in 2010 to 210 tonnes in 2015. In the latter region, estimates of ASGM emissions in China sharply declined (attributable to banning of mercury use in ASGM) but this was largely offset by increasing emissions in other countries, Indonesia in particular.

2.3.4 Comparing GMA global inventory estimates with national inventories

The target for the GMA 2018 air emissions inventory activity remains the production of a robust global inventory for the target year of 2015, for a defined set of sectors for which reliable global estimates can be produced. Although it presents emission estimates broken down by sector for each of some 200 countries, the applied methodology is directed at global/regional rather than national level application.

All methods and approaches associated with generation of emissions estimates (whether produced by measurements or theoretical calculations) have (often large) associated uncertainties. It should therefore not be expected that estimates produced using different approaches (global vs national, etc.) will necessarily be identical. Estimates may differ for several reasons including:

- use of activity data corresponding to different years or different sources
- differences in reporting/sector attribution
- differences in applied EFs
- assumptions applied in deriving annual emissions estimates from measurements

Differences between national/sector estimates that comprise the global inventory estimates presented in this report and national emission estimates from other sources provide an important part of estimate verification. Differences can often be explained, and even where this is not the case can reveal limitations in methodology or data that guide further attention and future work.

A major new development since the GMA2013 work is that a large number of countries are engaged in preparing new national inventories or national emission/release estimates, many of these associated with the Minamata Initial Assessments (MIAs) or Minamata National Action Plans (NAPs). This allows increased possibilities for comparing the global and nationally derived emissions estimates.

In relation to estimates compiled as part of the MIA process, most of the MIAs use an approach based on the UNEP Toolkit. The Toolkit was updated in 2013 to reflect new information compiled in developing the 2010 global inventory. In general, new refinements introduced in the work to produce the 2015 global inventory will not yet be reflected in the UNEP Toolkit.

Comparisons between GMA 2018 inventory estimates for the nominal year 2015 and national estimates will be compiled in Annex 7 [not yet available].

Information compiled as part of the GMA 2018 work, including information exchanged at international meetings (organized under the project inventory component) has identified the over 70 national inventories that may be suitable for comparison with the 2015 inventory estimates. These include:

i. Inventories prepared under the auspices of the UN ECE Convention on Long-range Transboundary Air Pollution (CLRTAP) reporting for 2015: 38 countries covering primarily the EU and CIS and Other European countries regions, but also Canada. An initial evaluation, based on total national mercury emission estimates for these countries indicated that GMA inventory estimates are generally somewhat higher than LRTAP reported emissions. For 5 countries (Bulgaria, Kazakhstan, Kyrgyzstan, Macedonia and Serbia) differences between GMA estimates and CLRTAP reported emissions are substantial and need further investigation. Excluding these countries, total estimated emissions to air are 66 tonnes in CLRTAP reporting compared with 81 tonnes in the GMA inventory.

   For most (ca. 2/3) of national CLRTAP inventories, the reported total emissions are lower than the GMA estimates, with GMA inventory estimates for individual countries on average ca. 60% greater than emissions reported to CLRTAP. It is not unlikely that there are gaps in CLRTAP national mercury inventories as in recent years efforts to improve CLRTAP reporting have largely been directed at greenhouse gas emissions, while mercury and some other air

pollutants (e.g. other heavy metals and Persistent organic pollutants, POPs) have received low priority.

ii. Inventories currently being compiled as part of MIAS for about 30 countries from the Sub-Saharan Africa, East and South-east Asia, South Asia, South America and Central America and the Caribbean regions. At the time of preparation of this draft, the majority of MIA inventories are preliminary, and not all were made available for preliminary consideration under the GMA activity. Therefore direct comparisons have not been completed but some provisional conclusions can be drawn based on results from some countries, and discussions with MIA national and regional coordinators.

Comparisons between GMA inventory results and results presented in (preliminary) MIA inventories gave rise to the following general observations:

- With few exceptions, MIAs are being prepared using the UNEP Toolkit which is available in two versions: Level 1 and Level 2. The Toolkit Level 1 approach is designed to be employed for producing first rough estimates of mercury emissions and releases. The Toolkit's Level 2 is designed to represent national circumstances at a more detailed level, supported by available national data. There can be very substantial differences between emissions/release estimates for individual countries produced using the UNEP Toolkit Level 1 and Toolkit Level 2. For this reason, comparisons made between GMA inventory and MIA results focus on MIAs produced using Toolkit Level 2.
- In general, estimates of national emission totals agree fairly well, but there can be significant differences on the sector level. These differences may be due to methodological differences in the approach for MIAs and GMA respectively, or use of different years of (activity) data, but can also be due to errors in national data collection for the MIAs, or regarding the GMA estimates, application of default emission factors and technology profiles not representative for that specific country.
- The GMA inventory is based on activity data for a particular year – nominally 2015 (but typically 2014). Most MIAs appear to be based on 'most recent available data' and often the exact year of activity data concerned is not defined. Activity data is a major factor determining estimated emissions using the GMA and Toolkit approaches, and consequently lack of consistency in this respect is a possible explanation for substantial differences between GMA and MIA inventory estimates.
- Other reasons identified on the basis of preliminary comparisons that may explain differences between the GMA estimates and the MIAs are:

  - MIA estimates associated with oil and gas extraction – a component currently not included in the GMA inventory.
  - MIA estimates associated with waste categories such as industrial waste and waste waters, currently not included in the GMA inventory
  - Estimates of emissions from large scale gold mining, where the default factor in the Toolkit is 3 times higher than that applied in the GMA inventory methodology; data necessary to improve quantification of emissions from this sector are largely lacking.

- For Cu production, the GMA approach may over-estimate the degree of application and effectiveness of abatement, at least for some African countries.
- For cement production there are differences in assumptions applied in calculating emission estimates.
- Some differences in ASGM/large-scale gold sector emissions estimates exist. The Toolkit default factors and methodology were revised in 2017; however many MIAs are still using earlier Toolkit versions.
- Caution should be applied to avoid double counting in totals for inputs to waste and releases to some pathways from products in MIA results, as prescribed in the Toolkit
- A major source of differences between GMA inventory estimates and preliminary MIA estimates can be traced to differences in estimates associated with use and disposal of waste (in particular waste burning) from mercury-added products. The methodology applied in the GMA work and the Toolkit approaches are very different. GMA emissions from waste are based on estimates of the amount of mercury in mercury-added products that are consumed in the country, while MIAs (using the UNEP Toolkit approach) calculate emissions using generic numbers for mercury-content of burned waste.
- Discrepancies exist between estimates of amounts of mercury reported in MIAs for mercury-containing products and regional consumption estimates presented in the UNEP Trade and Supply report (used as the basis for GMA estimates). In some MIAs, problems have been identified with data collection, especially for mercury-added products, including differentiation of, for example, consumption of mercury-containing lamps and batteries and mercury-free lamps and batteries. Generally, countries have substantial data gaps for products. These problems may be exacerbated by insufficiently detailed customs statistics and lack of resources to contact producers and importers for supplementary information. Consequently, there are indications that the default factors for Hg content in general waste burnt (applied in many of the MIAs) may be too high.

iii. National inventories provided by [Australia], Canada, Japan, Republic of Korea, Russia and United States.

Detailed comparisons between GMA estimates and national inventories provided by these countries are presented in Annex 7 [not yet complete]. Tables AC1-5; Table C1 below presents some example (preliminary) comparisons with GMA estimates for main sectors.

From this table it is apparent that estimates match to differing degrees for different sectors, and that this also varies between countries. However, in these example comparisons, the degree of consistency between national inventory estimates and the GMA estimates for this group of countries is generally good, and (with some exceptions) well within the bounds of associated uncertainties. Part of the difference can be explained by differences in the way emissions are assigned between sectors. This is particularly the case for some of the stationary combustion sectors and differentiation of power, industrial and

domestic/residential burning sources, and whether or not fuels are included under stationary combustion or individual industrial sectors. One identified potential inconsistency is that activity data from IEA (used in GMA 2018) do not always match with nationally reported activity data, e.g. for fuel consumption reported by Canada, where differences have been attributed to data set timing (monthly and annual, provisional and revised) and possible use of different factors for conversions from physical fuel units to energy units.

Some national inventories include additional emissions that are not yet quantified in the GMA inventory. Such 'other' sources include emissions from activities such as other chemical manufacturing processes; other mineral products (e.g., lime manufacturing), secondary non-ferrous metal production, oil and gas extraction, pulp and paper industry, and food industry, etc.). These emission sources are currently difficult to quantify at the global scale – largely due to lack of comprehensive activity data as well as lack of emission factors for highly variable process technologies. However, for the few (generally developed) countries reporting emissions from 'other' sources the contribution is approximately 5-20% of the national inventory totals, which extrapolated globally (on non-ASGM emissions totals) could represent additional emissions of the order of 100-200 tonnes.

2824 Table C1. [Example] Comparison between national inventory results and GMA 2015 (provisional) estimates

Sector	Australia		Canada*		Japan		Republic of Korea		Russia		USA			
	national	GMA 2015	national	GMA 2015	national	GMA 2015	national	GMA 2015	national	GMA 2015	national	GMA 2015	national	GMA 2015
Stationary combustion in power plants														
- coal			846	1748	1300	1264		1471			20750	22013		
- oil			0	11	13	155		30			39	40		
- gas			0	10	2	19		5			822	61		
Stationary combustion in industry														
- coal			251	129	240	341		214			986	2507		
- oil			60	19	2	71		25			4525	43		
- gas			0	4	1	3		2			1375	28		
Stationary combustion (domestic/ residential/other)														
- coal			0	5	0	0		0			1	205		
- oil			0	72	0	103		44			1772	363		
- gas			0	7	0	4		3			52	51		
Biomass burning			0	539	0	358		92			528	2441		
Cement			273	128	5500	3475		1258			2875	3131		
Ferrous metal production														
- primary pig iron and steel			617	200	2000	2219		687			1537	513		
- secondary steel			0	117	540	599		340			4140	1288		
Non-ferrous metal production														
- primary copper/lead/zinc			0	42	260	1623		295			573	108		
- primary aluminium			20	35	0	0		0			0	126		
- large-scale gold			0	339	0	16		0			521	485		
- mercury production			354	0	0	0		0			0	0		
Chlor-alkali industry			9	0	0	0		0			82	183		
VCM			0	0	0	0		0			0	0		
Oil refining			0	69	120	1135		968			240	1012		
ASGM			0	0	0	0					0	0		
Waste														
- controlled incineration			670	118	1500	1132		580			1812	1252		

- other (landfill, etc.)			304	309	3850	2246		683			2995	3296		
Cremation			247	89	69	101		41			1128	523		
Other			924	0	1351	0					3271			
Total			4574	3990	16747	14864		6739			50024	39668		

*Canada also reports emissions (totalling 4387 kg) under the CLRTAP reporting system.

2.4 Comparing 2010 and 2015 global inventory estimates

2.4.1 Cautionary Notes

Inventory methodologies are constantly improved as new information and data becomes available. With each new round of inventory development, methods are improved, both with respect to understanding of important factors/parameters and availability, and quality of essential data. This has implications for consistency over time. Changes in emissions estimates for different periods reflect both real-world trends and artefacts of improvements in inventory methods and data availability. Over-simplistic comparisons between the new inventory and previous inventories can result in misinterpretation and should therefore be avoided.

The increased focus on mercury emissions resulting from the adoption of the Minamata Convention, has also led to new research activities, national efforts and industrial focus related to mercury emissions. These efforts all contribute to providing more accurate and complete information on mercury emissions but unavoidably also introduce changes to both current and previous emission inventories.

It is inevitable that comparisons will be made between results presented in the GMA2013 (AMAP/UNEP, 2013) and the results in this update GMA – including comparing individual country-sector based estimates in the 2010 and 2015 inventories. If the implications of methodological refinements, addition of new sectors, improved quality of base information, etc. are not properly appreciated, such comparisons can result in inappropriate and misleading conclusions. It is strongly recommended that any such comparisons therefore refer to the information presented in this report only.

2.4.2 Observations on Changes from 2010 to 2015

As a first step in trying to address some of these issues and gain a reliable insight into whether apparent changes in emissions patterns between 2010 and 2015 represent real changes in emissions or are just artefacts of improved information and methodologies, an updated 2010 inventory was prepared in addition to the 2015 inventory. This updated 2010 inventory incorporated various 'improvements' including new (relevant) information on emission factors and application of APC technology, as well as updated activity data[1]. It also included a retrospective calculation of 2010 emissions for some sectors newly introduced in the 2015 inventory.

[1] In the 2010 inventory presented in the GMA 2013 much of the activity data used were preliminary, corresponding to the period for which latest-data were available (typically 2008 or 2009). The updated 2010 inventory values

Figure T1 compares the pattern of regional emissions in 2010 (GMA2013) with the updated-2010 inventory and the 2015 inventory. The updated estimate of total emissions to air for 2010 is very similar (at the global level) to the original global estimate for 2010 published in the GMA 2013 (AMAP/UNEP, 2013). This consistency is also apparent when considering aggregated emissions for (most) regions and sector groupings. The fact that changes in methods introduced for estimating emissions from specific sectors or country groups, the use of more representative 2010 activity data, and other 'artefacts' (including the introduction of at least one sector in 2015 not represented in the updated 2010 inventory) do not appear to have unduly influenced global or regional inventory results is considered a validation of the general approach employed for deriving global inventory estimates. At the same time, however, it should be noted that values for individual country-sector estimates have in some cases changed significantly.

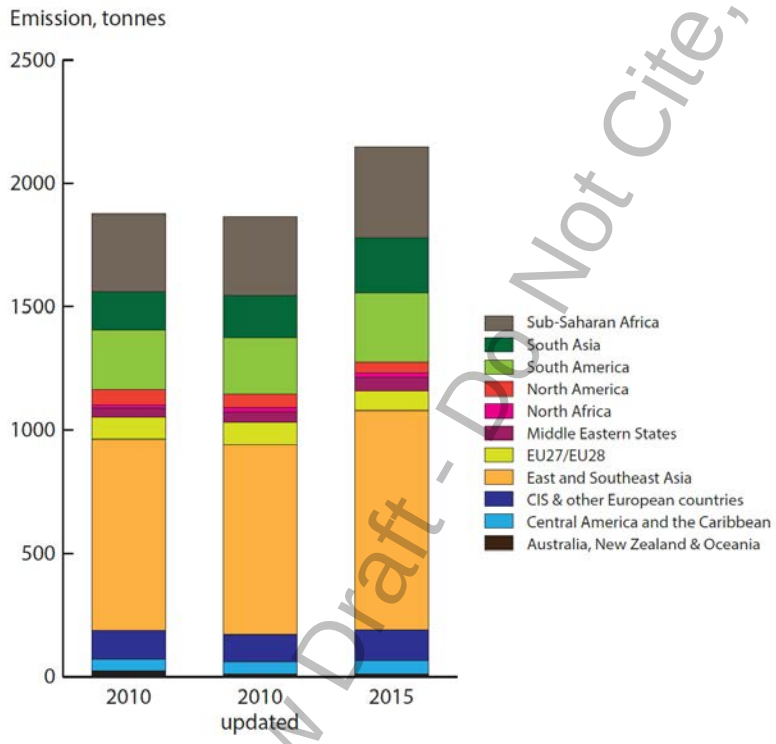

Figure T1: Regional breakdown of global emissions of mercury to air from anthropogenic sources in 2015 in relation to 2010.

presented in this report include a number that have been revised for 'final' 2010 activity data. The 2015 inventory presented in this report is largely based on latest available activity data (in most cases 2014).

Where relevant, the discussions in section 2.3.3 attempt to address the issue of whether apparent trends (between 2010 and 2015 estimates) reflect genuine changes in emissions over time or are artefacts related to improved information, etc. On the basis of this evaluation of apparent changes, the following observations are made:

Global emissions of mercury to the atmosphere in 2015 are approximately 12% higher than they were in 2010. Continuing action to reduce emissions has resulted in modest decreases in emissions in some regions (North America and EU) but increasing emissions in most other regions. Increased economic activity, as reflected in 'activity data' on consumption of fuels and raw materials and production of products is a major factor in driving up emissions associated with energy and industrial sectors in a number of regions. In this respect, differences between 2010 and 2015 may also reflect recovery following the economic down-turn that may have influenced global emissions in 2010. These factors appear to have more than offset any (technological) efforts to reduce mercury emissions.

Mercury emissions to air have decreased between 2010 and 2015 in three of the eleven world regions, namely in North America, in EU and in Australia, New Zealand & Oceania. In the case of North America in particular, shifts in fuel use (from coal to oil/gas) in the energy sector, combined with introduction of highly efficient APCD at major point sources appears to be a major factor in the changes observed. In both Canada and Australia closure or major changes in applied technology (including APC technology) at a few significant point sources associated with non-ferrous metal and large-scale gold production have resulted in decreasing national emissions.

In all other regions,, however, the estimated emissions to air increased.

Higher emissions in 2015 than in 2010 were estimated for a number of the large source sectors: cement production, coal combustion in power plants, non-ferrous metal production (primary Al, Cu, Pb, Zn), for mercury production, primary iron- and steel production, and for emissions from waste (mercury added products). For chlor-alkali production and for large scale gold production the estimated emissions decreased between 2010 and 2015. Other source sectors were comparatively smaller and/or estimated emissions were rather similar to 2010 (see table S1).

Table T1, below, presents an overview of the scale of changes in emissions in different areas for the main sectors addressed in the 2015 global emissions inventory. [Table to be developed]

2.5 Conclusions (emissions to air)

To be prepared following peer review – see also box with Key Findings/Messages at start of this chapter)

2.6 References

AMAP/UNEP, 2013. Technical Background Report for the Global Mercury Assessment 2013. Arctic Monitoring and Assessment Programme, Oslo, Norway/UNEP Chemicals Branch, Geneva, Switzerland. vi + 263 pp

BAT/BEP, 2017 – Guidance on best available techniques and best environmental practices (BAT/BEP) developed under the Minamata Convention, draft; status of February 2017 [cement, NFM, iron and steel methodology]

Boliden 2015 – Environmental report 2015 of the Boliden facility in Skelleftehamn, Sweden [cement, NFM, iron and steel methodology]

BREF CEM 2013 – Remus, R., Aguado Monsonet, M., Roudier, S., Delgado Sancho, L., 2013, Best Available Techniques (BAT) Reference Document for Iron and Steel Production [cement, NFM, iron and steel methodology]

BREF IS 2013 – Schorcht, F., Kourti, I., Scalet, B.M., Roudier, S., Delgado Sancho, L., 2013, Best Available Techniques (BAT) Reference Document for the Production of Cement, Lime and Magnesium Oxide [cement, NFM, iron and steel methodology]

BREF NFM 2014 – Joint Research Centre, 2014, Best Available Techniques (BAT) Reference Document for the Non-Ferrous Metal Industries, Final Draft (October 2014) [cement, NFM, iron and steel methodology]

Cementa 2015 – Environmental reports 2015 of the Cementa facilities in Slite, Dagerhamn, and Skövde, Sweden [cement, NFM, iron and steel methodology]

Chakraborty, 2013 – Chakraborty, L., Qureshi, A., Vadenbo, C. Hellweg, S., 2013, Anthropogenic Mercury Flows in India and Impacts of Emission Controls, Environmental Science and Technology, 47 (2013), 8105-8113 dx.doi.org/10.1021/es401006k [cement, NFM, iron and steel methodology] [VCM methodology]

CSGB, 2017. Cremation Society of Great Britain – Cremation Statistics (2014). http://www.srgw.info/CremSoc4/Stats/

EMEP/EEA 2016 – EMEP/EEA air pollutant emission inventory guidebook – 2016 [cement, NFM, iron and steel methodology]

Frey, C., Penman, J., Hanle, L., Monni, S., & Ogle, S. (2006). Chapter 3 Uncertainties: 2006 IPCC Guidelines for National Greenhouse Gas Inventories. Geneva: IPCC. [2.2.3]

Friedli, H.R., A.F. Arellano, S. Cinnirella and N. Pirrone (2009). Initial Estimates of Mercury Emissions to the Atmosphere from Global Biomass Burning. Environ. Sci. Technol., 2009, 43 (10), pp 3507–3513. DOI: 10.1021/es802703g [biomass methodology]

GNR, 2014. GNR database 2014 – WBCSD Sustainability Initiative, Getting the Numbers Right Project, Emissions Report 2014 http://www.wbcsdcement.org/index.php/key-issues/climate-protection/gnr-database [cement, NFM, iron and steel methodology]

Huang, X., Li, M., Friedli, H., Song, Y., Chang, D., & Zhu, L. (2011). Mercury Emissions from Biomass Burning in China. Environmental Science & Technology, 9442-9448. [biomass methodology]

Hui 2016 – Hui, M., Wu, Q., Wang, S., Liang, S., Zhang, L., Wang, F., Lenzen, M., Wang, Y., Xu, L., Lin, Z., Yang, H., Lin, Y., Larssen, T., Xu, M., Hao, J., 2016, Mercury flows in China and Global Drivers, Environmental Science and Technology, November 2016 [cement, NFM, iron and steel methodology]

Hylander, L., & Herbert, R. (2008). Global Emission and Production of Mercury during the Pyrometallurgical Extraction of Nonferrous Sulfide Ores. Environ. Sci. Technol. 42,, 5971–5977. [2.2.3]

IEA, 2005. International Energy Agency (2005). Energy Statistics Manual, OECD/IEA, 2005 [biomass methodology]

IEA, 2016. Database [biomass methodology]

IPIECA, 2012. Industry input to the UN global mercury treaty negotiations focus on oil and gas. By: Doll, B.E., B.M. Knickerbocker and E. Nucci. The global oil and gas industry association for environmental and social issues (IPIECA).

Kindbom, K., Munthe, J. (1998) Hur påverkas kvicksilver i miljön av olika energialternativ? - En förstudie fokuserad på biobränslen. IVL B 1299 [biomass methodology]

Kribek 2010 – Kribek, B., Majer, V., Veselovsky, F., Nyambe. I., 2010, Discrimination of lithogenic and anthropogenic sources of metals and sulphur in soils of the central-northern part of the Zambian Copperbelt Mining District: A topsoil vs. subsurface soil concept, Journal of Geochemical Exploration 104 (2010), 69-86 [cement, NFM, iron and steel methodology]

Kumari 2011 – Kumari, R., 2011, Preliminary mercury emission estimates from non-ferrous metal smelting in India, Atmospheric Pollution Research 2 (2011), 513-519 – OBS not the same Kumari 2011 as in GMA-2013 – another article!! [cement, NFM, iron and steel methodology]

Lin, Y., Wang, S., Wu, Q. and T. Larssen (2016). Material Flow for the Intentional Use of Mercury in China. Environ. Sci. Technol., 2016, 50 (5), pp 2337–2344. DOI: 10.1021/acs.est.5b04998 [VCM methodology]

LKAB 2015 – Environmental reports 2015 of the LKAB facilities in Malmberget and Kiruna, Sweden [cement, NFM, iron and steel methodology]

Maxson, P. (2016 / 2017) [VCM methodology] [Annex Tables from DRAFT - Summary of supply, trade and demand information on mercury, (UN-Environment – need final version as draft not for citation)]

Mlakar 2010 – Mlakar, T., Horvat, M., Vuk, T., Stergarsek, A., Kotnik, J., Tratnik, J., Fajon. V., 2010, Mercury species, mass flows and processes in a cement plant, Fuel 89 (2010), 1936-1945 [cement, NFM, iron and steel methodology]

Muntean 2014 – Muntean, M., Janssens-Maenhout, G., Song, S., Selin, N., Olivier, J., Guizzardi, D., Maas, R., Dentener, F., 2014, Trend analysis from 1970 to 2008 and model evaluation of EDGARv4 global gridded anthropogenic mercury emissions, Science of the Total Environment 494-495 (2014), 337-350 [cement, NFM, iron and steel methodology]

Obrist, D., D.W. Johnson, S. E. Lindberg, Y. Luo O. Hararuk, R. Bracho, J. J. Battles, D. B. Dail, R. L. Edmonds, R. K. Monson, S. V. Ollinger S. G. Pallardy, K. S. Pregitzer, and D. E. Todd. (2011). Mercury Distribution Across 14 U.S. Forests. Part I: Spatial Patterns of Concentrations in Biomass, Litter, and Soils. Environ. Sci. Technol. 2011, 45, 3974–3981. dx.doi.org/10.1021/es104384m [biomass methodology]

Pirrone, N., S. Cinnirella, X. Feng, R. B. Finkelman, H. R. Friedli, J. Leaner, R. Mason, A. B. Mukherjee, G. B. Stracher, D. G. Streets, and K. Telmer. Global mercury emissions to the atmosphere from anthropogenic and natural sources. Atmos. Chem. Phys., 10, 5951–5964, 2010. doi:10.5194/acp-10-5951-2010 [biomass methodology]

SSAB, 2015 – Environmental reports 2015 of the SSAB facilities in Luleå and Oxelösund, Sweden [cement, NFM, iron and steel methodology]

UNEP, 2011 – Toolkit for Identification and Quantification of Mercury Releases, Reference, Revised Inventory Level 2 Report Including Description of Mercury Source Characteristics, Version 1.1, 2011 [cement, NFM, iron and steel methodology]

UNEP, 2013. Global Mercury Assessment 2013: Sources, Emissions, Releases and Environmental Transport. UNEP Chemicals Branch, Geneva, Switzerland. 44pp

UNEP, 2013 – Technical report from GMA-2013 [cement, NFM, iron and steel methodology] [NB this ref. in these sections needs to be changed to AMAP/UNEP, 2013]

UNEP, 2015 – Toolkit for Identification and Quantification of Mercury Releases, Reference Report and Guideline for Inventory Level 2, Version 1.3, 2015 [cement, NFM, iron and steel methodology]

UNEP, 2017 – Toolkit for Identification and Quantification of Mercury Releases, Reference Report and Guideline for Inventory Level 2, Version 1.4, 2017 http://web.unep.org/chemicalsandwaste/what-we-do/technology-and-metals/mercury/toolkit-identification-and-quantification-mercury-releases [cement, NFM, iron and steel methodology] [biomass methodology]

VDZ, 2015 – The German Cement Works Association, 2015, Environmental Data of the German Cement Industry 2014 [cement, NFM, iron and steel methodology]

Wang, 2014 – Wang, S., Wang, F., Zhang, L., Yang, H., Wu., Q, Hao, J., 2014, Mercury Enrichment and its effects on atmospheric emissions in cement plants in China, Atmospheric Environment 92 (2014) 421-428 [cement, NFM, iron and steel methodology]

Wang, 2016 – Wang, S., Wang, F., Zhang, L., Yang, H., Wu, Q., Hao. J., 2016, Mercury mass flow in iron and steel production process and its implications for mercury emission control, Journal of Environmental Sciences, 43 (2016), 293-301 [cement, NFM, iron and steel methodology]

Won, 2012 – Won, J., Lee, T., 2012, Estimation of total annual mercury emissions from cement manufacturing facilities in Korea, Atmospheric Environment 62(2012), 265-271 [cement, NFM, iron and steel methodology]

Wu, Y., Streets, D.G., Wang, S.X., & Hao, J.M. (2010). Uncertainties in estimating mercury emissions from coal-fired power plants in China. Atmos. Chem. Phys., 10, 2937–2947. [2.2.3]

Wu, 2012 – Wu, Q., Wang, S., Zhang, L., Song, J., Yang, H., Meng, Y., 2012, Update of mercury emissions from China's primary zinc, lead and copper smelters, 2000-2010, Atmospheric Chemistry and Physics 12 (2012), 11153-11163 [cement, NFM, iron and steel methodology]

Wu, 2016 – Wu, Q., Wang, S., Zhang, L., Hui, M., Wang, F, Hao, J., 2016, Flow analysis of the Mercury Associated with Nonferrous Ore Concentrates: Implications on Mercury Emissions and Recovery in China, Environmental Science and Technology, January 2016 [cement, NFM, iron and steel methodology]
Yang, 2016 – Yang, M., Wang, S., Zhang, L., Wu, Q., Wang, F., Hui, M., Yang, H., Hao, J., 2016, Mercury emission and speciation from industrial gold production using roasting process, Journal of Geochemical Exploration, 170 (2016), 72-77 [cement, NFM, iron and steel methodology]
Zhang 2012 – Zhang, L., Wang, S., Wu, Q., Meng, Y., Yang, H., Wang, F., Hao, J., 2012, Were mercury emission factors for Chinese non-ferrous metal smelters overestimated? Evidence from onsite measurements in six smelters, Environmental Pollution, 171 (2012), 109-117 [cement, NFM, iron and steel methodology]
Zhang, W., Wei, W., Hu, D., Zhu, Y., & Wang, X. (2013). Emission of Speciated Mercury from Residential Biomass Fuel Combustion in China. Energy & Fuels 27, 6792-6800. [biomass methodology]
Zhang 2015 – Zhang, L., Wang, S., Wang, L., Wu, Y., Duan, L., Wu, Q., Wang, F., Yang, M., Yang, H., Hao, J., Liu, X., 2015, Updated emission inventories for speciated atmospheric mercury from anthropogenic sources in China, Environmental Science and Technology 49 (2015), 3185-3194 [cement, NFM, iron and steel methodology]

Personal comments:

National communication, South Africa – Rico Euripidou, mail 2016-11-11 [cement, NFM, iron and steel methodology]
National communication, Australia – Peter Nelson, mail February-March 2017 [cement, NFM, iron and steel methodology]
National communication, China – Qingru Wu, mail 2017-03-14 (clarifications) [cement, NFM, iron and steel methodology]
National communication, Korea – Yong-Chil Seo, mail 2016-02-25 [cement, NFM, iron and steel methodology]
AUST Cu - http://www.ga.gov.au/scientific-topics/minerals/mineral-resources/copper#heading-5 (link from Peter Nelson) [cement, NFM, iron and steel methodology]
NAM Zn - http://www.exxaro.com/pdf/icpr/a/mining_assets/base_metals.htm [cement, NFM, iron and steel methodology]

(Other references are as in GMA 2013 Technical report)

Appendix A. Details of methods for calculating Uncertainty Ranges

(i) Calculating uncertainties using the approach applied in the GMA, 2013

A relatively crude (and intentionally conservative) approach was adopted to provide some quantification of the scale of uncertainties in the estimates presented in the GMA 2013 (see Table U1).

Of the three major components contributing to the uncertainties associated with the emission estimates: uncertainties associated with activity data; uncertainties associated with (unabated) emission factors; and uncertainties associated with assumptions made regarding applied (Hg emissions control) technologies, only the first two were considered.

In general, the uncertainties associated with emission factors (including plant operating conditions and technologies used to reduce Hg emissions) are assumed to be considerably more important in determining uncertainties in the overall emissions estimates than those associated with activity data. For example, the EMEP/EEA (2009) air pollutant emission inventory guidebook assigns uncertainties associated with activity data (not specific to Hg) of the order of ± 5–10%. Evaluation of uncertainties associated with (emission factor-based) estimates depends on the procedures involved. For estimates based on a small number of measurements at representative facilities (or engineering judgment based on relevant facts) or engineering calculations based on assumptions alone – which between them cover the case for most Hg emissions estimates – the uncertainties are considered to be of the order of ± 50% to ± an order of magnitude.

For emissions based on Hg consumption in intentional use sectors, and associated waste handling, upper and lower range estimates were produced using the respective upper and lower ranges of the Hg consumption data. These however do not reflect the considerable uncertainties associated with the assumptions made regarding Hg flow in waste streams and associated emission factors. Consequently uncertainties in estimates associated with these sectors were assigned at ± a factor of 3. Uncertainties associated with the assumptions regarding assignment of countries to particular 'country groupings' for applied technology or waste handling procedures were not taken into account.

Table U1. Procedures adopted for calculating low/high range emissions estimates.

		Lower range estimate	Upper range estimate	Ref.
Activity data derived from IEA/official national sources	OECD countries	Activity minus 5%	Activity plus 5%	Modified after EMEP/EEA, 2009
Activity data derived from IEA/official national sources	Non-OECD countries	Activity minus 10%	Activity plus 10%	Modified after EMEP/EEA, 2009
Activity data derived from other sources		Activity minus 30%	Activity plus 30%	Based on AMAP/UNEP 2008
Unabated EFs	All countries	0.7*UEF# for coal sectors; 0.5*UEF# or 0.25*UEF for all other sectors	1.3*UEF# for coal sectors; 1.5*UEF# or 1.75* UEF for all other sectors	Assumptions applied in GMA 2013
Emissions estimates for intentional-use waste stream emissions and emissions from cremations		0.3 * mid-range estimate	3 * mid-range estimate	
Emissions estimates for ASGM		Mid-range estimate minus 15-100% depending on country	Mid-range estimate plus 15- 100% depending on country	

(ii) Introducing uncertainty associated with APC technology assumptions

In a modified version of the GMA2013 approach, uncertainties for technology profiles were introduced by considering 'average reduction efficiency', defined as the sum of the (weighted) abatement. The calculation of the average reduction efficiency for iron and steel production in country group 1 (48.7%) is illustrated in Table U2 below. The average reduction efficiency may also be derived by dividing the emission estimate with the activity data set and the unabated emission factor.

Table U2 Default technology profile applied for pig iron and steel production for country group 1

Technology	Emission reduction efficiency, %	Degree of application, %	Weighted reduction efficiency, %
Standard APC: ESP/CYC/FGD (sinter plant)	20	30	6
Efficient APC: ESP+FGD/ACT/ESP+ACT (sinter	55	60	33

plant)			
Very efficient APC: ESP+ACT/RAC (sinter plant)	97	10	9.7
		Average reduction efficency:	48.7

Uncertainty associated with the removal efficiency was then categorized into 4 different profiles, based on the average removal efficiency for that particular activity, see Table U3. It should be noted that this approach was only applied for 'by-product' sectors; no uncertainty on the removal efficiency was applied in the case of estimated emissions from artisanal gold mining or intentional-use waste streams.

Table U3. Procedures adopted for calculating low/high range technology profiles

Abatement profile	**Average reduction efficiency**	**Low bound**	**High bound**	**Ref.**
Low	0-30%	0% reduction	Average reduction efficiency plus 40%	Assumptions applied in this work
Medium	30-50%	Average reduction efficiency minus 20%	Average reduction efficiency plus 20%	Assumptions applied in this work
High	50-85%	Average reduction efficiency minus 10%	Average reduction efficiency plus 10%	Assumptions applied in this work
Very high	85-100%	Average reduction efficiency minus 5%	Average reduction efficiency plus 5%. However, a maximum bound of 99.99% is adopted.	Assumptions applied in this work

(iii) Employing the propagation of errors method to evaluate uncertainties associated with aggregated estimates

The error propagation method is a method for combining uncertainties. In the current assessment, an approach based on the procedure recommended in the IPCC guidelines for calculating the uncertainty for greenhouse gas emissions (Frey, et al., 2006) was used to evaluate the uncertainties associated with aggregated emissions estimates (regional and sectoral totals and the global inventory total).

The combined uncertainty for one activity (i.e. a national-sector/activity emission estimate) is calculated according the following equation:

$$U_{combined} = \sqrt{U_{AD}^2 + U_{TF}^2 + U_{UEF}^2}$$

where:

U_{AD}: Uncertainty associated with the activity data, see Table 2.1.

U_{UEF}: Uncertainty associated with the unabated emissions factor, see Table 2.1.

U_{TF}: Uncertainty associated with the average reduction efficiency, see Table 2.3.

The maximum uncertainty derived using the assumptions quantified in Table X2 and Table X3 were employed. The uncertainty for the activity data and the technology profile are assumed to be normally distributed around the mean. However, cut-offs were applied on the uncertainty for technology profiles to eliminate cases where the average removal efficiency would be greater than 100% or lower than 0%. The high / low uncertainty for the technology profiles can therefore differ in some cases.

Since the unabated emission factor is largely dependent on the mercury content of the fuel/raw material, the unabated emission factor is assumed to be log-normally distributed. This reflects common properties of such materials; see for example Wu et al (2010) for mercury content in coal, Hylander & Herbert (2008) for mercury content in nonferrous metal ores, and (REF) for mercury content in crude oils. The uncertainty around the unabated emission factor is thus assigned to a high and a low range uncertainty, based on the geometric mean and geometric standard deviation. The geometric mean is calculated with the following equation:

$$\mu_g = e^{\ln(\mu) - \frac{\ln\left(1+\left(\frac{U_{UEF}}{200}\right)^2\right)}{2}}$$

μ_g: Geometric mean

μ: Arithmetic mean, the unabated emission factor used in this study

U_{UEF}: The maximal uncertainty for the unabated emission factor

The geometric standard deviation is calculated with the following equation:

$$\sigma_g = e^{\sqrt{\ln\left(1+\left(\frac{U_{UEF}}{200}\right)^2\right)}}$$

σ_g Geometric standard deviation

The high and low uncertainty for the unabated emission factor is derived with help of two logarithmic transformations:

$$U_{UEF,low} = \frac{e^{\ln(\mu_g) - 1.96 \cdot \ln(\sigma_g)} - \mu}{\mu} \cdot 100$$

$$U_{UEF,high} = \frac{e^{\ln(\mu_g) + 1.96 \cdot \ln(\sigma_g)} - \mu}{\mu} \cdot 100$$

The following equation is used for combining the uncertainty:

$$U_{total} = \sqrt{\left(\frac{ee_1 \cdot U_{combined,1}}{EE}\right)^2 + \left(\frac{ee_2 \cdot U_{combined,2}}{EE}\right)^2 + \cdots + \left(\frac{ee_n \cdot U_{combined,n}}{EE}\right)^2}$$

where:

ee: Emission estimate for one activity in one country

EE: Emission estimate for the combined inventory. In this study the combined inventory is calculated at a global, sector and subcontinental level.

The IPCC guidelines are primary developed for calculating uncertainties associated with greenhouse gas emission estimates. Uncertainties associated with e.g. anthropogenic CO_2 emission factors are relatively small compared with those for mercury. The results of applying the error propagation method to mercury emissions may therefore be weak in some cases. Underestimation or overestimation of the uncertainties may also be a consequence where:

1. Distributions are non-Gaussian
2. Correlations exists between the activity data, the technology profiles and the unabated emission factor.

Notwithstanding these limitations, the uncertainty estimates obtained using the propagation of errors approach are considered to better represent the scale of the uncertainties for aggregated inventory estimates than those achieved by simply summing uncertainties for individual (country-sector) emission estimates.

3124

3125

Annex 1 Description of method used to estimate 2015 mercury emissions to air from main 'by-product' emission sectors and the chlor-alkali industry, including an example calculation

Annex 2 Description of method used to estimate 2015 mercury emissions to air from artisanal and small-scale gold mining, including an example calculation

Annex 3 Description of method used to estimate 2015 mercury emissions to air from wastes associated with mercury added products, including an example calculation

Annex 4 Description of method used to estimate 2015 mercury emissions to air from use in dental amalgam and human cremation

Annex 5 Activity data used in the calculation of emission estimates

Annex 6 Emission factors and technology profiles used in the calculation of emission estimates

Annex 7 Comparisons with National Inventories (to be completed)

Annex 8 Global Inventory Estimates 2015

Note to reader

This draft version of Chapter 3 in the Technical Background Report to the Global Mercury Assessment 2018 is made available for review by national representatives and experts. The draft version contains material that will be further refined and elaborated after the review process. Specific items where the content of this draft chapter will be further improved and modified are:

1. New data and trend analysis on Canadian monitoring data will be added
2. Maps and tables for data from USA will be revised and improved.
3. Additional information and evaluation of polar measurements will be added.
4. The map of ALL monitoring sites from all existing networks in section 2 will be further improved
5. References list will be further improved as soon as the revised final draft will be ready
6. Conclusions and main messages will be formulated.

GMA 2018 Draft Chapter 3. Levels of mercury in air. Nicola Pirrone, Mariantonia Bencardino, Sergio Cinnirella, Aurélien Dommergue, Joseph Timothy Dvonch, Ralf Ebinghaus, Xinbin Feng, Alessandra Fino, Xuewu Fu, Katarina Gårdfeldt, Antonella Macagnano, David Schmeltz, David Gay, Milena Horvat, Dan Jaffe, Joze Kotnic, Henrik Skov, Francesca Sprovieri, Helen Angot, Alexandra Steffen, Amanda Cole, Elsie Sunderland, Kjetil Torseth, Simon Wilson (Members of the UNEP Fate & Transport Partnership Group, - Air Subgroup Technical Expert Team)

Contents

6048

Chapter 3 Levels of Mercury in Air

3.1 Background

The aim of this chapter is to provide an up-to-date overview of mercury levels in air (since the GMA 2013). In particular, this chapter focuses on atmospheric mercury measurements and regional/worldwide spatial and temporal trends. The information presented here will include an overview of measurements currently collected in regional monitoring networks around the world. This chapter will also include an overview of high altitude and vertical profile measurements and mercury exchange fluxes at the air/water/soil/vegetation/snow-ice interfaces. A summary of new non-standard/conventional methods available (under development) for monitoring mercury in air is also be presented. The chapter will conclude with an overall assessment of the state of atmospheric mercury measurements and our current understanding of the state of the science.

Specifically, this chapter highlights recent key findings on:

- Atmospheric mercury measurements and trends worldwide and at the regional/continental scale with a focus on the spatial and temporal variability of Hg and its compounds concentrations at ground-based sites, at different altitudes and latitudes in the Southern and Northern Hemispheres.
- Atmospheric mercury in polar environment (Arctic and Antarctica) and the specific aspects related to these regions in terms of impact caused by Long Range Transport (LRT) and in-situ formation and transformation processes.
- Recent studies on vertical profile measurements over background regions and over impacted (industrial/urban) regions to support modelling uncertainty and advance our understanding of LRT and deposition/re-emission patterns.
- Temporal and spatial variability in Hg exchange fluxes between air and soil/vegetation/snow-ice interfaces, and also including contaminated sites (industrial, mining areas).
- Recent advances in monitoring applications using new/non-standard methods for measuring Hg species in the atmosphere.

3.2 Atmospheric mercury measurements and trends worldwide

3.2.1 Introduction

Atmospheric Hg is monitored in national programs driven by national legislation or international agreements and conventions. Extensive monitoring is also conducted as a part of long-term research programs. Many national networks operate in the context of international conventions or agreements and this cooperation also includes development of joint procedures both for measurements and reporting of data and for regular evaluation of trends and patterns. For example, in Europe, air monitoring data on Hg is reported to EMEP (The European Monitoring and Evaluation Programme) under the Convention on Long-range Transboundary Air Pollution (CLRTAP). Arctic countries report data to AMAP (The Arctic Monitoring and Assessment Program under the Arctic Council) and Asian/Pacific countries to APMMN (the Asia-Pacific Mercury Monitoring Network). National networks differ in terms of ambition level e.g. relating to sampling frequency and whether speciation of airborne mercury is included.

National monitoring can provide the basis and infrastructure for research programs where routine monitoring can be expanded to more advanced methodologies for e.g. speciation of airborne Hg, and also new sites in locations where measurement data were previously not available. Examples of programs contributing results to this chapter are the GMOS program and several research projects focussed on Polar regions. The GMOS network continues to operate many of the sites in coordination with national programs and regional agreements. Monitoring stations are located mostly at background sites in order to intercept major intercontinental and continental air mass transport patterns. Master sites provide atmospheric Hg measurement speciated data including total Hg in precipitation samples whereas secondary sites provide Total Gaseous Mercury (TGM) measurement data and total Hg in precipitation (see www.gmos.eu for further details).

According to data provided by Governments to UNEP within the 'Global Review of Mercury Monitoring networks' (UNEP, 2016), the national monitoring networks are reported in the Table 1.

Table 1: Global Review of mercury monitoring networks (UNEP, 2016).

National area	Program/ network/ inventory	Number of monitoring stations/ sites	Managing Institution	Main website
Andorra	Andorran Air Quality network	Not available	Department of Environment and Sustainability	
Australia	The Australian National Pollutant inventory (NPI)	Not available		https://data.gov.au/dataset/npi
Austria	Network for		Austrian Federal	Austrian Bio-indicator Grid

	Mercury impacts in forest foliage		Research Centre for Forests controls	
Brazil	Mercury monitoring Network	Not available	CETESB, the environmental agency of the State of São Paulo	http://www.cetesb.sp.gov.br/2014/10/27/cetesb-realiza-treinamentos-internacionais-sobre-pops-e-mercurio/
Canada	The Canadian Air and Precipitation Monitoring Network (CAPMoN) & others (including AMAP)	3 stat. for air meas..	CAPMoN	https://www.ec.gc.ca/rs-mn/default.asp?lang=En&n=6C2AD92E-1 **http://nadp.sws.uiuc.edu/**
		+7 stat. for air meas.	Environment Canada	
		+ 2 remote stat.	Canadian Northern Contaminants Program (NCP) – Environment Canada	
China (Taiwan)	Wet deposition Network	11 sampling sites + 1 remote site	Environmental Protection Administration	
European Union	Network under EU Directive 2004/107/EC		EEA	http://cdr.eionet.europa.eu/ https://www.eea.europa.eu/data-and-maps/data/aqereporting-2
Hungary	Hungarian Air Quality Monitoring Network	One sampling site	Hungarian Meteorological Service	
Korea		12 monitoring stations	National Institute of Environmental Research (NIER) in the Ministry of Environment	
Japan	2 Mercury Monitoring Networks	281 monitoring stations	National Institute for Minamata Disease (NIMD) and the National Institute for Environmental Studies (NIES)/Ministry of Environment (MOE).	
Poland	Polish State Environmental Monitoring programme	5 monitoring stations	Inspection of Environmental Protection	http://www.gios.gov.pl/en/state-of-the-environment/state-environmental-monitoring
Romania	Mercury Monitoring Network	Sites in 41 counties	Ministry of Environment, NEPA and the National Environmental Guard	
United Kingdom	National Metals Network and National Atmospheric Emission Inventory	2 monitoring stations	UK DEFRA	https://uk-air.defra.gov.uk/networks/network-info?view=metals http://naei.defra.gov.uk/overview/pollutants?pollutant_id=15
Vietnam	--------	1 monitoring station	Vietnamese Centre for Environmental Monitoring (CEM) of the Vietnam Environment Administration (VEA)	
Global network	GMOS	Several stations in both hemispheres	CNR-IIA Division of Rende, Italy	www.gmos.eu

Regional network	NADP	Several stations in USA, Canada	NADP Program Office Illinois State Water Survey, 2204 Griffith Drive Champaign, IL 61820-7495	http://nadp.sws.uiuc.edu/mdn/

The UNEP Review lists general information on existing national monitoring networks but doesn't include data on mercury concentrations and depositions.

Figure 1 provides a global picture of major monitoring networks that are part of global and regional networks mentioned in several sections of this chapter. It shows that though we have monitoring sites in both hemispheres, but there are regions (even large regions) that are completely lucking of monitoring data/sites which makes the evaluation of current situation in terms of geospatial distribution (gradients and variability) of Hg concentration in ambient air not feasible to do.

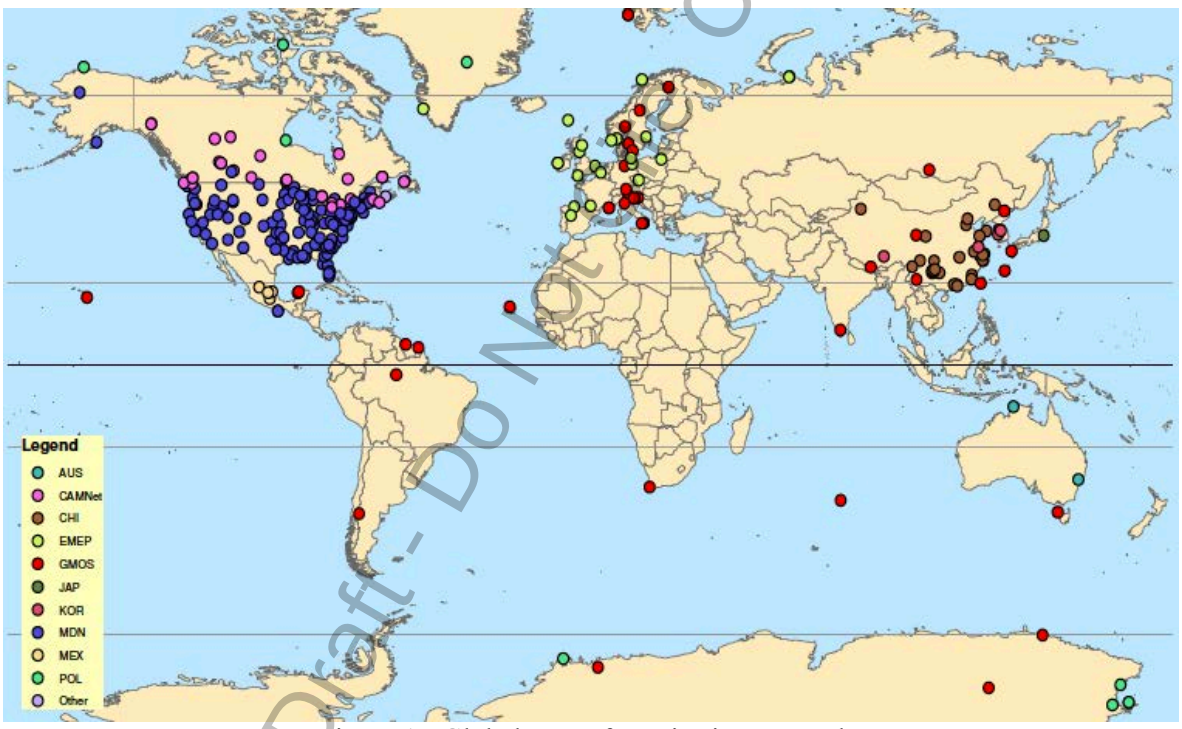

Figure 1 - Global map of monitoring networks

3.2.2 Spatial and temporal variability in the Southern and Northern Hemispheres

Extensive measurements and data analysis have been performed across several ground-based sites as part of the GMOS program network. GMOS will continue its operation by providing support to site operators for online QA/QC and technical assistance as necessary through the Global Observation System on Mercury (GOS4M) that is one of the four flagships of GEO (Group on Earth Observation) and

6117 will be financially supported through the ERA-PLANET (www.era-planet.eu) program. Tables 2 and 3
6118 show annual values for speciated Hg concentrations at all sites from 2012 to 2014. In both Tables 1 and
6119 2, the stations are ordered by latitude, thus describing the spatial atmospheric mercury variations
6120 moving from Northern to Southern Hemisphere. Mean GEM values of most of the sites located in the
6121 Northern Hemisphere were between 1.3 and 1.6 ngm^{-3},which is comparable to the concentrations
6122 measured at the long-term monitoring stations at Mace Head, Ireland (Ebinghaus et al., 2011; Slemr et
6123 al., 2011; Weigelt et al., 2015; Cole et al. 2014), and Zingst, Germany (Kock et al., 2005). In contrast,
6124 GEM concentrations from the EVK site, located at 5050 m above sea level in the Eastern Himalaya of
6125 Nepal, reported mean values below 1.3 ng m^{-3}. This value is comparable to free tropospheric
6126 concentrations measured in August 2013 over Europe (Weigelt et al., 2016). GEM concentration means
6127 observed at the stations in the Northern Hemisphere are also in good agreement with the overall mean
6128 concentrations observed at multiple sites in Canada (ranging from 1.23±0.37 to 3.75 ± 2.22 ng m^{-3}
6129 overall measurements collected from 1994-2011) (Cole et al., 2014) and those reported from 2 Arctic
6130 stations (VRS, PAL) (Sprovieri et al., 2016). Seasonal variations of GEM concentrations have also been
6131 observed at all European sites in the Northern Hemisphere, with most of them showing higher
6132 concentrations during the winter and spring and lower concentrations in summer and fall seasons.

6133 **Table 2:** Annually averaged GEM mean concentrations from 2012 to 2014 at the GMOS stations
6134 (Sprovieri et al. 2016).

	Code	Site	Elev (m asl)	Lat	Lon	Country	2012 GEM Mean ± St.Dev. ($ng\ m^{-3}$)	2013 GEM Mean ± St.Dev. ($ng\ m^{-3}$)	2014 GEM Mean ± St.Dev. ($ng\ m^{-3}$)
Northern Hemisphere	VRS	Villum Research Station	30	81.58033	-16.60961	Greenland	1.44 ± 0.27	1.61 ± 0.41	1.41 ± 0.35
	PAL	Pallas	340	68.00000	24.23972	Finland	- ± -	1.45 ± 0.11	1.47 ± 0.17
	RAO*	Råö	5	57.39384	11.91407	Sweden	1.33 ± 0.20	1.43 ± 0.16	1.48 ± 0.23
	MHE	Mace Head	5	53.32511	-9.90500	Ireland	** ± **	1.46 ± 0.17	1.41 ± 0.14
	LIS	Listvyanka	670	51.84670	104.89300	Russia	- ± -	1.34 ± 0.38	1.39 ± 0.40
	CMA	Col Margherita	2545	46.36711	11.79341	Italy	- ± -	- ± -	1.69 ± 0.29
	MCH*	Mt. Changbai	741	42.40028	128.11250	China	- ± -	1.78 ± 0.48	1.57 ± 0.42
	LON*	Longobucco	1379	39.39408	16.61348	Italy	- ± -	1.43 ± 0.33	- ± -
	MWA	Mt. Walinguan	3816	36.28667	100.89797	China	- ± -	1.33 ± 0.64	1.31 ± 0.60
	MIN	**Minamata**	**20**	**32.23056**	**130.40389**	**Japan**	1.95 ± 0.48	1.86 ± 0.40	1.91 ± 0.40
	EVK	Ev-K2	5050	27.95861	86.81333	Nepal	1.14 ± 0.17	1.11 ± 0.42	1.33 ± 0.22
	CHE*	**Cape Hedo**	**60**	**26.86430**	**128.25141**	**Japan**	2.12 ± 0.47	1.74 ± 0.38	1.78 ± 0.35
	MAL	Mt. Ailao	2503	24.53791	101.03024	China	- ± -	2.04 ± 0.64	1.33 ± 0.40
Tropics	SIS	Sisal	7	21.16356	-90.04679	Mexico	- ± -	1.20 ± 0.24	1.11 ± 0.37
	CAL	Calhau	10	16.86402	-24.86730	Cape Verde	- ± -	1.22 ± 0.14	1.20 ± 0.09
	KOD	Kodaicanal	2333	10.23170	77.46524	India	- ± -	1.54 ± 0.20	1.54 ± 0.26
	NIK	Nieuw Nickerie	1	5.95679	-57.03923	Suriname	- ± -	1.13 ± 0.42	1.28 ± 0.46
	MAN*	Manaus	110	-2.89056	-59.96975	Brazil	- ± -	1.08 ± 0.23	0.99 ± 0.23
Southern Hemisphere	AMS*	Amsterdam Island	70	-37.79604	77.55095	Terres Australes et Antarctiques Françaises	1.03 ± 0.07	1.03 ± 0.09	1.05 ± 0.05
	CPT	Cape Point	230	-34.35348	18.48983	South Africa	1.07 ± 0.10	1.03 ± 0.11	1.09 ± 0.12
	BAR	Bariloche	801	-41.12873	-71.42010	Argentina	1.01 ± 0.11	0.89 ± 0.15	0.87 ± 0.15
	DDU	Dumont d'Urville	40	-66.66281	140.00292	Antarctica	0.91 ± 0.2	0.85 ± 0.19	0.86 ± 0.38
	DMC	Concordia Station	3220	-75.10170	123.34895	Antarctica	0.76 ± 0.24	0.84 ± 0.27	- ± -

** *to be included*

* *GMOS Master stations with speciation Hg data*

in bold External GMOS Partners

Table 3: Annually-averaged PBM and GOM mean concentrations from 2012 to 2014 at the GMOS stations (Sprovieri et al. 2016).

							2012		2013		2014	
	Code	Site	Elev (m asl)	Lat	Lon	Country	PBM Mean ± St.Dev. ($pg\,m^{-3}$)	GOM Mean ± St.Dev. ($pg\,m^{-3}$)	PBM Mean ± St.Dev. ($pg\,m^{-3}$)	GOM Mean ± St.Dev. ($pg\,m^{-3}$)	PBM Mean ± St.Dev. ($pg\,m^{-3}$)	GOM Mean ± St.Dev. ($pg\,m^{-3}$)
NH	RAO	Råö	5	57.39384	11.91407	Sweden	2.89 ± 3.27	0.63 ± 1.73	3.96 ± 3.77	0.54 ± 0.85	4.41 ± 5.87	1.25 ± 1.87
NH	MCH	Mt. Changbai	741	42.40028	128.11250	China	-	-	17.10 ± 14.25	4.96 ± 6.33	-	-
NH	LON	Longobucco	1379	39.39408	16.61348	Italy	-	-	3.28 ± 3.82	11.33 ± 29.90	-	-
NH	MWA	Mt. Walinguan	3816	36.28667	100.89797	China	-	-	98.59 ± 37.79	12.32 ± 6.33	-	-
NH	**CHE**	**Cape Hedo**	**60**	**26.86430**	**128.25141**	**Japan**	1.77 ± 2.46	1.10 ± 1.80	3.70 ± 3.60	1.46 ± 2.19	4.03 ± 5.25	2.26 ± 3.71
T	MAN	Manaus	110	-2.89056	-59.96975	Brazil	-	-	5.04 ± 4.13	1.72 ± 0.72	1.45 ± 1.81	1.61 ± 1.75
SH	AMS	Amsterdam Island	70	-37.79604	77.55095	Terres Australes et Antarctiques Françaises	1.76 ± 1.20	1.65 ± 0.82	2.05 ± 1.37	1.53 ± 0.45	2.22 ± 1.83	2.03 ± 1.44

Table 4 summarizes the summary of the annual wet deposition fluxes and the weighted THg concentrations observed at the 17 GMOS sites from the Northern, Tropical, and Southern Hemispheres between 2011 and 2015 (Sprovieri et al., 2017). Seasonal trend analysis of THg in precipitation showed increasing Hg concentrations and Hg deposition during the spring and summer months. However, the patterns of THg concentrations and precipitation amounts reveal that, at most of the sites, the seasonal THg wet deposition maximum corresponds to the maximum in precipitation amounts collected. The dominant factor in determining the Hg wet deposition loading recorded at all the European sites was then generally related to the amounts of the collected precipitation.

Table 4: Annual wet deposition fluxes [$\mu g m^{-2} yr^{-1}$] and weighted THg concentrations [ngL^{-1}] observed at GMOS stations from 2011 to 2015 (Sprovieri et al. 2017).

	Code	Station	Elev (m asl)	Lat	Lon	Country	2011		2012		2013		2014		2015	
							Annual Wet Dep. Flux [μg m^{-2} yr^{-1}]	Weighted HgT [ng L^{-1}]	Annual Wet Dep. Flux [μg m^{-2} yr^{-1}]	Weighted HgT [ng L^{-1}]	Annual Wet Dep. Flux [μg m^{-2} yr^{-1}]	Weighted HgT [ng L^{-1}]	Annual Wet Dep. Flux [μg m^{-2} yr^{-1}]	Weighted HgT [ng L^{-1}]	Annual Wet Dep. Flux [μg m^{-2} yr^{-1}]	Weighted HgT [ng L^{-1}]
Northern Hemisphere	NYA	Zeppelin	474	78.90806	11.88139	Norway	-	-	0.9	**3.8**	0.9	**4.1**	1.7	**5.7**	0.8	**4.4**
	PAL	Pallas	340	68	24.23972	Finland	2.9	**7.1**	1.9	**6.8**	1.3	**4.5**	2.3	**6.1**	-	-
	RAO	Råö	5	57.393835	11.914066	Sweden	5.8	**8.9**	6.5	**10.4**	4.2	**8.2**	6.3	**9.9**	-	-
	MHE	Mace Head	5	53.325106	-9.905	Ireland	-	-	0.9	**2.2**	4.8	**4.6**	4.1	**6.6**	-	-
	LIS	Listvyanka	670	51.8467	104.893	Russia	-	-	0.2	**9.7**	0.1	**2.6**	-	-	-	-
	CMA	Col Margherita	2545	46.36711	11.79341	Italy	-	-	-	-	-		4.4	**7.8**	-	-
	ISK	Iskrba	520	45.561217	14.858047	Slovenia	5.1	**7.5**	8.4	**6.2**	7.2	**5.3**	10.0	**6.1**	3.0	**3.0**
	MCH	Mt. Changbai	741	42.40028	128.11250	China	2.8	**10.6**	4.8	**8.4**	1.2	**3.9**	1.0	**5.4**	-	-
	LON	Longobucco	1379	39.39408	16.61348	Italy	-	-	0.3	**3.9**	3.1	**6.6**	-	-	-	-
	MWA	Mt. Waliguan	3816	36.28667	100.89797	China	-	-	0.3	**4.3**	0.4	**6.4**	2.2	**15.0**	-	-
	MAL	Mt. Ailao	2503	24.53791	101.03024	China	4.3	**2.8**	3.2	**3.3**	5.5	**5.3**	0.2	**6.7**	-	-
Tropics	SIS	Sisal	7	21.16356	-90.04679	Mexico	-	-	-	-	7.4	**11.0**	6.5	**9.1**	-	-
	CST	Celestun	3	20.85838	-90.38309	Mexico	-	-	2.4	**8.1**	0.1	**13.5**	-	-	-	-
Southern Hemisphere	AMS	Amsterdam Island	70	-37.79604	77.55095	Terres Australes et Antarctiques Françaises	-	-	-	-	1.95	**2.34**	1.55	**1.80**	-	-
	CPT	Cape Point	230	-34.35348	18.48983	South Africa	0.3	**2.1**	3.8	**14.6**	5.2	**19.6**	0.57	**1.84**	0.6	**3.0**
	CGR	Cape Grim	94	-40.683333	144.689444	Australia	-	-	-	-	3.1	**4.0**	3.8	**6.7**	3.1	**6.5**
	BAR	Bariloche	801	-41.12873	-71.42010	Argentina	-	-	-	-	-	-	0.1	**0.4**	0.5	**0.6**

3.2.1.1 Atmospheric Hg concentrations and pattern analysis in the Southern Hemisphere (SH)

For the sites located in the SH as part of GMOS network (see Table 2), mean GEM concentrations (~ 1.0 ngm^{-3}) are lower than those reported in the Northern Hemisphere (~ 1.5 ngm^{-3}) but are in good agreement with the previously reported southern hemispherical background levels (Sprovieri et al., 2010; Angot et al., 2014; Slemr et al., 2015) and the expected range for remote sites in this region. A small (within ~ 0.1 ngm^{-3}) seasonal variability in GEM concentrations was observed at Cape Point and Amsterdam Island with highest values during austral winter and lowest values in summer (Slemr et al., 2015) but the variability in concentrations is much lower than in the Northern Hemisphere. GEM concentrations are comparable at all SH monitoring sites, whereas the lower concentrations of GEM observed (<1ngm^{-3}), were associated with air masses coming from the southern Indian Ocean and the Antarctic continent (Angot et al., 2014).

3.2.1.2 Wet deposition at Tropical Sites and in the SH

Hg deposition measurements are scarce in tropical latitudes; hence there have been few scientific publications within the past decade from this region (Shanley et al., 2015 and references therein). The tropics are a particularly important region with regard to global atmospheric chemistry and 49% of total Hg(II) deposition globally occurs in the tropical oceans (Horowitz et al., 2017). Due to intense ultraviolet radiation and high water-vapour concentrations, high OH concentrations oxidize inorganic and organic gases, and induce an efficient removal from the atmosphere of the oxidized products. To address the

regional gap of information, the GMOS program initiated Hg deposition measurements in Mexico at Sisal station (see Table 3). High wet Hg deposition flux at this site suggested that other tropical areas maybe hotspots for Hg deposition as well. A number of studies have suggested that this could be due to higher precipitation and the scavenging ratios from the global pool in the subtropical free troposphere where high concentrations of oxidized Hg species exist (Selin and Jacob, 2008). These findings were also highlighted in previous studies in the south of Florida and the Gulf of Mexico coastal areas, confirming that local and regional Hg emissions play only a minor role in wet Hg deposition (Sillman et al., 2013) and suggesting that the primary source of scavenged oxidized Hg could be the global pool. In remote areas such as the Southern Hemisphere, far from any local sources, atmospheric deposition has been recognized as the main source of Hg to the ocean (Lindberg et al., 2007; Pirrone et al., 2008; Sunderland and Mason, 2007). Total mercury (THg) exhibited annual and seasonal patterns in Hg wet deposition samples. Inter-annual differences in total wet deposition are mostly linked with precipitation volume, with the greatest deposition flux occurring in the wettest years (see Table 4) (Sprovieri et al., 2017).

3.2.2 Spatial and temporal variability in U.S.A.

3.2.2.1 NADP's Mercury Deposition Network

The National Atmospheric Deposition Program's Mercury Deposition Network (MDN) makes long-term measurements of mercury in precipitation (wet deposition) across North America. The MDN began monitoring in 1996. The MDN sites follow standard procedures, and uniform precipitation collectors and rain gages to make weekly-integrated measurements of total mercury in a combined precipitation measurement (wet only) from Tuesday to Tuesday. Some daily samples are available. Sample bottles are pre-charged with acid to preserve the mercury sample. Currently, the MDN has 106 active sites. All MDN samples are analysed for total mercury concentration using Cold Vapour Atomic Florescence Spectroscopy (CVAFS). Invalid samples are identified using standard protocols. Subsamples for some sites are analysed for methyl mercury (MeHg). Valid and invalid results are provided for use by the scientific community (http://nadp.isws.illinois.edu/ mdn/).

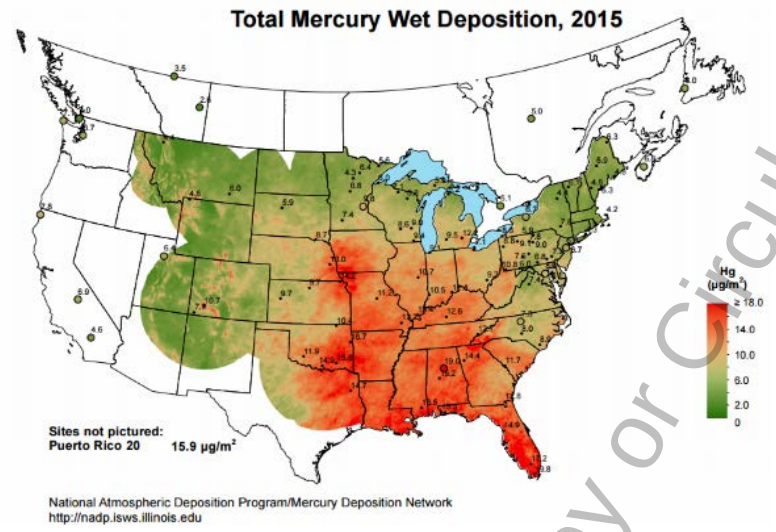

Figure 2: Total mercury wet depositions recorded in North America (2015). All years available at http://nadp.isws.illinois.edu

	Mercury Concentrations (ng/L)		
Year	N valid obs.	PW Mean	Median
2010	4,495	8.51	6.33
2011	4,286	9.01	6.99
2012	4,357	9.15	7.03
2013	4,391	9.02	7.17
2014	4,848	8.83	6.98
2015	4,798	8.04	6.4

All observations are used to determine total mercury deposition over North America in annual maps of precipitation weighted mean concentration (ng/L) and flux (ug/m^2 year, see figure). Precipitation-weighted average concentrations for 2015 are shown in the nearby Figure (??), and annual basic statistics are provided in the Table 5 (??).

Over the MDN measurement area, significant wet deposition is found along the U.S. Gulf Coast, and somewhat inland. Wet mercury deposition in these areas strongly correlates with higher precipitation (40-60 inches per year or >1000 cm/year). This pattern is repeated annually. Highest concentrations are found in the western areas where precipitation is lowest, and dominated by winter snow.

Trends over time in MDN data have been investigated by several research groups (Butler et al., 2008; Prestbo and Gay, 2009; Risch et al., 2012; Weiss-Penzias et al., 2016). Evaluating data through the mid 2000s, Butler et al. showed general decreases in eastern U.S. concentrations, with significant decreases

at about half of these sites. Fewer significant trends were seen in the Southeast, but the general tendency was for decreasing concentrations. Prestbo and Gay found significant decreasing concentration trends at about half of the sites (mostly in the East), particularly across Pennsylvania and extending up through the Northeast, and fully consistent with Butler et al. Two sites in the West (Colorado, Washington) showed the same decreases. No significant concentration increases were noted, with little change in the Upper Midwest concentration or deposition. Risch et al., focusing on the Great Lakes region, found only "small localized decreases" in Hg concentration. Deposition trends were present, but not at these same sites; Overall, mercury deposition in the Great Lakes area remained unchanged between 2002 and 2008.

Weiss-Penzias et al reported wet concentrations almost exclusively decreasing between 1997 and 2013, with over 50% of the MDNsites showing significant decreases (of 19 sites). However, for the time period 2007–2013 (with 71 sites), increasing concentrations were just as numerous as decreasing concentrations, and this increased with one shorter time period, and positive tendencies were wide spread. Regional trend analyses revealed significant positive trends in Hg concentration in the Rocky Mountains, Plains, and Upper Midwest regions for the more recent time periods.

3.2.2.2 NADP's Atmospheric Mercury Network

The NADP's Atmospheric Mercury Network (AMNet) measures atmospheric mercury that contributes to mercury deposition using automated, continuous measurement systems, and standardized methods. Currently, there were 21 AMNet sites, and data from the AMNet are available on the NADP website (http://nadp.isws.illinois.edu/ amn). AMNet observations have been made since 2009 and are made continuously (five-minute and two-hour averages).

Network	Year	Mercury in Precipitation (wet deposition)				
NADP's MDN		Species	Valid Observations	PW Mean	Median	Units
	2010	total mercury	4,495	8.51	6.33	ng/L
	2011		4,286	9.01	6.99	ng/L
	2012		4,357	9.15	7.03	ng/L
	2013		4,391	9.02	7.17	ng/L
	2014		4,848	8.83	6.98	ng/L
	2015		4,798	8.04	6.4	ng/L

Table 2

		Atmospheric Mercury Concentrations	Valid Observations	Mean	Median	Units
NADP's AMNet	2010	GEM	51,289	1.57	1.43	ng/m3
		GOM	38,744	6.5	1.39	pg/m3
		PBM	38,099	6.67	3.78	pg/m3
	2011	GEM	54,541	1.59	1.44	ng/m3
		GOM	44,864	15.92	1.35	pg/m3
		PBM	44,817	8.23	4.09	pg/m3
	2012	GEM	42,924	1.47	1.42	ng/m3
		GOM	36,226	19.74	1.22	pg/m3
		PBM	37,386	13.13	4.18	pg/m3
	2013	GEM	39,078	1.49	1.44	ng/m3
		GOM	30,806	14.35	1.29	pg/m3
		PBM	30,919	10.33	4.45	pg/m3
	2014	GEM	49,348	1.47	1.4	ng/m3
		GOM	35,390	12.64	1.52	pg/m3
		PBM	35,238	10.99	4.96	pg/m3
	2015	GEM	52,938	1.58	1.38	ng/m3
		GOM	44,179	12.47	1.59	pg/m3
		PBM	43,022	8.62	4.11	pg/m3

Data are qualified and averaged to one-hour (GEM in ng m^{-3}) and two-hour values (GOM, and $PBM_{2.5}$, in pg m^{-3}).

Valid data are released for use by the scientific community, and also released in annual figures of mercury variability for sites meeting certain criteria. Annual average statistics are shown in the Table 5.

The median GEM concentration found in the network is 1.38 ng/m3, and varies somewhat across the network. However, larger differences were present between sites for GOM and PBM concentrations in AMNet. GOM concentrations are generally higher in the urban environment, with lowest concentrations along the Pacific Ocean and other coastal sites. $PBM_{2.5}$ concentrations measured were generally the same as with GOM. The occurrence of very high outlier concentrations were noted at almost all of the sites (figure).

Investigations of AMNet trends over time are currently ongoing.

Table 5: Annual average statistics……(title TO BE COMPLETED)

	Atmospheric Mercury Concentrations	Valid Observations	Mean	Median	Units
2010	GEM	51,289	1.57	1.43	ng/m3
	GOM	38,744	6.5	1.39	pg/m3
	PBM	38,099	6.67	3.78	pg/m3
2011	GEM	54,541	1.59	1.44	ng/m3
	GOM	44,864	15.92	1.35	pg/m3
	PBM	44,817	8.23	4.09	pg/m3
2012	GEM	42,924	1.47	1.42	ng/m3
	GOM	36,226	19.74	1.22	pg/m3
	PBM	37,386	13.13	4.18	pg/m3
2013	GEM	39,078	1.49	1.44	ng/m3
	GOM	30,806	14.35	1.29	pg/m3
	PBM	30,919	10.33	4.45	pg/m3
2014	GEM	49,348	1.47	1.4	ng/m3
	GOM	35,390	12.64	1.52	pg/m3
	PBM	35,238	10.99	4.96	pg/m3
2015	GEM	52,938	1.58	1.38	ng/m3
	GOM	44,179	12.47	1.59	pg/m3
	PBM	43,022	8.62	4.11	pg/m3

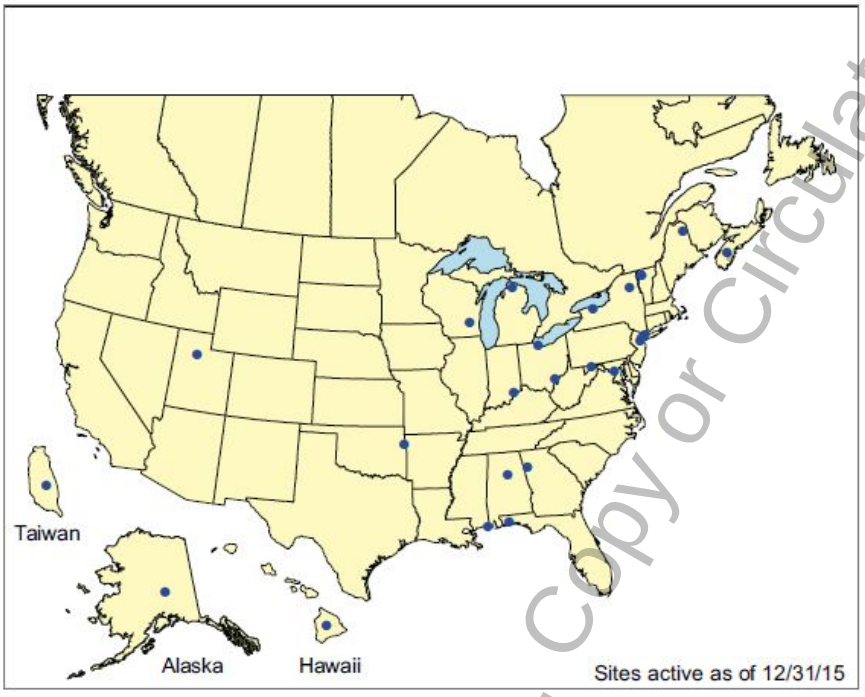

AMNet sites as of 12/31/2015.

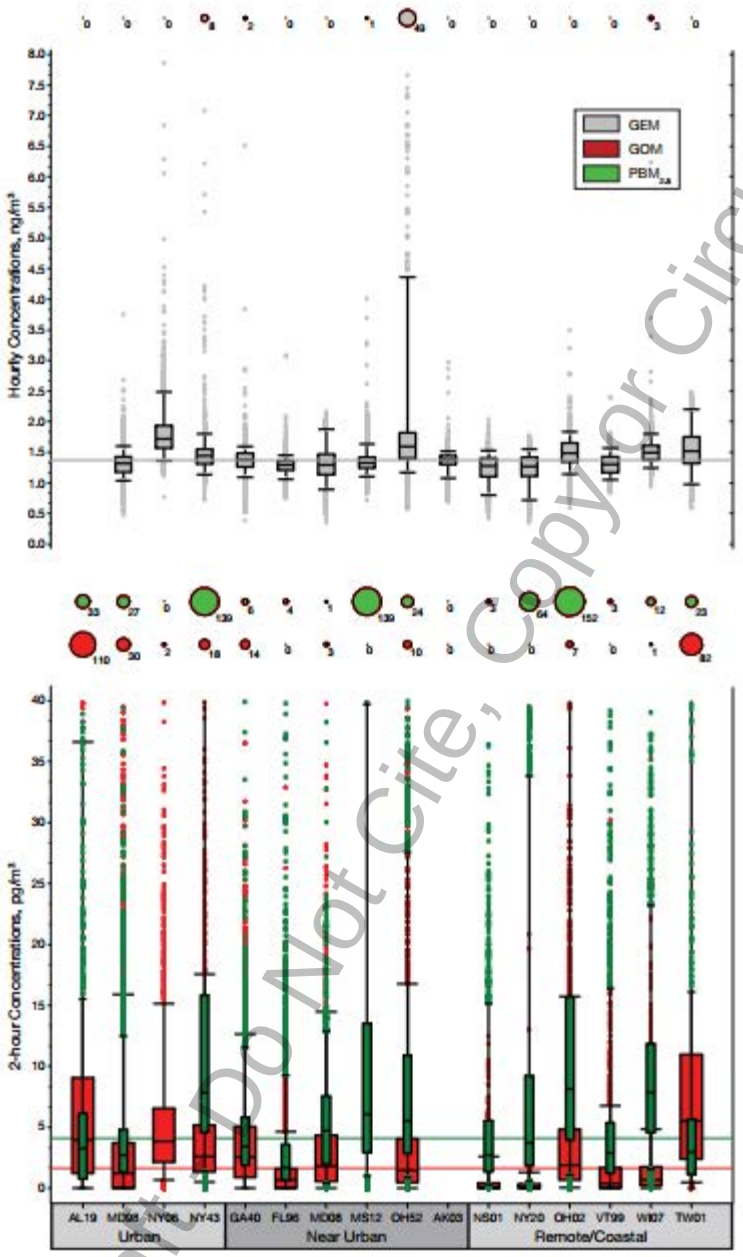

Figure @@: Hourly GEM concentrations in ng/m3 for each AMNet site (top) and 2-hour GOM and PBM2.5 concentrations in pg/m3 for each AMNet site (bottom), 2015. The bubble charts indicate the number of valid observations for GEM values above 8 ng/m3 , and GOM and PBM2.5 above 40 pg/m3 , the upper limit shown with the box plots. Horizontal lines in each graph represent the respective 2015 median values. From NADP, 2016.

Reference: National Atmospheric Deposition Program, 2016. National Atmospheric Deposition Program 2015 Annual Summary. NADP Data Report 2016-02. Illinois State Water Survey, University of Illinois at Urbana-Champaign, IL.

3.2.3 Canadian Atmospheric Mercury Network

Since 1994, considerable atmospheric Hg monitoring and research has taken place across Canada through both ongoing networks and independent research programs. Over time, the parameters measured have evolved, and the breadth and volume of data collected are significant. Most monitoring began as independent research programs to measure total gaseous mercury (TGM) in the early 1990s. Realizing the benefits of a community, researchers joined forces to create the Canadian Atmospheric Mercury Measurement Network (CAMNet) in 1994. CAMNet was operated by Environment and Climate Change Canada (ECCC) from 1994 to 2007, with between 7 and 15 sites across Canada. Later, some of these sites were transferred to the Canadian Atmospheric and Precipitation Monitoring Network (CAPMoN), which still operates these sites today and to other networks. The remainder of the currently operated ECCC sites are either part of the Northern Contaminants Program (NCP) or are run as part of ECCC measurement programs. As of 2017, these individual programs have been consolidated and fall under **Environment and Climate Change Canada – Atmospheric Mercury Monitoring or ECCC-AMM**. Table 6 shows all the atmospheric mercury measurements that have been taken across Canada. Figure XX shows the time periods from each site what measurements were made. Currently, there are 12 sites in Canada that collect continuous TGM and are highlighted in grey. In 1996, the United States-led Mercury Deposition Network (MDN) began collecting wet deposition samples for total mercury (THg) and, at some sites, methyl mercury (MeHg). Canada has joined forces with the MDN and has had up to 18 precipitation monitoring sites operating as part of the network over time. The sites where these precipitation measurements have been made over time are listed in Table XX. Currently, there are 7 sites in Canada that collect wet deposition measurements of mercury and are highlighted in grey. Finally, during the early 2000s, to meet increasing research needs, considerable advancements were made in instrument capabilities to collect and analyse mercury species in the air. From 2002 onward, some CAMNet sites began continuous measurements that could distinguish among gaseous elemental mercury (GEM), reactive gaseous mercury (RGM) and particulate mercury (TPM) (termed speciated atmospheric mercury). The sites which have made these measurements over time are listed in Table 6. Currently, there are 6 sites in Canada that collect continuous termed speciated atmospheric mercury and are highlighted in grey. As of January 2017, The ECCC-AMM monitors TGM at 12 sites, atmospheric speciated mercury at 6 sites and wet deposition at 5 sites. Figure 3 shows a map of the ECCC-AMM sites.

6321 **Table 6:** Mean concentrations of mercury data collected in Canada. The location of each site and the
6322 previous network or program under which the data was collected.

Station	Long (°W) Lat (°W)	Measurement period TGM	Mean TGM (ng m^{-3})	Measurement period Speciated Hg	Mean GEM (ng m^{-3})	Mean RGM (pg m^{-3})	Mean PHg (pg m^{-3})	Measurement period wet deposition	Mean Total Hg (ng L^{-1})
Little Fox Lake YK [a,g]	135.63 61.35	Jun 2007 – Oct 2011	1.28	-	-	-	-	-	-
Ucluelet BC [b]				-	-	-	-	-	-
Reifel Island BC [c, d]	123.17 49.10	Mar 1999 – Feb 2004	1.67	-	-	-	-	-	-
Saturna BC [c, d, e]	123.13 48.78	Mar 2009 – Dec 2010	1.43	-	-	-	-	Sep 2009 – Jan 2011	4.5
Whistler BC [b]	122.93 50.07	Aug 2008 – Oct 2011	1.21	-	-	-	-	-	-
Fort Vermilion AB [f]	116.02 58.38	-	-	-	-	-	-	Dec 2006 – Jan 2008	4.3
Meadows AB	114.64 53.53	May 2005 – Dec 2008	1.51	-	-	-	-	-	-
Genesee AB [b,d]	114.20 53.30	Mar 2004 – Dec 2010	1.53	Jan - Sep 2009	1.4	5.0	4.5	Jul 2006 – Jan 2011	12.8
Crossfield AB [f]	114.00 51.29	-	-	-	-	-	-	May 2006 – Dec 2007	9.3
Fort Chipewyan AB [c]	111.12 58.78	Jun 2000 – July 2001	1.36	-	-	-	-	-	-
Henry Kroeger AB [d]	110.83 51.42	-	-	-	-	-	-	Oct 2004 – Jan 2011	11.7
Esther AB [d, e]	110.20 51.67	Jun 1998 – Apr 2001	1.65					Apr 2000 – May 2001	14.2
Fort McKay South AB [h]	111.64 57.15	Aug 2013 – Dec 2016		Aug 2013 – Dec 2016				-	-
Patricia McInnis AB [h]	111.48 56.75	Oct 2010 – Dec 2016		-	-	-	-	-	-
Bratt's Lake SK [d,e]	104.71 50.20	May 2001 – Dec 2010	1.44	-	-	-	-	Jun 2001 – Jan 2011	11.2
Flin Flon MB [b]	101.88 54.77	Jul 2008 – Jun 2011	3.75	Jul 2010 – Mar 2011	2.06	3.4	10.4	Sep 2009 – Dec 2010	59.9
Churchill MB [f, i]	94.07 58.75	-	-	Mar – Apr 2004	1.52	100.9	168.5	Jun 2006 – Dec 2007	5.3
ELA ON [d,e,i]	93.72 49.66	-	-	May 2005 – Dec 2010	1.4	3.7	6.5	Nov 2009 – Jan 2011	9.6
Dorset ON [d, j, k]	78.93 45.22	-	-	Jul 2008 – Mar 2010	1.38	2.7	5.9	Jan 1997 – Dec 1998	9.7
Windsor ON [l]	83.01 42.18	Jan 2007 – Dec 2008	1.93	-	-	-	-	-	-
Burnt Island ON [c]	82.95 45.81	May 1998 – Dec 2007	1.55					Nov 2001 – Mar 2003	9.2
Mississauga ON [k]	79.65 43.54			Jan – Dec 2009	1.4	3.7	6.5		
Egbert ON [c,d,e]	79.78 44.23	Dec 1996 – Dec 2010	1.58	-	-	-	-	Mar 2000 – Jan 2011	8.4
Buoy ON [c]	79.45	Jul – Sep 2005	1.70	-	-	-	-	-	-

	43.40								
Kuujjuarapik QC [c]	77.73 55.30	Aug 1999 – Sep 2009	1.68	-	-	-	-	-	-
Point Petre ON [c]	77.15 43.84	Nov 1996 – Dec 2007	1.75	-	-	-	-	Nov 2001 – Mar 2003	9.1
Chapais QC [d,e]	74.98 49.82	-	-	-	-	-	-	Dec 2009 – Jan 2011	6.4
St. Anicet QC [b,c,d]	74.03 45.20	Aug 1994 – Dec 2009	1.60	Jan 2003 – Dec 2010	1.52	3	17.5	Apr 1998 – Aug 2007	7.9
St. Andrews NB [c,d]	67.08 45.08	Jan 1996 – Jul 2007	1.38	-	-	-	-	Jul 1996 – Dec 2003	6.6
Kejimkujik NS [c,d,e]	65.21 44.43	Jan 1996 – Dec 2010	1.40	Jan 2009 – Dec 2011	1.34	0.5	4.2	Jul 1996 – Jan 2011	5.2
Halifax NS [b]	63.67 44.67			Oct 2009 – Dec 2011	1.68	2.1	2.3		
Mingan QC [b,c]	64.17 50.27	Jan 1997 – Dec 2000	1.57	-	-	-	-	Apr 1998 – Aug 2007	5.0
Southampton PE [c]	62.58 46.39	Jan 2005 – Dec 2006	1.23	-	-	-	-	-	-
Alert NU [a]	62.33 82.50	Jan 1995 – Dec 2011	1.51	Jan 2002 – Dec 2011	1.26	21.8	41.1	-	-
Stephenville NL [d,e]	58.57 48.56	-	-	-	-	-	-	Feb 2010 – Jan 2011	5.6
Cormak NL [d,e]	57.38 49.32	-	-	-	-	-	-	May 2000 – Jul 2010	4.2

Legenda: a) Northern Contaminants Program (NCP); b) Clean Air Regulatory Agenda Mercury Science Program (CARA) currently Climate Change and Air Pollution program (CCAP); c) Canadian Atmospheric Mercury Measurement Network (CAMNet); d) The Mercury Deposition Network (MDN); e) The Canadian Air and Precipitation Monitoring Network (CAPMoN); f) Geological Survey of Canada (GSC); g) Intercontinental Atmospheric Transport of Anthropogenic Pollutants to the Arctic (INCATPA); h) Joint Oil Sands Monitoring Program (JOSM); i) University of Alberta; j) Ontario Ministry of the Environment (MOE); k) University of Toronto; l) University of Windsor. Long = Longitude; Lat = Latitude.

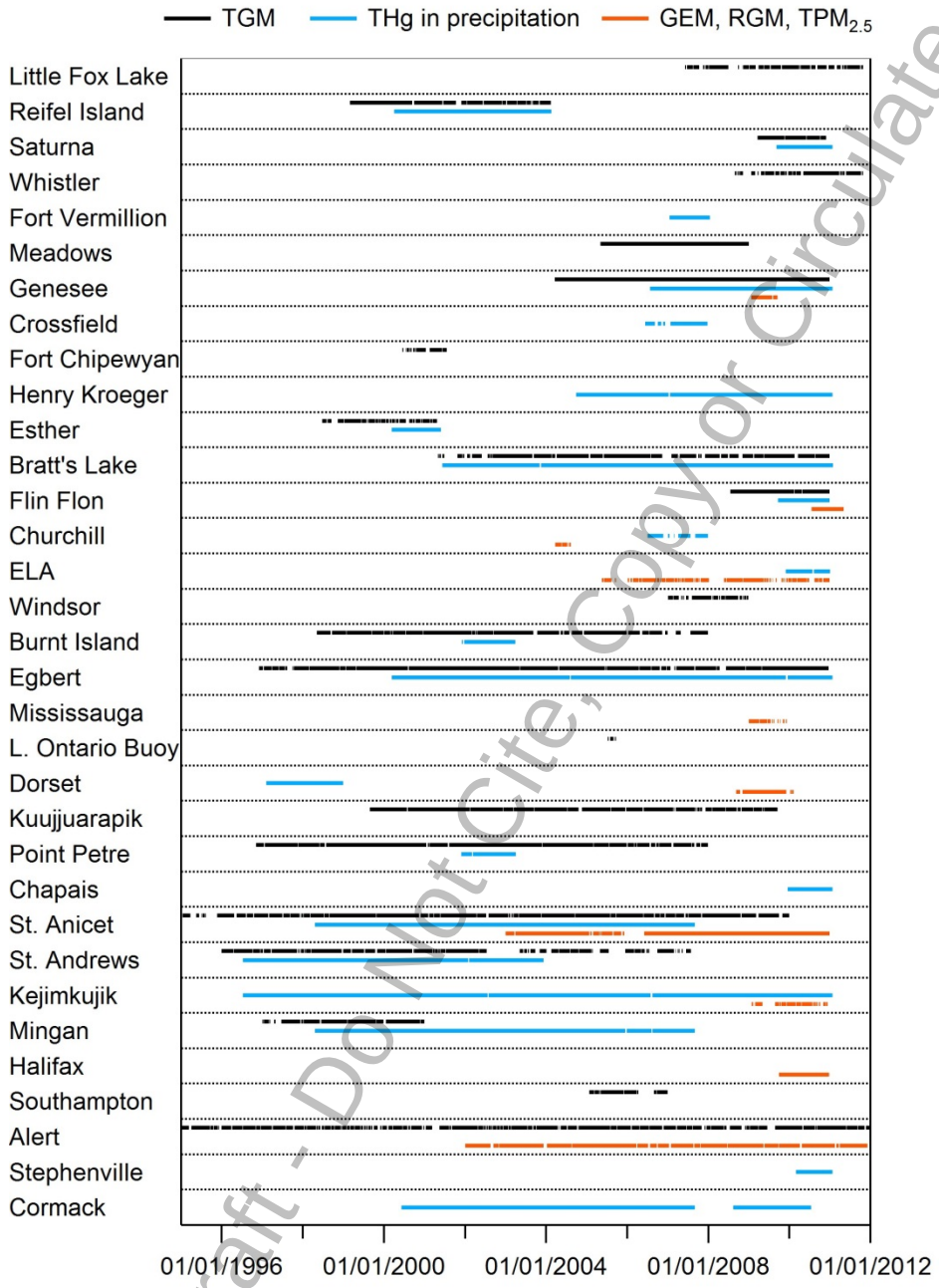

Figure 2: Time period of mercury measurements at Canadian monitoring sites

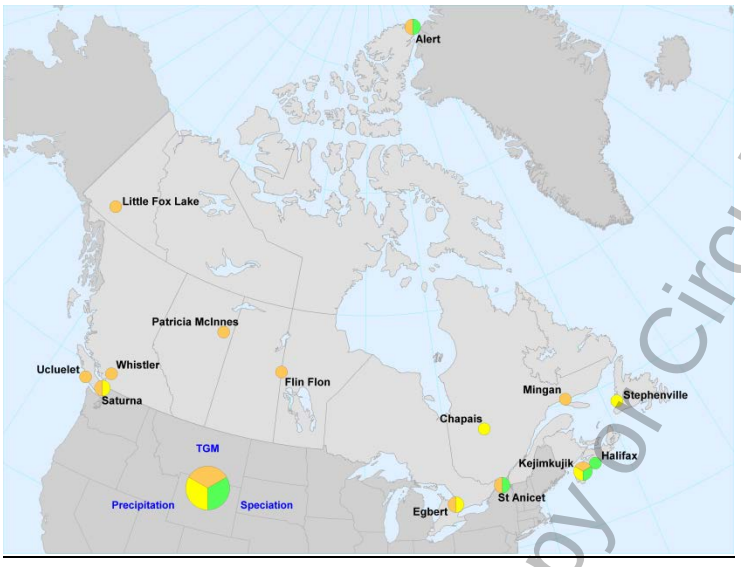

Figure 3: Environment and Climate Change Canada – Atmospheric Mercury Monitoring sites currently operating in Canada as of January 2017.

Trends of mercury over time have been investigated for many Canadian measurement sites for all 3 atmospheric mercury parameters including TGM, speciated mercury and mercury in precipitation (Cole et al., 2014). A minimum of 5 yr. of data were required to perform the trend analysis. The time period over which data are reported differs for each location. As a result, linear trends were estimated for all available data from each site rather than limiting the analysis to only overlapping time periods. Trends were calculated using the seasonal Kendall test for trend and the related Sen's slope calculation (Gilbert, 1987; van Belle and Hughes, 1984). This method is an extension of the non-parametric Mann-Kendall test for trend, which is recommended when there are missing values and when the data are not normally distributed; both of these conditions apply to these datasets.[1] Table XX summarizes the calculated trends of mercury in Canada over time for data sets that fall within the above parameters. The areas shaded in blue are currently operated sites in Canada.

[1] In the seasonal Kendall method, data from the 12 months are treated as 12 separate datasets. For each month, the presence of a trend is confirmed or rejected by the Mann-Kendall test, and a slope is estimated using Sen's nonparametric estimator of slope. An overall annual trend is estimated from the monthly trend statistics; however, this estimate may be questionable if the monthly trends are not homogeneous. Thus, to ensure reliability of the data, a test for seasonal homogeneity was performed as well. If seasonal trends were homogeneous, the results were used to determine an overall trend for the entire period. If they were not homogeneous, or when there was insufficient data in certain months, only trends for individual months were reported. The disadvantage of this technique is that it produces a linear trend over the entire period and can miss complex patterns such as a decrease followed by an increase.

6350

Station	Measurement period TGM	Trend TGM (% yr^{-1})	Measurement period GEM/RGM/PHg	Trend GEM	Trend RGM	Trend PHg	Measurement period wet deposition	Trend Total Hg in precip
Little Fox Lake YK	Jun 2007 – Oct 2011		-	-	-	-	-	-
Ucluelet BC			-	-	-	-	-	-
Reifel Island BC	Mar 1999 – Feb 2004	-3.3 (-4.2 to -2.4)	-	-	-	-	-	-
Saturna BC	Mar 2009 – Dec 2010		-	-	-	-	Sep 2009 – Jan 2011	
Whistler BC	Aug 2008 – Oct 2011		-	-	-	-	-	-
Genesee AB	Mar 2004 – Dec 2010	-0.4 (ns) (-1.4 to +0.1)	-	-	-	-	Jul 2006 – Jan 2011	
Fort McKay South, AB			-	-	-	-	-	-
Patricia McInnis AB	Oct 2010 – Dec 2016		-	-	-	-	-	-
Henry Kroeger AB	-	-	-	-	-	-	Oct 2004 – Jan 2011	-
Bratt's Lake SK	2001 – 2010	-2.5 (-3.4 to -1.6)	-	-	-	-	-	-
Flin Flon MB	Jul 2008 – Jun 2011		-	-	-	-	-	-
ELA ON	-	-	May 2005 – Dec 2010	-	-	-	-	-
Burnt Island ON	1998 –2007	-2.5 (-3.4 to -1.6)		-	-	-	-	-
Egbert ON	1996 – 2010	-1.3 (-1.7 to -1.0)	-	-	-	-	2000-2010	-2.1 (-3.7 to -0.6)
Point Petre ON	1996 – 2007	-1.7 (-2.2 to -1.2)	-	-	-	-	-	-
Chapais QC	-	-	-	-	-	-	Dec 2009 – Jan 2011	
St. Anicet QC	1995 – 2009	-1.5 (-1.8 to -1.2)	Jan 2003 – Dec 2010				1998 – 2007	-3.7 (-6.5 to -0.3)
St. Andrews NB	1996 - 2007	-1.0 (-1.4 to -0.5)	-	-	-	-	Jul 1996 – Dec 2003	-
Kejimkujik NS	1996 – 2010	-0.9 (-1.1 to -0.6)	Jan 2009 – Dec 2011				1996 – 2011	-2.2 (-3.5 to +0.3)

6351 **Table 7** Annual trends over time of mercury data collected in Canada

6352 ### 2.2.4 Atmospheric mercury in Asia

6353 Before the establishment of the GMOS global network independent programs and networks for
6354 monitoring atmospheric Hg species and deposition have been developed in Asia, such as those in Korea,
6355 Japan, China, and Chinese Taiwan supported by the National Science Foundation in each of the Asian
6356 countries and region. Since 2010, some of these Asian sites have been incorporated within the global
6357 network (Sprovieri et al., 2016), including Mt. Waliguan, Mt. Ailao, Shangri-La and Mt. Changbai in
6358 mainland China, Lulin in Chinese Taiwan, Cape Hedo, Okinawa and Minamata, Kyushu islands in Japan,
6359 Kanghwa Island in Korea, and Kodaikanal in India. A statistical summary of speciated atmospheric Hg
6360 concentrations and associated site information (urban and remote areas) in Asia is shown in Table 8
6361 whereas Table 9 reports Hg concentrations and deposition fluxes in precipitation, throughfall, and

litterfall. GEM and PBM concentrations recorded at remote Chinese sites are elevated compared to that observed at background/remote areas in Europe and North America, and at others sites in the Northern Hemisphere (Sprovieri et al., 2016; Fu et al., 2015). In Chinese urban areas, the highly elevated GEM, GOM and PBM were mainly derived from local anthropogenic Hg emissions, whereas regional anthropogenic emissions and long-range transport from domestic source regions are the primary causes of the elevated GEM and PBM concentrations at remote sites (Fu et al., 2015). Mean GOM concentrations at remote sites in China ranged from 2.2 to 10.1 pgm^{-3}, significantly lower than those observed in the Chinese urban areas but comparable to the values in Europe and North America (Fu et al., 2015; Table 4).

Wet-only deposition fluxes of THg and MeHg ranged between 1.8–7.0 $\mu gm^{-2}\ yr^{-1}$ and 0.01–0.06 $\mu gm^{-2}yr^{-1}$, respectively, at remote sites, and 13.4-56.5 $\mu g\ m^{-2}\ yr^{-1}$ and 0.05–0.28 $\mu g\ m^{-2}\ yr^{-1}$ at urban sites, respectively. Wet deposition fluxes of THg and MeHg at urban sites in China were higher compared to those in North America and Europe, but wet deposition fluxes of THg at remote sites were in the lower range of those observed in North America and Europe. Regarding the Chinese GMOS sites, details on THg recorded from 2011 to 2015 are reported in Table 9.

Table 8: Atmospheric Hg concentrations at ground-based stations in Asia (Fu et al., 2015).

Site	Country	Elev (m asl)	Lat	Lon	Type	Study period	TGM or GEM Mean ± St.Dev. (ng m^{-3})	PBM/TPM Mean ± St.Dev. (pg m^{-3})	GOM Mean ± St.Dev. (pg m^{-3})	Reference
An-myun	Korea	45.7	36.533°N	126.317°E	Background	12/2004-04/2006	4.61 ± 2.21	-	-	Nguyen et al. (2007)
Beijing	China	48	38.898° N	116.392° E	Urban	02&09/1998	10.40 ± 3.25	-	-	Liu et al. (2002)
						01-12/2006	-	272	-	Schleicher et al. (2015)
							-	573 ± 551*	-	
Cape Hedo	Japan	60	26.864° N	128.251° E	Background	01/2011-03/2015	1.91 ± 0.48	3.17 ± 4.41	1.89 ± 3.16	Sprovieri et al. (2016a)
Changchun	China	270	43.824° N	125.319° E	Urban	-/2001	18.4	276*	-	Fang et al. (2004)
Chemgshantou	China	30	37.38° N	122.68° E	Remote coast	07&10/2007, 01&04/2009	2.31 ± 0.74		-	Ci et al. (2011)
Chongming Island	China	11	31.522° N	121.908° E	Remote coast	9/12/2009	2.50 ± 1.50	-	-	Dou et al. (2013)
Chongqing	China	350	29.6° N	106.5° E	Urban	08/2006-09/2007	6.74 ± 0.37	-	-	Yang et al. (2009)
Guangzhou	China	60	23.124° N	113.355° E	Urban	11/2010-10/2011	4.60 ± 1.60	-	-	Chen et al. (2013)
Guiyang	China	1040	26.57°N	106.72° E	Urban	11/2011-11/2012	8.40 ± 4.87	-	-	Feng et al. (2004)
						12/2009-11/2010	10.2 ± 7.06	-	-	Fu and Feng (2015)
						08-12/2009	9.72 ± 10.2	368 ± 276	35.7 ± 43.9	Fu et al. (2011)
Jeju Island	Korea	60	33.283°N	120.167°E	Remote coast	05/2006-05/2007	3.85 ± 1.68	-	-	Nguyen et al. (2010)
Jiaxing	China	10	30.833° N	120.7° E	Urban	09/2005	5.40 ± 4.10	-	-	Wang et al. (2007)
Lanzhou	China	1540	36.067° N	103.79° E	Urban	-/2004	28.6	-	-	Su et al. (2007)
						04&07&10&12/1994	-	955*	-	Duan and Yang (1995)
Lulin	Chinese Taipei	2862	23.51°N	120.92° E	Background	04/2006-12/2007	1.73 ± 0.61	2.3 ± 3.9	12.1 ± 20.0	Sheu et al. (2010)
Minamata[T]	Japan	20	32.231°N	130.403° E	Rural	04/2011-12/2014	1.89 ± 0.43	-	-	Sprovieri et al. (2016a)
Miyun	China	220	40.481°N	116.775° E	Remote forest	12/2008-11/2009	3.22 ± 1.94	98.2 ± 113	10.1 ± 18.8	Zhang er al. (2013)
Mt. Ailao	China	2450	24.533°N	101.017° E	Remote forest	05/2011-05/2012	2.09 ± 0.63	31.3 ± 28.0	2.2 ± 2.3	Zhang et al. (2015b)
Mt. Changbai	China	740	42.402°N	128.112° E	Remote forest	10/2008-10/2010	1.60 ± 0.51	-	-	Fu et al. (2012b)
						07/2013-07/2014	1.73 ± 0.48	18.9 ± 15.6	5.7 ± 6.8	Fu et al. (2014)
Mt. Damei	China	550	29.632°N	121.565° E	Remote forest	04/2011-04/2013	3.31 ± 1.44	154 ± 104	6.3 ± 3.9	Yu et al. (2015)
Mt. Dinghu	China	700	23.164°N	112.549° E	Remote forest	09/2009-04/2010	5.07 ± 2.89	-	-	Chen et al. (2013)
Mt. Gongga	China	1640	29.649° N	102.117° E	Remote forest	05/2005-07/2007	3.98 ± 1.62	30.7 ± 32.0*	6.2 ± 3.9	Fu et al. (2008)
Mt. Jiuxian	China	1700	25.71° N	118.11° E	Remote forest	11/2010. 01&04&08/2010	-	24.0 ± 14.6	-	Xu et al. (2013)
Mt. Leigong	China	2178	26.39° N	108.2° E	Remote forest	05/2008-05/2009	2.80 ± 1.51	-	-	Fu et al. (2010)
Mt. Walinguan	China	3816	36.287°N	100.898°E	Remote grassland	09/2007-09/2008	1.98 ± 0.98	19.4 ± 18.0	7.4 ± 4.8	Fu et al. (2012a)
Nanjing	China	100	32.05° N	118.78° E	Urban	01-12/2011	7.90 ± 7.00	-	-	Zhu et al. (2012)
						06/2011-02/2012		1100 ± 570*	-	Zhu et al. (2014)
Ningbo	China	10	29.867° N	121.544° E	Urban	10/2007-01/2008	3.79 ± 1.29	-	-	Nguyen et al. (2011)
Qingdao	China	40	36.16° N	120.5° E	Urban	01/2013	2.80 ± 0.90	245 ± 174*	-	Zhang er al. (2014)
Seul	Korea	17	37.514° N	127.001° E	Urban	02/2005-02/2006	3.22 ± 2.10	23.9 ± 19.6	27.2 ± 19.3	Kim et al. (2009)
Shangai	China	19	31.23° N	121.54° E	Urban	08-09/2009	2.70 ± 1.70	-	-	Friedli et al. (2011)
						07/2004-04/2006	-	560 ± 220*	-	Xiu et al. (2009)
Shangri-La	China	3580	28.017° N	99.733° E	Remote forest	11/2009-10/2010	2.55 ± 2.73	37.8 ± 31.0	7.9 ± 7.9	Zhang er al. (2015)
Southeastern coastal cities	China	-	-	-	Urban	11/2010, 01&04&08/2011	-	141 ± 128	-	Xu et al. (2013)
Tokai-mura	Japan	15	36.27°N	140.36°E	Urban	10/2005-08/2006	3.78 ± 1.62	-	-	Osawa et al. (2007)
Wanqingsha	China	3	22.7° N	113.55° E	Remote coast	11/12/2009	2.94	-	-	Li et al. (2011)
Wuhan	China	20	30.6° N	114.3° E	Urban	-/2002	14.8		-	Xiang and Liu (2008)
Xiamen	China	7	24.60° N	118.05° E	Urban	03/2012-02/2013	3.50 ± 1.61	174 ± 280	61 ± 69	Xu et al. (2015)

*(PBM/TPM: * Indicates TPM (total particulate-bound mercury) and the rest indicate PBM (particulate-bound mercury on particles with an aerodynamic diameter < 2.5 μm)*

6378
6379

6380 **Table 9:** Hg concentrations and deposition fluxes in precipitation, throughfall, and litterfall in China
6381 (from Fu et al., 2015).
6382

Site	Elev (m asl)	Lat	Lon	Type	Study period	Samples	Hg concentration (ng L^{-1} or ng g^{-1})		Deposition flux ($\mu g\ m^{-2}\ yr^{-1}$)		Reference
							THg	MeHg	THg	MeHg	
Mt. Ailao, Yunnan	2500	24,53	101,02	Remote	06/2011-05/2012	Precipitation	3,0	-	5,4	-	Zhou et al. (2013)
						Litterfall	54,0	-	71,2	-	
Mt. Leigong, Guizhou	2178	26,39	108,20	Remote	05/2008-05/2009	Precipitation	4,0	0,04	6,1	0,06	Fu et al. (2010b)
						Throughfall	8,9	0,1	10,5	0,12	
						Litterfall	91,0	0,48	39,5	0,28	
Mt. Damei, Zhejiang	550	29,63	121,57	Remote	08/2012-07/2013	Precipitation	4,1	-	7,0	-	Lang (2014)
						Litterfall	46,6	-	26,0	-	
Nam Co, Tibet	4730	30,77	90,99	Remote	07/2009-07/2011	Precipitation	4,8	0,03	1,8	0,01	Huang et al. (2012)
Mt. Gongga[1], Suchuan	1640	29,65	102,12	Remote	12/01/06	Precipitation*	9,9	-	9,1	-	Fu et al. (2008)
Mt. Gongga[2], Suchuan	3000	29,58	101,93	Remote	05/2005-04/2007	Precipitation*	14,2	0,16	26,1	0,3	Fu et al. (2010a)
						Throughfall	40,2	0,3	57,1	0,43	
						Litterfall	35,7	-	35,5	-	
Mt. Changbai, Jilin	750	42,40	128,47	Remote	08/2005-07/2006	Precipitation*	13,4	-	8,4	-	Wan et al. (2000a)
Puding, Guizhou	1145	26,37	105,80	Remote	08/2005-07/2006	Precipitation*	20,6	0,18	24,8	0,22	Guo et al. (2008)
Hongjiadu, Guizhou	1130	26,88	105,85	Remote	08/2005-07/2006	Precipitation*	39,4	0,18	34,7	0,16	Guo et al. (2008)
Yinzidu, Guizhou	1088	26,57	106,12	Remote	08/2005-07/2006	Precipitation*	35,7	0,18	38,1	0,19	Guo et al. (2008)
Dongfeng, Guizhou	970	26,85	106,13	Remote	08/2005-07/2006	Precipitation*	37,4	0,2	36,3	0,19	Guo et al. (2008)
Wujiangdu, Guizhou		27,32	106,77	Remote	08/2005-07/2006	Precipitation*	57,1	0,25	39,6	0,17	Guo et al. (2008)
Guiyang	1040	26,57	106,72	Urban	09/07/08	Precipitation	13,3	0,05	13,4	0,05	Liu et al. (2011)
Xiamen	50	24,60	118,31	Urban	07/2013-02/2014	Precipitation	26,6	-	30,4	-	Wu (2014)
Chongqing				Urban	06/2010-06/2011	Precipitation	30,7	0,31	28,7	0,28	Wang et al. (2012); Y.M. Wang et al. (2014)
Tieshanping, Chongqing	500	29,63	104,68	Urban	03/2005-03/2006	Precipitation	32,3	-	29,0	-	Wang er al. (2009)
						Throughfall	69,7	-	71,3	-	
						Litterfall	105	-	220	-	
Nanjing	100	32,05	118,78	Urban	06/2011-02/2012	Precipitation	52,9	-	56,5	-	Zhu et al. (2014)

*(Precipitation: * indicates bulk precipitation and the rest indicate wet-only precipitation. Mt. Gongga: [1] elevation of the sampling site was 1600m above sea level. [2] Elevation of the sampling site was 3000m above sea level).*

6383
6384
6385

6386 3.2.5 Mercury concentrations and pattern analysis in polar areas (Arctic and
6387 Antarctica)

6388 Arctic ecosystems and indigenous communities are particularly vulnerable to methylmercury exposures
6389 due to its biomagnification in many traditionally consumed foods such as birds, fish and marine
6390 mammals. In order to reduce negative health effects associated with methylmercury exposures, the
6391 pathway from emissions to human and environmental impacts needs to be understood. Atmospheric
6392 modelling provides a first step by tracing the link from emissions to deposition onto environmental
6393 surfaces. Deposition of mercury in a particular region depends on the magnitude and speciation of
6394 domestic and foreign emissions and on the oxidative capacity of the atmosphere that transforms
6395 gaseous elemental mercury (GEM) to deposited divalent species (UNEP, 2015). Atmospheric deposition
6396 is partly offset by the re-emission of a fraction of deposited mercury. Atmospheric Hg deposition from
6397 different models compares fairly well (add reference). Further detailed information on modelling
6398 uncertainty and scenario analysis can be found in Chapter 4 of this GMA report.

Located far from anthropogenic emissions, Polar Regions can be seen as open-air laboratories to improve our understanding of these atmospheric processes.

The Arctic Monitoring and Assessment Programme (AMAP) established in 1991, is a coordinated air monitoring programme covering the circum-Arctic areas of North America and Eurasia. The AMAP programme has an active ambient air Hg monitoring component with sites in Canada, USA, Russia, Norway and Greenland (Denmark). The Global Atmospheric Watch (GAW) site at Alert operated by Environment and Climate Change Canada – and funded through the Northern Contaminants Program (NCP) of Indigenous and Northern Affairs Canada (INAC) – has the longest continuous record of GEM (22 years) and Hg speciation (15 years) in the Arctic (Cole et al., 2013; Steffen et al., 2014). Continuous monitoring for long periods has also occurred at: (1) Amderma (Russia) (Steffen et al., 2005), (2) GAW Ny-Ålesund 'Zeppelin' site (Svalbard, Norway) (Berg et al., 2013), (3) AMAP Villum Research Station at Station Nord (hereafter named Station Nord, Greenland-Denmark) (Skov et al., 2004), and (4) Andøya (northern Norway) (Berg et al., 2001). Four multi-year records over the 2011-2015 period from high arctic (Alert, Station Nord and Zeppelin) and European sub-arctic (Andøya) sites were recently analysed (Angot et al., 2016a). Additionally, summertime measurements were performed in 2004 over the North Atlantic Ocean (Aspmo et al., 2004), and in 2005, 2010 and 2012 in the marine boundary layer over the Arctic Ocean (Sommar et al., 2010, Yu et al., 2014).

		ALT	SND	NYA	AND	TR	DC	DDU
2011	*n*	8040	4712	8173	7444	5978	NA	NA
	mean	1.39	1.26	1.51	1.61	0.95	NA	NA
	median	1.35	1.34	1.59	1.61	0.99	NA	NA
	SD	0.45	0.32	1.61	0.15	0.20	NA	NA
2012	*n*	8447	7932	8181	8428	7808	3761	5949
	mean	1.21	1.44	1.51	1.61	0.98	0.76	0.91
	median	1.21	1.44	1.54	1.61	0.97	0.70	0.92
	SD	0.35	0.26	0.21	0.13	0.15	0.24	0.20
2013	*n*	8048	6605	6980	7862	8197	2900	5121
	mean	1.31	1.57	1.47	1.53	0.90	0.84	0.85
	median	1.39	1.49	1.52	1.56	0.93	0.87	0.85
	SD	0.46	0.44	0.30	0.15	0.15	0.27	0.19
2014	*n*	8358	4991	6730	8146	7421	NA	1958
	mean	1.45	1.36	1.48	1.50	0.95	NA	0.85
	median	1.45	1.36	1.57	1.51	1.00	NA	0.82
	SD	0.33	0.35	0.33	0.16	0.21	NA	0.38
2015	*n*	NA	1059	8342	7146	3670	8383	3114
	mean	NA	1.11	1.49	1.50	0.94	1.06	0.86
	median	NA	1.11	1.49	1.50	0.93	1.12	0.87
	SD	NA	0.32	0.21	0.10	0.31	0.41	0.19

Table 10: Annually based statistics (number of hourly-averaged data (n.), mean, median, standard deviation (SD), of Hg(0) concentrations (in ng m^{-3}) at ground-based polar sites over the 2011-2015 period.

While the Arctic has been extensively monitored, with hundreds of publications focusing on AMDEs, measurements are more sporadic in Antarctica. Several short-term ambient air measurements campaigns were carried out in summer in the 2000s at Terra Nova Bay, McMurdo, South Pole and Concordia stations (Sprovieri et al., 2002; Brooks et al., 2008a, b; Dommergue et al., 2012). A year-round record (January 2000-February 2001) was reported at Neumayer (Ebinghaus et al., 2002; Temme et al., 2003) while multi-year records of GEM were initiated at the Norwegian Antarctic Research Station, Troll (TR) in 2007 (Pfaffhuber et al., 2012). In 2012, GMOS (2011-2015) supported the implementation of two other monitoring stations: Dumont d'Urville on the East Antarctic coast and Concordia station on the East Antarctic ice sheet (Angot et al., 2016b, c). Monitoring at Concordia station is now supported by the French Polar Institute IPEV. Additionally, short-term field campaigns dedicated to atmospheric Hg (Nerentorp Mastromonaco et al., 2016; Wang et al., 2016) and Hg deposition (Han et al., 2011; 2014; 2017) were performed in recent years over the Austral Ocean and the East Antarctic ice sheet, producing supplementary data. In Nerentorp Mastromonaco et al., 2016, the authors suggested a seasonal increase of total mercury in the sea-water due to a contribution of Hg(II) deposition combined with contributions from melting sea ice and snow.

First discovered in 1995 (Schroeder et al., 1998), atmospheric mercury depletion events (AMDEs) are observed in springtime throughout the Arctic (Lindberg et al., 2001; Berg et al., 2003a; Poissant and Pilote, 2003; Skov et al., 2004; Steffen et al., 2005) as a result of the oxidation of GEM by reactive bromine species (Lu et al., 2001; Brooks et al., 2006; Sommar et al., 2007). AMDEs can lead to the deposition of ~100 t of mercury per year to the Arctic (Ariya et al., 2004; Skov et al., 2004; Dastoor et al., 2015). The fraction of mercury retained in snowpack during AMDEs is still a matter of debate in the scientific mercury community because a number of studies have observed rapid revolatilization (Steffen et al., 2008; Soerensen et al., 2016).

Several studies have reported significant re-emission (e.g., Ferrari et al., 2005; Brooks et al., 2006; Kirk et al., 2006; Sommar et al., 2007; Dommergue et al., 2010a) reducing the amount of mercury that accumulates within the snowpack (Hirdman et al., 2009; Larose et al., 2010). Until today no one has determined a net accumulation based on flux measurements of wet deposition, dry deposition and reemission. During AMDEs, dramatically higher levels of both gaseous oxidised mercury (GOM; formerly named reactive gaseous mercury, RGM) and/or $PBM_{2.5}$ are observed (Lu et al., 2001; Lindberg et al., 2002; Lu and Schroeder, 2004; Sprovieri et al., 2005; Steffen et al., 2008). Lindberg et al. (2002) for instance reported GOM concentrations up to 900 pg m^{-3} during an AMDE at Barrow (Alaska) and

showed a strong positive correlation between GOM production and both UV-B radiation and surface snow Hg concentrations. Preliminary multi-year trends of GOM and $PBM_{2.5}$ concentrations at Alert were analysed (Cole et al., 2013), indicating increases from 2002 to 2009 in both GOM and $PBM_{2.5}$ during spring when concentrations are highest. Steffen et al. (2014) investigated the behaviour of the GOM and $PBM_{2.5}$ over 10 years at Alert and showed that there is a transition to a regime of high $PBM_{2.5}$ levels in March and April to a regime of high GOM levels in May. This transition was found to be driven by air temperature and presence of springtime particles (sea salts and arctic haze). They further reported that the highest deposition of mercury to the snow occurs when the GOM levels peak and not when $PBM_{2.5}$ levels are highest. They concluded that, using this information, one can predict when the most mercury will be deposited to the snow and ice surfaces in the high Arctic. Despite the significant challenges in the measurements, the behaviour of mercury over the Arctic sea ice has been investigated (Nghiem et al., 2012; Steffen et al., 2013; Moore et al, 2014). Nghiem et al (2012) showed that the ever decreasing amount of perennial sea ice in the Arctic Ocean will impact the amount of active bromine in this area. Since the depletion of GEM is driven by the bromine photochemistry, the decrease in perennial sea ice will certainly impact the amount of mercury depleted in the atmosphere over the Arctic sea ice. Further, Moore et al. (2014) showed that with the changes of sea ice from perennial to annual, the dynamics of the sea ice also change. Annual sea ice creates more dynamic sea ice, enabling it to provide more turbulence within the ice and produce more open leads. These open leads cause convective forcing of the overlying atmosphere to pull down air masses that contain more mercury than those which are depleted at the surface and replenish the pool of mercury available for conversion and eventual deposition. Finally, it has also been shown that some of the mercury deposited to the surfaces is reemitted to the atmosphere (references above); however, several studies have shown that photo-reduction of the mercury in the snow is dependent on the amount of chlorine in the surface snow (Poulain et al., 2004 and Lehnherr and St Louis, 2009). Thus, the more chlorine in the snow, the less mercury will reemit. Steffen et al. (2013) demonstrated that there is significantly more GEM re-emitted to the atmosphere from inland snow that from snow over the sea ice. All of these studies combined demonstrate that the mercury chemistry in the Arctic is very dependent on the sea ice and its overlying atmosphere. With significant changes occurring in the Arctic and the dynamics of the sea ice, the springtime mercury cycle will be impacted including the amount of mercury deposited and retained in the Arctic ecosystem.

As presented in Fig. 4, a different seasonal pattern is observed in the high Arctic (ALT, SND, NYA – latitude ranging from 78 to 82°N) as compared to lower latitudes (AND, northern Norway - 69°N). As noted by Angot et al. (2016a), a variability is observed at high Arctic sites in spring due to the occurrence of AMDEs (see above). Summertime (June-August) measurements also differ from what is seen at lower latitudes likely due to re-emission of GEM by the Arctic Ocean and/or by snow surfaces (Angot et al. 2016a and references therein). Yu et al. (2014) reported highly variable GEM concentrations (0.15-4.58 ng m^{-3}) over the central Arctic Ocean in summer, highlighting the need for additional oceanographic campaigns to better understand and constrain oceanic fluxes of GEM.

The analysis of ten-year trends of TGM (GEM+GOM) concentrations (Cole et al., 2013) revealed discrepancies among Arctic sites. While no trend was observed at Zeppelin station, a slight decreasing trend (-0.9% per year) was reported at Alert. This difference in trends may be due to several factors including different air masses origin and local scale processes (e.g., oceanic evasion).

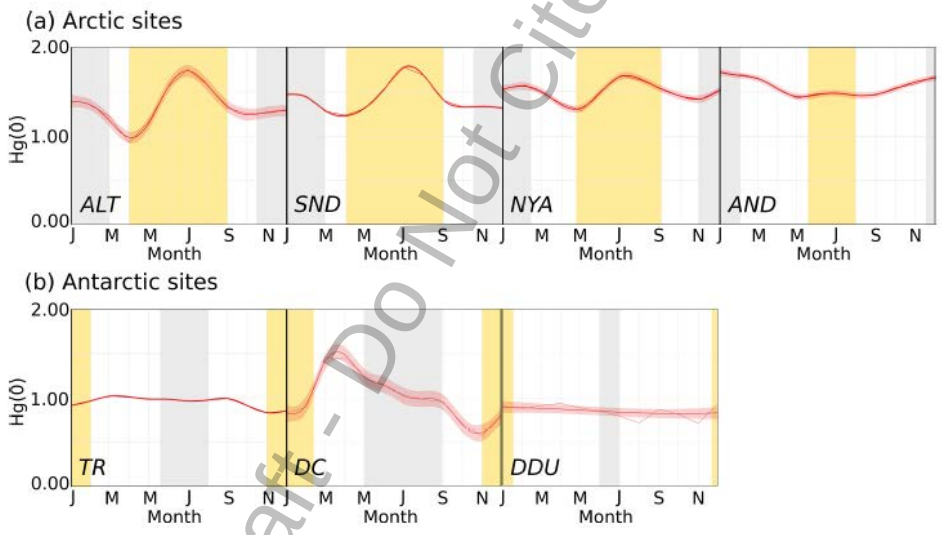

Figure 4: Seasonal variation (monthly mean along with the 95% confidence interval for the mean) of GEM (Hg(0)) concentrations (in ngm^{-3}) at (a) four Arctic and (b) three Antarctic sites for the period 2011-2015 (Angot et al., 2016a). ALT: Alert, SND: Villum Research Station at Station Nord, NYA: Zeppelin station at Ny-Ålesund, AND: Andøya, TR: Troll, DC: Concordia Station at Dome C, DDU: Dumont d'Urville. Periods highlighted in yellow (grey) refer to 24h sunlight (darkness).

Similar to the Arctic, AMDEs can be observed at coastal Antarctic sites after polar sunrise (e.g., Ebinghaus et al., 2002). However, major differences between the Artic and the Antarctic Hg atmospheric cycles have been identified in recent studies, primarily because of their different geography; While the Arctic is a semi-enclosed ocean almost completely surrounded by land, Antarctica is a land mass –

covered with an immense ice shelf – surrounded by ocean. In summer (November to mid-February, permanent sunlight), GEM concentrations exhibit a distinct diurnal cycle on the East Antarctic ice sheet, with a maximum at noon, attributed to a dynamic daily cycle of GEM oxidation, deposition to the snowpack, and re-emission from the snowpack (Dommergue et al., 2012, Angot et al., 2016c, Wang et al., 2016). Additionally, GEM depletion events can be observed on the ice sheet in summer, with GEM concentrations remaining low (~ 0.40 ng m^{-3}) for several weeks (Angot et al., 2016c). These depletion events do not resemble the ones observed in springtime in the Arctic since they are not associated with depletion of ozone. They are observed when air masses stagnate over the East Antarctic ice sheet, likely favouring an accumulation of oxidants within the shallow (few hundreds of meters) atmospheric boundary layer. These observations, along with GOM/ $PBM_{2.5}$ concentrations up to 1 000 pg m^{-3} recorded at South Pole (Brooks et al., 2008), suggest that the inland atmospheric reservoir is depleted in GEM and enriched in GOM in summer. Observations at coastal Antarctic stations suggest that divalent Hg species produced inland can be transported – due to the large-scale airflow pattern flowing from the East Antarctic ice sheet towards the coast (katabatic winds) – leading to Hg deposition and accumulation in coastal ecosystems (Angot et al., 2016b, Bargagli, 2016). Atmospheric models are currently unable to reproduce this complex reactivity (Angot et al., 2016a). Field studies also show that the sea ice environment is a significant interphase between the polar ocean and the atmosphere and should be accounted for when studying how climate change may affect the mercury cycle in polar regions (Nerentorp Mastromonaco et al., 2016b).

3.2.6 Atmospheric mercury measurements and trends in Europe

Heavy metals were considered by the Convention on Long-Range Transboundary Air Pollution (CLRTAP) beginning in the 1980s. At that time, mercury was only of secondary priority, as it was considered that measurements of the relevant chemical forms, and the understanding of chemistry involved, was not mature enough for any regional scale harmonized monitoring to be initiated (EMEP-CCC, 1985). The European Monitoring and Evaluation Programmes (EMEP) first data report on heavy metals (EMEP, 1986) does thus not include any Hg data, even though first measurements were already available at that time. By 1990, the number of sites measuring mercury in air had increased to seven, with sites located in Norway, Sweden, Denmark, Germany and the UK. Mercury was included in the first priority list of measurements for the late 1990s, and since then the number of sites have increased gradually. The CLRTAP Aarhus Protocol on Heavy metals was adopted in 1998, and countries agreed to reduce their

6536 emission rates compared to year 1990 levels. Currently monitoring efforts include about 37 sites across
6537 17 countries (Fig. 5). Considering all years, the total number of sites is 64 sites and 23 countries.

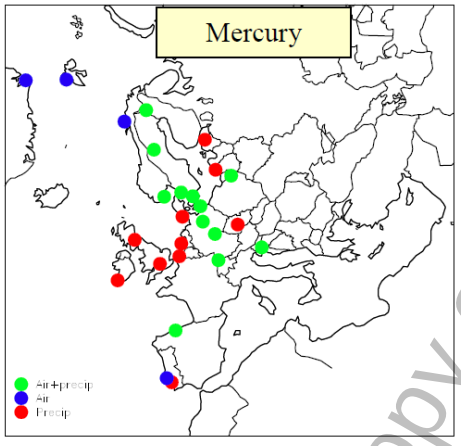

6538
6539 **Figure 5:** EMEP Mercury observation network.
6540

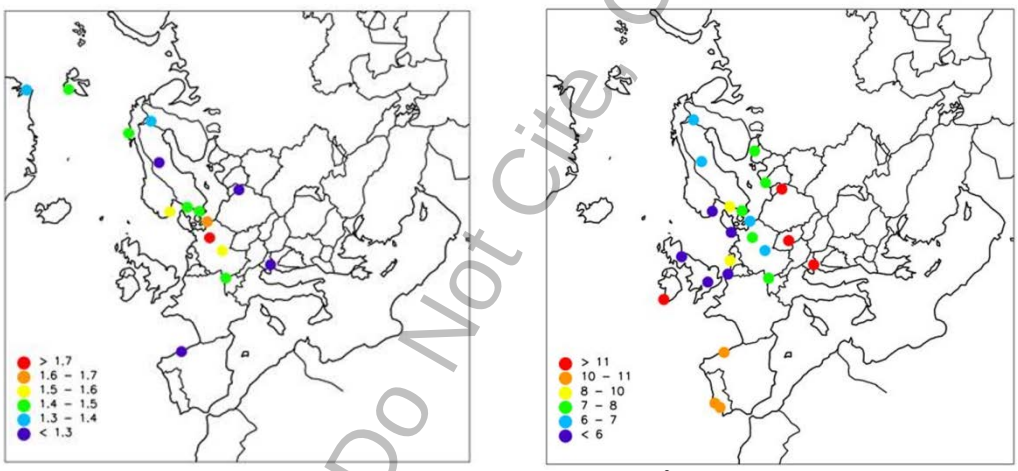

6541
6542 **Figure 6:** Concentration levels of Mercury in air (left, unit: ng/m^3) and precipitation (right, unit ng/L) at
6543 EMEP sites, year 2014.

6544 Compared to other heavy metals, relatively few stations are measuring mercury in precipitation in
6545 Europe, and many of them are related to the OSPARCOM programme. There are several sites (in PT, LV,
6546 IE) with high detection limits and these are only giving an indication of upper concentration limit. There
6547 is no clear regional distribution of mercury in precipitation; the highest concentration is seen at NL0091
6548 with 10 µg/L (when excluding uncertain data from Portugal and Ireland), followed by sites in Czech
6549 Republic and Sweden with concentrations of 8 µg/L, while the lowest levels (less than 5 µg/L) are seen in
6550 Great Britain (7).

6551 Annual averages of Hg concentrations in precipitation and in air in 2014 are presented in Figure 6. There
6552 is indication of elevated level in central Europe as expected due to influence from anthropogenic

sources like coal combustion. An interesting observation is that the coastal Arctic sites in Norway has slightly higher levels than what is observed at Greenland and more inland in Finland and Sweden, which might be due to the summertime evasion from the ocean or due to the fact that Svalbard receives several direct transport episodes from the continent, especially in winter and spring. PL05 and SI08 show unexpected low concentration, 1.2 ng m^{-3} and 0.8 ng m^{-3} respectively. The latter concentration level is even lower than observed in Antarctica (Pfaffhuber et al, 2012). Given the locations of these stations and the proximity to emission sources, it seems like there may be a bias in the concentration level for these two sites. This bias is larger at ES08, which has an annual mean of 0.3 ng m^{-3}, which obviously cannot be correct.

Results from a field intercomparison study of mercury measurement within EMEP performed in 2005 showed that most participating labs performed well and within the +-30% uncertainty EMEP data quality objective (Umweltbundesamt, 2006, Weigelt et al., 2013). However, the biased concentration results reported above highlights the importance to follow QA/QC procedures. These three laboratories need to evaluate their methodology as it seems evident that there is an issue with either calibration or gold trap poisoning, or a combination of both. In precipitation, the highest levels are seen in Eastern Europe (SI, PL and CZ), which seem reasonable since the anthrophonic emission sources are highest in this region. Taking into account that precipitation measurements of mercury are more complex than air measurements, and that the expected measurement uncertainty is 42% (Umweltbundesamt, 2006), the observed concentrations and spatial pattern seems reasonable, for Poland most of the data is below detection limit so it is difficult to fully assess the spatial concentration pattern. Also, Ireland and Portugal report most of the data below detection limit.

Two recent publications and reports present the spatial and temporal trends of mercury in EMEP, namely Tørseth et al. (2012) and Colette et al. (2016). The first paper study provides a very broad introductory overview of the full dataset available, but does not go into any details on site level and individual time series. The latter report focuses primarily on the period 1990-2012, and relies heavily on model results from the EMEP-MSC-E model, using official emissions data. An overall assessment based on these two publications is given below.

Figure 7 presents annual time series of mercury measured at sites with long-term data series across Europe. As can be seen, most of these sites are located in Northern Europe, and there are obvious gaps in the time series in the early 1990s. Inter-annual variability is large, but a significant reduction has

6583 occurred since. Trends based on this analysis suggest reductions in the order of 5-10% since the late
6584 1990s. More recent work by Zhang et al. (2016) suggests declines of greater than 2% per year since the
6585 mid-1990s in Western Europe and a total reduction of greater than 30% due to declines in primary
6586 anthropogenic source releases.

6587

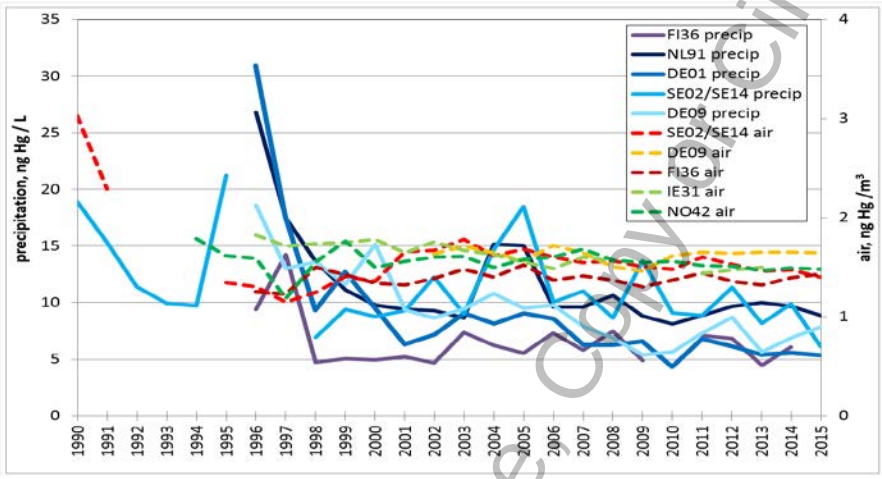

6588
6589
6590 **Figure 7:** Time series of mercury in air and precipitation at selected EMEP stations, 1990-2015.
6591

6592 Tørseth el al., 2012 also include reference to various studies on trends in emissions and observations, to
6593 assess the levels before the late 1980ies. They conclude that a major decline of the European Hg
6594 emissions occurred at the end of the 1980s. The measurements of total gaseous mercury (TGM) for the
6595 period from 1980 to about 1993 indicate a dramatic decrease of about 60% in ambient concentrations.
6596 Concentration changes reflect the emission change in Europe. Reduced emissions in Europe and the long
6597 lifetime of Hg have resulted in an increased focus on non-European sources (HTAP, 2010).
6598 Measurements of total gaseous mercury indicate e.g. a dramatic decrease in concentrations during 1980
6599 to about 1993.

6600 For mercury, the European sources have been reduced significantly resulting in a relatively large
6601 contribution from non-European sources to ambient levels. The monitoring efforts within Europe have
6602 gradually improved in Northern Europe, while other regions have little data.

6603 ### 3.2.7 Northern–Southern Hemispheric gradients

6604 A summary of descriptive statistics of GEM, GOM and PBM from all GMOS sites in the Northern and
6605 Southern Hemispheres as well as in the Tropical area is reported in Tables 2 and 3, whereas Figure 8

shows a focus on GEM yearly distribution for 2013 (blue) and 2014 (green). The sites have been organized in the graphic as well as in the tables according to their latitude from those in the Northern Hemisphere to those in the tropics and in the Southern Hemisphere. The box-and-whisker plot of GEM shows a downward trend with the 13 northern sites which had significantly higher median concentrations than the southern sites did, confirming the assessment made on long-term monitoring sites such as Mace Head (MHD), Ireland (Ebinghaus et al., 2011; Weigelt et al., 2015), and at Cape Point (CPT), South Africa (Slemr et al., 2015). At MHD the annual baseline GEM means observed by Ebinghaus et al. (2011) decreased from 1.82 ngm^{-3} earlier in 1996 to 1.4 ngm^{-3} in 2011, showing a downwards trend of 1.4–1.8% per year. Recently across the GMOS network, a decrease of 1.6% at MHD from 2013 and 2014 was observed and a slight increase in Hg concentrations at CPT from 2007 to 2013 that continued through 2014 (Slemr et al., 2015). The clear north–south gradient, in line also with previous studies (Soerensen et al., 2010a, b, 2012; Sommar et al., 2010; Lindberg et al., 2007; Sprovieri et al., 2010), has in addition confirmed by the probability density functions (PDFs) of the data (Sprovieri et al., 2016).

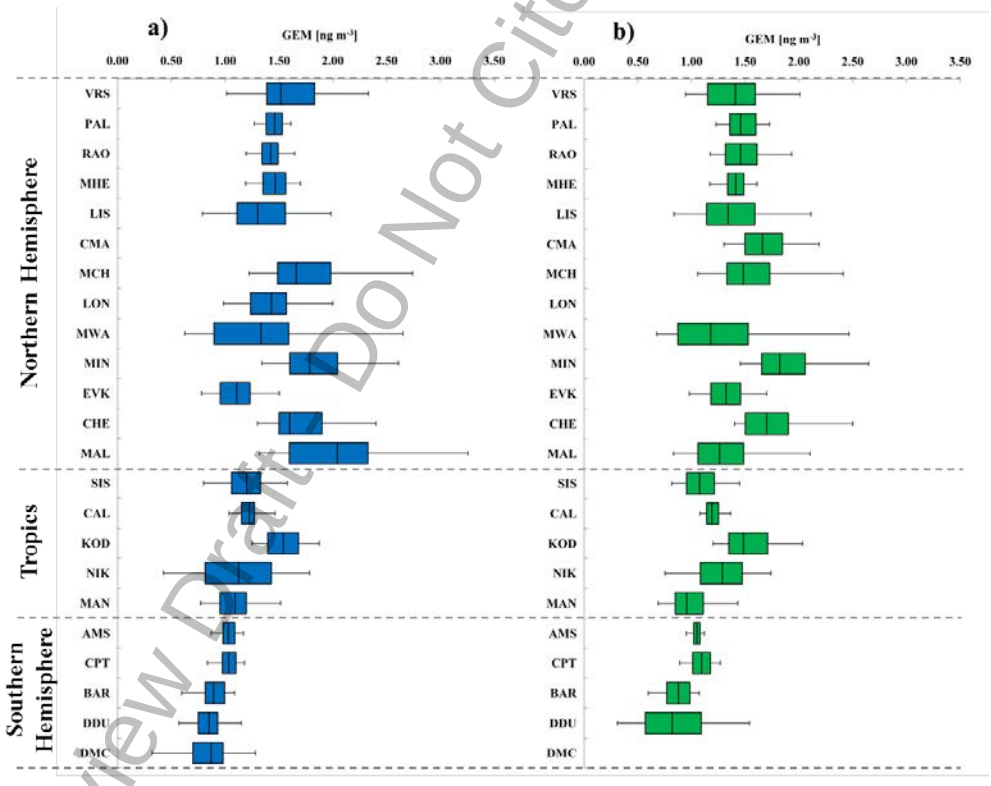

Figure 8: Box-and-whisker plots of GEM yearly distribution at the GMOS stations for (a) 2013 and(b) 2014. The sites are organized according to their latitude from the northern to the southern locations. Each box includes median(midline), 25th and 75th percentiles (box edges), 5th and 95th percentiles (whiskers) (Sprovieri et al. 2016).

3.3 Vertical profile and UTLS measurements

3.3.1 Vertical profiles

Vertical profiling of GEM from inside the boundary layer to the free troposphere was carried out during European Tropospheric Mercury Experiment (ETMEP) flights in 2013 (Weigelt et al. 2015). Several flights were performed with a CASA-212 research aircraft equipped with scientific instruments to measure GEM, GOM, and TGM as well as the trace gases CO, O_3, SO_2, NO, NO_2, and meteorological parameters temperature, pressure, and relative humidity. A specially designed gas inlet system was installed at the aircraft fuselage. In total five vertical profiles were flown over flat and mountainous rural- and industrialized sites in Slovenia and Germany. On the contrary to previously measured vertical profiles, a significant difference between boundary layer- and free tropospheric air was detected. While the free tropospheric overall GEM background concentration over central Europe is ~ 1.3 ng m^{-3} inside the boundary layer the GEM background concentration was found to be 10 to 30% higher (~ 1.6 ng m^{-3}). At all measurement locations, neither in the boundary layer, nor in the free troposphere a clear vertical gradient was apparent. This finding indicates that inside the particular layers of the atmosphere, GEM is homogeneously distributed. The combination of ETMEP measurements over Leipzig with CARIBIC measurement over Western Europe (Fig. 9) revealed for the first time a complete vertical profile from 0.5 km (lower boundary layer) to 10.5 km (upper free troposphere). From above the boundary layer to the free troposphere's top the GEM background concentration is on average 1.3 ng m^{-3}. All concentrations are given at STP (0°C, 1013.25 hPa).

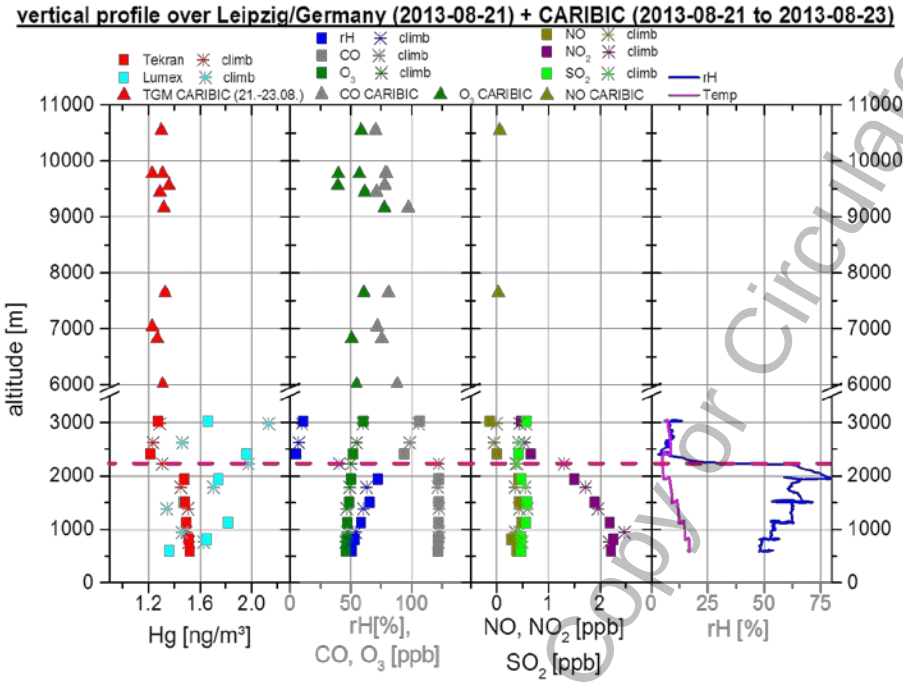

Figure 9: Vertical profile of GEM, CO, O3, SO2, NO, NO2, T, RH over Leipzig, Germany during ETMEP and CARIBIC flights.

3.3.2 Aircraft-based emission estimates for point and area sources

On several Nitrogen, Oxidants, Mercury and Aerosol Distributions, Sources and Sinks (NOMADSS) project flights large Hg point sources were sampled, mainly coal-fired power plants (CFPP) in the Southeast U.S. Ambrose et al. (2015), developed a unique method to use the NOMADSS data to evaluate Hg point source emissions. This method relies on the simultaneous C-130 observations of NO_x, SO_2, CO and CO_2 observations. A key conclusion is that for some CFPPs, including some of the largest Hg emitters in the US, the observations suggest substantially higher Hg emissions compared to the emission inventories.

During ETMEP flights over central Europe significant mercury emissions were measured from a modern coal fired power plant south of Leipzig/Germany. Inside the plume GEM peaked to 10 ng/m³. The denuder sample inside the plume indicated, modern coal-fired power plants may be an overestimated source of GOM. The measured fraction of GOM inside the plume was between 0.5% and 2%. This is in contrast to the 40%, given by the "AMAP/UNEP geospatially distributed mercury emissions dataset 2010v1" (AMAP/UNEP, 2013). The yearly emission of gaseous mercury from that power plant was estimated to 268-283kg/a for GEM and 2-12 kg/a for GOM. (Weigelt et al. 2015).

The Chicago-Gary area is highly industrialized with significant emissions of Hg and other pollutants. Using data from NOMADSS flight RF-15, Gratz et al. (2016) developed a novel method to evaluate the Hg

emission inventory from this region. The observations showed a region of enhanced Hg, CO, SO2 and NOx. Combining the observations with the Flexpart model allowed for the characterization of the "footprint" of the observations and therefore a good comparison between the observations and expectations based on the emission inventory. Gratz' analysis indicated "that there are many small emission sources that are not fully accounted for within the inventory, and/or that the re-emission of legacy Hg is a significant source of THg to the atmosphere in this region (Gratz et al., 2016).

3.3.3 Large-scale Tropospheric distribution and plumes

During the Civil Aircraft for the Regular Investigation of the atmosphere Based on an Instrument Container (CARIBIC) project more than 100 large-scale pollution plumes have been detected in the global upper troposphere. The largest plume with an extension of 1000 km was detected on a flight from Frankfurt to Osaka between the Korean peninsula and the Yellow Sea. This mixed plume could be attributed to large forest fires in Southern Siberia as well as industrial sources in Chinese provinces of Shandong, Henan, Shanxi and Hebei.

Most of the plumes were found over East Asia during the flights from Frankfurt to Guangzhou, Osaka, Seoul and Manila, in the African equatorial region during the flights to South Africa, over South America during the flights to Sao Paulo and Santiago de Chile, and over Pakistan and India during the flights to Chennai. The plumes encountered over the African equatorial region and over South America originate from biomass burning as evidenced by low Hg/CO emission ratios and elevated mixing ratios of acetonitrile, CH_3Cl and CH_3Br. Backward trajectories point to the region around Rift Valley and Amazon basin with its outskirts as the source areas. The plumes encountered over the East Asia and over Pakistan and India are predominantly of urban/industrial origin, sometimes mixed with products of biomass/biofuel burning. Numerous plumes with elevated mercury concentrations were encountered during the tropospheric sections of the CARIBIC flights since May 2005. Mercury correlated significantly with CO in more than 50% of the observed plumes and with CO_2 in about 30% of the plumes for which CO_2 data were available. Extensive ancillary data on chemical fingerprint of the air within these plumes and backward trajectories provide additional means to identify the origin and the type of the source (Slemr et al., 2014).

Large plumes over equatorial Africa were observed during all flights between Frankfurt and South Africa. These plumes which extend over thousands of km are embedded in north-south gradient of mercury, CO, and CO_2, and consist of a number of overlapping smaller plumes. Due to the changing background,

the inhomogeneity of the plumes and low precision of the mercury measurements only a few of the plume encounters provided significant Hg vs. CO correlations. Most plumes were observed over Far East Asia and relative to the number of flights to Far East destinations the yield of plumes with significant Hg vs CO correlations was the second highest after the African flights. Lower yields of plume occurrence were found for flights to South America and to South Asia. Only one plume was encountered over North America and one over Europe. (Slemr et al., 2009, Slemr et al., 2013, Slemr et al., 2014)

The Hg/CO emission ratios derived from these correlations are consistent with the previous data and tend to smaller values of ~1 pg m^{-3} ppb^{-1} for plumes from biomass burning and larger values of ~6 pg m^{-3} ppb^{-1} for urban/industrial emissions. Most of the plumes observed over South America and Africa originate from biomass burning and one plume observed over mid-Atlantic could be attributed to forest fires in south eastern US. The plumes observed over the Far East Asia are mostly of urban/industrial or mixed origin. Only a few Hg/CO_2 emission ratios have been reported so far. The range of the Hg/CO_2 emission ratios from CARIBIC flights is comparable to the range observed at Cape Point (Brunke et al., 2012). The Hg/CO_2 emission ratios of 107 – 964 pg m^{-3} ppm^{-1} observed in the plumes over Far East, however, are substantially higher than 2 – 30 pg m^{-3} ppm^{-1} calculated by Brunke et al. (2012) for coal burning. If confirmed by further measurements the higher observed than calculated Hg/CO_2 emission ratios would imply substantial other mercury emissions than from coal burning. Generally it can be concluded from CARIBIC data that the major industrial sources for atmospheric mercury are located in East-Asia, Pakistan and India whereas major contribution to mercury emissions from biomass burning are originating from Equatorial Africa (Rift-Valley) and the Amazon region.

In the tropospheric CARIBIC data an El Niño Southern Oscillation (ENSO) signal could be detected. (Slemr et al., 2016a). The highest mercury concentrations are always found at the most negative SOI values i.e. are related to the El Niño events. A cross-correlation reveals that peak mercury concentrations are delayed by 6 – 12 months against SOI. This delay is similar to the delay of CO which has been shown to originate from biomass burning in aftermath of El Niño events. Slemr et al. (2016) suggested that the ENSO signal in the worldwide mercury concentrations is also due to mercury emissions from biomass burning (Slemr et al., 2009, Slemr et al., 2013, Slemr et al., 2014).

3.3.4 Airborne observations of speciated Hg

Mercury observations on the NCAR C-130 were made by the University of Washington in summer 2013 with specially developed Detector for Oxidized Hg Species (DOHGS) (Ambrose et al., 2015), which

measures both gaseous elemental mercury (Hg0), gaseous oxidized mercury (GOM), plus a fraction of particle-bound oxidized Hg. GOM is believed to consist of Hg(II) compounds, such as $HgCl_2$, $HgBr_2$, etc. The measurements were routinely calibrated in-flight with a high precision source of Hg0, and in the laboratory with sources of gaseous $HgBr_2$ and $HgCl_2$. The dual channel difference method avoids problems with earlier measurements based on KCl denuders, which are known to have significant interferences. We believe these are the most carefully calibrated and accurate measurements of speciated Hg made to date on an aircraft platform. Details on the methodology and further information on calibrations, accuracy, and precision are given in Ambrose et al. (2015). On several flights, substantial concentrations of Hg(II) were identified. Although the location and timing of these events were correct in the GEOS-Chem Hg model, the concentrations were much higher (2–4x). Figure 10 shows an example from research flight 6 (RF-06), along with the base simulations from GEOS-Chem (Gratz et al., 2015). This flight was also one of the few with detectable concentrations of BrO. We concluded that the likely source of Hg(II) on this flight was oxidation of gaseous elemental mercury (GEM) by Br radicals. This was supported by a detailed chemical mechanism and box-model calculation. This is a major finding and has implications for both Hg and halogens. Note that the halogen chemistry and mercury oxidation mechanism in the GEOS-Chem model were recently updated, as reported in Horowitz et al. (2017).

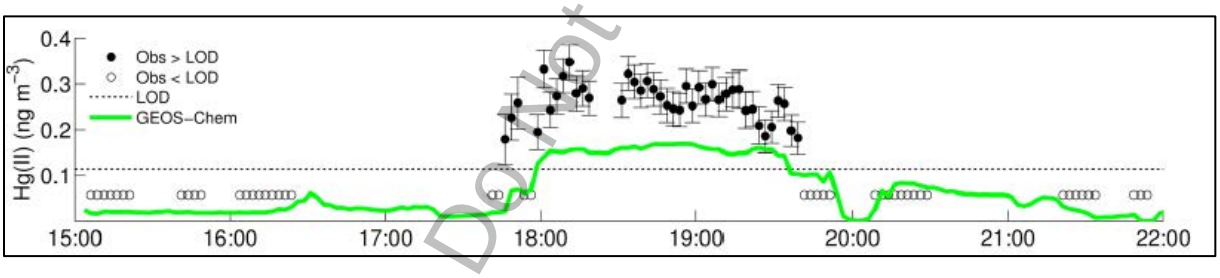

Figure 10: Oxidized Hg (Hg(II); ng m^{-3}) concentrations measured during RF-06 on June 19, 2013, (black points) and modelled Hg(II) from the base model simulations (green line).

Shah et al. (2016) further analysed the origins of oxidized mercury using a variety of sensitivity studies with the GEOS-Chem model. For observations above the detection limit it was found that modelled Hg(II) concentrations are a factor of 3 too low (observations: 212 ± 112 ng m^{-3}, model: 67 ± 44 ng m^{-3}). The highest Hg(II) concentrations, 300–680 pg m^{-3}, were observed in dry (RH < 35 %) and clean air masses during two flights over Texas at 5–7 km altitude and off the North Carolina coast at 1–3 km. The GEOS-Chem model, back trajectories and observed chemical tracers for these air masses indicate subsidence and transport from the upper and middle troposphere of the subtropical anticyclones, where fast oxidation of elemental mercury (Hg0) to Hg(II) and lack of Hg(II) removal lead to efficient

accumulation of Hg(II). Shah et al. (2016) suggested that the most likely explanation for the model bias is a systematic underestimate of the Hg0 +Br reaction rate, which has now been updated in Horowitz et al. (2017). It was shown that sensitivity simulations with tripled bromine radical concentrations or a faster oxidation rate constant for Hg0 +Br, result in 1.5–2 times higher modelled Hg(II) concentrations and improved agreement with the observations. The modelled tropospheric lifetime of Hg0 against oxidation to Hg(II) decreases from 5 months in the base simulation to 2.8–1.2 months in our sensitivity simulations. In order to maintain the modelled global burden of THg, we need to increase the in-cloud reduction of Hg(II) was increased, thus leading to faster chemical cycling between Hg0 and Hg(II). Observations and model results for the NOMADSS campaign suggest that the subtropical anticyclones are significant global sources of Hg(II).

In the lower stratosphere, TGM concentrations always decrease with increasing PV and O_3. This behaviour is similar to all trace species with ground sources and stratospheric sinks such as CO and CH_4. Opposite to such species, mercury as an element can only be transformed to other mercury species such as GOM or particle bound mercury (TPM). The transformation rate of TGM to particle bound mercury can be calculated using SF_6 as a timer. SF_6 is a very long-lived tracer whose concentration increases by about 0.230 ppt yr-1. Correlations of TGM with SF_6 suggest a seasonally dependent TGM conversion rate of about 0.43 ng m-3 yr-1 resulting in a stratospheric TGM lifetime of about 2 yr. This lifetime is longer than several weeks claimed recently by Lyman and Jaffe (2012) but is closer to 1 yr estimated by Holmes et al. (2010) using the GEOS-Chem model with included bromine oxidation chemistry.

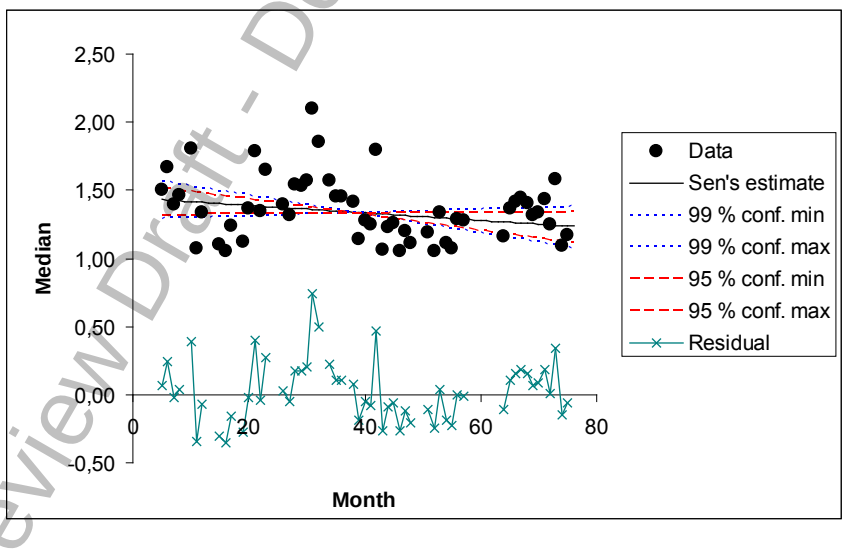

Figure 11: Monthly averages of TGM concentrations in the troposphere (PV < 1.5 PVU) north of 15°N from May 2005 to April 2011 with Sen´s slope estimate.

3.4 Temporal and spatial variability of Hg exchange fluxes between air and soil/vegetation/snow-ice

Re-emission of previously deposited Hg to terrestrial and aquatic surfaces is an essential component of the global biogeochemical Hg cycle, accounting for approximately 2/3 of inputs to the atmosphere each year (Amos et al., 2013; 2014). The magnitude of reemissions fluxes has grown substantially over the history of human use of mercury that has enriched terrestrial and aquatic ecosystems globally (Amos et al., 2013; 2015). Most evasion occurs as elemental Hg (Hg(0)) but in marine regions, dimethylmercury evasion ($(CH_3)_2Hg$) can also be important (Soerensen et al., 2016).

Globally, evasion of Hg(0) from the oceans in comparable in magnitude to primary anthropogenic emissions (Soerensen et al., 2010a). Concentrations of dissolved Hg(0) in seawater are driven by the supply of Hg(II) for reduction (total seawater Hg concentrations), biological and photochemical reduction rates mediated by light and bacterial activity, and the stability of Hg(II) complexes in seawater. Several recent studies have shown the composition of dissolved organic matter (DOM) in seawater can have a strong influence on the amount of Hg(II) that is reduced and subsequently evaded back to the atmosphere, with terrestrial DOM in particular effectively reducing reactivity of sorbed Hg (Soerensen et al., 2014; Schartup et al., 2015; Zhang et al., 2015). Net flux of mercury to the atmosphere through air-sea exchange is thought to range between 1940-4150 Mg per year, with a mean flux of 3200 predicted by Amos et al. (2013).

Air–soil (or vegetation covered) exchange fluxes are an important part of global and regional Hg biogeochemical cycle (Lindberg et al. 2007, Gustin et al. 2008, Gustin et al. 2010, Pierce et al. 2015). Much of Hg(II) deposited in precipitation or taken up plants is subject to reduction to Hg(0) and may be evaded back to the atmosphere. Smith-Downey et al. (2010) estimated based on a global terrestrial mercury model that evasion of mercury linked to decomposition of soil organic carbon pools and subsequent liberation of Hg(II) sorbed to soil organic matter is greater than 700 Mg per year, reflecting the large pool of Hg stored in terrestrial ecosystems globally (>240 Gg). In total, this study estimated 56% of Hg deposited to terrestrial ecosystems is reemitted. Similarly, Graydon et al. (2012) found that 45-70% of isotopically labelled Hg(II) wet deposited to a forested watershed had been reemitted to the atmosphere after one year. Recent observations suggest the evasion flux of mercury from global soils may be slightly lower and the reservoir even higher (e.g., Hararuk et al., 2013).

Hg exchange flux between soil (vegetation) depends on several environmental factors (soil moisture, soil porosity substrate temperature, etc.), chemical factors (Hg species and its content in soil, organic matter, atmospheric oxidants, etc.), meteorological factors (e.g. pressure, air temperature, wind speed and turbulence, solar radiation, snow cower) and surface characteristics (e.g. type of vegetation, substrate type, roughness of the surface) (Schroeder et al. 2005, Gustin et al. 2004). These factors are leading to highly variable Hg fluxes in different landscapes and determine spatial and temporal variability in deposition or evasion of GEM (Schroeder et al. 2005). All forms of atmospheric Hg can be deposited from atmosphere to soils or differently vegetated surfaces by wet or by dry deposition processes (Gustin 2011) where it can either remain in terrestrial system and undergo further biogeochemical cycle or emitted back to atmosphere with relative importance of different controlling factors (Gustin 2011). Changes in direction of the flux were observed on several soil types covered by different types of vegetation (Gustin and Jaffe 2010, Poissant et al. 2005), and can happen quickly, within few hours (Bash and Miller 2008, Converse et al. 2010).

Soil types, moisture, and Hg content and speciation in soil are important factors influencing GEM flux between soil and air (Kocman and Horvat 2010, Lin et al. 2010). Soil porosity and disturbance promote Hg(II) reduction and GEM transport from soil (Fu et al. 2012, Bash and Miller 2007). Soils with small grain size, silt and clay with higher surface area showed higher GEM fluxes to air (Gustin et al. 2002). Rainfall and soil moisture promote GEM emission by order of magnitude (Lindberg et al. 1999). Irrigation of soil enhances Hg (II) reduction and added water replaces GEM binding sites and thus promotes GEM emission. Organic matter in soil was reported to be one of main factors affecting GEM emissions as organic matter forms stable complexes with Hg(II) and thus reduce GEM flux (Grigal 2003, Skyllberg et al. 2006, Yang et al. 2007). Microbial activity in soil and increasing soil pH may promote GEM flux by Hg(II) reduction (Fritshe et al. 2008, Choi and Holsen 2009, Yang et al. 2007). High ambient air GEM concentrations were reported to reduce GEM flux by reducing Hg(0) concentration gradient and thus deposition is dominated despite influence of other factors (Xin and Gustin 2007, Bash and Miller 2007, Wang et al. 2007, Zhu et al. 2016). Flux measured from background soils was between -51.7 to 97.8 with mean of 2.1 ng $m^{-2}h^{-1}$ (Zhu et al. 2016 and references therein).

Vegetation is changing environmental factors at ground surfaces by reducing solar radiation, temperature, wind velocity (Gustin et al. 2004), and serve as surface for Hg uptake (Zhu et al. 2016). Deforestation can increase GEM emissions due to higher flor irradiation and temperature (Zhu et al. 2016, Carpi et al. 2014, Mazur et al. 2014). Recent measurements showed that GEM exchange flux

6835 between plants and air is bidirectional and that growing plants acts as a net sink (Ericksen et al. 2003,
6836 Stamenković et al. 2008, Hartman et al. 2009, Zhu et al. 2016). Most fluxes measured in forest foliage
6837 and grasslands were between -9.6 and 37 (6.3), and -19 to 41 (5.5) ng $m^{-2}h^{-1}$, respectively (Zhu et al.
6838 2016 and references therein).

6839 Air-snow exchange fluxes were mostly investigated in polar regions. During AMDEs air GEM is oxidized
6840 and deposited in snow as GOM and PBM which can be rapidly volatilized back to atmosphere by
6841 photochemical reduction on snow or in melted snow (Dommergue et al. 2003, Fain et al. 2007, Kirk et al.
6842 2006). Photo-reduction was found to be predominant factor for re-emission from snow and was linearly
6843 correlated to UV intensity (Lalonde et al. 2002, Mann et al. 2015). Important factor controlling snow-air
6844 fluxes is temperature also by changing solid-liquid water ratio (Mann et al. 2015). Similar factors as in
6845 polar regions control snow-air Hg exchange in temperate regions (Maxwell et al. 2013). Measured fluxes
6846 from snowpack are within same range reported for vegetation cower and were between -10.8 to 40 ng
6847 $m^{-2}h^{-1}$ with mean of 5.7 ng $m^{-2}h^{-1}$ (Zhu et al. 2016 and references therein).

6848 Polar air-sea water exchange of elemental mercury was for the first time measured continuously in the
6849 remote seas of western Antarctica. The measurements were performed during winter and spring (2013)
6850 in the Weddell Sea and during summer (2010/2011) in the Bellingshausen, Amundsen and Ross Seas,
6851 and show spatial and seasonal variations. The average DGM concentration in surface water in open sea
6852 was highest during spring (12±7pgL-1) and lowest during summer (7±6.8pgL-1), resulting in a net evasion
6853 of mercury during spring (1.1±1.6ngm-2 h-1) and a net deposition during summer (-0.2±1.3ngm-2 h-1).
6854 In open sea, higher average concentrations of GEM (or TGM) and DGM were found close to the Drake
6855 Passage compared to in the Bellingshausen and Weddell Seas. Emission sources from the South
6856 American continent, identified with back trajectories, were suggested to explain the observed
6857 variations. The yearly mercury evasion from open sea surfaces in the Southern Ocean was estimated to
6858 30 (-450-1700) tons, using the average (and min and max) flux rates obtained in this study. Higher DGM
6859 was measured under sea ice (19-62pgL-1) compared to in open sea due to a capsuling effect, resulting in
6860 a theoretical prevented evasion of 520 (0-3400) tons per year. Diminishing sea ice and higher water
6861 temperatures in polar regions could result in increased mercury evasion to the atmosphere. However,
6862 the contribution of the Southern Ocean to the global modelled annual emissions of mercury from sea
6863 surfaces would probably only be a few percent. (Nerentorp et al 2017).

Hg evasion from contaminated or naturally enrich soils was recognized as important input to regional and global budget (Ferrara et al. 1998, Kotnik et al. 2005). The average evasion flux over urbanized areas and agricultural fields is 5 to 10 times higher than over background soils (Zhu et al. 2016). Measured Hg exchange fluxes over natural enriched surfaces were reported to be 5.5 to 239 (5.6) μg $m^{-2}h^{-1}$, and from anthropogenically contaminated sites 0.001 to 14 (0.6) μg $m^{-2}h^{-1}$ (Zhu et al. 2016 and references therein).

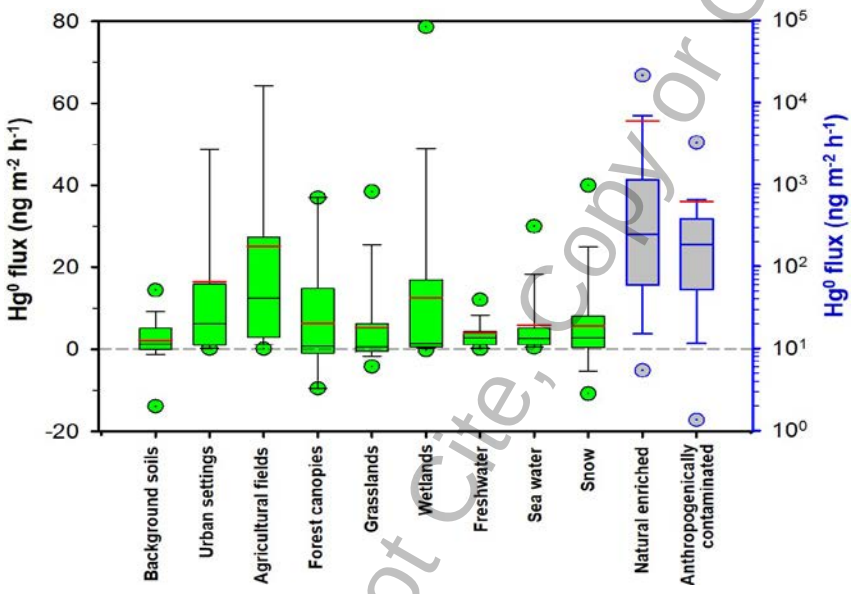

Figure 12: Box and whisker plots of global field-observed GEM fluxes obtained from various landscapes. The two box horizontal border lines indicate 25th and 75th percentiles, whiskers represent 10th and 90th percentiles and outliers (green circles) indicate 5th and 95th percentiles from bottom to top. Red line and black line indicate mean and median flux. Figure from Zhu et al. 2016.

Fluxes from soils, mines and snow surfaces, where GEM can be formed due to photoreduction, are typically higher during daytime as during nighttime (Zhu et al. 2016). Higher evasion flux was observed during warm than cold seasons from different soils and enriched surfaces (Zhu et al. 2016). Hg fluxes measurements over soil, vegetation or snow covered surfaces were consistently higher in E Asia than those measured in Europe, N and S America, Australia and S Africa. This is explained by higher anthropogenic emissions and re-emissions of deposited Hg (Zhu et al. 2016 and references therein).

3.5 Existing data by new monitoring technologies and new methods

Complex commercial instruments as well as sensors and sensing systems have been recently redesigned and improved by introducing innovative technologies. Thus, many sensors have been developed to detect the several forms of mercury making use of nanotechnology. Over the last 20 years, biomolecules, macromolecules, nanostructures (rods, tubes, fibres, particles, dots) and nanocomposite based systems have been found to be the most intriguing and effective detecting devices for mercury detection in several environmental compartments. Most of them have exploited the strong affinity between mercury and gold, others the affinity of mercury ions to specific biomolecules. The possibility to manipulate and investigate the features of the nanomaterials allowed the chance of fabricating selective and more sensitive tools. The Table 11 comprises some of the most recent technologies used to develop sensors and devices for mercury detection.

Table 11: Recent technologies used to develop sensors and devices for mercury detection.

Sampling	Materials/device	Linearity range	LOD	Samples	Reference
Hg ions	CV-AAS +SDS-coated chromosorb P + 2-mercaptobenzoxazole	0.05-85.6 $ngml^{-1}$ 0.09-9.6 $ugml^{-1}$	0.01$ngml^{-1}$	Real samples in liquids	Ghaedi, M. et al., 2006, Anal Lett. 39 1171-1185
TGM-Continuous Emission Monitor	Catalysts to oxidize + polymer composites to absorb + chemicals to remove (CVA-AFS)	0.5-1900 ugm^{-3}	0.05ugm^{-3}	Real samples	TEKRAN331OXi (www.tekran.com)
Optical sensors: Hg^{2+}, FRET bio-sensor (gold nanoparticles-DNA)	Fluorescence quenching		40 nM	Water	Miyake, Y. et al., J. Am. Chem. Soc. 2006, 128, 2172−2173
Optical sensors: Hg^{2+}, surface energy transfer probe-Rhodamine B-AuNPs	Fluorescence quenching		2 ppt	Buffer solution, water, river water, contaminated soil	Darbha, G.K., et al., ACS Nano 2007, 1, 208−214.
Optical sensor: surface-enhanced resonance Raman scattering (SERRS) sensor	structure-switching double stranded DNAs (dsDNAs)		100 pM	Aqueous solution	Kang T., et al. Chemistry. 2011 17(7):2211-4
Electrochemical sensors: Hg^{2+}, array of 256 gold microelectrodes	anodic stripping voltammetry	$5x10^{-8}$-$1x10^{-6}$ M	3.2 µg L^{-1} (16 nM)	Chloride media	Ordeig, O., eta al., Electroanalysis 2006 18 573-578
FET sensors: Hg^{2+}	Thioglycolic acid (TGA)-functionalized -AuNPs-reduced graphene oxide		$2.5x10^{-8}$ M	Aqueous solution	Chen, K., et al., Anal. Chem. 2012, 84, 4057-406

	(rGO)				
Colorimetric sensors: Hg^{2+} (naked eye)	Au-nanorods/glass	2.0 μgl^{-1} to 0.58 mgl^{-1}	$1ugl^{-1}$	Aqueous solution	Chemnasiri W., et al., Sens Actuat B 173 (2012) 322-328
LSPR (prediction model)	Au-nanorods (shift wavelength)		4.5 attograms (mass)	Hg^0 vapour	James J.Z., et al., Analyst 2013
Conductive sensors	CNT-AuNP		2 ppbv	Hg^0 vapour	McNicholas T.P., et al., J. Phys. Chem. C, 2011, 115 13927–13931
Conductive sensors	TiO2NFs-AuNPs (tens of min)		2pptv	Hg^0 vapour	Macagnano A., et al. (a), Sensors and Actuators B 247 (2017) 957–967
Conductive sensors	TiO2NF-AuNPs	20-100 ppbv	1.5 ppbv	Hg^0 vapour	Macagnano et al. (b), ACP 2017 (acp-2016-1077)
QCM sensor (AT cut quartz)	nanostructured gold electrode		2.5 ppbv	Hg^0 vapour	Kabir K.M., et al., Journal of Sensors 2015 ID 727432
Jerome® J405 Mercury Vapour Analyzer	gold thin film (750 ccmin-1)	0.5-999ugm^{-3}	0.5ugm^{-3}	Hg^0 vapour	www.azi.com

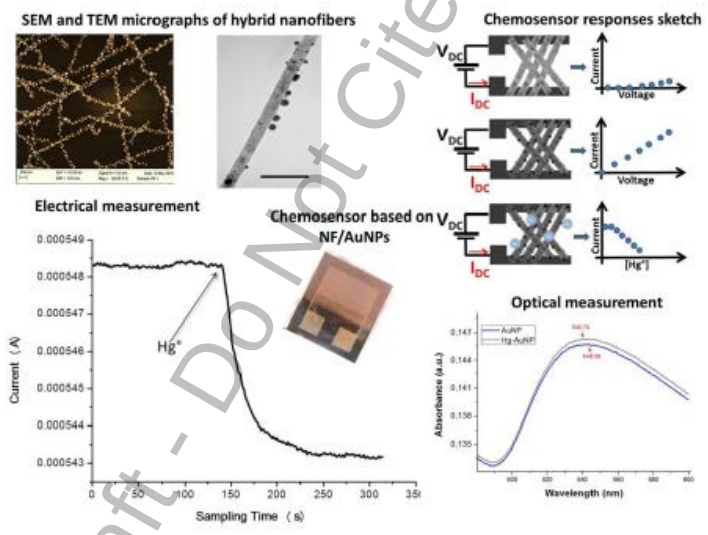

Figure 13: Recent results about sensors based on electrospinning technology: nanofibers of titania doped with AuNPs to detect traces of elemental mercury in air (*Macagnano et al., 2017, a,b).*

However, given the uncertainty and restrictions associated with automated measurements, passive sampling systems currently are a useful alternative for making regional and global estimates of air Hg concentrations. Some passive samplers applied for Hg have been biological materials. Further passive samplers have been designed using a variety of synthetic materials (like sulphur-impregnated carbon (SIC), chlorine-impregnated carbon (CIC), bromine-impregnated carbon (BIC) gold-coated (GCS)

sorbents, etc.) (Li, H. et al., 2017) and housings for Hg collection (McLagan et al., 2016). These latter samplers work on the basis of diffusion. Additionally, surrogate surfaces have been developed for passive measurement of Hg dry deposition. Most commercially available passive/diffusive samplers are planar or axial in shape and offer lower sampling rates and limited sampling capacity. As a result, sensitivity can suffer during short-term analysis (due to low sampling rates), or long-term sampling (analyte back-diffusion due to low capacity). (Huang et al. 2014). Alternatively, radial samplers, consisting of a columnar sorbent surrounded by a cylindrical diffusive barrier, have the purpose to increase the sampling rate by maximizing the surface area across which diffusion occurs (Radiello®, Krol et al., 2010). PASs have been designed with also external shields to protect the sampler components from direct wind, sunlight, and precipitation and to reduce turbulent airflow. A collection of passive samplers more recently developed has been reported in Table 12.

Table 12 – Passive and active samplers developed in recent years to measure TGM [ng m^3] and GOM [pg m^3].

Target	Location	TGM GOM	Materials/sampler	Sampling rate (ml min^{-1})	Blank	DL (pg m^3)	Influences	Reference
TGM	Rural	i) 1-4 ii) 0.8-1.5	i) Gold coated plate ii) silver wire /radial sampler	i) 87 (lab); 51+/-19 (field); 260 theoretical ii) 20 (measured); 33 (theoretical)	i) ii) 80 pg	i) 90 (3 days) ii) 430 (3 days)		Gustin et al., Atmos. Environ., 2011, 45, 5805–5812
TGM	Industrial	25	Gold solution with LDPE/passive integrative mercury sampler (PIMS)	1.4	0.3 ng	2000 (4 weeks)		Brumbaugh et al., Chemosphere: Global Change Sci., 2000, 2, 1–9
TGM	Chamber	10	Gold coated tube/laboratory scale	57 (measured) 114 (theoretical)	0.02 ng	50 (2.8 days); 140 (1 day)	Wind speed	Skov et al., Environ. Chem., 2007, 4, 75–80
TGM	Chamber, indoor, outdoor	2-3.5	Gold-coated silica/axial sampler	0.22 (measured) 0.32 (theoretical)		30% (uncertainty)		Brown et al., J. Environ. Monit., 2012, 14, 2456–2463
TGM	Industrial, suburban, rural	2-5.5	Sulphur-impregnated carbon/axial sampler	90		80 (30 days)	Wind speed	Zhang et al., Atmos. Environ., 2012, 47, 26–32.
TGM	Industrial	2	Gold-coated filter-cation exchange membrane/two-bowl sampler	460 (measured) 556 (theoretical)	0.17 ng	10 (3 days)	Wind speed; humidity	Huang et al., J. Environ. Monit., 2012, 14, 2976–2982
TGM	Chamber, indoor,	1.35−2.16 ng m^{-3}	Sulphur impregnated	0.158-0.121 $m^3 day^{-1}$		11-12 months		Mc. Lagan D., et al.,

	outdoor	(indoor); d 1.17–3.29 ng m^{-3} (outdoor)	carbon sampler/radial in a protective shield	(indoor-outdoor)				Environ. Sci. Technol. Lett. 2016, 3, 24–29
GOM	Rural, suburban	DL-65	Cation-exchange membrane/multiple configurations	0.7-3.2 (measured) 0.055 (theoretical)	0.27 ng to 0.68 ng	5 (2 weeks)	Wind speed	Lyman et al., Atmos. Environ., 2010, 44, 246–252
GOM	Remote	DL-67	Cation-exchange membrane/aerohead configuration		0.56 ng	2.3 (2 weeks)	Wind speed	Wright et al., Science of The Total Environment, 2013, 470–471, 1099–1113
GOM	Industrial, suburban, rural	DL-35	Cation-exchange membrane/ two-bowl sampler	1042 (measured) 486 (theoretical)	0.02-0.04 ng	3 (3 days)	Wind speed; humidity	Huang et al., J. Environ. Monit., 2012, 14, 2976–2982

3.6 Conclusions

To be completed with key highlights on:

- Regional distributions / gradients and time trends
- Gaps in air monitoring spatial coverage
- Limitation of current methods/technology for Hg monitoring in ambient air and fluxes
- The need to foster the development of advanced sensor technology for monitoring mercury concentrations in ambient air, deposition fluxes and gaseous mercury evasions.

In order to come up with a feasible and sustainable strategy for long-term monitoring of Hg in air it is necessary to promote a close cooperation between existing monitoring networks (national, regional, global) with the aims:

- To ensure sustainability of a long-term monitoring program covering both hemispheres
- To assure comparability among different monitoring data sets by promoting the adoption of common SOPs and QA/QC criteria/methods
- To promote intercomparison experiments for testing and validating new methods and technologies for mercury monitoring
- To support Nations in developing their own monitoring programs by promoting a continuous capacity building and transfer of knowledge program in cooperation with UN Environment.

6942 Many experiences already done in past years in the framework of different programs and
6943 projects may be of great help in the future.

6944

3.7 References

Aas, W., Pfaffhuber, K.A., & Nizzetto, P.B. (2016). Heavy metals and POP measurements, 2014 (EMEP/CCC, 04/2016). Kjeller: NILU.

Ambrose, J.L., Gratz, L.E., Jaffe, D.A., Campos, T., Flocke, F., Knapp, D., Stechman, D., Stell, M., Weinheimer, A., Cantrell, C., and Mauldin, R. Mercury Emission Ratios from Coal-Fired Power Plants in the Southeastern United States during NOMADSS. Envir. Sci. Tech. 49 (17), 10389–10397, doi: 10.1021/acs.est.5b01755, 2015.

Amos, H.M., D.J. Jacob, D.G. Streets, E.M. Sunderland. 2013. Legacy impacts of all-time anthropogenic emissions on the global mercury cycle. Global Biogeochemical Cycles. 27, 1-12.

Amos, H.M., D.J. Jacob, D. Kocman, H.M. Horowitz, Y. Zhang, S. Dutkiewicz, M. Horvat, E.S. Corbitt, D.P. Krabbenhoft, E.M. Sunderland. 2014. Global biogeochemical implications of mercury discharges from rivers and sediment burial. Environmental Science and Technology. 48, 9514-9522.

Angot, H., Barret, M., Magand, O., Ramonet, M., and Dommergue, A.: A 2-year record of atmospheric mercury species at a background Southern Hemisphere station on Amsterdam Island, Atmos. Chem. Phys., 14, 11461–11473, doi:10.5194/acp-14-11461-2014, 2014.

Angot, H., Dastoor, A., De Simone, F., Gårdfeldt, K., Gencarelli, C.N., Hedgecock, I.M., Langer, S., Magand, O., Mastromonaco, M.N., Nordstrøm, C., Pfaffhuber, K.A., Pirrone, N., Ryjkov, A., Selin, N.E., Skov, H., Song, S., Sprovieri, F., Steffen, A., Toyota, K., Travnikov, O., Yang, X., Dommergue, A., 2016a. Chemical cycling and deposition of atmospheric mercury in polar regions: review of recent measurements and comparison with models. Atmos Chem Phys 16, 10735–10763. doi:10.5194/acp-16-10735-2016

Angot, H., Dion, I., Vogel, N., Legrand, M., Magand, O., Dommergue, A., 2016b. Multi-year record of atmospheric mercury at Dumont d'Urville, East Antarctic coast: continental outflow and oceanic influences. Atmos Chem Phys 16, 8265–8279. doi:10.5194/acp-16-8265-2016.

Angot, H., Magand, O., Helmig, D., Ricaud, P., Quennehen, B., Gallée, H., Del Guasta, M., Sprovieri, F., Pirrone, N., Savarino, J., Dommergue, A., 2016c. New insights into the atmospheric mercury cycling in central Antarctica and implications on a continental scale. Atmos Chem Phys 16, 8249–8264. doi:10.5194/acp-16-8249-2016.

Ariya, P.A., Dastoor, A.P., Amyot, M., Schroeder, W.H., Barrie, L., Anlauf, K., Raofie, F., Ryzhkov, A., Davignon, D., Lalonde, J., Steffen, A., 2004. The arctic: a sink for mercury. Tellus 56B, 397cling.

Aspmo, K., Temme, C., Berg, T., Ferrari, C., Gauchard, P-A., Fain, X., Wibetoe, G., 2004. Mercury in the atmosphere, snow and melt water ponds in the North Atlantic Ocean during Arctic summer. Environ. Sci. Thecnol 40, 4083–4089.

Banic, C.M., Beauchamp, S.T., Tordon, R.J., Schroeder, W.H., Steffen, A., Anlauf, K.A., Wong, K.H.T. Vertical distribution of gaseous elemental mercury in Canada, J. Geophys. Res. 108, D9, 4264.

Bargagli, R., 2016. Atmospheric chemistry of mercury in Antarctica and the role of cryptogams to assess deposition patterns in coastal ice-free areas. Chemosphere 163, 202–208. doi:10.1016/j.chemosphere.2016.08.007

Bash, J. O. and Miller, D. R.: A note on elevated total gaseous mercury concentrations downwind from an agriculture field during tilling, Sci. Total Environ., 388, 379–388, 2007.

Bash, J. O. and Miller, D. R.: A relaxed eddy accumulation system for measuring surface fluxes of total gaseous mercury, J. Atmos. Ocean. Tech., 25, 244–257, 2008.

Berg, T., Bartnicki, J., Munthe, J., Lattila, H., Hrehoruk, J., Mazur, A., 2001. Atmospheric mercury species in the European Arctic: measurements and modelling. Atmos. Environ. 35, 2569016/j.

Berg, T., Pfaffhuber, K.A., Cole, A.S., Engelsen, O., Steffen, A., 2013. Ten-year trends in atmospheric mercury concentrations, meteorological effects and climate variables at Zeppelin, Ny-Alesund. Atmospheric Chem. Phys. 13, 6575–6586.

Berg, T., Sommar, J., W.A. Cg, Gardfeldt, K., Munthe, J., Schroeder, B., 2003. Arctic mercury depletion events at two elevations as observed at the Zeppelin Station and Dirigibile Italia, Ny-Ålesund, spring 2002. J Phys IV Fr. 107, 151–154.

Brenninkmeijer, C.A.M. P., Crutzen, T., Dauer, D.B., Ebinghaus, R., Filippi, D., Fischer, H., Franke, H., Freiß, U. J., Heintzenberg, H.M., Kock, H.H., Leuenberger, M., Martinsson, B.G., Miemczyk, S., Nguyen, H.N., Oram, D., O'Sullivan, S., Penkett, U., Platt, M., Pupek, M., Ramonet, B., Reichelt, R.M., Rhee, T.S., Rohwer, J., Rosenfeld, K., Scharffe, D., Schlager, H., Schumann, U., Slemr, F., Sprung, D., Stock, P., Thaler, R., van Velthoven, P., Waibel, A., Wandel, A., Waschitschek, K., Wiedensohler, A., Zahn, A., Zech, U., Ziereis H.(2007): Civil Aircraft for the Regular Investigation of the Atmosphere Based on an

Instrumented Container; the new CARIBIC system, Atmospheric Chemistry and Physics, 7, 5277–5339, 2007.

Brooks, S., Saiz-Lopez, A., Skov, H., Lindberg, S.E., Plane, J.M.C., Goodsite, M.E., 2006. The mass balance of mercury in the springtime arctic environment. Geophys. Res. Lett. 33, L13812. doi:10.1029/2005GL025525.

Brooks, S.B., Arimoto, R., Lindberg, S.E., Southworth, G., 2008a. Antarctic polar plateau snow surface conversion of deposited oxidized mercury to gaseous elemental mercury with fractional long-term burial. Atmos. Environ. 42, 2877–2884.

Brooks, S.B., Lindberg, S.E., Southworth, G., Arimoto, R., 2008b. Springtime atmospheric mercury speciation in the McMurdo, Antarctica coastal region. Atmos. Environ. 42, 2885th fra.

Butler, T. J., Cohen, M. D., Vermeylen, F. M., Likens, G. E., Schmeltz, D., & Artz, R. S. (2008). Regional precipitation mercury trends in the eastern USA, 1998–2005: Declines in the Northeast and Midwest, no trend in the Southeast. Atmospheric Environment, 42(7), 1582-1592.

Carbone, F., M. S. Landis, C. N. Gencarelli, A. Naccarato, F. Sprovieri, F. De Simone, I. M. Hedgecock, **N. Pirrone** (2016) Sea surface temperature variation linked to elemental mercury concentrations measured on Mauna Loa. *Geophysical Research Letters*, *43*, doi:10.1002/2016GL069252.

Carpi, A., Fostier, A. H., Orta, O. R., dos Santos, J. C., and Gittings, M.: Gaseous mercury emissions from soil following forest loss and land use changes: Field experiments in the United States and Brazil, Atmos. Environ., 96, 423–429, 2014.

Choi, H. D. and Holsen, T. M.: Gaseous mercury emissions from unsterilized and sterilized soils: The effect of temperature and UV radiation, Environ. Poll., 157, 1673–1678, 2009.

Cole, A.S., Steffen, A., Pfaffhuber, K.A., Berg, T., Pilote, M., Poissant, L., Tordon, R., Hung, H., 2013. Ten-year trends of atmospheric mercury in the high Arctic compared to Canadian sub-Arctic and mid-latitudes sites. Atmospheric Chem. Phys. 13, 1535–1545.

Cole, A. S., Steffen, A., Eckley, C. S., Narayan, J., Pilote, M., Tordon, R., Graydon, J. A., St Louis, V. L., Xu, X., & Branfireun, B. (2014). A Survey of Mercury in Air and Precipitation across Canada: Patterns and Trends. Atmosphere, 5, 635-668.

Colette, A., Aas, W., Banin, L., Braban, C.F., Ferm, M., González Ortiz, A., Ilyin, I., Mar, K., Pandolfi, M., Putaud, J.-P., Shatalov, V., Solberg, S., Spindler, G., Tarasova, O., Vana, M., Adani, M., Almodovar, P., Berton, E., Bessagnet, B., Bohlin-Nizzetto, P., Boruvkova, J., Breivik, K., Briganti, G., Cappelletti, A., Cuvelier, K., Derwent, R., D'Isidoro, M., Fagerli, H., Funk, C, Garcia Vivanco, M., González Ortiz, A., Haeuber, R., Hueglin, C., Jenkins, S., Kerr, J., de Leeuw, F., Lynch, J., Manders, A., Mircea, M., Pay, M.T., Pritula, D., Putaud, J.-P., Querol, X., Raffort,V., Reiss, I., Roustan, Y., Sauvage, S., Scavo, K., Simpson, D., Smith, R.I., Tang, Y.S., Theobald, M., Tørseth, K., Tsyro, S., van Pul, A., Vidic, S., Wallasch, M., Wind, P. (2016). Air pollution trends in the EMEP region between 1990 and 2012. Joint Report of the EMEP Task Force on Measurements and Modelling (TFMM), Chemical Co-ordinating Centre (CCC), Meteorological Synthesizing Centre-East (MSC-E), Meteorological Synthesizing Centre-West (MSC-W) (EMEP: TFMM/CCC/MSC-E/MSC-W Trend Report) (EMEP/CCC, 01/2016). Kjeller: NILU.

Converse, A. D., Riscassi, A. L., and Scanlon, T. M.: Seasonal variability in gaseous mercury fluxes measured in a high-elevation meadow, Atmos. Environ., 44, 2176–2185, 2010. doi:10.1029JD002116, 2003.

D'Amore F., M. Bencardino, S. Cinnirella, F. Sprovieri, **N. Pirrone** (2015) Data quality through a web-based QA/QC system: implementation for atmospheric mercury data from the Global Mercury Observation System. *Environmental Science: Processes Impacts*, 2015, DOI:10.1039/C5EM00205B.

Dastoor, A., Ryzhkov, A., Durnford, D., Lehnherr, I., Steffen, A., Morrison, H., 2015. Atmospheric mercury in the Canadian Arctic. Part II: Insight from modeling. Sci. Total Environ., Special Issue: Mercury in Canada's North 509–510, 16–27. doi:10.1016/j.scitotenv.2014.10.112

Dommergue, A., Barret, M., Courteaud, J., Cristofanelli, P., Ferrari, C.P., Gall 2015. Atmospheric mercury in the Canadian Arctic. Part II: Insight frondary layer of the Antarctic Plateau. Atmos Chem Phys 12, 11027–11036. doi:10.5194/acp-12-11027-2012

Dommergue, A., Larose, C., Faurteaud, J., Cristofanelli, P., Ferrari, C.P., Gall 2015. Atmospheric mercury in the Canadian Arctic. Part II: Insight frondar-Ålesund Area (79°N) and Their Transfer during Snowmelt. Environ. Sci. Technol. 44, 901–907. doi:10.1021/es902579m.

Dommergue, A., Ferrari, C. P., Gauchard, P.-A., Boutron, C. F., Poissant, L., Pilote, M., Jitaru, P., and Adams, F. C.: The fate of mercury species in a sub-arctic snowpack during snowmelt, Geophys. Res. Lett., 30, 1621, doi:10.1029/2003GL017308, 2003.

7054 Ebinghaus, R., Jennings, S., Kock, H., Derwent, R., Manning, A., and Spain, T.: Decreasing trends in total gaseous
7055 mercury observations in baseline air at Mace Head, Ireland from 1996 to 2009, Atmos. Environ., 45, 3475–
7056 3480, 2011.
7057 Ebinghaus, R., Kock, H. H., Coggins, A. M., Spain, T. G., Jennings, S. G., and Temme, C.: Long-term
7058 measurements of atmospheric mercury at Mace Head, Irish west coast, between 1995 and 2001, Atmos.
7059 Environ., 36, 5267–5276, 2002.
7060 Ebinghaus, R., Kock, H.H., Temme, C., Einax, J.W., Lowe, A.G., Richter, A., Burrows, J.P., Schroeder, W.H.,
7061 2002. Antarctic springtime depletion of atmospheric mercury. Environ. Sci. Technol. 36, 123876, 20.
7062 Ebinghaus, R., Slemr, F. Aircraft measurements of atmospheric mercury over southern and eastern Germany,
7063 Atmos. Environ. 34, 895-903, 2000.
7064 Ebinghaus, R., Slemr, F., Brenninkmeijer, C.A.M., van Velthoven, P., Zahn, A., Hermann, M., O´Sullivan,
7065 D.A.,Oram, D.E. Emissions of gaseous mercury from biomass burning in South America in 2005 observed
7066 during CARIBIC flights, Geophys. Res. Lett. 34, L08813, doi:10.1029/2006GL028866, 2007.
7067 Ericksen, J. A., Gustin, M. S., Schorran, D. E., Johnson, D. W., Lindberg, S. E., and Coleman, J. S.: Accumulation
7068 of atmospheric mercury in forest foliage, Atmos. Environ., 37, 1613–1622, 2003.
7069 Faïn, X., Grangeon, S., Bahlmann, E., Fritsche, J., Obrist, D., Dommergue, A., Ferrari, C. P., Cairns, W., Ebinghaus,
7070 R., and Barbante, C.: Diurnal production of gaseous mercury in the alpine snowpack before snowmelt, J.
7071 Geophys. Res.-Atmos., 112, D21311, doi:10.1029/2007JD008520, 2007.
7072 Ferrara, R., Maserti, B. E., Andersson, M., Edner, H., Ragnarson, P., Svanberg, S., and Hernandez, A.: Atmospheric
7073 mercury concentrations and fluxes in the Almadén district (Spain), Atmos. Environ., 32, 3897–3904, 1998.
7074 Ferrari, C.P., Gauchard, P.-A., Aspmo, K., Dommergue, A., Magand, O., Bahlmann, E., Nagorski, S., Temme, C.,
7075 Ebinghaus, R., Steffen, A., Banic, C., Berg, T., Planchon, F., Barbante, C., Cescon, P., Boutron, C.F., 2005.
7076 Snow-to-air exchanges of mercury in an arctic seasonal snowpack in Ny-Alesund, Svalbard. Atmos.
7077 Environ. 39, 7633–7645.
7078 Fisher, J.A., D.J. Jacob, A.L. Soerensen, H.M. Amos, A. Steffen, E.M. Sunderland. 2012. Riverine source of Arctic
7079 Ocean mercury inferred from atmospheric observations. Nature Geoscience. 5: 499-504.
7080 Friedli, H.R., Radke, L.F., Lu, J.Y., Banic, C.M., Leaitch, W.R., MacPherson, J.I. Mercury emissions from burning
7081 of biomass from temperate North American forests: laboratory and airborne measurements, Atmos.
7082 Environ, 37, 253-267, 2003.
7083 Fritsche, J., Obrist, D., Zeeman, M. J., Conen, F., Eugster, W., and Alewell, C.: Elemental mercury fluxes over a
7084 sub-alpine grassland determined with two micrometeorological methods, Atmos. Environ., 42, 2922–2933,
7085 2008.
7086 Fu, X., Feng, X., Zhang, H., Yu, B., and Chen, L.: Mercury emissions from natural surfaces highly impacted by
7087 human activities in Guangzhou province, South China, Atmos. Environ., 54, 185– 193, 2012a.
7088 Fu, X.W., Zhang, H., Yu, B.,Wang, X., Lin, C.-J., and Feng, X. B.: Observations of atmospheric mercury in China:
7089 a critical review, Atmos. Chem. Phys., 15, 9455–9476, doi:10.5194/acp-15-9455- 2015, 2015.
7090 Gratz, L., et al. Airborne Observations of Mercury Emissions from the Chicago/Gary Urban/Industrial Area during
7091 the 2013 NOMADSS Campaign. Atmos. Env., 145, 415–423, doi: 10.1016/j.atmosenv.2016.09.051, 2016.
7092 Gratz, L.E., et al. Oxidation of mercury by bromine in the subtropical Pacific free troposphere. Geophys. Research
7093 Letters, 42, 10492–10502, doi: 10.1002/2015GL066645, 2015.
7094 Graydon, J.A., V. St. Louis, S. Lindberg, K.A. Sandilands, J.W.M. Rudd, C.A. Kelly, R. Harris, M. Tate, D.P.
7095 Krabbenhoft, C.A. Emmerton, H. Asmath, M. Richardson. The role of terrestrial vegetation in atmospheric
7096 Hg deposition: Pools and fluxes from the METAALICUS experiment. Global Biogeochemical Cycles,
7097 2012, 2610.1029/2011GB004031.
7098 Grigal, D. F.: Mercury sequestration in forests and peatlands: A review, J. Environ. Qual., 32, 393–405, 2003.
7099 Gustin, M. and Jaffe, D.: Reducing the Uncertainty in Measurement and Understanding of Mercury in the
7100 Atmosphere, Environ. Sci. Technol., 44, 2222–2227, 2010.
7101 Gustin, M. S., Biester, H., and Kim, C. S.: Investigation of the light-enhanced emission of mercury from naturally
7102 enriched substrates, Atmos. Environ., 36, 3241–3254, 2002.
7103 Gustin, M. S., Ericksen, J. A., Schorran, D. E., Johnson, D. W., Lindberg, S. E., and Coleman, J. S.: Application of
7104 controlled mesocosms for understanding mercury air-soil-plant exchange, Environ. Sci. Technol., 38,
7105 6044–6050, 2004.
7106 Gustin, M. S.: Exchange of mercury between the atmosphere and terrestrial ecosystems, in: Environmental
7107 Chemistry and Toxicology of Mercury, edited by: Liu, G. L., Cai, Y., and O'Driscoll, N., 423–451, 2011.
7108 Gustin, M.; Jaffe, D. Reducing the uncertainty in measurement and understanding of mercury in the atmosphere.
7109 Environ. Sci. Technol. 2010, 44, 2222–2227.

7110 Gustin, M.S.; Lindberg, S.E.; Weisberg, P.J. An update on the natural sources and sinks of atmospheric mercury.
7111 Appl. Geochem. 2008, 23, 482–493.
7112 Han, Y., Huh, Y., Hong, S., Hur, S.D., Motoyama, H., 2014. Evidence of air-snow mercury exchange recorded in
7113 the snowpack at Dome Fuji, Antarctica. Geosci. J. 18, 105i, 3. doi:10.1007/s12303-013-0054-7.
7114 Han, Y., Huh, Y., Hong, S., Hur, S.D., Motoyama, H., Fujita, S., Nakazawa, F., Fukui, K., 2011. Quantification of
7115 total mercury in Antarctic surface snow using ICP-SF-MS: spatial variation from the coast to Dome Fuji.
7116 Bull. Korean Chem. Soc. 32, 4258–4264.
7117 Han, Y., Huh, Y., Hur, S.D., Hong, S., Chung, J.W., Motoyama, H., 2017. Net deposition of mercury to the
7118 Antarctic Plateau enhanced by sea salt. Sci. Total Environ. 583, 81patial variation from thtenv.2017.01.008.
7119 Hararuk, O., D. Obrist, Y. Luo. 2013. Modeling the sensitivity of soil mercury to climate-induced changes in soil-
7120 carbon pools. Biogeosciences. 10, 2393-2407.
7121 Hartman, J. S., Weisberg, P. J., Pillai, R., Ericksen, J. A., Kuiken, T., Lindberg, S. E., Zhang, H., Rytuba, J. J., and
7122 Gustin, M. S.: Application of a rule-based model to estimate mercury exchange for three background
7123 biomes in the Continental United States, Environ. Sci. Technol., 43, 4989–4994, 2009.
7124 Hirdman, D., Aspmo, K., Burkhart, J.F., Eckhardt, S., Sodemann, H., Stohl, A., 2009. Transport of mercury in the
7125 Arctic atmosphere: Evidence for a spring-time net sink and summer-time source. Geophys. Res. Lett. 36,
7126 L12814. doi:10.1029/2009GL038345.
7127 Horowitz, HM, DJ Jacob, Y Zhang, TS Dibble, HM Amos, JA Schmidt, ES Corbitt, EA Marais, EM Sunderland.
7128 (2017). A new mechanism for atmospheric mercury redox chemistry: implications for the global mercury
7129 budget. Atmospheric Chemistry and Physics. 17, 6353-6371.
7130 Kalinchuk, V.V., Mishukov, V.F., Astakhov, A.S., 2017. Arctic source for elevated atmospheric mercury (Hg0) in
7131 the western Bering Sea in the summer of 2013. J. Environ. Sci. doi:10.1016/j.jes.2016.12.022
7132 Kim, S. H., Han, Y. J., Holsen, T. M., & Yi, S. M. (2009). Characteristics of atmospheric speciated mercury
7133 concentrations (TGM, Hg (II) and Hg (p)) in Seoul, Korea. Atmospheric Environment, 43(20), 3267-3274.
7134 Kirk, J. L., St. Louis, V. L., and Sharp, M. J.: Rapid reduction and reemission of mercury deposited into snowpacks
7135 during atmospheric mercury depletion events at Churchill, Manitoba, Canada, Environ. Sci. Technol., 40,
7136 7590–7596, 2006.
7137 Kock, H., Bieber, E., Ebinghaus, R., Spain, T., and Thees, B.: Comparison of long-term trends and seasonal
7138 variations of atmospheric mercury concentrations at the two European coastal monitoring stations Mace
7139 Head, Ireland, and Zingst, Germany, Atmos. Environ., 39, 7549–7556, 2005.
7140 Kocman, D. and Horvat, M.: A laboratory based experimental study of mercury emission from contaminated soils in
7141 the River Idrijca catchment, Atmos. Chem. Phys., 10, 1417–1426, doi:10.5194/acp-10-1417-2010, 2010.
7142 Kotnik, J., Horvat, M., and Dizdarevic, T.: Current and past mercury distribution in air over the Idrija Hg mine
7143 region, Slovenia, Atmos. Environ., 39, 7570–7579, 2005.
7144 Król, S., Zabiegała, B., and Namiesnik, J.: Monitoring VOCs in atmospheric air II. Sample collection and
7145 preparation, TRACTrend. Anal. Chem., 29, 1101–1112, 2010.
7146 Kwon, S.Y., Selin, N.E., 2016. Uncertainties in Atmospheric Mercury Modeling for Policy Evaluation. Curr. Pollut.
7147 Rep. 2, 103–114. doi:10.1007/s40726-016-0030-8.
7148 Lalonde, J. D., Poulain, A. J., and Amyot, M.: The role of mercury redox reactions in snow on snow-to-air mercury
7149 transfer, Environ. Sci. Technol., 36, 174–178, 2002.
7150 Larose, C., Dommergue, A., De Angelis, M., Cossa, D., Averty, B., Marusczak, N., Soumis, N., Schneider, D.,
7151 Ferrari, C., 2010. Springtime changes in snow chemistry lead to new insights into mercury methylation in
7152 the Arctic. Geochim. Cosmochim. Acta 74, 6263–6275.
7153 Lehnherr, I., & St. Louis, V. (2009). Importance of ultraviolet radiation in the photodemethylation of methylmercury
7154 in freshwater ecosystems. Environmental Science and Technology, 43(15), 5692-5698.
7155 Lin, C. J., Gustin, M. S., Singhasuk, P., Eckley, C., and Miller, M.: Empirical models for estimating mercury flux
7156 from soils, Environ. Sci. Technol., 44, 8522–8528, 2010.
7157 Lin, H., Zhang, W., Deng, C. et al. Evaluation of passive sampling of gaseous mercury using different sorbing
7158 materials, Environ Sci Pollut Res (2017) 24: 14190. doi:10.1007/s11356-017-9018-1
7159 Lindberg, S. E., Zhang, H., Gustin, M., Vette, A., Marsik, F., Owens, J., Casimir, A., Ebinghaus, R., Edwards, G.,
7160 Fitzgerald, C., Kemp, J., Kock, H. H., London, J., Majewski, M., Poissant, L., Pilote, M., Rasmussen, P.,
7161 Schaedlich, F., Schneeberger, D., Sommar, J., Turner, R.,Wallschlager, D., and Xiao, Z.: Increases in
7162 mercury emissions from desert soils in response to rainfall and irrigation, J. Geophys. Res.-Atmos., 104,
7163 21879–21888, 1999.

Lindberg, S.; Bullock, R.; Ebinghaus, R.; Engstrom, D.; Feng, X.B.; Fitzgerald, W.; Pirrone, N.; Prestbo, E.;Seigneur, C. A synthesis of progress and uncertainties in attributing the sources of mercury in deposition. Ambio 2007, 36, 19–32.

Lindberg, S.E., Brooks, S., Lin, C.-J., Scott, K., Meyers, T., Chambers, L., Landis, M., Stevens, R., 2001. Formation of Reactive Gaseous Mercury in the Arctic: Evidence of Oxidation of Hg. Res.-Atd irrigation, J. Geophys. Resrctic Sunrise. Water Air Soil Pollut. Focus 1, 295–302. doi:10.1023/a:1013171509022

Lindberg, S.E., Brooks, S., Lin, C.-J., Scott, K.J., Landis, M.S., Stevens, R.K., Goodsite, M.E., Richter, A., 2002. Dynamic oxidation of gaseous mercury in the arctic troposphere at polar sunrise. Environ. Sci. Technol. 36, 1245ic Sun.

Lu, J.Y., Schroeder, W.H., 2004. Annual time-series of total filterable atmospheric mercury concentrations in the Arctic. Tellus 56B, 213–222.

Lu, J.Y., Schroeder, W.H., Barrie, L.A., Steffen, A., Welch, H.E., Martin, K., Lockhart, L., Hunt, R.V., Boila, G., Richter, A., 2001. Magnification of atmospheric mercury deposition to polar regions in springtime: the link to tropospheric ozone depletion chemistry. Geophys. Res. Lett. 28, 3219–3222.

Lyman, S.N., Jaffe, D.A. Formation and fate of oxidized mercury in the upper troposphere and lower stratosphere, Nature Geoscience, doi:10.1038/NGEO1353, 2011.

Macagnano A., Perri V., Zampetti E., Bearzotti A., De Cesare F., Sprovieri F., Pirrone N. A smart nanofibrous material for adsorbing and detecting elemental mercury in air. Atmos. Chem. Phys., 17, 6883-6893, 2017. Https://doi.org/10.5194/acp-17-6883-2017 (b)

Macagnano A., Perri V., Zampetti E., Ferretti A.M., Sprovieri F., Pirrone N., Bearzotti A., Esposito G., De Cesare F. Elemental mercury vapor chemoresistors employing TIO_2 nanofibers photocatalytically decorated with Au-nanoparticles. Sensors and Actuators B 247 (2017) 957–967 (a)

Mann, E. A., Mallory, M. L., Ziegler, S. E., Avery, T. S., Tordon, R., and O'Driscoll, N. J.: Photoreducible mercury loss from Arctic snow is influenced by temperature and snow age, Environ. Sci. Technol., 49, 12120–12126, 2015.

Maxwell, J. A., Holsen, T. M., and Mondal, S.: Gaseous elemental mercury (GEM) emissions from snow surfaces in Northern New York, PloS One, 8, e69342, 2013.

Mazur, M., Mitchell, C. P. J., Eckley, C. S., Eggert, S. L., Kolka, R. K., Sebestyen, S. D., and Swain, E. B.: Gaseous mercury fluxes from forest soils in response to forest harvesting intensity: A field manipulation experiment, Sci. Total Environ., 496, 678–687, 2014.

McLagan D.S., Mazur M.E.E., Mitchell C.P.J., Wania F. Passive air sampling of gaseous elemental mercury: a critical review. Atmos. Chem. Phys., 16, 3061-3076, 2016. Http://www.atmos-chem-phys.net/16/3061/2016/; doi:10.5194/acp-16-3061-2016.

Moore, C. W., Obrist, D., Steffen, A., Staebler, R. M., Douglas, T. A., Richter, A., & Nghiem, S. V. (2014). Sea Ice Lead-induced Convective Forcing of Mercury and Ozone in the Arctic Boundary Layer. Nature

Nerentorp Mastromonaco, M., G, Eckley, C. S., Eggert, S. L., Kolka, R. K., Sebfors, A., Ahnoff, M., Dommergue, A., Meld manipulation experiment, Sci. Total Environ., 496, 678harvesting intensity: A field manipulation experimentn. 129, 125l Env.

Nerentorp Mastromonaco, M., Gårdfeldt, K., Langer, S., Dommergue A., Seasonal Study of Mercury Species in the Antarctic Sea Ice Environment. Environ. Sci. Technol. 50 (23), pp 12705–12712, 2016b.

Nerentorp Mastromonaco, M., Gårdfeldt, K., , Assmann, K M., Langerc, S., Delalid, T., Shlyapnikovd, M Y., Zivkovicd, I., Horvat, M. Speciation of mercury in the waters of the Weddell, Amundsen and Ross Seas (Southern Ocean) Marine Chemistry Volume 193, 20 July 2017, Pages 20–33, 2017.

Nerentorp Mastromonaco, M., Gårdfeldt, K., Jourdain, B., Abrahamsson, K., Granfors, A., Anhoff, M., Dommergue, A., Mejan, G., Jacobi, H-W. 2016 a Antarctic winter mercury and ozone depletion events over sea ice. Atmospheric Environment, 129:125-132, 2016a.

Nerentorp Mastromonaco, M., Gårdfeldt, K., Langer, S. Seasonal Flux of mercury over west Antarctic Seas. Marine Chemistry 193 20:44-54, 2017.

Nghiem, S., Rigor, I., Richter, A., Burrows, J. P., Shepson, P. B., Bottenheim, J., Barber, D. G., Steffen, A., Latonas, J., Wang, F., Stern, G., Clemente-Colón, P., Martin, S., Hall, D. K., Kaleschke, L., Tackett, P., Neumann, G., & Asplin, M. J. (2012). Field and satellite observations of the formation and distribution of Arctic atmospheric bromine above a rejuvenated sea ice cover. Journal of Geophysical Research D: Atmospheres, 117(5), D00S05.

Nguyen, H. T., Kim, K. H., Kim, M. Y., Hong, S., Youn, Y. H., Shon, Z. H., & Lee, J. S. (2007). Monitoring of atmospheric mercury at a global atmospheric watch (GAW) site on An-Myun Island, Korea. Water, air, and soil pollution, 185(1-4), 149-164.

Nguyen, H. T., Kim, M. Y., & Kim, K. H. (2010). The influence of long-range transport on atmospheric mercury on Jeju Island, Korea. Science of the Total Environment, 408(6), 1295-1307.

Osawa, T., Ueno, T., & Fu, F. (2007). Sequential variation of atmospheric mercury in Tokai‐mura, seaside area of eastern central Japan. Journal of Geophysical Research: Atmospheres, 112(D19).

Pacyna, E. G., Pacyna, J. M., Fudala, J., Strzelecka-Jastrzab, E., Hlawiczka, S., and Panasiuk, D.: Mercury emissions to the atmosphere from anthropogenic sources in Europe in 2000 and their scenarios until 2020, Sci. Total Environ., 370, 147–156, 2006.

Pfaffhuber, K.A., Berg, T., Hirdman, D., Stohl, A., 2012. Atmospheric mercury observations from Antarctica: seasonal variation and source and sink region calculations. Atmos Chem Phys 12, 3241–3251. doi:10.5194/acp-12-3241-2012.

Pierce, A.H.; Moore, C.W.; Wohlfahrt, G.; HÖrtang, L.; Kljun, N.; Obrist, D. Eddy covariance flux measurements of gaseous elemental mercury using cavity ring-down spectroscopy. Environ. Sci. Technol. 2015, 49, 1559–1568.

Pirrone, N., Hedgecock, I., and Sprovieri, F.: Atmospheric mercury, easy to spot and hard to pin down: impasse?, Atmos. Environ., 42, 8549–8551, doi:10.1016/j.atmosenv.2008.09.004, 2008.

Poissant, L., Pilote, M., 2003. Time series analysis of atmospheric mercury in Kuujjuarapik/Whapmagoostui (Quebec). J Phys IV Fr. 107, 10798551,

Poissant, L.; Pilote, M.; Beauvais, C.; Constant, P.; Zhang, H.H. A year of continuous measurements of three atmospheric mercury species (GEM, RGM and Hgp) in southern Quebec, Canada. Atmos. Environ. 2005, 39, 1275–1287.

Poulain, A. J., Lalonde, J. D., Amyot, J. D., Shead, J. A., Raofie, F., & Ariya, P. A. (2004). Redox transformations of mercury in an Arctic snowpack at springtime. Atmospheric Environment, 38, 6763-6774.

Prestbo, E. M., & Gay, D. A. (2009). Wet deposition of mercury in the US and Canada, 1996–2005: Results and analysis of the NADP mercury deposition network (MDN). Atmospheric Environment, 43(27), 4223-4233.

ResSteffen, A., Douglas, T., Amyot, M., Ariya, P., Aspmo, K., Berg, T., Bottenheim, J., Brooks, S., Cobbett, F., Dastoor, A., Dommergue, A., Ebinghaus, R., Ferrari, C., Gardfeldt, K., Goodsite, M.E., Lean, D., Poulain, A.J., Scherz, C., Skov, H., Sommar, J., Temme, C., 2008. A synthesis of atmospheric mercury depletion event chemistry in the atmosphere and snow. Atmos Chem Phys 8, 1445–1482. doi:10.5194/acp-8-1445-2008.

Risch, M. R., Gay, D. A., Fowler, K. K., Keeler, G. J., Backus, S. M., Blanchard, P., ... & Dvonch, J. T. (2012). Spatial patterns and temporal trends in mercury concentrations, precipitation depths, and mercury wet deposition in the North American Great Lakes region, 2002–2008. Environmental pollution, 161, 261-271.

Schartup, AT, U. Ndu, P.H. Balcom, R.P. Mason, E.M. Sunderland. 2015. Contrasting effects of marine and terrestrially derived organic matter on mercury speciation and bioavailability in seawater. Environmental Science and Technology. 49: 5965-5972.

Schroeder, W. H., Beauchamp, S., Edwards, G., Poissant, L., Rasmussen, P., Tordon, R., Dias, G., Kemp, J., Van Heyst, B., and Banic, C. M.: Gaseous mercury emissions from natural sources in Canadian landscapes, J. Geophys. Res.-Atmos., 110, D18302, 2005.

Schroeder, W.H., Anlauf, K.G., Barrie, L.A., Lu, J.Y., Steffen, A., Schneeberger, D.R., Berg, T., 1998. Arctic spingtime depletion of mercury. Nature 394, 331 sout.

Selin, N. E., Jacob, D. J., Yantosca, R. M., Strode, S., Jaeglé, L., and Sunderland, E. M.: Global 3-D land-ocean-atmosphere model for mercury: Present-day versus preindustrial cycles and anthropogenic enrichment factors for deposition, Global Biogeochem. Cy., 22, GB2011, doi:10.1029/2007GB003040, 2008.

Shah, V., Jaeglé, L., Gratz, L.E., Ambrose, J.L., Jaffe, D.A., Selin, N.E., Song, S., Giang A., et al. Origin of oxidized mercury in the summertime free troposphere over the Southeast United States. Atmos. Chem. Phys., 16, 1511–1530, doi: 10.5194/acp-16-1511-2016, 2016.

Shanley, J. B., Engle, M. A., Scholl, M., Krabbenhoft, D. P., Brunette, R., Olson, M. L., & Conroy, M. E. (2015). High mercury wet deposition at a “clean air” site in Puerto Rico. Environmental Science & Technology, 49(20), 12474-12482.

Sheu, G. R., Lin, N. H., Wang, J. L., Lee, C. T., Yang, C. F. O., & Wang, S. H. (2010). Temporal distribution and potential sources of atmospheric mercury measured at a high-elevation background station in Taiwan. Atmos. Environ. 2010, *44*(20), 2393-2400.

Sillman, S., Marsik, F., Dvonch, J. T., & Keeler, G. J. (2013, January). Assessing atmospheric deposition of mercury in Florida, USA: Local versus global sources and models versus measurements. In E3S Web of Conferences (Vol. 1). EDP Sciences.

Skov, H. Brooks, S. Goodsite, M.E. Lindberg, S.E. Meyers, T.P. Landis, M.S. Larsen, M.R.B. Jensen, B. McConville, G. Christensen, J. (2006) Measuring reactive gaseous mercury flux by relaxed eddy accumulation. Atm. Env. vol 40, 5452-5463.

Skov, H. Christensen, J. Goodsite, M.E. Heidam, N.Z. Jensen, B. Wåhlin, P. and Geernaert, G. (2004) "The fate of elemental mercury in Arctic during atmospheric mercury depletion episodes and the load of atmospheric mercury to Arctic" ES & T. vol. 38, 2373-2382. . doi:10.1021/es030080h.

Skov, H. Sørensen, B.T. Landis, M.E. Johnson, M.S. Lohse, C. Goodsite, M.E. and Sacco, P. (2007) Performance of a new diffusive sampler for Hgo determination in the troposphere. Environmental Chemistry, vol. 4. 75-80.

Skov, H., Christensen, J.H., Goodsite, M.E., Heidam, N.Z., Jensen, B., With reduced sulfur groups, Environ. Sci. T. Sci. Tr groups, Environ. Sci. Tci. Ton with reduced sulfur groups, Environ. Sci. Tn. Sci. Tn.hnol., 40, 4174si180, 2006.iences.viron. Sci. Technol. 38, 2373–2382. doi:10.1021/es030080h

Skyllberg, U., Bloom, P. R., Qian, J., Lin, C. M., and Bleam, W. F.: Complexation of mercury(II) in soil organic matter: EXAFS evidence for linear two-coordination with reduced sulfur groups, Environ. Sci. Technol., 40, 4174–4180, 2006.

Slemr, F., Angot, H., Dommergue, A., Magand, O., Barret, M., Weigelt, A., Ebinghaus, R., Brunke, E.-G., Pfaffhuber, K. A., Edwards, G., Howard, D., Powell, J., Keywood, M., and Wang, F.: Comparison of mercury concentrations measured at several sites in the Southern Hemisphere, Atmos. Chem. Phys., 15, 3125–3133, doi:10.5194/acp-15-3125-2015, 2015.

Slemr, F., Brunke, E.-G., Ebinghaus, R., and Kuss, J.: Worldwide trend of atmospheric mercury since 1995, Atmos. Chem. Phys., 11, 4779–4787, doi:10.5194/acp-11-4779-2011, 2011.

Slemr, F., Ebinghaus, R., Brenninkmeijer, C.A.M., Hermann, M., Kock, H.H., Martinsson, B.G., Schuck, T.,Sprung, D., van Velthoven, P., Zahn, A., Ziereis, H. Gaseous mercury distribution in the upper troposphere and lower stratosphere observed onboard the CARIBIC passenger aircraft, Atmos. Chem. Phys. 9, 1957-1969, 2009.

Slemr, F., Ebinghaus, R., Brenninkmeijer, C.A.M., Hermann, M., Kock, H.H., Levine, I., Martinsson, B., Schuck, T., Sprung, D., van Velthoven, P., Zahn, A., Ziereis H.: Gaseous mercury distribution in the upper troposphere and lower stratosphere observed during the CARIBIC flights from Frankfurt to southern China and to South America, Atmospheric Chemistry and Physics, 9 (6): 1957-1969, 2009.

Slemr, F., Ebinghaus, R., Weigelt, A., Kock, H. H., Brenninkmeijer, C. A. M., Schuck, T., Hermann, M., et al.: CARIBIC observations of gaseous mercury in the upper troposphere and lower stratosphere. E3S Web of Conferences, 1(2013), 17001. (doi:10.1051/e3sconf/20130117001), 2013.

Slemr, F.; Brenninkmeijer, C.A.; Rauthe-Schöch, A.; Weigelt, A.; Ebinghaus, R.; Brunke, E.-G.; Martin, L.; Spain, T.G.; O´Doherty, S.: El Niño–Southern Oscillation influence on tropospheric mercury concentrations. Geophysical Research Letters 43, 1766–1771 (doi:10.1002/2016GL067949), 2016a.

Slemr, F.; Weigelt, A.; Ebinghaus, R.; Brenninkmeijer, C.; Baker, A.; Schuck, T.; Rauthe-Schöch, A.; Riede, H., Leedham, E.; Hermann, M.; van Velthoven, P.; Oram, D.; O'Sullivan, D.; Dyroff, C.; Zahn, A.; Ziereis, H.: Mercury Plumes in the Global Upper Troposphere Observed during Flights with the CARIBIC Observatory from May 2005 until June 2013, Atmosphere, 5, 342-369; doi:10.3390/atmos5020342, 2014.

Slemr, F.; Weigelt, A.; Ebinghaus, R.; Kock, H.H.; Bödewadt, J.; Brenninkmeijer, C.A.M.; Rauthe-Schöch, A.; Weber, S.; Hermann, M.; Becker, J.; Zahn, A.; Martinsson, B.: Atmospheric mercury measurements onboard the CARIBIC passenger aircraft. Atmospheric Measurement Techniques 9, 2291–2302 (doi: 10.5194/amt-9-2291-2016), 2016b.

Smith-Downey, N.V., E.M. Sunderland, D.J. Jacob. 2010. Anthropogenic impacts on global storage and emissions of mercury from terrestrial soils: Insights from a new global model. Journal of Geophysical Research, 115, G03008.

Soerensen, A., Skov, H., Soerensen, D. J. B., and Johnson, M.: Global concentrations of gaseous elemental mercury and reactive gaseous mercury in the marine boundary layer, Environ. Sci. Technol., 44, 7425–7430, doi:10.1021/es903839n, 2010a.

Soerensen, A., Sunderland, E., Holmes, C., Jacob, D., Yantosca, R., Skov, H., Christensen, J., Strode, S., and Mason, R.: An improved global model for air-sea exchange of mercury: high concentrations over the North Atlantic, Environ. Sci. Technol., 44, 8574–8580, doi:10.1021/es102032g, 2010b.

Soerensen, A.L., D.J. Jacob, A.T. Schartup, J.A. Fisher, I. Lehnherr, V.L. St. Louis, L-E. Heimberger, J.E. Sonke, D.P. Krabbenhoft, E.M. Sunderland. (2016). A mass budget for mercury and methylmercury in the Arctic Ocean. Global Biogeochemical Cycles, 30, 560–575, doi:10.1002/2015GB005280.

7329 Soerensen, A.L., D.J. Jacob, D.G. Streets, M.L.I. Witt, R. Ebinghaus, R.P. Mason, M. Andersson, E.M. Sunderland.
7330 2012. Multi-decadal decline of mercury in the North Atlantic atmosphere explained by changing subsurface
7331 seawater concentrations. Geophysical Research Letters, 39, L21810.
7332 Soerensen, A.L., R.P. Mason, P.H. Balcom, D.J. Jacob, Y. Zhang, J. Kuss, E.M. Sunderland. 2014. Elemental
7333 mercury concentrations and fluxes in the tropical atmosphere and ocean. Environmental Science and
7334 Technology. 48, 11312-11319.
7335 Soerensen, A.L., R.P. Mason, P.H. Balcom, E.M. Sunderland. 2013. Drivers of surface ocean mercury
7336 concentrations and air-sea exchange in the West Atlantic Ocean. Environmental Science and Technology.
7337 47, 7757-7765.
7338 Sommar, J., Andersson, M. E., and Jacobi, H.-W.: Circumpolar measurements of speciated mercury, ozone and
7339 carbon monoxide in the boundary layer of the Arctic Ocean, Atmos. Chem. Phys., 10, 5031–5045,
7340 doi:10.5194/acp-10-5031-2010, 2010.
7341 Sommar, J., W, Sunderland, E., Holmes, C., Jacob, D., Yantosca, R., Skov, H., Christensen, J., Strode, S., and
7342 Mason, R.: ACircumpolar transport and air-surface exchange of atmospheric mercury at Ny- over the North
7343 ASvalbard, spring 2002. Atmos Chem Phys 7, 151–166. doi:10.5194/acp-7-151-2007.
7344 Sprovieri F., N. Pirrone, M.S. Landis, R.K. Stevens (2005a) Oxidation of gaseous elemental mercury to gaseous
7345 divalent mercury during 2003 polar sunrise at Ny-Alesund. Environmental Science & Technology 39 (23),
7346 9156-9165.
7347 Sprovieri F., N. Pirrone, M.S. Landis, R.K. Stevens (2005b) Atmospheric mercury behavior at different altutudes at
7348 Ny Alesund during Spring 2003. Atmospheric Environment 39 (39), 7646-7656.
7349 Sprovieri, F., Pirrone, N., Bencardino, M., D'Amore, F., Angot, H., Barbante, C., Brunke, E.-G., Arcega-Cabrera, F.,
7350 Cairns, W., Comero, S., Diéguez, M. D. C., Dommergue, A., Ebinghaus, R., Feng, X. B., Fu, X., Garcia, P.
7351 E., Gawlik, B. M., Hageström, U., Hansson, K., Horvat, M., Kotnik, J., Labuschagne, C., Magand, O.,
7352 Martin, L., Mashyanov, N., Mkololo, T., Munthe, J., Obolkin, V., Ramirez Islas, M., Sena, F., Somerset,
7353 V., Spandow, P., Vardè, M., Walters, C., Wängberg, I., Weigelt, A., Yang, X., and Zhang, H.: Five-year
7354 records of mercury wet deposition flux at GMOS sites in the Northern and Southern hemispheres, Atmos.
7355 Chem. Phys., 17, 2689-2708, doi:10.5194/acp-17-2689-2017, 2017.Temme, C., Blanchard, P., Steffen, A.,
7356 Banic, C., Beauchamp, S., Poissant, L., Tordon, R., andWiens, B.: Trend, seasonal and multivariate
7357 analysis study of total gaseous mercury data from the Canadian atmospheric mercury measurement network
7358 (CAMNet), Atmos. Environ., 41, 5423–5441, 2007.
7359 Sprovieri, F., Pirrone, N., Bencardino, M., D'Amore, F., Angot, H., Barbante, C., Brunke, E.-G., Arcega-Cabrera, F.,
7360 Cairns, W., Comero, S., Diéguez, M. D. C., Dommergue, A., Ebinghaus, R., Feng, X. B., Fu, X., Garcia, P.
7361 E., Gawlik, B. M., Hageström, U., Hansson, K., Horvat, M., Kotnik, J., Labuschagne, C., Magand, O.,
7362 Martin, L., Mashyanov, N., Mkololo, T., Munthe, J., Obolkin, V., Ramirez Islas, M., Sena, F., Somerset,
7363 V., Spandow, P., Vardè, M., Walters, C., Wängberg, I., Weigelt, A., Yang, X., and Zhang, H.: Five-year
7364 records of mercury wet deposition flux at GMOS sites in the Northern and Southern hemispheres, Atmos.
7365 Chem. Phys., 17, 2689-2708, doi:10.5194/acp-17-2689-2017, 2017.Stamenkovic, J., Gustin, M. S., Arnone,
7366 J. A., Johnson, D. W., Larsen, J. D., and Verburg, P. S. J.: Atmospheric mercury exchange with a tallgrass
7367 prairie ecosystem housed in mesocosms, Sci. Total Environ., 406, 227–238, 2008.
7368 Sprovieri, F., Pirrone, N., Ebinghaus, R., Kock, H., and Dommergue, A.: A review of worldwide atmospheric
7369 mercury measurements, Atmos. Chem. Phys., 10, 8245–8265, doi:10.5194/acp-10-8245-8265, 2010, 2010.
7370 Sprovieri, F., Pirrone, N., Hedgecock, I.M., Landis, M.S., Stevens, R.K., 2002. Intensive atmospheric mercury
7371 measurements at Terra Nova Bay in antarctica during November and December 2000. J. Geophys. Res.
7372 107, 4722. doi:10.1029/2002JD002057
7373 Steffen, A., Bottenheim, J., Cole, A., Douglas, T. A., Ebinghaus, R., Friess, U., Netcheva, S., Nghiem, S., Sihler, H.,
7374 & Staebler, R. (2013). Atmospheric mercury over sea ice during the OASIS-2009 campaign. Atmospheric
7375 Chemistry and Physics, 13, 7007-7021.
7376 Steffen, A., Bottenheim, J., Cole, A., Ebinghaus, R., Lawson, G., Leaitch, W.R., 2014. Atmospheric mercury
7377 speciation and mercury in snow over time at Alert, Canada. Atmospheric Chem. Phys. 14, 2219-2231.
7378 Steffen, A., Schroeder, W., Macdonald, R., Poissant, L., Konoplev, A., 2005. Mercury in the Arctic atmosphere: An
7379 analysis of eight years of measurements of GEM at Alert (Canada) and a comparison with observations at
7380 Amderma (Russia) and Kuujjuarapik (Canada). Sci. Total Environ., Sources, Occurrence, Trends and
7381 Pathways of Contaminants in the ArcticBidleman S.I. 342, 185–198. doi:10.1016/j.scitotenv.2004.12.04.
7382 Sunderland, EM, RP Mason. (2007) Human impacts on open ocean mercury concentrations. Global Biogeochemical
7383 Cycles. GB4022, doi:10.1029/2006GB002876, 2007.

Swartzendruber, P. C., Jaffe, D.A., Finley, B., 2009. Development and First Results of an Aircraft-Based, High Time Resolution Technique for Gaseous Elemental and Reactive (Oxidized) Gaseous Mercury. Environ. Sci. Technol. 43, 7484–7489.

Temme, C., Einax, J.W., Ebinghaus, R., Schroeder, W.H., 2003. Measurements of atmospheric mercury species at a coastal site in the antarctic and over the atlantic ocean during polar summer. Environ. Sci. Technol. 37, 22ol.

Tørseth, K., Aas, W., Breivik, K., Fjæraa, A.M., Fiebig, M., Hjellbrekke, A.G., Lund Myhre, C., Solberg, S., Yttri, K.E. (2012). Introduction to the European Monitoring and Evaluation Programme (EMEP) and observed atmospheric composition change during 1972-2009. Atmospheric Chemistry and Physics, 12, 5447-5481. doi:10.5194/acp-12-5447-2012.

UNEP, 2015. Global mercury modelling: update of modelling results in the global mercury assessment 2013.

UNEP, GLOBAL REVIEW OF MERCURY MONITORING NETWORKS, 1- 48, November 2016.

Wang, J., Zhang, L., Xie, Z., 2016. Total gaseous mercury along a transect from coastal to central Antarctic: Spatial and diurnal variations. J. Hazard. Mater. 317, 362 Guizhou,:10.1016/j.jhazmat.2016.05.068

Wang, S. F., Feng, X. B., Qiu, G. L., Fu, X. W., and Wei, Z. Q.: Characteristics of mercury exchange flux between soil and air in the heavily air-polluted area, eastern Guizhou, China, Atmos. Environ., 41, 5584–5594, 2007.

Weigelt, A., Ebinghaus, R., Manning, A., Derwent, R., Simmonds, P., Spain, T., Jennings, S., and Slemr, F.: Analysis and interpretation of 18 years of mercury observations since 1996 at Mace Head, Ireland, Atmos. Environ., 100, 85–93, doi:10.1016/j.atmosenv.2014.10.050, 2015.

Weigelt, A., Ebinghaus, R., Pirrone, N., Bieser, J., Bödewadt, J., Esposito, G., Slemr, F., van Velthoven, P. F. J., Zahn, A., and Ziereis, H.: Tropospheric mercury vertical profiles between 500 and 10 000m in central Europe, Atmos. Chem. Phys., 16, 4135–4146, doi:10.5194/acp-16-4135-2016, 2016.

Weigelt A., Franz Slemr, Ralf Ebinghaus, Nicola Pirrone, Johannes Bieser, Jan Bödewadt, Giulio Esposito, and Peter F. J. van Velthoven (2016) Mercury emissions of a coal-fired power plant in Germany**.** *Atmospheric Chemistry & Phys*ics, 16, 13653-13668, doi:10.5194/acp-16-13653-2016, 2016.

Weigelt, A.; Temme, C.; Bieber, E.; Schwerin, A.; Schuetze, M.; Ebinghaus, R.; Kock, H.H. : Measurements of atmospheric mercury species at a German rural background site from 2009 to 2011 – methods and results, Environmental Chemistry, 10(2), 102-110 (DOI: 10.1071/EN12107), 2013.

Weiss-Penzias, P. S., Gay, D. A., Brigham, M. E., Parsons, M. T., Gustin, M. S., & ter Schure, A. (2016). Trends in mercury wet deposition and mercury air concentrations across the US and Canada. Science of the Total Environment, 568, 546-556.

Xin, M. and Gustin, M. S.: Gaseous elemental mercury exchangewith low mercury containing soils: Investigation of controlling factors, Appl. Geochem., 22, 1451–1466, 2007.

Yang, Y. K., Zhang, C., Shi, X. J., Lin, T., andWang, D. Y.: Effect of organic matter and pH on mercury release from soils, J. Environ. Sci., 19, 1349–1354, 2007.

Yu, J., Xie, Z., Kang, H., Li, Z., Sun, C., Bian, L., Zhang, P., 2014. High variability of atmospheric mercury in the summertime boundary layer through the central Arctic Ocean. Sci. Rep. 4, 6091. doi:10.1038/srep06091.

Zhang, Y., D.J. Jacob, H.M. Horowitz, L. Chen, H.M. Amos, D.P. Krabbenhoft, F. Slemr, V.L. St. Louis, E.M. Sunderland. Observed dcrease in atmospheric mercury explained by global decline in anthropogenic emissions. Proceedings of the United States National Academy of Sciences. 113(3): 526-531.

Zhang, Y., D.J. Jacob, S. Dutkiewicz, H.M. Amos, M.S. Long, E.M. Sunderland. (2015). Biogeochemical drivers of the fate of riverine mercury discharged to the global and Arctic oceans. Global Biogeochemical Cycles, 29, 854-864.

Zhu W., Lin CJ., Wang X., Sommar J., Fu X., and Feng X., Global observations and modeling of atmosphere–surface exchange of elemental mercury: a critical review. Atmos. Chem. Phys., 16, 4451–4480, 2016.

Note to reader

This draft version of Chapter 4 in the Technical Background Report to the Global Mercury Assessment 2018 is made available for review by national representatives and experts. The draft version contains material that will be further refined and elaborated after the review process. Specific items where the content of this draft chapter will be further improved and modified are:

1. Modelling results based on the new GMA 2018 emissions inventory will be added and sent out for separate review.
2. Introduction will be updated in line with the new modelling results.
3. Internal references to other parts of the GMA report will be updated.
4. Conclusions and main messages will be finalised.

GMA 2018 Draft Chapter 4 Atmospheric Pathways, transport and fate. Oleg Travnikov, Johannes Bieser, Mark Cohen, Ashu Dastoor, Ian Hedgecock, Che-Jen Lin, Noelle Selin and Xun Wang.

8023

8024 # Contents

8042

8043
8044

8045

8046

Chapter 4 Atmospheric pathways

4.1. Introduction

Mercury (Hg) has a long environmental lifetime and cycles between the atmosphere, ocean, and land. Mercury released to the atmosphere can travel globally: it undergoes atmospheric redox reactions, deposits to the Earth's surface, and can continue to cycle between surface and atmosphere for decades to centuries. Using a combination of models and measurement, work since GMA 2013 has addressed aspects of Hg's transport and fate, including emissions, atmospheric chemistry, removal processes, modelling, and historical trends. In addition, a number of other studies have provided additional insights into regional and local mercury cycling.

Emissions and their speciation: The emergence of new regional and global emissions inventories provide alternatives to the UNEP/AMAP inventories for the present day as well as new historical estimates. Uncertainties remain in quantifying emissions, particularly from certain regions and sectors and in mercury speciation.

Atmospheric chemistry: New information has solidified our knowledge about mercury oxidation reactions, including the primary importance of Br chemistry in mercury oxidation. Models including these reactions have shorter mercury lifetimes, and can reproduce some free tropospheric observations. Recent model intercomparisons have shown that there remain challenges in reproducing observed concentrations and patterns in several areas. In particular, uncertainty remains in atmospheric speciation (Jaffe et al., 2014), the potential importance of heterogeneous chemistry (Ariya et al, 2015), and the mechanism and rate of atmospheric reduction reactions (de Foy et al., 2016).

Removal Processes: Wet deposition measurement-model comparisons, in particular in convective storms, have provided insight into the vertical distribution of mercury in the troposphere as well as oxidation processes. Dry deposition remains more poorly quantified than wet deposition, and there remains disagreement among models on its global magnitude. New measurement analyses of dry deposition have shown the importance of gaseous elemental mercury uptake into the terrestrial environment, in addition to deposition of oxidized mercury forms.

Mercury modelling: Recent model development has advanced our ability to simulate Hg transport in the atmosphere between different geographical regions and account for multi-media cycling of Hg, including the importance of legacy Hg (*this paragraph will be updated based on new simulation results)*.

Historical trends and future scenarios: Recent declines have been observed in both atmospheric mercury and wet deposition, on the order of 1-2% per year, that differ by region. Some modelling studies have reproduced these trends, attributing some regional variations to declines in emissions. Observed trends, however, are small compared with uncertainties in surface-atmosphere fluxes, anthropogenic sources, and attributable fraction. Future changes under policy scenarios could reduce mercury deposition in the future; however, the influence of climate change and legacy mercury complicates our ability to assess these potential future changes in models.

4.2. Atmospheric processes

In GMA 2013 the atmospheric chemistry section focussed on emission speciation, atmospheric Hg redox chemistry, the processes governing the exchange of Hg at environmental interfaces and atmospheric Hg dynamics. Since then progress has been made in all key areas of interest regarding atmospheric Hg chemistry and also in some which were not included, although it may seem that more questions have been posed than have been answered. Atmospheric Hg processes have been studied or inferred using theoretical, experimental, monitoring and modelling techniques and more often than not a combination of these. The chemical nature of atmospheric Hg, whether it is elemental, oxidised or bound (tightly or loosely) to atmospheric particulate matter, and its interconversion between these forms, continues to pose a challenge for the emission inventory, modelling and measurement communities alike.

4.2.1. Emissions and their speciation

Other estimates in addition to the AMAP/UNEP emission inventories of 2008 and 2013 (*AMAP/UNEP,* 2008; 2013) are now available. An alternative global anthropogenic emission inventory is available from 1970 (*Muntean et al*., 2014) which uses different approaches to determine emissions from anthropogenic activity sectors, and differs in both Hg emissions total and speciation from the AMAP/UNEP. All-time emissions to the atmosphere have been also developed in combination with estimates of releases (*Streets et al*., 2011; 2017). There have also been improvements to regional inventories (*Rafaj et al*., 2014; *Wu et al*., 2016), to estimates of historical and legacy emissions (*Amos et al.*, 2013; 2015), and also the contribution made by the past and current use of Hg in commercial products (*Horowitz et al*., 2014). A modelling comparison of the influence of using different global emission inventories on worldwide Hg deposition fields was performed recently (*De Simone et al*., 2016).

The importance of accurate emission inventories and how their uncertainty relates to the implementation of the Minamata Convention has been discussed in *Kwon and Selin* (2016). The observed decrease in atmospheric Hg species concentrations (e.g. *Zhou et al*., 2016) has led to some

authors to call into question the accuracy of current emission inventories, particularly in their estimation of European and North American sources (*Zhang et al*., 2016), and suggest that there has been a 20% decrease in total Hg emissions between 1990 and 2010, with a 30% decrease in elemental Hg.

Since GMA 2013 the discussion of emission speciation has continued. Regional and global modelling studies have also called into question the speciation in emission inventories for specific areas (*Kos et al.*, 2013; *Beiser et al*., 2014; *Zhang et al*., 2015). The partitioning of Hg(II) compounds between the gas and particulate phases is still difficult to determine. In part this is due to the lack of information concerning the Hg(II) chemical species present in the atmosphere, but also because of the vast range of particulate chemical composition. *Ariya et al*. (2015) discuss in some detail heterogeneous reactions of Hg and also interactions between Hg and fly ash which is particularly important in combustion processes leading to Hg emissions.

4.2.2. Atmospheric chemistry

Atmospheric redox reactions can occur homogeneously in the gas and aqueous phase, and heterogeneously on the surface of fog/cloud droplets and atmospheric particulate matter. At first sight the homogeneous reactions would appear to be straightforward, while it is clear that the heterogeneous reactions may be somewhat more complex to study due to the very wide range of composition of the surfaces at which reactions may take place. A recent review by *Ariya et al.* (2015) provides an in depth overview of Hg reactions and transformations in environmental media.

Perhaps the major obstacle to understanding the processes by which Hg is oxidised, reduced, adsorbed and desorbed in the atmosphere and both in and on atmospheric particles is the fact that the nature of the oxidised Hg compounds in the atmosphere remains uncertain. While it seems clear that O_3, OH, and Br are all implicated in the oxidation of atmospheric Hg, the precise nature of the reactions occurring and identity (and phase) of the products remains the subject of speculation. Recent theoretical studies have given further insight into the Br initiated oxidation of Hg; this reaction proceeds via an unstable $HgBr^*$ intermediate which may react further or decompose back to Hg and Br (*Goodsite et al.,* 2004, 2012). A series of theoretical studies have investigated the possibility, or not, that $HgBr^*$ may react with a series of small atmospheric compounds (*Dibble et al,* 2012, 2013, 2014; *Jiao and Dibble,* 2015; 2017) and also recently with VOCs (*Dibble and Schwid,* 2017). It now seems likely that the $HgBr^*$ intermediate may react further with the relatively abundant radicals HO_2 and NO_2. Meanwhile the likelihood that elemental Hg is oxidised by molecular halogens has been shown to be improbable and that oxidation to Hg halides requires either halogen atom initiation or the presence of a reactive surface (*Auzmendi-Murua et al*., 2014).

Considering only oxidation reactions can lead to atmospheric lifetimes for elemental Hg which cannot be reconciled with its global distribution and relatively uniform background hemispheric concentrations. Given the experimental and observational (in particular the rapid depletion of elemental Hg concentrations seen during AMDEs) evidence as well as the collaborative results from modelling studies that point to an atmospheric lifetime against oxidation of less than 3 months based on two recent model studies (*Shah et al.,* 2016; *Horowitz et al*., 2017). This is shorter than the estimated overall lifetime of around 12 months (*Schroeder and Munthe*, 1998). There is, therefore, likely to be Hg reduction taking place in the atmosphere, and over the years a number of mechanisms have been suggested, most of which have involved the atmospheric aqueous phase, cloud and fog droplets and deliquesced aerosols, as the reaction medium. A thorough discussion of possible reduction pathways can be found in *Ariya et al*. (2015). Most recently it has been suggested that atmospheric reduction occurs in cloud droplets via the photo-reduction of organic Hg compounds, and a model study using modelled organic aerosol concentrations as an indicator of organic Hg compound concentrations (*Horowitz et al*., 2017), based a regional modelling study which included the reduction of Hg(II) by dicarboxylic acids (*Bash et al.,* 2014). However, it should be pointed out that the rate of reduction in global models is largely tuned to reproduce observed Hg species concentrations.

Further information concerning Hg oxidation at different levels in the atmosphere has been obtained as a result of the increasing amount of observational data available from high-altitude measurement sites, observations combined with modelling can help determine which Hg atmospheric oxidation pathways are more or less likely (see for example *Weiss-Penzias et al*., 2015). In this study it was found that in one high Hg(II) free tropospheric event there was almost quantitative oxidation of Hg(0) to Hg(II). Interestingly a better model reproduction of the observations (using the GEOS-Chem model) was found when employing the O_3/OH rather than the $HgBr^*$ oxidation scheme. However, it should be pointed out that was not the most recent HgBr* scheme as described in (*Horowitz et al*., 2017). Recent model-measurement comparisons have shown episodes of high oxidized mercury concentrations that can be explained by Br oxidation (*Coburn et al.,* 2016; *Gratz et al*., 2015), and that this is consistent with constraints from global biogeochemical cycling (*Shah et al.*, 2016). These studies collectively show that measurements in free tropospheric air can significantly aid understanding of the atmospheric chemistry and dynamics of Hg. Uncertainties in measuring oxidized mercury (*Jaffe et al.,* 2014), however, challenge our ability to further advance model-measurement comparison of mercury species (*Gustin et al*., 2015).

Kos et al. (2013) performed a detailed analysis of the uncertainties associated with Hg(II) measurement and modelling. A number of model sensitivity runs were carried out to evaluate different chemical mechanisms and speciation of anthropogenic Hg emissions. In particular, they found evident inconsistencies between the emission speciation in existing emission inventories and the measured Hg(II) concentration in surface air. Besides, the OH oxidation chemistry provided better agreement with observations at simulation of the seasonal cycle of wet deposition in North America.

A complex analysis of the major Hg oxidation mechanisms was carried out by *Travnikov et al.* (2017) involving both measured data from ground-based sites and simulation results from four global chemical transport models. It was shown that the Br oxidation mechanism can reproduce successfully the observed seasonal variation of the Hg(II)/Hg(0) ratio in the near-surface air, but it predicts a wet deposition maximum in spring instead of in summer as observed at monitoring sites in North America and Europe. Model runs with OH chemistry correctly simulate both the periods of maximum and minimum values and the amplitude of observed seasonal variation but shift the maximum Hg(II)/Hg(0) ratios from spring to summer. O_3 chemistry does not predict significant seasonal variation of Hg oxidation. The possibility of more complex chemistry and/or multiple Hg oxidation pathways occurring concurrently in various parts of the atmosphere was suggested.

Bieser et al. (2017) used the same model ensemble and variety of aircraft observations to study vertical and hemispheric distributions of atmospheric Hg. They also found that different chemical mechanisms were better at reproducing observed Hg(II) patterns depending on altitude. Increased Hg(II) concentrations above the planetary boundary layer in spring and summer could only be reproduced by models using O_3 and OH chemistry. On the other hand, the Br oxidation mechanism allowed to better agreement with observed intercontinental gradients of total Hg in the upper troposphere.

4.2.3. Removal process

Hg removal from the atmosphere occurs via wet and dry deposition. Studies of Hg deposition are providing insights into atmospheric oxidation through the study of Hg in precipitation according to precipitation type (*Dvonch et al., 2005; Holmes et al*., 2016; *Kaulfus et al*., 2017). These studies show that precipitation system morphology influences Hg deposition, with convective systems showing enhanced Hg deposition by a factor of 1.6, season and region also influence the deposition. However, the nature of the precipitation system is of interest as convective systems scavenge Hg from much higher than stratiform systems. Thus indirectly these studies provide information regarding the atmospheric oxidation of Hg because the scavenging height of different cloud types differ

8209 significantly and combined with information on the vertical distribution of potential Hg oxidants,
8210 modelling studies can help to evaluate possible, probable and unlikely oxidation mechanisms at
8211 varying levels in the troposphere. This does of course require the models to more or less accurately
8212 reproduce precipitation system morphologies. More sites measuring Hg in precipitation would clearly
8213 help estimate ecosystem deposition fluxes and refine models.

8214 *Nair et al.* (2013) carried out cloud-resolving simulations of Hg wet deposition processes in several
8215 case studies in the Northeastern and Southeastern U.S. This study is of particular interest as many
8216 modelling simulations have tended to underpredict Hg wet deposition in the Southeastern U.S. It was
8217 found that wet deposition in typical Northeastern thunderstorms would generally be less than
8218 comparable storms in the Southeast – assuming identical atmospheric concentrations of Hg – due to
8219 difference in typical cloud dynamics between the two regions. In addition, it was found that
8220 stratiform precipitation typically only scavenges Hg from the lowest ~4 km of the atmosphere, while
8221 Southeastern thunderstorms can scavenge Hg up to ~10 km.

8222 In another wet deposition process analysis, apparent scavenging ratios, based on ground-level
8223 measurements of speciated air concentrations of Hg and total Hg in precipitation, were studied at
8224 four sites in the Northeastern U.S. (*Huang et al*., 2013). While the use of ground-based
8225 measurements introduced inherent uncertainties, the authors suggested that GOM concentrations
8226 may be underestimated by current measurements, as scavenging ratios based on existing GOM
8227 measurements appeared anomalously high.

8228 Several studies investigated Hg dry deposition processes. *Zhang et al.* (2012) compared CMAQ and
8229 GRAHM modelled dry deposition against field measurements in the Great Lakes region for 2002 and
8230 in some cases, for 2005. Dry deposition from the different models varied by as much as a factor of 2
8231 at regional scales, and larger variations were found at local scales. The authors suggested that the
8232 model-estimated dry deposition values were upper estimates given the tendency of the models to
8233 produce atmospheric concentrations of GOM and PBM significantly greater than measured
8234 concentrations. Following a proposed methodology to estimate bidirectional GEM surface exchange
8235 (*Wright and Zhang*, 2015) dry deposition of Hg was estimated at 24 measurement sites in the U.S.
8236 and Canada (*Zhang et al*., 2016). In this analysis, the dry deposition flux of GEM was estimated to be
8237 significantly larger than that of GOM or PBM at most of the sites. Importance of GEM dry deposition
8238 was also supported by Obrist et al. (2017) who showed that most of the Hg (about 70%) in the
8239 interior Arctic tundra is derived from GEM deposition, with only minor contributions from the
8240 deposition of Hg(II) from precipitation or AMDEs. Additional work is required to reconcile these
8241 results with those of many fate-and-transport models (e.g., *Selin et al*., 2007; *Holmes et al.,* 2010; *Lei*

et al., 2013; *Song et al*., 2015; *Cohen et al*., 2016) and estimates based on field measurement surveys (e.g., *Pirrone et al*., 2010; *Denkenberger et al*., 2012; *Eckley et al.,* 2016) that suggest that the overall net flux of GEM from terrestrial surfaces is upward.

Another aspect of Hg removal from the atmosphere has been studied by a number of groups and is the subject of ongoing monitoring, and that is the deposition of Hg via litterfall, forest canopies seem to be effective sinks for both particulate and oxidised Hg (*Fu et al*., 2016, *Wang et al*., 2016, *Wright et al*. 2016).

4.3. Global mercury atmospheric transport and fate modelling

4.3.1. Overview of recent modelling studies

Since GMA 2013 and GMA Update 2015 a number of modelling studies have addressed the problem of Hg dispersion and fate on a global scale. Global chemical transport models were used for simulations of Hg atmospheric transport, source apportionment of Hg deposition in various geographical regions, and study of processes governing Hg cycling in the atmosphere.

Transport and deposition of Hg on a global scale was studied with the global climate-chemistry model CAM-Chem/Hg for current (*Lei et al*., 2013) and future (*Lei et al*., 2014) conditions. The model generally reproduced global observed TGM levels but overestimated concentrations in South Africa which was explained by the effect of emissions. The analysis also revealed predominant influence of precipitation on the wet deposition pattern. Sensitivity experiments showed that around 22% of total Hg deposition in the United States resulted from domestic anthropogenic sources, and only 9% was contributed by transpacific transport from Asia.

A newly developed global nested GNAQPMS-Hg model was applied for simulations of Hg concentration and deposition levels and evaluation of trans-boundary transport of Chinese anthropogenic emissions (*Chen et al*., 2015). It was shown that Hg emitted from Chinese sources accounts for 62% of total deposition over the country. Contribution of Chinese anthropogenic emissions to deposition over neighbouring regions varies from 15.2% for the Korean Peninsula to 5.9% for Japan. However, for remote regions, such as North America and Europe, the contributions from China do not exceed 5%.

Dastoor et al. (2015) analysed the sources of Hg in the Canadian Arctic with the GRAHM chemical transport model. They found that the total contribution from Hg emissions originating in East Asia to annual Hg deposition in Canadian Arctic (26 to 28%) is more than twice that of the next biggest contributors, the U.S. (7 to 9%) and Europe (6 to 7%), in 2005. Global anthropogenic emissions,

terrestrial emissions, and oceanic emissions were simulated to contribute approximately 30%, 40% and 30% of Hg deposition in the Canadian Arctic, respectively.

A comprehensive analysis of source-receptor relationships of Hg concentration and deposition on a global scale was performed by *Chen et al.* (2014) using the global GEOS-Chem model. It was found that global natural sources are the main contributors for Hg deposition over all regions except East Asia. Deposition over East Asia is dominated by anthropogenic emissions with relative contribution of domestic sources of 50%. Besides, 16% of Hg deposition over North America originates from East Asia, indicating that transpacific transport of East Asian emissions is the major foreign source of Hg deposition in North America. Europe, Southeast Asia, and the Indian subcontinent also make significant contributions to Hg deposition in some receptor regions.

GEOS-Chem was also used by Song et al. (2015) for inverse modelling aimed at constraining present-day atmospheric Hg emissions and relevant physiochemical parameters. Based on the inversion results the authors updated the global estimate of Hg emission from the ocean and terrestrial ecosystems as well as anthropogenic emissions from Asian sources. Re-evaluation of the Hg long-term global biogeochemical cycle showed that legacy Hg becomes more likely to reside in the terrestrial ecosystems than in the ocean. The same model was used by *Shah et al.* (2016) to interpret aircraft measurements and to place new constraints on Hg chemistry in the free troposphere. They found that standard model simulations significantly underestimated observed reactive Hg and that use of faster oxidation mechanism could improve agreement with observations. Recently, the GEOS-Chem model was updated by implementing a new mechanism for atmospheric Hg redox chemistry to gain new insights into the global Hg budget and the patterns of Hg deposition (*Horowitz et al*., 2017).

A new global, Eulerian version of the HYSPLIT-Hg model was applied to simulate global atmospheric transport and deposition of Hg to the Great Lakes (*Cohen et al.*, 2016). The objective of the study was to estimate the amount and source-attribution for atmospheric Hg deposition to each lake, information needed to prioritize amelioration efforts. As shown, the contribution of U.S. direct anthropogenic emissions to total Hg deposition varied from 46% to 11% for different lakes. On average, the U.S. was the largest contributor for Hg deposition to the Great lakes, followed by China, contributing 25% and 6%, respectively. The results of the study also illustrated the importance of atmospheric chemistry, emissions strength, speciation, and proximity, to the amount and source-attribution of Hg deposition.

A number of modelling studies were performed with the global ECHMERIT model addressing impacts of different Hg oxidation mechanisms on the model performance when simulating Hg concentration

and deposition patterns (*De Simone et al*., 2014), contribution of biomass burning to Hg deposition worldwide (*De Simone et al*., 2015), and uncertainties associated with utilizing different global Hg emissions inventories for simulations of Hg atmospheric dispersion (*De Simone et al*., 2016). In particular, it was found that the net effect of biomass burning is to liberate Hg from lower latitudes and disperse it towards higher latitudes where it is eventually deposited. Anthropogenic Hg emissions contribute 20-25% to present-day Hg deposition and roughly two-thirds of primary anthropogenic Hg is deposited to the world's ocean.

An ensemble of four global chemical transport models for Hg (GLEMOS, GEOS-Chem, GEM-MACH-Hg, and ECHMERIT) was recently used in a series of modelling studies focused on assessment of Hg levels over the globe and evaluation of model performance in different geographical regions (*Angot et al*., 2016; *Travnikov et al*., 2017; *Bieser et al*., 2017). *Travnikov et al.* (2017) performed analysis of spatial and temporal variations of Hg surface concentrations and deposition fluxes as well as key processes governing Hg dispersion in the atmosphere. Vertical and interhemispheric distributions and speciation of Hg from the planetary boundary layer to the lower stratosphere were studied by *Bieser et al.* (2017). *Angot et al*. (2016) provided a combined analysis of the model simulations and atmospheric Hg monitoring data in the Arctic and Antarctica.

Many of the above mentioned modelling studies were focussed on assessing source-receptor relationships i.e. how emissions in one region or country contribute to deposition in others. These assessments are based on emission inventories describing current anthropogenic emissions. All models also include estimates of emissions from natural surfaces. These emissions are a mixture of natural emissions and re-emissions of anthropogenic Hg previously emitted from anthropogenic activities in previous years. The anthropogenic contributions to the re-emissions from natural surfaces can originate from both recent deposition (e.g. within 10 years) but also contains contributions from considerably longer time periods (decades to centuries). The percentage contribution of deposition from one region to the other represents the current anthropogenic emissions only.

GMA 2013 noted that multi-compartment modelling of Hg, taking into account the dynamic coupling of atmospheric Hg with the upper ocean and parts of the lithosphere, had advanced over the previous four to five years (*Selin et al*., 2008; *Sunderland et al*., 2009; *Smith-Downey et al*., 2010). Of the models used in the 2015 update, two (GLEMOS and GMHG) were mainly atmospheric models, and one (GEOS-Chem) simulated dynamic cycling. Recent work has advanced observational constraints on Hg biogeochemical cycling, using worldwide measurements (*Agnan et al*., 2016; *Lamborg et al.*, 2014; *Wang et al*., 2016) as well as inverse modelling (*Song et al*., 2015). A key

conclusion of these studies, taken together, is that legacy emissions from land may be smaller than previously assumed in global models. Further multimedia analyses have added to our understanding of the anthropogenic enrichment of the global biogeochemical cycle of Hg (*Amos et al*., 2015), and in particular the role of legacy Hg. See also discussion below in Section 4.4.

4.3.2. Mercury atmospheric loads to terrestrial and aquatic regions

(To be added based on new simulation results)

4.3.3. Source apportionment of mercury deposition

(To be added based on new simulation results)

4.3.4. Contribution of different emission sectors to mercury deposition

(To be added based on new simulation results)

4.4. Historical trends and future scenarios

Evaluation of historical changes of Hg atmospheric concentration and deposition to other environmental media is important because it helps understanding how legacy of previous anthropogenic emissions affects the present-day Hg pollution levels and future environmental responses to expected emission control measures. Human disturbance of Hg natural cycling in the environment by mining and industrial activities led to significant enrichment of atmospheric Hg since pre-industrial times (e.g. *Fitzgerald et al.,* 1998; *Lindberg et al*., 2007; *Biester et al*., 2007). Recently, *Amos et al*. (2013; 2014; 2015) applied a multi-media box model coupling the atmosphere, ocean, and terrestrial reservoirs to reconstruct Hg historical cycling among the geochemical reservoirs on the millennium scale. They found that the present-day atmospheric deposition has increased by a factor of 2.6 from the preindustrial period (ca. 1850), which consistent with sediment archives. Moreover, all-time anthropogenic emissions (ca. since 2000 BC) have enriched the present-day Hg levels in the atmosphere, surface ocean, and deep ocean by factors of 7.5, 5.9, and 2.1, respectively, relative to natural conditions (*Amos et al*., 2013). Besides, *Amos et al*. (2014) showed that accounting for the additional loss of Hg to ocean margin sediments suggests twice as large as the all-time relative enrichment in surface reservoirs. Both model simulations and natural archives provide evidence for peak atmospheric Hg concentrations during the second half of the 20th century and declines in more recent decades (*Amos et al*., 2015).

Changes of Hg atmospheric deposition over two last decades in different geographical regions were evaluated in a number of recent modelling studies. Long-term trends of Hg deposition in Europe were analysed within the framework of the Task Force on Measurements and Modelling under the EMEP Co-operative Programme for Monitoring and Evaluation of the Long-range Transmission of Air

Pollutants in Europe (*Colette et al*., 2016). According to the modelling results presented in the study Hg total deposition in the considered EMEP region (Europe and Central Asia) decreased on average by 23% during the period 1990-2012 (about -1% y^{-1}). However, the deposition trend was essentially non-linear with the rates of deposition reduction being higher at the beginning and lower at the end of the period. Besides, the deposition changes differ significantly between individual countries ranging from 70% decrease to 10% increase in some countries. Generally, the decrease of deposition was larger in the European Union (35% for the period 1990-2012 or -1.5% y^{-1}) than in other parts of the region. Similar rates (-1.5±0.7% y^{-1}) of Hg wet deposition reduction at a number of monitoring sites in Western Europe were simulated for the period 1996-2008 (*Muntean et al*., 2014), which was twice as lower as the observed trend at these sites. *Zhang et al.* (2016) estimated somewhat steeper trend of Hg wet deposition in the same region (-2.0±0.14% y^{-1}). *Muntean et al*. (2014) estimated Hg wet deposition decline in North America as of -2.4±0.7 % y^{-1} for the period 1996-2008. *Zhang et al*. (2016) utilized an updated emissions inventory and obtained somewhat smaller decline -1.4±0.1 % y^{-1} for longer period (1996-2013) in the same region.

Soerensen et al. (2012) used a global Hg model (GEOS-Chem) that coupled the atmosphere, soil, and the surface ocean to analyse a long-term decline in Hg^0 concentration over the Northern Atlantic. They found that existing inventories of Hg anthropogenic emissions cannot explain substantial decrease of observed Hg^0 concentration (-2.5% y^{-1}) for the period 1990-2009 since significant emissions reduction in North America and Europe are balanced by the rise of Hg emissions in East Asia. The model application allowed attributing this decrease to reduction of Hg emissions from the ocean as a result of declining subsurface seawater Hg concentrations. It was hypothesized that the declining trend can be explained by decreased riverine and wastewater inputs at ocean margins (*Soerensen et al*., 2012). However, later *Amos et al*. (2014) showed that the inputs of Hg to the North Atlantic from rivers also did not contribute substantially to these changes. On the other hand, *Zhang et al.* (2016) demonstrated that revised anthropogenic emissions can explain the observed decline in Hg concentration over the past two decades. Therefore, the model evaluation of long-term changes of Hg concentration and deposition levels highly depends on availability of reliable data on historical Hg emissions.

Despite increases in global anthropogenic emissions over the past several decades (*Streets et al.,* 2011), Arctic atmospheric Hg levels have decreased or remained constant (*Cole and Steffen*, 2010; *Cole et al*., 2013, *Berg et al*. 2013). Implications of climate change related factors such as rise in air temperatures (particularly in spring) and reduced sea ice extent and thickness to the Hg levels in the

Arctic ecosystems are complex and multidirectional (*Stern et al.,* 2012; *Bekryaev et al*., 2010; *Cavalieri et al*., 2012).

Fisher et al. (2013) investigated the factors controlling Hg(0) trends in the Arctic from 1979-2008 using global historical anthropogenic emissions inventory of *Streets et al.* (2011) using GEOS-Chem. The model simulated a small increasing trend in Hg(0) concentrations over 30 years mainly reflecting the growth in emissions. Besides, the authors suggested that climate warming may lead to decreased fluxes of Hg from the atmosphere to the cryosphere and increased Hg(0) concentrations in the Arctic. *Chen et al*. (2015) extended the study by *Fisher et al*. (2013) to quantitatively determine the contributions of changes in environmental variables and anthropogenic emissions to Hg trends in the Arctic using anthropogenic emission inventories from AMAP/UNEP for the years 2000, 2005, and 2010. In addition to confirming the results by *Fisher et al*. (2013) in spring and summer, the study found that decrease in Atlantic ocean evasion of Hg at lower latitudes contributed to the decrease in Hg(0) concentrations in the Arctic from November–March.

Dastoor et al. (2015) assessed the impact of changing anthropogenic emissions and meteorology on Hg(0) concentrations and deposition in the Canadian Arctic from 1990-2005 using GEM-MACH-Hg and AMAP anthropogenic emissions (*AMAP*, 2011). Changes in meteorology and anthropogenic emissions were found to contribute equally to the decrease in surface air Hg(0) concentrations in the Canadian Arctic with an overall decline of ~12% from 1990-2005 in agreement with measurements at Alert (*Cole and Steffen*, 2010; *Cole et al.,* 2013). In contrast, the model simulated 15% increase and 5% decrease in net deposition in the High Arctic due to changes in meteorology and decline in emissions in North America and Europe, respectively, resulting in an overall increase of 10% in Hg deposition over a period of 1990-2005. Although the link between Hg deposition and lake sediment fluxes is not fully understood, an increase in deposition of Hg in the Arctic appears to be consistent with observed increases in Hg fluxes in some Arctic lake sediments in recent decades (*Goodsite et al*., 2013).

Despite modelling differences, all studies suggested a dominant role of climate warming related changes in environmental factors on Hg trends in the Arctic. Current Hg models lack a complete representation of the complexity of climate sensitive Hg processes. Fully interactive atmosphere-land-ocean biogeochemical Hg models including detailed representation of sea-ice dynamics are required to close the gap in modelling results.

Future changes of Hg atmospheric concentration and deposition to the ground as a result of changes in anthropogenic emissions, land use and land cover as well as climate change were also investigated

in a number of modelling studies. *Pacyna et al.* (2016) used two chemical transport models (GLEMOS and ECHMERIT) to evaluate future changes of Hg depositions in various geographical regions for three anthropogenic emissions scenarios of 2035 (Fig. 1). The "Current Policy" scenario (CP 2035) predicted a considerable decrease (20-30%) of Hg deposition in Europe and North America and strong (up to 50 %) increase in South and East Asia. According to the "New Policy" scenario (NP 2035) a moderate decrease in Hg deposition (20-30%) was predicted in all regions except for South Asia. Model predictions based on the "Maximum Feasible Reduction" scenario (MFR 2035) demonstrated consistent Hg deposition reduction on a global scale. It should be noted that the geogenic and legacy sources were assumed to be unchanged in this study.

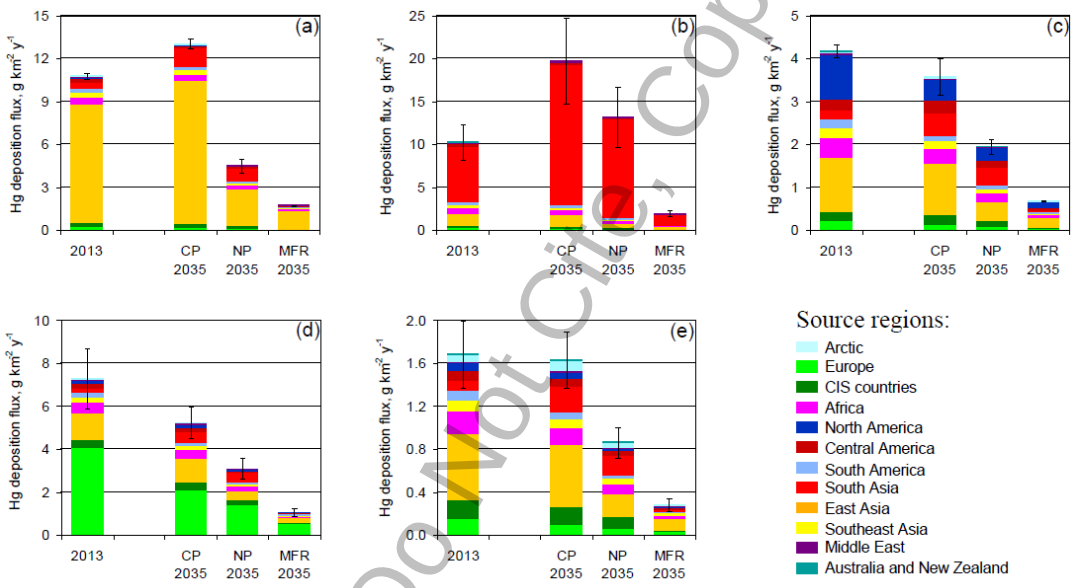

Figure 1. *Source apportionment of Hg deposition from direct anthropogenic sources (average of two models) in 2013 and 2035 in various geographical regions: (a) East Asia, (b) South America, (c) North America, (d) Europe, (e), and the Arctic. Whiskers show deviation between the models. Contribution of natural and secondary emissions are not shown. Source: Pacyna et al. (2016).*

A combined effect of emissions changes and temperature increase associated with climate change was studied by *Lei et al.* (2014) with the CAM-Chem model using three emissions scenarios of 2050 (B1, A1B, A1FI) based on projections developed by the Intergovernmental Panel on Climate Change (IPCC). It was found that all three scenarios predict general increase of total gaseous Hg concentration around the globe due to increasing use in fossil fuel energy. The increase in temperature enhances emissions from land and ocean and accelerates oxidation of Hg^0 leading to increased deposition. The effect of climate change as well as alteration of land cover/land use on

future Hg levels were studied more thoroughly by *Zhang et al.* (2016) by combining a chemical transport model (GEOS-Chem), a general circulation model (GISS GCM 3), and a dynamic vegetation model (LPJ). Using the IPCC A1B scenario for the simulation of 2000-2050 climate change they found that the surface Hg^0 concentration is to increase globally with significant changes occurring over most continental and ocean regions due to changes in atmospheric Hg redox chemistry. Changes in natural vegetation and anthropogenic land use lead to general increases in Hg^0 dry deposition. The gross Hg deposition flux will increase over most continental regions driven by combined changes in climate and land use/land cover. However, these results do not take into account the possible feedback of the deep ocean and terrestrial reservoirs to the future emissions and climate changes.

Amos et al. (2013) used a fully coupled biogeochemical model and showed that even if anthropogenic emissions stay unchangeable, Hg deposition will continue to increase due to effect of the legacy of anthropogenic production emissions accumulated in the ocean. Generally, the atmosphere responds quickly to the termination of future emissions, but long-term changes are sensitive to a number of factors, including historical changes in anthropogenic emissions, air-sea exchange, and Hg burial in deep ocean and coastal sediments (*Amos et al.*, 2014, 2015).

4.5. Region-specific modelling studies

4.5.1. Polar regions

Since GMA 2013, three global Hg models have been applied to study Hg cycling in polar regions - GLEMOS (*Travnikov and Ilyin*, 2009), GEOS-Chem (*Fisher et al*. 2012; *Holmes et al*., 2010), and GEM-MACH-Hg (formerly GRAHM; *Dastoor et al*., 2008; *Durnford et al*., 2012; *Kos et al*., 2013). The largest differences among models in the polar-regions are related with the representation of Hg(0)-Br oxidation rates, Br concentrations, parameterization of photo-reduction and re-emission of Hg(0) from the snowpack, and Hg evasion fluxes from the Arctic Ocean (*Angot et al.,* 2016). *Durnford et al*. (2012) developed and implemented a dynamic multi-layer snowpack-meltwater parameterization in GEM-MACH-Hg. *Fisher et al.* (2012) and *Durnford et al*. (2012) introduced enhanced evasion of Hg from the Arctic Ocean during summer to explain the observed summertime maximum in Hg(0) concentrations (*Steffen et al*. 2005; *Berg et al.* 2013). *Dastoor and Durnford* (2014) found that the summertime concentrations in the Arctic are characterized by two distinct summertime maxima with the peaks varying in time with location and the year. Using GEM-MACH-Hg, the authors demonstrated that early summer peak in Hg(0) concentrations is supported primarily by re-emission of Hg from melting snowpack and meltwater and the late summer peak is supported by evasion of Hg(0) from the Arctic Ocean. *Toyota et al*. (2014) developed a detailed one-dimensional air–snowpack model for interactions of bromine, ozone, and Hg in the springtime Arctic which provided

a physicochemical mechanism for AMDEs and concurrently occurring ozone depletion events (ODEs). The authors also developed a temperature dependent GOM-PBM partitioning mechanism explaining its observed seasonal transition (*Steffen et al*., 2014) and demonstrated that PBM is mainly produced as $HgBr_4^{2-}$ through uptake of GOM into bromine-enriched aerosols after ozone is significantly depleted in the Arctic air masses.

Dastoor and Durnford (2014) conducted a comprehensive evaluation of GEM-MACH-Hg simulated concentrations of Hg(0) and Hg(II) in air, total Hg (THg) concentrations in precipitation and seasonal snowpack, and snow/air Hg fluxes with measurements from 2005-2009 at 4 Arctic sires – Alert, Ny-Ålesund, Amderma, and Barrow (see Fig. 2 for the sites location). The model median concentrations of Hg(0) and Hg(II) were found within the range of observed medians at all locations. Hg concentrations in snow collected during springtime (AMDEs season) are significantly higher at Barrow than at Alert, which was well simulated by the model. Modelled Hg concentrations in seasonal snowpack were also within the measured range.

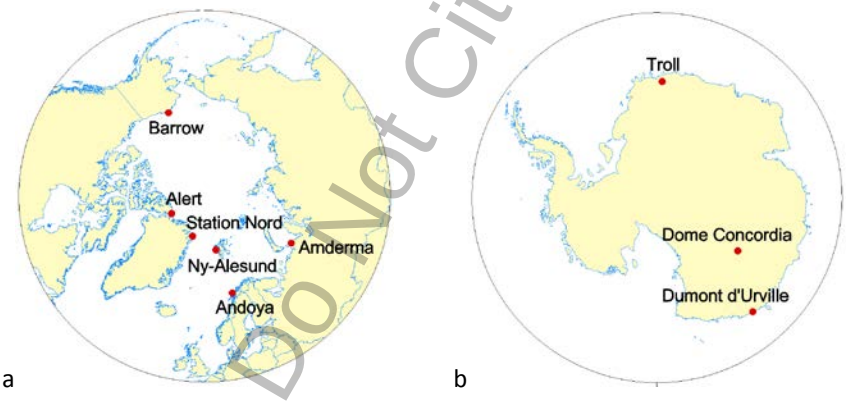

Figure 2: *Location of Arctic (a) and Antarctic (b) ground-based sites used for model evaluation.*

Angot et al. (2016) evaluated GEM-MACH-Hg, GEOS-Chem and GLEMOS using atmospheric monitoring data of Hg concentrations for 2013 at 4 Arctic sites (Alert, Station Nord, Ny-Ålesund and Andøya) and 3 Antarctic sites (Troll, Dome Concordia, and Dumont d'Urville) shown in Fig. 2. In addition, interannual variability in Hg(0) concentrations were evaluated using GEOS-Chem and GEM-MACH-Hg simulations from 2011-2014. The models captured the broad spatial and seasonal patterns in Hg(0) concentrations observed in the Arctic. The decline in Hg(0) concentrations from Andøya, the site closest to European industrialized areas, to Alert, the most northerly site, was well reproduced by the models and suggests transport of anthropogenic Hg from lower latitudes to the Arctic. A more

pronounced seasonal cycle observed at Alert and Station Nord than Ny-Ålesund and Andøya was also captured by the models (Fig. 3).

All models reproduced the characteristic low Hg(0) concentrations in spring and high Hg(0) concentrations in summer. Consistent with observations, the models simulated enhanced total oxidized Hg concentrations (i.e., oxidized gaseous and particulate Hg) at Alert and Ny-Ålesund during the AMDEs season but underestimated the values compared to measurements. At Ny-Ålesund all the models overestimated wet deposition along with overestimation of precipitation amount. The model-measurement discrepancy was attributed to lower collection efficiency of precipitation in polar regions due to frequent strong winds and blowing snow conditions (*Lynch et al*., 2003 and *Prestbo and Gay*, 2009) and to the uncertainties in gas-particle partitioning of oxidized Hg in the models.

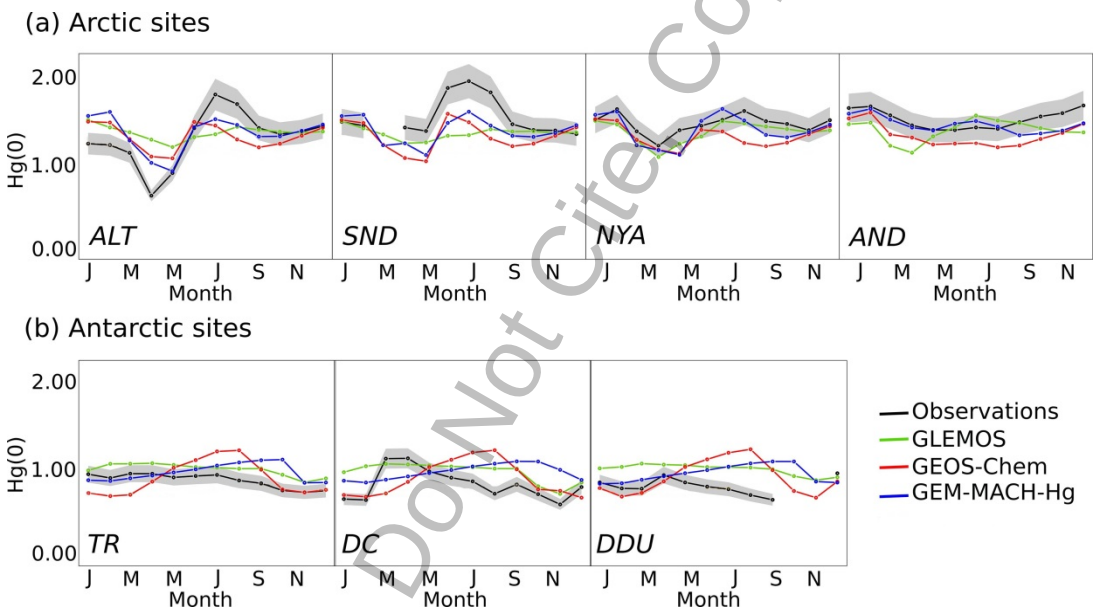

Figure 3: *Year 2013 monthly-averaged Hg(0) concentrations (in ng m^{-3}) at (a) Arctic and (b) Antarctic ground-based sites: observations (in black) and concentrations according to the three global models (GLEMOS in green, GEOS-Chem in blue, GEM-MACH-Hg in red). The grey shaded regions indicate a 10% uncertainty for observations. Adapted from Angot et al. (2016). Only models that explicitly implement high-latitude specific processes are shown.*

Simulated Hg(0) interannual variability in GEOS-Chem and GEM-MACH-Hg in winter was lower than measured which suggests an impact of interannual variability in anthropogenic emissions; the models used 2010 global anthropogenic Hg emissions (*AMAP/UNEP*, 2010) for simulations from 2011-2014. Interannual variability in the frequency of AMDEs was fairly well reproduced by GEM-

MACH-Hg but not by GEOS-Chem. Real-time modelling of the distribution of bromine concentrations and sea-ice dynamics is needed to improve the models (*Moore et al*., 2014).

In contrast, at Antarctic sites, the models overestimated Hg(0) concentrations and failed to reproduce observed seasonal patterns in Hg(0) concentrations (Fig. 3). GEM-MACH-Hg and GEOS-Chem simulated increasing Hg(0) concentrations at all sites over the course of winter in contradiction with observations; whereas, GLEMOS simulated lower than observed wintertime decline in Hg(0) concentrations at Dumont d'Urville and Dome Concordia (*Angot et al*., 2016). High summertime variability and strong diurnal cycle in Hg(0) concentrations observed at Dumont d'Urville and Dome Concordia were also not well reproduced by the models. GEM-MACH-Hg did not simulate the infrequent AMDEs observed at Troll and Dumont d'Urville in spring; whereas, GEOS-Chem simulated AMDEs at DDU with somewhat higher frequency than observed. *Angot et al*. (2016) attributed poor model simulation of Hg at the Antarctic sites to missing local Hg(0) oxidation pathways involving OH, O_3, NOx, and RO_2 radicals and air circulation, and bias in southern hemispheric emissions including oceanic evasion in the models.

Modelling estimates of Hg mass fluxes in the Arctic including the Arctic Ocean were provided by *Fisher et al.* (2012), *Durnford et al.* (2012) and *Dastoor and Durnford* (2014). Using GEOS-Chem, *Fisher et al.* (2012) estimated Hg deposition of 55 Mg y^{-1} (i.e., 25 Mg y^{-1} directly to open ocean, 20 Mg y^{-1} to ocean via snow melt on sea ice, and 10 Mg y^{-1} to land via snow melt), evasion from ocean of 90 Mg y^{-1} and a net surface loss of 35 Mg y^{-1} in the Arctic north of 70°. In contrast, using GEM-MACH-Hg, *Durnford et al*. (2012) estimated Hg deposition of 153 Mg y^{-1} (i.e., 58 Mg y^{-1} directly to open ocean, 50 Mg y^{-1} to ocean via snow melt on sea ice, 29 Mg y^{-1} directly to land, and 16 Mg y^{-1} to land via snow melt), emission of 36 Mg y^{-1} (i.e., 33 Mg y^{-1} from ocean and 3 Mg y^{-1} from land) and a net surface gain of 117 Mg y^{-1} in the Arctic north of 66.5°. Thus, *Fisher et al.* (2012) concluded that Arctic Ocean is a net source of Hg to the atmosphere, i.e., 45 Mg y^{-1}; whereas, *Durnford et al*. (2012) concluded that Arctic Ocean is a sink of atmospheric Hg, i.e., 75 Mg y^{-1}. In comparison, GLEMOS estimated the yearly net gain of Hg in the Arctic to be 131 Mg y^{-1} (*Travnikov and Ilyin*, 2009).

Model disagreements in the estimates of atmosphere-ocean-snowpack Hg fluxes indicate sources of uncertainties in the models. Constraining models in the polar regions is challenging due to insufficient measurements (*Dastoor and Durnford*, 2014; *Angot et al*., 2016). *Fisher et al*. (2012) inferred that 95 Mg y^{-1} input of Hg from circumpolar rivers (and coastal erosion) resulting in 90 Mg y^{-1} evasion of Hg from the Arctic Ocean was required to balance the observed summertime peak in Hg(0) concentrations at the Arctic sites. In contrast, *Durnford et al*. (2012) found that 33 Mg y^{-1} Hg evasion from the Arctic Ocean was sufficient to reproduce the summertime peak Hg(0)

concentrations in the Arctic. *Dastoor and Durnford* (2014) estimated riverine Hg export to the Arctic Ocean from North American, Russian and all Arctic watersheds in the range of 2.8-5.6, 12.7-25.4 and 15.5-31.0 Mg y^{-1}, respectively, based on GEM-MACH-Hg simulated Hg in meltwater. Using MITgcm ocean model and GEOS-Chem, *Zhang et al*. (2015) concluded that an input of 63 Mg y^{-1} of Hg discharge from rivers and coastal erosion to the Arctic Ocean was needed to reproduce the observed summer maximum in atmospheric Hg(0) concentrations. Riverine discharge to the Arctic Ocean is poorly constrained by observations with estimates ranging from 12.5 to 44 Mg y^{-1} (*Outridge et al*., 2008; *Amos et al*., 2014). *Zhang et al*. (2015) noted that enhanced turbulence associated with sea ice dynamics facilitates increased evasion of Hg discharged by Arctic rivers in estuaries resulting in a much larger portion of riverine Hg in the Arctic Ocean subjected to evasion than estimated in *Fisher et al*. (2012). In addition, *Fisher et al*. (2012) assumed that the Hg input from rivers is uniformly distributed in the entire Arctic Ocean; whereas, latitudinal variation in Hg evasion from the Arctic Ocean was considered in *Durnford et al*. (2012) and *Zhang et al*. (2015) which is supported by observations (*Andersson et al*., 2008; *Hirdman et al*. 2009; *Sommar et al*, 2010). Other sources of differences in models were related with the parameterizations of bromine concentrations and Hg snowpack/meltwater processes (*Dastoor and Durnford*, 2014).

4.5.2. Europe

In recent years, the development of regional atmospheric Hg models for Europe was supported by the FP7 project GMOS (Global Mercury Observations System). Mercury chemistry was implemented into the on-line coupled meteorological CTM WRF-Chem by *Gencarelli et al.* (2014) and the CCLM-CMAQ model was further developed (*Bieser et al.,* 2014; *Zhu et al.,* 2015). These models have been used to evaluate key processes and identify their impact on Hg dispersion and deposition in Europe (*Gencarelli et al*., 2016; *Bieser et al*., 2017).

As it follows from recent estimates by *Muntean et al*. (2014) Hg emissions in Europe continue to decrease, but with different rates for each Hg species. Due to technological development, emissions of GOM are declining faster than total Hg emissions, which affects the regional deposition and global transport patterns. This finding was further confirmed by model studies were the models tendency to overestimate ground based GOM concentrations could be attributed to the speciation of primary anthropogenic Hg emissions (*Bieser et al*., 2014; 2017). Moreover, airborne in situ measurements at a modern coal fired power plant did not detect any GOM 1 km downwind from the stack (*Weigelt et al.,* 2016).

The models have in common, that the modelled annual wet deposition fluxes are in good agreement with observations. This was found for regional (*Gencarelli et al*., 2014; *Bieser et al.,* 2014) and global

models (*Muntean et al*., 2014). At the same time, models tend to underestimate TGM concentrations for Europe. A behaviour which is also seen in the results from global models (*Muntean et al.*, 2014; *Chen et al*., 2013). The reason for this is not understood yet. In a global long term simulation with the GEOS-Chem model *Muntean et al*. (2014) showed that modelled TGM concentrations were closer to observations in the 1990s but that the model overestimates the decreasing tend over the last decades. Thus, the emission inventories might play a role for this. This is also in line, with the fact that new regional emission models lead to higher estimates for European Hg emissions (*Rafaj et al*., 2014).

Moreover, a recent study with a newly developed regional multi-media model indicates that an underestimation of the air-sea exchange from regional oceans could be a source for the model bias in Europe (*Bieser and Schrum*, 2016). Figure 4 depicts the impact of air-sea exchange on Hg concentrations at two ground based stations in Europe. It can be seen, that close to the ocean (Zingst) air-sea exchange has a large impact on GEM concentrations. This effect, albeit less pronounced, was also observed at a station 200 km inland (Waldhof).

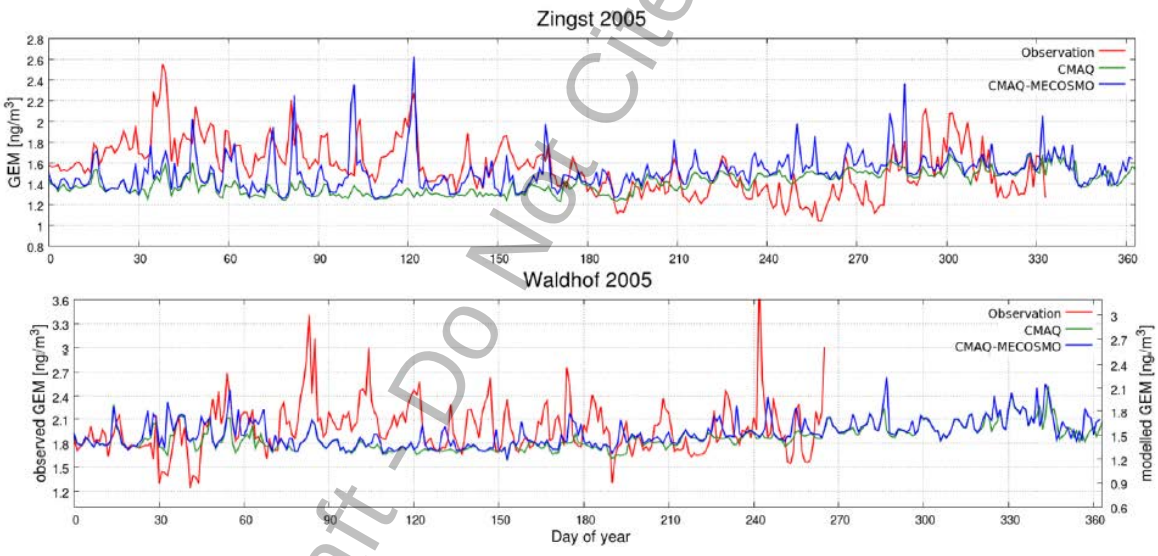

Figure 4: *Impact of air-sea exchange on atmospheric Hg concentrations at two ground based observations sites in Germany: observation (red), atmospheric model (green), coupled ocean-atmospheric model (blue) (Bieser and Schrum, 2016).*

A first model analysis on the vertical distribution of Hg in Europe was recently published (*Bieser et al.,* 2017). Based on aircraft based observations, it was found that models are generally able to reproduce the GEM gradient from the surface up to the tropopause (Fig. 4). Moreover, models were able to reproduce the GOM gradient inside the planetary boundary layer, in those cases where a low

GOM fraction in the anthropogenic emissions was assumed. This is in line with the findings on decreasing GOM fraction in European Hg emissions discussed earlier.

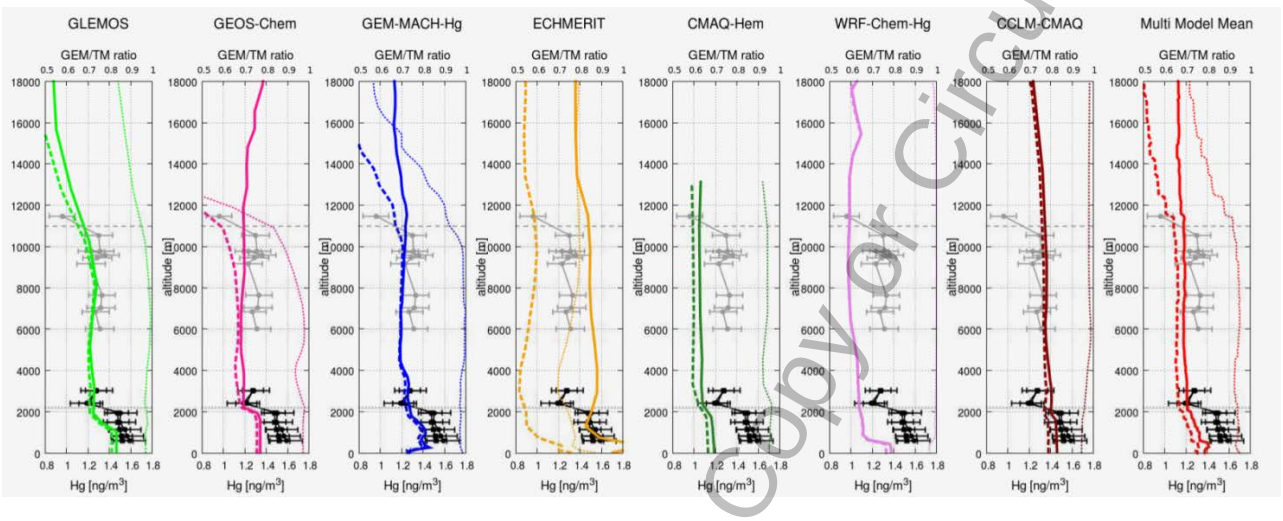

Figure 4: *Vertical profiles at Leipzig, Germany 23rd August 2013 from two aircraft campaigns and simulations with seven atmospheric chemistry transport models. Black dots are observations from the European Tropospheric Mercury Experiment (ETMEP), grey dots are observations from the CARIBIC civil passenger aircraft. The coloured lines indicate modelled TM (solid) and GEM (dashed) concentrations. The dotted lines depict the GEM/TM ratio. Source: Bieser et al. (2017).*

The impact of long range transport on European Hg deposition has been addressed before (*UNEP*, 2015). Since then, there has been a new study on the global transport of Hg from Asia (*Chen et al.,* 2015). Here, the estimated contribution of Chinese emissions to Hg deposition in Europe is only 3.5%, which is much smaller than previous estimates of 20% (*UNEP,* 2015). The impact of long range transport on regional Hg deposition in Europe is strongly dependent on the lifetime of Hg in the atmospheric models. A new study by *Horowitz et al*. (2017) indicates that organic aerosols mediate photolytic reduction of oxidized Hg species in the aqueous phase leading to an increased life time of Hg in the atmosphere. Due to the high concentration of organic aerosols in China current models might underestimate the long range transport due to an overestimation of atmospheric oxidation. *De Simone et al*. (2015, 2016) investigated the impact of biomass burning on atmospheric Hg concentrations and deposition. Especially wild fires in the boreal forests can have a large impact on regional Hg concentration and deposition. For Europe, they estimate the fraction of Hg deposition due to biomass burning between 5% and 10%.

4.5.3. North America

CMAQ, with global boundary conditions estimated with the MOZART model, was used to estimate atmospheric Hg deposition to the Great Lakes for 2005 (*Grant et al.*, 2014). U.S. emissions from power plants had the largest impact on Lake Erie. The model tended to overestimate wet deposition in the Great Lakes region. In another CMAQ-based investigation, the model was used with boundary conditions from GEOS-Chem, and alternatively, GRAHM, to estimate atmospheric Hg deposition in the United States (*Myers et al*., 2013) in a series of 2001-2005 case studies. Simulation results were significantly influenced by the choice of boundary conditions. CMAQ, with a new aqueous-phase oxidized Hg reduction chemical mechanism (involving dicarboxylic acids) and GEOS-Chem boundary conditions, was used to simulate Hg fate and transport in the U.S. during 2001-2002. Results for wet deposition with the new chemical mechanism were found to be more consistent with observations than earlier mechanisms used in CMAQ. Using a weight-of-evidence approach, *Sunderland et al*. (2016) argued that historical EPA CMAQ-based modelling may have underestimated the impact of local and regional sources on near-field Hg deposition in the U.S., and consequently underestimated the benefits of Hg emissions reductions.

The GEOS-Chem model was used to estimate the cumulative benefits of domestic and international Hg controls for atmospheric deposition – and subsequent public health impacts – in the U.S. through 2050 (*Giang and Selin*, 2016). For the same amount of avoided Hg emissions, domestic reductions were estimated to have nearly an order of magnitude higher public health benefit than international actions. The CAM-Chem-Hg model was used to estimate present day (ca. 2000) (*Lei et al*., 2013) and future (ca. 2050) (*Lei et al*., 2014) atmospheric Hg concentrations and deposition in the U.S., as influenced by different scenarios of changes in U.S. and global emissions, and different climate change scenarios. Concentrations and deposition in the U.S. increased significantly in scenarios with higher future emissions and higher atmospheric temperatures. Under the most impacted scenario considered, climate change alone caused an approximate 50-100% increase in atmospheric Hg concentrations in the U.S. When increased Hg emissions in this scenario were included, the average Hg(0), GOM, and PBM concentrations in the U.S. increased by a factors of ~2.5x, ~5x, and ~3x, respectively. The GRE-CAPS model – which included a version of the regional CAMx model - was used to investigate the influence of climate change on atmospheric Hg deposition in the Eastern U.S. (*Megaritis et al.*, 2014). Simulations for the present day (ca. 2000's) were compared with climate-change-influenced simulations for the year 2050, assuming constant 2001 Hg emissions. The study found that average deposition in the U.S. increased by about ~5% due to climate-change impacts (e.g., enhanced atmospheric oxidation of GEM at higher temperatures), but regional differences were found (e.g., related to changes in precipitation patterns).

The HYSPLIT-Hg model was used to estimate 2005 atmospheric Hg deposition to the Great Lakes (*Cohen et al.*, 2016). Results for a base case and 10 alternative model configurations were developed, examining the sensitivity of the results to different assumptions regarding atmospheric reaction rates and chemical mechanisms. Model evaluation against measurements in the Great Lakes region showed good agreement between modelled and measured wet deposition and Hg(0) concentrations, but the model tended to overpredict reported GOM and PBM concentrations. The total deposition and source-attribution for that deposition was similar to that found by *Grant et al.* (2014) (e.g., see Figure 5). Lake Erie, downwind of significant local/regional emissions sources, was estimated by the model to be the most impacted by direct anthropogenic emissions (58% of the base case total deposition), while Lake Superior, with the fewest upwind local/regional sources, was the least impacted (27%). The U.S. was the largest national contributor, followed by China, contributing 25% and 6%, respectively, on average, for the Great Lakes. The contribution of U.S. direct anthropogenic emissions to total Hg deposition varied between 46% for the base case (with a range of 24–51% over all model configurations) for Lake Erie and 11% (range 6–13%) for Lake Superior. The relative contributions of different sources are illustrated in Figure 6 for the base case simulation. These results were used in an International Joint Commission report (*IJC*, 2015) which called for increased monitoring and modelling of atmospheric Hg in the Great Lakes region.

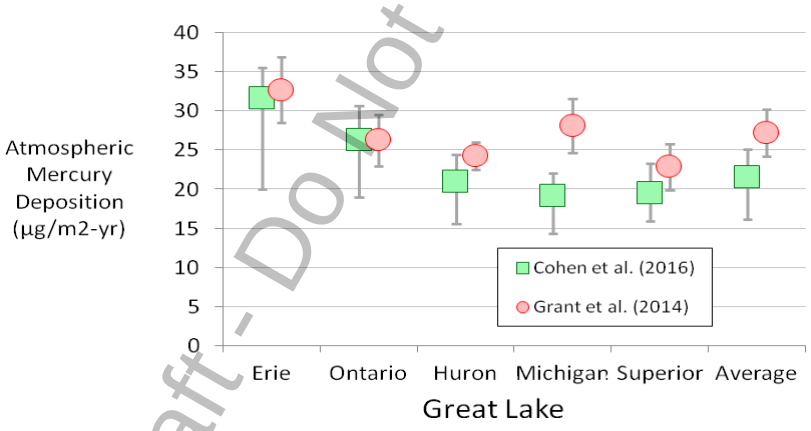

Figure 5. *Atmospheric Hg deposition flux to the Great Lakes for 2005, estimated by CMAQ (Grant et al., 2014) and HYSPLIT-Hg (Cohen et al., 2016). CMAQ error bars shown are the reported range in estimates for each lake. HYSPLIT-Hg error bars shown are the range found in the 10 alternate model configurations used in the analysis. The Great Lakes summary values shown are based on an area-weighted average of individual-lake results.*

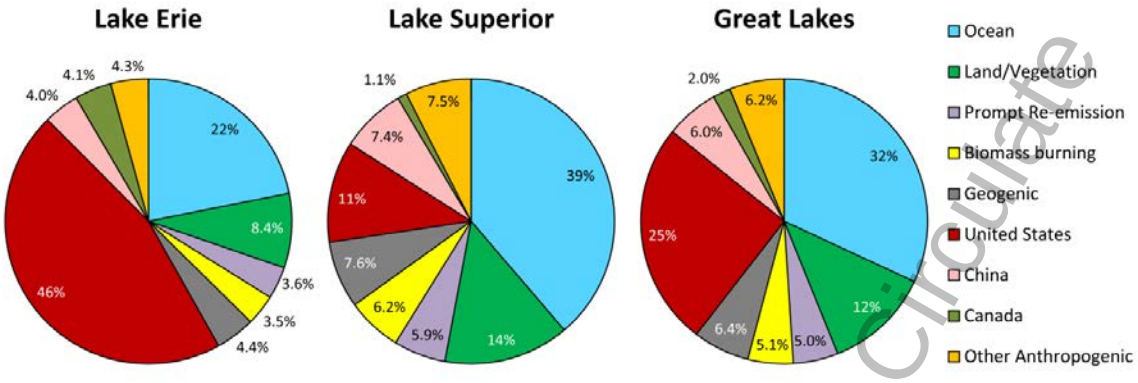

Figure 6. *Relative contributions of different source categories to 2005 atmospheric Hg deposition to Lake Erie, Lake Superior, and an area-weighted average for the Great Lakes, estimated by the HYSPLIT-Hg model (Cohen et al., 2016) (base-case simulation). The values shown for specific countries (United States, China, and Canada) and for all other countries ("Other Anthropogenic") include only the contributions from direct, anthropogenic emissions and do not include contributions arising from re-emissions of previously deposited material from terrestrial or oceanic surfaces.*

A number of analyses were conducted in which measurements of atmospheric concentrations were combined with back-trajectory and other receptor-based modelling approaches to assess the relative importance of different source regions and other factors to the atmospheric Hg arriving at the measurement site (see Table 1 for references). In most cases, the HYSPLIT model (*Stein et al.,* 2015) was used for simulating back-trajectories. Similar studies were carried out for flight-based measurements of atmosphere Hg concentrations above the surface, utilizing back-trajectories and/or other model simulations, above Tullahoma, TN (*Brooks et al*., 2014), Texas and the Southeastern U.S. (*Ambrose et al.,* 2015; *Gratz et al*., 2015; *Shah et al*., 2016), and Lake Michigan (*Gratz et al*., 2016).

Table 1. Measurement sites analysed with receptor-based modelling

Measurement site	Country	Back-trajectory Study
Beltsville, MD	USA	*Ren et al*., 2016
Celestun, Yucatan	MEX	*Velasco et al*., 2016
Chicago, IL	USA	*Gratz et al*., 2013a
Dartmouth, NS	CAN	*Cheng et al*., 2013a; *Cheng et al*., 2016
Grand Bay, MS	USA	*Ren et al.,* 2014; *Rolison et al*., 2013
Holland MI	USA	*Gratz et al*., 2013a
Huntington Forest, NY	USA	*Zhou et al*., 2017; *Choi et al*., 2013; *Cheng et al*., 2013b
Illinois (several sites)	USA	*Gratz et al*., 2013b; *Lynam et al*., 2014
Kejimkujik, NS	CAN	*Cheng et al*., 2013a; *Cheng et al*., 2016
Oxford, MS	USA	*Jiang et al*., 2013
Pensacola, FL	USA	*Huang et al*., 2016; *Demers et al*., 2015
Piney Reservoir, MD	USA	*Castro and Sherwell,* 2015
Reno, NV	USA	*Gustin et al*., 2016

Rochester, NY	USA	*Choi et al.*, 2013
Steubenville, OH	USA	*White et al*., 2013
Underhill, VT	USA	*Zhou et al.*, 2017
Western U.S. (several sites)	USA	*Wright et al*., 2014; *Huang and Gustin*, 2015; *Gustin et al*., 2016
Windsor, ON	CAN	*Xu et al.,* 2014

In a hybrid analysis combining fate-and-transport modelling with measurements, GEOS-Chem was used to examine trends in Hg wet deposition over the United States over the 2004-2010 period (*Zhang and Jaegle*, 2013). The modelling results were subtracted from the observations to assess the roles of changing meteorology and emissions on observed wet deposition at 47 U.S. sites. In the Northeast and Midwest U.S., approximately half of the decreasing trend in Hg concentrations in precipitation could be explained by decreasing U.S. emissions over the study period.

4.5.4. East Asia

East Asia (including Southeast Asia) is the largest source region of atmospheric Hg release worldwide, with China as the largest emitter. According to *GMA 2013*, Hg release in East and Southeast Asia accounts for 40% of global anthropogenic emission in 2010. Mercury outflow from East Asia has been regarded as a concern to global Hg pollution (*Jaffe et al*., 2005; *Lin et al*., 2010; *Chen et al*., 2014).

The rapid economic growth and improving air emission control in East Asia change the anthropogenic Hg emission and speciation readily within a relatively short period of time. As better emission data become available, reassessment using updated emission data is necessary. For example, *Wu et al*. (2016) applied updated industrial activity statistics and emission factors to estimate anthropogenic Hg release in China from 1978 to 2014, and found that the emission varied significantly over time due to increased industrial production, energy use and implementation of emission control measures. Atmospheric Hg emission in China peaked in 2011 at 565 Mg y^{-1} and then dropped to 531 Mg y^{-1} in 2014. More importantly, the emission speciation gradually shifted to a larger fraction of oxidized Hg (56/43/3 for Hg0/HgII/Hgp in 2014). Such an emission speciation shift indicates increased local deposition and reduced emission outflow.

Wang et al. (2016b) re-evaluated the natural release of elemental Hg vapour from soil, vegetation and water surfaces using new soil Hg data in China and updated model schemes with physicochemical parameters reported recently. They found a distinct spatial distribution of estimated Hg release compared to the data reported by *Shetty et al*. (2008), despite a similar net natural release at ~460 Mg y^{-1} in China. Such a spatial distribution transition also has an impact on regional model results.

A number of regional and global scale modelling studies simulated atmospheric Hg levels in China and the East Asia region (e.g. *Lin et al*., 2010; *Pan et al*., 2010; *Chen et al*., 2014; *Chen et al*., 2015; *Zhu et al*., 2015; *Wang et al*., 2016a). It should be noted that most model results are not directly comparable due to differences in the emission inventory (particularly, natural emissions since many earlier studies did not specify the quantity and spatial distribution), Hg chemistry and model configuration. In general, regional models reproduced Hg concentrations more representative of the observed elevated levels in urban and industrial areas. Most global model results appear to be relatively consistent, estimating that Asian emissions contribute to 16-25% of Hg deposition in North America and 10-15% in the European region, except for one study (*Chen et al.,* 2014) reporting <5% of contribution in both regions.

The results of two regional modelling studies using CMAQ-Hg with identical model specifications are directly comparable (*Lin et al*., 2010; *Wang et al.* 2016a). The two modelling assessments use the same model configuration of CMAQ-Hg with different emission inventories: from (*Street et al.,* 2005; *Shetty et al*., 2008) in the former, and from (*Wu et al.,* 2016; *Wang et al*., 2016b) in the latter. The difference in the annual budgets is mainly caused by the reduced anthropogenic emission in the region, increased fraction of HgII, and a change in the spatial distribution of natural emission. Given the changes in emissions, the transport budget from East Asia by *Wang et al.* (2016a) is 25% lower than the earlier estimate by *Lin et al.* (2010), as shown in Figure 7. In addition, the greater Hg mass accumulated within the regional domain in *Wang et al.* (2016a) also better explain the elevated atmospheric Hg concentrations in China. More modelling studies are still needed in this region. Recent observational data obtained from the ambient monitoring network in China (*Fu et al.,* 2015) provide a unique opportunity to better understand the chemical transport of atmospheric in a region undergoing dynamic emission changes.

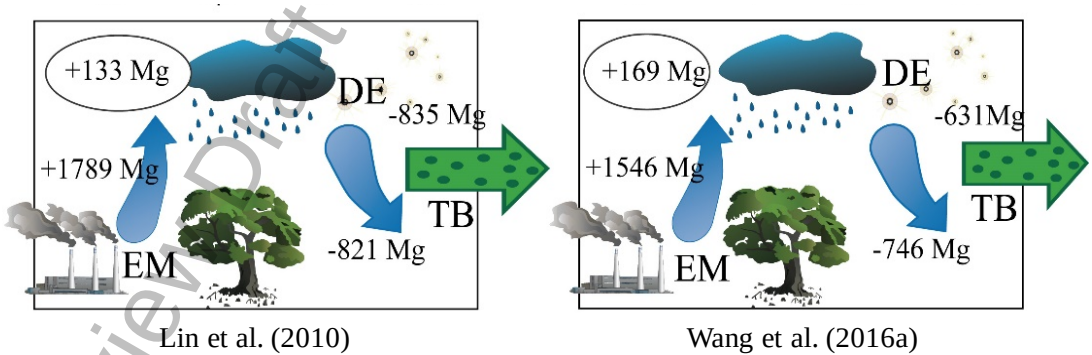

Lin et al. (2010) Wang et al. (2016a)

Figure 7: *Comparison of annual Hg mass budget in East Asia by Lin et al. (2010) and Wang et al. (2016a). EM is emission; DE is deposition; TB is transport budget.*

4.6. Conclusions

A number of regional and global models have been used to simulate the atmospheric fate and transport of Hg, using meteorological data and emissions inventories as inputs and atmospheric measurements to evaluate the results. Significant uncertainties remain in model physics (e.g., gas-particle partitioning and deposition processes) and chemistry (e.g., elemental Hg oxidation mechanisms), as well as in model inputs (e.g., emissions amounts and speciation) and measurements used for evaluation. Nevertheless, the scientific understanding of atmospheric Hg as represented in the models has progressed to the point where useful policy-relevant information about source-receptor relationships can be derived. This also implies that models can be used to provide first estimates of the effects on Hg-deposition of emission reductions, both regionally and globally. As improvements are made in understanding and model-related data, uncertainties in model results will be lessened and will become even more useful.

Atmospheric measurements are essential to evaluate and improve models; given the uncertainties noted above, models must continually be tested by comparison against measurements. At the same time, measurements alone cannot provide the depth of source-receptor and trend explanation information that can be obtained by models. Likewise, uncertainties in emissions inventories have emerged as a critical limitation in atmospheric model analyses, and the improvement of these fundamental model inputs is essential to improve model accuracy.

(To be updated based on new simulation results)

References

Agnan Y., T. Le Dantec, C. W. Moore, G. C. Edwards, and D. Obrist (2016) New Constraints on Terrestrial Surface-Atmosphere Fluxes of Gaseous Elemental Mercury Using a Global Database, *Environmental Science and Technology*, *50*(2), 507–524, doi:10.1021/acs.est.5b04013.

AMAP (2014) Global Anthropogenic Emissions of Mercury to the Atmosphere, www.amap.no/mercury-emissions/datasets.

AMAP (2011) AMAP assessment 2011: mercury in the Arctic. Oslo, Norway: Arctic Monitoring and Assessment Programme (AMAP); (pp. xiv +193).

Ambrose J.L., Gratz L.E., Jaffe D.A., Campos T., Flocke F.M., Knapp D.J., Stechman D.M., Stell M., Weinheimer A. J., Cantrell C.A., and Mauldin R.L. (2015) Mercury Emission Ratios from Coal-Fired Power Plants in the Southeastern United States during NOMADSS, *Environmental Science & Technology*, 49, 10389-10397, 10.1021/acs.est.5b01755.

Amos H.M., Jacob D.J., Streets, D.G. , and Sunderland E.M. (2013) Legacy impacts of all-time anthropogenic emissions on the global mercury cycle, *Global Biogeochemical Cycles* **27**(2), 410--421.

Amos H.M., D.J. Jacob, D. Kocman, H.M. Horowitz, Y. Zhang, S. Dutkiewicz, M. Horvat, E.S. Corbitt, D.P. Krabbenhoft, and E.M. Sunderland (2014) Global biogeochemical implications of mercury discharges from rivers and sediment burial, *Environ. Sci. Technol*., 48(16), 9514–9522.

Amos H.M., Sonke J.E., Obrist D., Robins N., Hagan N., Horowitz H.M., Mason R.P., Witt M., Hedgecock I.M., Corbitt E.S., and Sunderland E.M. (2015) Observational and Modelling Constraints on Global Anthropogenic Enrichment of Mercury, *Environ. Sci. Technol.* 49(7), 4036--4047.

Andersson, M.; Sommar, J.; Gårdfeldt, K.; Lindqvist, O. (2008) Enhanced concentrations of dissolved gaseous mercury in the surface waters of the Arctic Ocean. *Mar. Chem.*, *110* (3-4), 190–194; DOI 10.1016/j.marchem.2008.04.002.

Angot H., Dastoor A., De Simone F., Gårdfeldt K., Gencarelli C.N., Hedgecock I.M., Langer S., Magand O., Mastromonaco M.N., Nordstrøm C., Pfaffhuber K.A., Pirrone N., Ryjkov A., Selin N.E., Skov H., Song S., Sprovieri F., Steffen A., Toyota K., Travnikov O., Yang X., and Dommergue A. (2016) Chemical cycling and deposition of atmospheric mercury in polar regions: review of recent measurements and comparison with models*, Atmos. Chem. Phys*., 16, 10735-10763, doi:10.5194/acp-16-10735-2016.

Ariya P.A., Amyot M., Dastoor A., Deeds D., Feinberg A., Kos G., Poulain A., Ryjkov A., Semeniuk K., Subir M. & Toyota K. (2015) Mercury Physicochemical and Biogeochemical Transformation in the Atmosphere and at Atmospheric Interfaces: A Review and Future Directions, *Chemical Reviews* 115(10), 3760-3802.

Auzmendi-Murua I., Castillo Ál. & Bozzelli J.W. (2014) Mercury Oxidation via Chlorine, Bromine, and Iodine under Atmospheric Conditions: Thermochemistry and Kinetics, *The Journal of Physical Chemistry A* 118(16), 2959-2975.

Bekryaev R.V., Polyakov I.V., Alexeev V.A. (2010) Role of polar amplification in long-term surface air temperature variations and modern arctic warming. *J. Clim.,* 23(14), 3888-3906.

Berg T., Pfaffhuber K.A., Cole A.S., Engelsen O. and Steffen A. (2013) Ten-year trends in atmospheric mercury concentrations, meteorological effects and climate variables at Zeppelin, Ny-Alesund, Atmospheric Chemistry and Physics, 13, 6575-6586.

Bieser, J., Slemr, F., Ambrose, J., Brenninkmeijer, C., Brooks, S., Dastoor, A., DeSimone, F., Ebinghaus, R., Gencarelli, C. N., Geyer, B., Gratz, L. E., Hedgecock, I. M., Jaffe, D., Kelley, P., Lin, C.-J., Jaegle, L., Matthias, V., Ryjkov, A., Selin, N. E., Song, S., Travnikov, O., Weigelt, A., Luke, W., Ren, X., Zahn, A., Yang, X., Zhu, Y., and Pirrone, N. (2017) Multi-model study of mercury dispersion in the atmosphere: vertical and interhemispheric distribution of mercury species, Atmos. Chem. Phys., 17, 6925-6955, https://doi.org/10.5194/acp-17-6925-2017.

Bieser J. and Schrum C. (2016) Impact of marine mercury cycling on coastal atmospheric mercury concentrations in the North- and Baltic Sea region. Elementa 111, doi: 10.12952/journal.elementa.000111.

Bieser J., De Simone F., Gencarelli C.N., Hedgecock I.M., Matthias V., Travnikov O., Weigelt A. (2014) A diagnostic evaluation of modelled mercury wet deposition in Europe using atmospheric speciated high-resolution observations, *Environ. Science and Pollution Research* 21 (16).

Brooks S., Ren X., Cohen M., Luke W.T., Kelley P., Artz R., Hynes A., Landing W., and Martos B. (2014) Airborne Vertical Profiling of Mercury Speciation near Tullahoma, TN, USA, *Atmosphere*, 5, 557-574, 10.3390/atmos5030557.

Castro M.S. and Sherwell J. (2015) Effectiveness of Emission Controls to Reduce the Atmospheric Concentrations of Mercury, *Environmental Science & Technology*, 49, 14000-14007, 10.1021/acs.est.5b03576.

Cavalieri D.J. and Parkinson C.L. (2012) Arctic sea ice variability and trends, 1979-2010. *The Cryosphere*, 6(4): 881-889.

Chen G.Q., J.S. Li, B. Chen, C. Wen, Q. Yang, A. Alsaedi, and T. Hayat (2016) An overview of mercury emissions by global fuel combustion: The impact of international trade, *Renewable and Sustainable Energy Reviews*, *65*, 345–355, doi:10.1016/j.rser.2016.06.049.

Cheng I., Zhang L., and Xu X. (2016) Impact of Measurement Uncertainties on Receptor Modelling of Speciated Atmospheric Mercury, *Scientific Reports*, 6, 10.1038/srep20676.

Chen H.S., Wang Z.F., Li J., Tang X., Ge B.Z., Wu X.L., Wild O., Carmichael G.R. (2015) GNAQPMS-Hg v1.0, a global nested atmospheric mercury transport model: model description, evaluation and application to trans-boundary transport of Chinese anthropogenic emissions. *Geosci. Model Dev*., 8, 2857–2876. doi:10.5194/gmd-8-2857-2015.

Chen L., Y. Zhang, D.J. Jacob, A.L. Soerensen, J.A. Fisher, H.M. Horowitz, E.S. Corbitt, and X. Wang (2015) A decline in Arctic Ocean mercury suggested by differences in decadal trends of atmospheric mercury between the Arctic and northern midlatitudes, *Geophysical Research Letters*, *42*(14), 6076–6083, doi:10.1002/2015GL064051.

Cheng I., X. Xu, and L. Zhang (2015) Overview of receptor-based source apportionment studies for speciated atmospheric mercury, *Atmospheric Chemistry and Physics*, *15*(14), 7877–7895, doi:10.5194/acp-15-7877-2015.

Chen L., H.H. Wang, J.F. Liu, Y.D. Tong, L.B. Ou, W. Zhang, D. Hu, C. Chen, and X. J. Wang (2014) Intercontinental transport and deposition patterns of atmospheric mercury from anthropogenic emissions, *Atmospheric Chemistry and Physics*, *14*(18), 10163–10176, doi:10.5194/acp-14-10163-2014.

Cheng I., Zhang L., Blanchard P., Dalziel J., and Tordon R. (2013a) Concentration-weighted trajectory approach to identifying potential sources of speciated atmospheric mercury at an urban coastal site in Nova Scotia, Canada, *Atmospheric Chemistry and Physics*, 13, 6031-6048, 10.5194/acp-13-6031-2013.

Cheng I., Zhang L., Blanchard P., Dalziel J., Tordon R., Huang J., and Holsen T.M. (2013b) Comparisons of mercury sources and atmospheric mercury processes between a coastal and inland site, *Journal of Geophysical Research-Atmospheres*, 118, 2434-2443, 10.1002/jgrd.50169.

Choi H.-D., Huang J., Mondal S., and Holsen T. M. (2013) Variation in concentrations of three mercury (Hg) forms at a rural and a suburban site in New York State, *Science of the Total Environment*, 448, 96-106, 10.1016/j.scitotenv.2012.08.052, 2013.

Coburn S., B. Dix, E. Edgerton, C. D Holmes, D. Kinnison, Q. Liang, A. Ter Schure, S. Wang, and R. Volkamer (2016) Mercury oxidation from bromine chemistry in the free troposphere over the southeastern US, *Atmospheric Chemistry and Physics*, *16*(6), 3743–3760, doi:10.5194/acp-16-3743-2016.

Cohen M.D., Draxler R.R., Artz R.S., Blanchard P., Gustin M.S., Han Y., Holsen T.A., Jaffe D.A., Kelley P., Lei H., Loughner C.P., Luke W.T., Lyman S.L., Niemi D., Pacyna J.M., Pilote M., Poissant L., Ratte D., Ren X., Steenhuisen F., Steffen A., Tordon R., and Wilson S. (2016) Modelling the global atmospheric transport and deposition of mercury to the Great Lakes, Elementa, 4:000118, 10.12952/journal.elementa.000118.

Cole A.S. and Steffen A. (2010) Trends in long-term gaseous mercury observations in the Arctic and effects of temperature and other atmospheric conditions, *Atmos. Chem. Phys*., 10, 4661-4672, 10.5194/acp-10-4661-2010.

Cole A.S., Steffen A., Pfaffhuber K.A., Berg T., Pilote M., Poissant L., Tordon R., and Hung H. (2013) Ten-year trends of atmospheric mercury in the high Arctic compared to Canadian sub-Arctic and mid-latitudes sites, *Atmospheric Chemistry and Physics*, 13, 1535-1545.

Dastoor A.P. and Durnford D.A. (2014) Arctic ocean: is it a sink or a source of atmospheric mercury?, *Environmental Science and Technology*, 48, 1707-1717.

Dastoor A.P., Davignon D., Theys N., Van Roozendael M., Steffen A., and Ariya P.A. (2008) Modelling dynamic exchange of gaseous elemental mercury at polar sunrise, *Environmental Science and Technology*, 42, 5183-5188.

Dastoor A., Ryzhkov A., Durnford D., Lehnherr I., Steffen A., and Morrison H. (2015) Atmospheric mercury in the Canadian Arctic. Part II: Insight from modelling, *Science of The Total Environment*, 509–510, 16-27, http://dx.doi.org/10.1016/j.scitotenv.2014.10.112.

De Simone F., Cinnirella S., Gencarelli C.N., Yang X., Hedgecock I.M., Pirrone N. (2015) Model Study of Global Mercury Deposition from Biomass Burning, *Environmental Science and Technology* 49 (11) 6712-6721.

De Simone F., Cinnirelli S., Gencarelli C.N., Carbone F., Hedgecock I.M., Pirrone N. (2016) Particulate-Phase Mercury Emissions during Biomass Burning and Impact on Resulting Deposition: a Modelling Assessment. *Atmos. Chem. Phys. Disc*., doi:10.5194/acp-2016-685 (under review).

De Simone F., Gencarelli C.N., Hedgecock I.M., and N. Pirrone (2016) A Modelling Comparison of Mercury Deposition from Current Anthropogenic Mercury Emission Inventories, *Environmental Science and Technology*, *50*(10), 5154–5162, doi:10.1021/acs.est.6b00691.

Deeds D.A., Banic C.M., Lu J., and Daggupaty S. (2013) Mercury speciation in a coal-fired power plant plume: An aircraft-based study of emissions from the 3640 MW Nanticoke Generating Station, Ontario, Canada, *Journal of Geophysical Research-Atmospheres*, 118, 4919-4935, 10.1002/jgrd.50349.

Demers J.D., Sherman L.S., Blum J.D., Marsik F.J. and Dvonch J.T. (2015) Coupling atmospheric mercury isotope ratios and meteorology to identify sources of mercury impacting a coastal urban-industrial region near Pensacola, Florida, USA, *Global Biogeochemical Cycles*, 29, 1689-1705, 10.1002/2015gb005146.

Denkenberger J.S., Driscoll C.T., Branfireun B.A., Eckley C.S., Cohen M. and Selvendiran P. (2012) A synthesis of rates and controls on elemental mercury evasion in the Great Lakes Basin, *Environmental Pollution*, 161, 291-298, 10.1016/j.envpol.2011.06.007.

Durnford D., Dastoor A., Ryzhkov A., Poissant L., Pilote M., and Figueras-Nieto D. (2012) How relevant is the deposition of mercury onto snowpacks? – Part 2: A modelling study, *Atmos. Chem. Phys*., 12, 9251-9274, 10.5194/acp-12-9251-2012.

Eckley C.S., Tate M.T., Lin C.J., Gustin M., Dent S., Eagles-Smith C., Lutz M.A., Wickland K.P., Wang B., Gray J.E., Edwards G.C., Krabbenhoft D.P., and Smith D.B. (2016) Surface-air mercury fluxes across Western North America: A synthesis of spatial trends and controlling variables, *Science of the Total Environment*, 568, 651-665, 10.1016/j.scitotenv.2016.02.121.

Fisher J.A., Jacob D.J., Soerensen A.L., Amos H.M., Corbitt E.S., Streets D.G., Wang Q., Yantosca R.M., Sunderland E.M. (2013) Factors driving mercury variability in the Arctic atmosphere and ocean over the past 30 years. *Global Biogeochemical Cycles* 27: 1226-1235.

Fisher J.A., Jacob D.J., Soerensen A.L., Amos H.M., Steffen A., and Sunderland E.M. (2012) Riverine source of Arctic Ocean mercury inferred from atmospheric observations, *Nature Geosci*, 5, 499-504.

Foy B. de, Y. Tong, X. Yin, W. Zhang, S. Kang, Q. Zhang, G. Zhang, X. Wang, and J. J. Schauer (2016) First field-based atmospheric observation of the reduction of reactive mercury driven by sunlight, *Atmospheric Environment*, *134* (March), 27–39, doi:10.1016/j.atmosenv.2016.03.028.

Fu X., Yang X., Lang X., Zhou J., Zhang H., Yu B., Yan H., Lin C.-J., & Feng X. (2016) Atmospheric wet and litterfall mercury deposition at urban and rural sites in China, *Atmospheric Chemistry and Physics* 16(18), 11547--11562.

Gencarelli C.N., Bieser J., Crabone F., De Simone F., Hedgecock I.M., Matthias V., Travnikov O., Yang X., Pirrone N. (2016) Sensitivity study of regional mercury dispersion in the atmosphere. *Atmos. Chem. Phys. Discuss.*, doi:10.5194/acp-2016-663 (under review).

Gencarelli C.N., De Simone F., Hedgecock I.M., Sprovieri F., Pirrone N. (2014) Development and application of a regional-scale atmospheric mercury model based on WRF/Chem: a Mediterranean area investigation, *Environmental Science and Pollution Research* 21 (6), 4095-4109.

Giang A., and Selin N.E. (2016) Benefits of mercury controls for the United States, Proceedings of the National Academy of Sciences of the United States of America, 113, 286-291, 10.1073/pnas.1514395113.

Giang A., L.C. Stokes, D.G. Streets, E.S. Corbitt, and N.E. Selin (2015) Impacts of the Minamata Convention on Mercury Emissions and Global Deposition from Coal-Fired Power Generation in Asia, *Environmental Science & Technology*, *49*, 5236–5335, doi:10.1021/acs.est.5b00074.

Goodsite M.E., Outridge P.M., Christensen J.H., Dastoor A., Muir D., Travnikov O., Wilson S. (2013) How well do environmental archives of atmospheric mercury deposition in the Arctic reproduce rates and trends depicted by atmospheric models and measurements? *Science of The Total Environment*, 452–453,196–207.

Grant S.L., Kim M., Lin, P., Crist K.C., Ghosh S., and Kotamarthi V.R. (2014) A simulation study of atmospheric mercury and its deposition in the Great Lakes, *Atmospheric Environment*, 94, 164-172, 10.1016/j.atmosenv.2014.05.033.

Gratz, L. E. et al. (2015), Oxidation of mercury by bromine in the subtropical Pacific free troposphere, *Geophysical Research Letters*, *42*(23), 10494–10502, doi:10.1002/2015GL066645.

Gratz L.E., Ambrose J.L., Jaffe D.A., Knote C., Jaegle L., Selin N.E., Campos T., Flocke F.M., Reeves M., Stechman D., Steil M., Weinheimer A.J., Knapp D.J., Montzka D.D., Tyndall G.S., Mauldin R.L., Cantrell C.A., Apel E.C., Hornbrook R.S., and Blake N.J. (2016) Airborne observations of mercury emissions from the Chicago/Gary urban/industrial area during the 2013 NOMADSS campaign, *Atmospheric Environment*, 145, 415-423, 10.1016/j.atmosenv.2016.09.051.

Gratz L.E., Ambrose J.L., Jaffe D.A., Shah V., Jaegle L., Stutz J., Festa J., Spolaor M., Tsai C., Selin N.E., Song S., Zhou X., Weinheimer A.J., Knapp D.J., Montzka D.D., Flocke F.M., Campos T.L., Apel E., Hornbrook R., Blake N.J., Hall S., Tyndall G.S., Reeves M., Stechman D., and Stell M. (2015) Oxidation of mercury by bromine in the subtropical Pacific free troposphere, *Geophysical Research Letters*, 42, 10.1002/2015gl066645.

Gratz L.E., Keeler G.J., Marsik F.J., Barres J.A., and Dvonch J.T. (2013a) Atmospheric transport of speciated mercury across southern Lake Michigan: Influence from emission sources in the Chicago/Gary urban area, *Science of the Total Environment*, 448, 84-95, 10.1016/j.scitotenv.2012.08.076.

Gratz L.E., Keeler G.J., Morishita M., Barres J.A., and Dvonch J.T. (2013b) Assessing the emission sources of atmospheric mercury in wet deposition across Illinois, *Science of the Total Environment*, 448, 120-131, 10.1016/j.scitotenv.2012.11.011.

Gustin M.S., H.M. Amos, J. Huang, M.B. Miller, and K. Heidecorn (2015) Measuring and modelling mercury in the atmosphere: a critical review, *Atmospheric Chemistry and Physics*, *15*(10), 5697–5713, doi:10.5194/acp-15-5697-2015.

Gustin M.S., Pierce A.M., Huang J., Miller M.B., Holmes H.A., and Loria-Salazar S.M. (2016) Evidence for Different Reactive Hg Sources and Chemical Compounds at Adjacent Valley and High Elevation Locations, *Environmental Science & Technology*, 50, 12225-12231, 10.1021/acs.est.6b03339.

Gustin M.S., Amos H.M., Huang J., Miller M.B. & Heidecorn K. (2015) Measuring and modelling mercury in the atmosphere: a critical review, *Atmospheric Chemistry and Physics* **15**(10), 5697--5713.

Hirdman D., Aspmo K., Burkhart J.F., Eckhardt S., Sodemann H., Stohl A. (2009) Transport of mercury in the Arctic atmosphere: evidence for a spring-time net sink and summer-time source. *Geophys Res Lett*; 36. http://dx.doi.org/10.1029/2009GL038345.

Holmes C.D., Jacob D.J., Corbitt E.S., Mao J., Yang X., Talbot R., and Slemr F. (2010) Global atmospheric model for mercury including oxidation by bromine atoms, *Atmospheric Chemistry and Physics*, 10, 12037-12057.

Holmes C.D., Krishnamurthy N.P., Caffrey J.M., Landing W.M., Edgerton E.S., Knapp K.R., and Nair U.S. (2016) Thunderstorms Increase Mercury Wet Deposition, *Environmental Science & Technology* 50(17), 9343-9350.

Horowitz H.M., D.J. Jacob, H.M. Amos, D.G. Streets, and E.M. Sunderland (2014) Historical Mercury Releases from Commercial Products: Global Environmental Implications, *Environmental Science and Technology*, *48*, 10242–10250, doi:dx.doi.org/10.1021/es501337j.

Horowitz H.M., Jacob D.J., Zhang Y., Dibble T.S., Slemr F., Amos H.M., Schmidt J.A., Corbitt E.S., Marais E.A., and Sunderland E.M. (2017) A new mechanism for atmospheric mercury redox chemistry: Implications for the global mercury budget, *Atmospheric Chemistry and Physics Discussions*, 1-33, doi:10.5194/acp-2016-1165.

Huang J., and Gustin M.S. (2015) Use of Passive Sampling Methods and Models to Understand Sources of Mercury Deposition to High Elevation Sites in the Western United States, *Environmental Science & Technology*, 49, 432-441, 10.1021/es502836w.

Huang J., Chang F.-C., Wang S., Han Y.-J., Castro M., Miller E., and Holsen T. M. (2013) Mercury wet deposition in the eastern United States: characteristics and scavenging ratios, *Environmental Science-Processes & Impacts,* 15, 2321-2328, 10.1039/c3em00454f.

Huang J., Miller M.B., Edgerton E., and Gustin M.S. (2016) Deciphering the Chemical Forms of Gaseous Oxidized Mercury in Florida, USA, *Atmos. Chem. Phys. Discuss.*, 1-26, 10.5194/acp-2016-725.

Hui M. et al. (2016) Mercury Flows in China and Global Drivers, *Environmental Science & Technology*, acs.est.6b04094, doi:10.1021/acs.est.6b04094.

IJC (2015) Atmospheric Deposition of Mercury in the Great Lakes Basin, International Joint Commission, Windsor, Ontario, 23p.

Jaffe D.A. et al. (2014) Progress on Understanding Atmospheric Mercury Hampered by Uncertain Measurements, *Environmental Science and Technology*, *48*, 7204–7206, doi:dx.doi.org/10.1021/es5026432.

Jiang Y., Cizdziel J.V., and Lu D. (2013) Temporal patterns of atmospheric mercury species in northern Mississippi during 2011-2012: Influence of sudden population swings, *Chemosphere*, 93, 1694-1700, 10.1016/j.chemosphere.2013.05.039.

Jiao Y. and Dibble T.S. (2015) Quality Structures, Vibrational Frequencies, and Thermochemistry of the Products of Reaction of BrHg• with NO2, HO2, ClO, BrO, and IO, *The Journal of Physical Chemistry A* **119**(42), 10502-10510.

Jiao Y. and Dibble T.S. (2017) First kinetic study of the atmospherically important reactions BrHg(radical dot) + NO2 and BrHg(radical dot) + HOO, *Phys. Chem. Chem. Phys.* **xx**, xx.

Kaulfus A.S., Nair U.S., Holmes C.D., and Landing W.M. (0), Mercury Wet Scavenging and Deposition Differences by Precipitation Type, *Environmental Science & Technology* **0**(ja), null.

Kocman D., M. Horvat, N. Pirrone, and S. Cinnirella (2013) Contribution of contaminated sites to the global mercury budget, *Environmental Research*, *125*, 160–170, doi:10.1016/j.envres.2012.12.011.

Kos G., Ryzhkov A., Dastoor A., Narayan J., Steffen A., Ariya P.A., and Zhang L. (2013) Evaluation of discrepancy between measured and modelled oxidized mercury species, *Atmospheric Chemistry and Physics*, 13, 4839-4863.

Kos G., Ryzhkov A., Dastoor A., Narayan J., Steffen A., Ariya P.A. and Zhang L. (2013) Evaluation of discrepancy between measured and modelled oxidized mercury species, *Atmospheric Chemistry and Physics*, 13, 4839-4863, 10.5194/acp-13-4839-2013.

Kwon S.Y. and N.E. Selin (2016) Uncertainties in Atmospheric Mercury Modelling for Policy Evaluation, *Current Pollution Reports*, doi:10.1007/s40726-016-0030-8.

Lamborg C.H., C.R. Hammerschmidt, K.L. Bowman, G.J. Swarr, K.M. Munson, D.C. Ohnemus, P.J. Lam, L.-E. Heimbürger, M.J.A. Rijkenberg, and M.A. Saito (2014) A global ocean inventory of anthropogenic mercury based on water column measurements, *Nature*, *512*(7512), 65–68, doi:10.1038/nature13563.

Lei H., D.J. Wuebbles, X.-Z. Liang, Z. Tao, S. Olsen, R. Artz, X. Ren, and M. Cohen (2014) Projections of atmospheric mercury levels and their effect on air quality in the United States, *Atmospheric Chemistry and Physics*, *14*(2), 783–795, doi:10.5194/acp-14-783-2014.

Lei H., Liang X.Z., Wuebbles D.J. and Tao Z. (2013) Model analyses of atmospheric mercury: present air quality and effects of transpacific transport on the United States, *Atmospheric Chemistry and Physics*, 13, 10807-10825, 10.5194/acp-13-10807-2013.

Lei H., Wuebbles D. J., Liang X.Z., Tao Z., Olsen S., Artz R., Ren X., and Cohen M. (2014) Projections of atmospheric mercury levels and their effect on air quality in the United States, *Atmospheric Chemistry and Physics*, 14, 783-795, 10.5194/acp-14-783-2014.

Lynam M.M., Dvonch J.T., Hall N.L., Morishita M., and Barres J.A. (2014) Spatial patterns in wet and dry deposition of atmospheric mercury and trace elements in central Illinois, USA, Environmental *Science and Pollution Research*, 21, 4032-4043, 10.1007/s11356-013-2011-4.

Megaritis A.G., Murphy B.N., Racherla P.N., Adams P.J., and Pandis S.N. (2014) Impact of climate change on mercury concentrations and deposition in the eastern United States, *Science of the Total Environment*, 487, 299-312, 10.1016/j.scitotenv.2014.03.084.

Moore C.W., Obrist D., Steffen A., Staebler R.M., Douglas T.A., Richter A., and Nghiem S.V. (2014) Convective forcing of mercury and ozone in the Arctic boundary layer induced by leads in sea ice, *Nature*, 506, 81-84, 10.1038/nature12924.

Muntean M., Janssens-Maenhout G., Song S., Selin N.E., Jos Oliver J.G.J., Guizzardi D., Maas R., Dentener F., (2014) Trend analysis from 1970 to 2008 and model evaluation of EDGARv4 global gridded anthropogenic mercury emissions. Science *of the Total Environment* 494-495, 337-350.

Myers T., Atkinson R.D., Bullock O.R., Jr., and Bash J.O. (2013) Investigation of effects of varying model inputs on mercury deposition estimates in the Southwest US, *Atmospheric Chemistry and Physics*, 13, 997-1009, 10.5194/acp-13-997-2013.

Nair U.S., Wu Y., Holmes C.D., Ter Schure A., Kallos G., and Walters J.T. (2013) Cloud-resolving simulations of mercury scavenging and deposition in thunderstorms, *Atmospheric Chemistry and Physics*, 13, 10143-10157, 10.5194/acp-13-10143-2013.

Outridge P., Macdonald R., Wang F., Stern G., Dastoor A. (2008) A mass balance inventory of mercury in the Arctic Ocean. *Environ. Chem.*, *5* (2), 89–111; DOI 10.1071/EN08002.

Pacyna J.M., Travnikov O., De Simone F., Hedgecock I.M., Sundseth K., Pacyna E.G., Steenhuisen F., Pirrone N., Munthe J., Kindbom K. (2016) Current and future levels of mercury atmospheric pollution on a global scale. *Atmos. Chem. Phys*. 16, 12495-12511. doi:10.5194/acp-16-12495-2016

Pirrone N., Cinnirella S., Feng X., Finkelman R.B., Friedli H.R., Leaner J., Mason R., Mukherjee A.B., Stracher G.B., Streets D.G., and Telmer K. (2010) Global mercury emissions to the atmosphere from anthropogenic and natural sources, *Atmospheric Chemistry and Physics*, 10, 5951-5964, 10.5194/acp-10-5951-2010.

Prestbo E.M., and Gay D.A. (2009) Wet deposition of mercury in the U.S. and Canada, 1996–2005: Results and analysis of the NADP mercury deposition network (MDN), *Atmospheric Environment*, 43, 4223-4233, http://dx.doi.org/10.1016/j.atmosenv.2009.05.028.

Rafaj P., Cofala J., Kuenen J., Wyrwa A., Zysk J. (2014) Benefits of European Climate Policies for Mercury Air Pollution, *Atmosphere* 5 (1), 45-59. doi:10.3390/atmos5010045.

Ren X., Luke W.T., Kelley P., Cohen M.D., Artz R., Olson M.L., Schmeltz D., Puchalski M., Goldberg D.L., Ring A., Mazzuca G.M., Cummings K.A., Wojdan L., Preaux S., and Stehr J.W. (2016) Atmospheric mercury measurements at a suburban site in the Mid-Atlantic United States: Inter-annual, seasonal and diurnal variations and source-receptor relationships, *Atmospheric Environment*, 146, 141-152 10.1016/j.atmosenv.2016.08.028.

Ren X., Luke W.T., Kelley P., Cohen M., Ngan F., Artz R., Walker J., Brooks S., Moore C., Swartzendruber P., Bauer D., Remeika J., Hynes A., Dibb J., Rolison J., Krishnamurthy N., Landing W.M., Hecobian A., Shook J., and Huey L.G. (2014) Mercury Speciation at a Coastal Site in the Northern Gulf of Mexico: Results from the Grand Bay Intensive Studies in Summer 2010 and Spring 2011, *Atmosphere*, 5, 230-251, 10.3390/atmos5020230.

Rolison J.M., Landing W.M., Luke W., Cohen M., and Salters V.J.M. (2013) Isotopic composition of species-specific atmospheric Hg in a coastal environment, *Chemical Geology*, 336, 37-49, 10.1016/j.chemgeo.2012.10.007.

Schroeder W.H. & Munthe J. (1998) Atmospheric mercury—An overview', *Atmospheric Environment* 32(5), 809 - 822.

Selin N.E. (2014) Global change and mercury cycling: challenges for implementing a global mercury treaty, *Environmental Toxicology and Chemistry*, *33*(6), 1202–10, doi:10.1002/etc.2374.

Selin N.E., Jacob D.J., Park R.J., Yantosca R.M., Strode S., Jaegle L., and Jaffe D. (2007) Chemical cycling and deposition of atmospheric mercury: Global constraints from observations, *Journal of Geophysical Research-Atmospheres,* 112, 10.1029/2006jd007450.

Shah V., Jaegle L., Gratz L.E., Ambrose J.L., Jaffe D.A., Selin N.E., Song S., Campos T.L., Flocke F.M., Reeves M., Stechman D., Stell M., Festa J., Stutz J., Weinheimer A.J., Knapp D.J., Montzka D.D., Tyndall G.S., Apel E.C., Hornbrook R.S., Hills A.J., Riemer D.D., Blake N.J., Cantrell C.A., and Mauldin R.L. (2016) Origin of oxidized mercury in the summertime free troposphere over the southeastern US, *Atmospheric Chemistry and Physics,* 16, 1511-1530, 10.5194/acp-16-1511-2016.

Sommar J., M.E. Andersson, and H.W. Jacobi (2010) Circumpolar measurements of speciated mercury, ozone and carbon monoxide in the boundary layer of the Arctic Ocean, *Atmos. Chem. Phys*., 10(11), 5031–5045.

Song S., Selin N.E., Soerensen A.L., Angot H., Artz R., Brooks S., Brunke E.G., Conley G., Dommergue A., Ebinghaus R., Holsen T.M., Jaffe D.A., Kang S., Kelley P., Luke W.T., Magand O., Marumoto K., Pfaffhuber K.A., Ren X., Sheu G.R., Slemr F., Warneke T., Weigelt A., Weiss-Penzias P., Wip D.C., and Zhang Q. (2015) Top-down contents on atmospheric mercury emissions and implications for global biogeochemical cycling, *Atmos. Chem. Phys*., 15, 7103-7125.

Steffen A., Bottenheim J., Cole A., Ebinghaus R., Lawson G. and Leaitch W.R. (2014) Atmospheric mercury speciation and mercury in snow over time at Alert, Canada, *Atmospheric Chemistry and Physics*, 14, 2219-2231.

Steffen A., Schroeder W., Macdonald R., Poissant L., and Konoplev A. (2005) Mercury in the Arctic atmosphere: An analysis of eight years of measurements of GEM at Alert (Canada) and a comparison with observations at Amderma (Russia) and Kuujjuarapik (Canada), *Science of The Total Environment*, 342, 185-198, http://dx.doi.org/10.1016/j.scitotenv.2004.12.048.

Stein A.F., Draxler R.R., Rolph G.D., Stunder B.J.B., Cohen M.D., and Ngan F. (2015) NOAA's HYSPLIT atmospheric transport and dispersion modelling system, Bulletin of the American Meteorological Society, 10.1175/BAMS-D-14-00110.1.

Stern G.A., Macdonald R.W., Outridge P.M., Wilson S., Chételat J., Cole A., Hintelmann H., Loseto L.L., Steffen A., Wang F., Zdanowicz C. (2012) How does climate change influence Arctic mercury? *Sci Total Environ*.; 414:22-42. doi: 10.1016/j.scitotenv.2011.10.039.

Streets D.G., M.K. Devane, Z.F. Lu, T.C. Bond, E.M. Sunderland, and D.J. Jacob (2011) All-time releases of mercury to the atmosphere from human activities, *Environ. Sci. Technol.*, 45(24), 10, 485–10,491, doi:10.1021/es202765m.

Sunderland E.M., and N.E. Selin (2013) Future trends in environmental mercury concentrations: implications for prevention strategies., *Environmental health : a global access science source*, *12*, 2, doi:10.1186/1476-069X-12-2.

Sunderland E.M., Driscoll C.T., Hammitt J.K., Grandjean P., Evans J.S., Blum J.D., Chen C.Y., Evers D.C., Jaffe D.A., Mason R.P., Goho S., and Jacobs W. (2016) Benefits of Regulating Hazardous Air Pollutants from Coal and Oil Fired Utilities in the United States, *Environmental Science & Technology*, 50, 2117-2120, 10.1021/acs.est.6b00239.

Toyota K., Dastoor A.P., and Ryzhkov A. (2014) Air–snowpack exchange of bromine, ozone and mercury in the springtime Arctic simulated by the 1-D model PHANTAS – Part 2: Mercury and its speciation, Atmos. Chem. Phys., 14, 4135-4167, doi:10.5194/acp-14-4135-2014.

Toyota K., Dastoor A.P., and Ryzhkov, A. (2016) Parameterization of gaseous dry deposition in atmospheric chemistry models: Sensitivity to aerodynamic resistance formulations under statically stable conditions, *Atmospheric Environment* 147, 409 - 422.

Travnikov O. and I. Ilyin (2009) The EMEP/MSC-E mercury modelling system. In: Pirrone N, Mason RP, editors. Mercury Fate and Transport in the Global Atmosphere. Dordecht: *Springer*. pp. 571−587.

Travnikov O., Angot H., Artaxo P., Bencardino M., Bieser J., D'Amore F., Dastoor A., De Simone F., Diéguez M. D. C., Dommergue A., Ebinghaus R., Feng X. B., Gencarelli C. N., Hedgecock I. M., Magand O., Martin L., Matthias V., Mashyanov N., Pirrone N., Ramachandran R., Read K. A., Ryjkov A., Selin N. E., Sena F., Song S., Sprovieri F., Wip D., Wängberg I., and Yang X. (2017) Multi-model study of mercury dispersion in the atmosphere: atmospheric processes and model evaluation, Atmos. Chem. Phys., 17, 5271-5295, doi:10.5194/acp-17-5271-2017.

UNEP (2015) Global Mercury Modelling: Update of Modelling Results in the Global Mercury Assessment 2013.

Velasco A., Arcega-Cabrera F., Oceguera-Vargas I., Ramirez M., Ortinez A., Umlauf G., and Sena F. (2016) Global Mercury Observatory System (GMOS): measurements of atmospheric mercury in Celestun, Yucatan, Mexico during 2012, *Environmental Science and Pollution Research*, 23, 17474-17483, 10.1007/s11356-016-6852-5.

Wang F., A. Saiz-Lopez, A.S. Mahajan, J.C. Gómez Martín, D. Armstrong, M. Lemes, T. Hay, and C. Prados-Roman (2014a) Enhanced production of oxidised mercury over the tropical Pacific Ocean: a key missing oxidation pathway, *Atmospheric Chemistry and Physics*, *14*(3), 1323–1335, doi:10.5194/acp-14-1323-2014.

Wang L., S. Wang, L. Zhang, Y. Wang, Y. Zhang, C. Nielsen, M. B. McElroy, and J. Hao (2014b), Source apportionment of atmospheric mercury pollution in China using the GEOS-Chem model, *Environmental Pollution*, *190*, 166–175, doi:10.1016/j.envpol.2014.03.011.

Wang X., Z. Bao, C. J. Lin, W. Yuan, and X. Feng (2016), Assessment of Global Mercury Deposition through Litterfall. *Environmental Science and Technology*, *50*(16), 8548–8557, doi:10.1021/acs.est.5b06351.

Weigelt A., Slemr F., Ebinghaus R., Pirrone N., Bieser J., Bödewadt J., Esposito G., Van Velthoven P. (2016) Mercury emissions of a coal fired power plant in Germany. *Atmos. Chem. Phys*. 16, 13653-13668. doi: 10.5194/acp-16-13653-2016

Weiss-Penzias P., Amos H.M., Selin N.E., Gustin M.S., Jaffe D.A., Obrist D., Sheu G.R., and Giang A. (2015) Use of a global model to understand speciated atmospheric mercury observations at five high-elevation sites, *Atmospheric Chemistry and Physics*, 15(3), 1161-1173, 10.5194/acp-15-1161-2015.

White E.M., Landis M.S., Keeler G.J., and Barres J.A. (2013) Investigation of mercury wet deposition physicochemistry in the Ohio River Valley through automated sequential sampling, *Science of the Total Environment*, 448, 107-119, 10.1016/j.scitotenv.2012.12.046.

Wright G., Gustin M.S., Weiss-Penzias P., and Miller M.B. (2014) Investigation of mercury deposition and potential sources at six sites from the Pacific Coast to the Great Basin, USA, *Science of the Total Environment*, 470, 1099-1113, 10.1016/j.scitotenv.2013.10.071.

Wright L.P., and Zhang L. (2015) An approach estimating bidirectional air-surface exchange for gaseous elemental mercury at AMNet sites, *Journal of Advances in Modelling Earth Systems*, 7, 35-49, 10.1002/2014ms000367.

Wright L.P., Zhang L., and Marsik F.J. (2016) Overview of mercury dry deposition, litterfall, and throughfall studies, *Atmospheric Chemistry and Physics* 16(21), 13399--13416.

Wu Q., Wang S., Li G., Liang S., Lin C.-J., Wang Y., Cai S., Liu K., and Hao J. (2016) Temporal Trend and Spatial Distribution of Speciated Atmospheric Mercury Emissions in China During 1978–2014, *Environmental Science & Technology* 50(24), 13428-13435.

Xu X.H., Akhtar U., Clark K., and Wang X.B. (2014) Temporal Variability of Atmospheric Total Gaseous Mercury in Windsor, ON, Canada, *Atmosphere*, 5, 536-556, 10.3390/atmos5030536.

Zhang H., C.D. Holmes and S. Wu (2016a), Impacts of changes in climate, land use and land cover on atmospheric mercury, *Atmospheric Environment*, *141*, 230–244, doi:10.1016/j.atmosenv.2016.06.056.

Zhang L., Blanchard P., Johnson D., Dastoor A., Ryzhkov A., Lin C.J., Vijayaraghavan K., Gay D., Holsen T.M., Huang J., Graydon J.A., St Louis V.L., Castro M.S., Miller E.K., Marsik F., Lu J., Poissant L., Pilote M., and Zhang K.M. (2012) Assessment of modelled mercury dry deposition over the Great Lakes region, *Environmental Pollution*, 161, 272-283, 10.1016/j.envpol.2011.06.003.

Zhang L., Wu Z., Cheng I., Wright L.P., Olson M.L., Gay D.A., Risch M.R., Brooks S., Castro M.S., Conley G.D., Edgerton E.S., Holsen T.M., Luke W., Tordon R., and Weiss-Penzias P. (2016) The Estimated Six-Year Mercury Dry Deposition Across North America, *Environmental Science & Technology*, 10.1021/acs.est.6b04276.

Zhang Y.X. and Jaegle L. (2013) Decreases in Mercury Wet Deposition over the United States during 2004-2010: Roles of Domestic and Global Background Emission Reductions, *Atmosphere*, 4, 113-131, 10.3390/atmos4020113.

Zhang Y., D.J. Jacob, H.M. Horowitz, L. Chen, H.M. Amos, D.P. Krabbenhoft, F. Slemr, V.L. St Louis, and E.M. Sunderland (2016b) Observed decrease in atmospheric mercury explained by global decline in anthropogenic emissions, *Proceedings of the National Academy of Sciences of the United States of America*, *113*(3), 526–31, doi:10.1073/pnas.1516312113.

Zhang Y., D.J. Jacob, S. Dutkiewicz, H.M. Amos, M.S. Long, and E.M. Sunderland (2015) Biogeochemical drivers of the fate of riverine mercury discharged to the global and Arctic oceans, *Global Biogeochem. Cycles*, 29, 854–864, doi:10.1002/2015GB005124.

Zhang Y., L. Jaeglé, L. Thompson, and D.G. Streets (2014) Six centuries of changing oceanic mercury, *Global Biogeochemical Cycles*, *28*(11), 1251–1261, doi:10.1002/2014GB004939.

Zhang Y., Jacob D.J., Horowitz H.M., Chen L., Amos H.M., Krabbenhoft D.P., Slemr F., St. Louis, V.L., and Sunderland E.M. (2016) Observed decrease in atmospheric mercury explained by global decline in anthropogenic emissions, *Proceedings of the National Academy of Sciences* 113(3), 526-531.

Zhou H., Zhou C., Lynam M.M., Dvonch J.T., Barres J.A., Hopke P.K., Cohen M. and Holsen T.M. (2016) Atmospheric Mercury Temporal Trends in the Northeastern United States from 1992 to 2014: Are Measured Concentrations Responding to Decreasing Regional Emissions?, *Environmental Science and Technology Letters*, (submitted).

Zhu J., Wang T., Bieser J., Matthias V. (2015) Source attribution and process analysis for atmospheric mercury in eastern China simulated by CMAQ-Hg. *Atmos. Chem. Phys*. 5 (15).

9170

9171

Note to reader

This draft version of Chapter 5 in the Technical Background Report to the Global Mercury Assessment 2018 is made available for review by national representatives and experts. The draft version contains material that will be further refined and elaborated after the review process. Specific items where the content of this draft chapter will be further improved and modified are:

1. Comparison of results with independent estimates for Hg releases to water.
2. Quantification of the uncertainties for sectors where this information is currently missing and update of for some others
3. Geospatial distribution of releases
4. Paragraph on the results of the inventory in the context of global Hg cycle will be added
5. Detailed harmonisation and cross reference with Chapter 2 including integration of Annexes (e.g. Annex on methodological approaches used for Hg-added products sector)

GMA 2018 Draft Chapter 5 Releases of Hg to the aquatic environment from anthropogenic sources.

David Kocman, Milena Horvat

10030 ## Contents

10063
10064

Chapter 5 Releases of Hg to the aquatic environment from anthropogenic sources

5.1 Introduction

This chapter is an extension to work on the global inventory of air emissions discussed in Chapter 2. The results presented represent an attempt to compile a comprehensive global inventory of releases of mercury to water from anthropogenic sources for which sufficient information is available. The work builds on, updates and extends the aquatic Hg release inventory prepared as a part of the UNEP global mercury assessment 2013 (AMAP/UNEP, 2013).

This is the second time only that the content of the updated report has been expanded to include information on Hg releases to aquatic environments. General lack of data in the literature reporting Hg releases to aquatic systems and related information needed for estimation of the releases (e.g. waste-water amounts) is still an issue restricting accuracy and completeness of these estimates. Therefore, methods employed to derive the estimates are largely driven by the type and the amount of information available for various source category. Part of this work is directly linked to the air emissions inventory work and utilise factors employed in the UNEP Toolkit are used to derive releases to water from sectors responsible for emissions to air. Releases from other sectors not covered by the Toolkit but recognised as relevant with respect to releases to water, are also addressed, using independent methods and assumptions to derive the estimates.

To the extent possible, our estimates are compared with available national and other estimates/inventories of releases to water. For some of the release sectors covered in the 2015 inventory - to evaluate if obtained results are realistic - alternative release estimates were made using independent assumptions and information. Information regarding global releases of Hg to aquatic systems is still incomplete, and therefore a substantial part of this chapter is devoted to discussion on data sources and their availability, data gaps and associated uncertainties, as well as different methods and approaches/assumptions made for estimating the releases.

10090 The focus of this chapter is on Hg released from current anthropogenic sources to adjacent freshwater
10091 systems. The exception is oil and gas production sector, where offshore releases with produced water
10092 are also included. If should be pointed out that this inventory does not represent the total global load of
10093 Hg to aquatic systems. Namely, in addition to primary anthropogenic sources for which lack of
10094 information prevented reliable quantification, diffuse releases associated with legacy Hg accumulated in
10095 terrestrial environments can also be important contributors. In this chapter, relative contribution and
10096 significance of sources quantified is assessed by comparing inventory results with magnitudes of sources
10097 and pathways of other components of the global Hg cycle as established before.

10098 In contrast to air emission estimates (Chapter 2), the numbers presented here do not necessarily
10099 correspond to the year 2015. For example, the underlying assumptions for estimating Hg releases with
10100 industrial wastewaters are based on information corresponding to latest available information, while
10101 releases from point sources were derived from atmospheric inventory data for 2015 presented in
10102 Chapter 2.

10103 Inventory results are summarised using two types of regionalisation. The first is distribution of the
10104 estimates according to sub-continental regions. The purpose of this regionalisation is comparability with
10105 air emissions inventory. However, in case of aquatic releases it is more relevant to track Hg from its
10106 source and through catchments all the way to its ultimate delivery into the oceans. Therefore, additional
10107 regionalisation is used based on major drainage basins of the world (see Section 2.5 for details).

10108 It should be noted that the fate of terrestrial Hg once entering aquatic systems will largely depend on
10109 site-specific environmental conditions that govern its transport and transformation processes within
10110 catchments, and have the control over its ultimate delivery to downstream marine environments. This is
10111 not addressed in the inventory as the focus of this chapter is on quantification of releases only.

10112 5.2 Estimating global anthropogenic mercury releases for 2010-
10113 2015: Methodology

10114 A key component of this work to update the 2010 Global Atmospheric Mercury Assessment: Sources,
10115 Emissions and Transport report (AMAP/UNEP, 20013) is the production of a new global inventory of
10116 anthropogenic Hg releases to aquatic systems. This new inventory has the target year of 2015 – however

recognising that information required to produce such inventories may not yet be available for all countries and release categories the basis for most of this new inventory is latest available data which dates in the 2000–2015 period.

5.2.1 Methods for estimating releases

Various methods are employed to estimate releases of Hg at the plant/facility, national, regional and global level. The approaches used and underlying assumptions depend on the data availability. In general, they fall under one of the three main groups schematically shown in Figure 1. In order to avoid confusion with the atmospheric and other independent inventories, we named our inventory of global primary anthropogenic aquatic Hg releases *Global Mercury Assessment Aquatic Release* (GMAAR) inventory.

Often assumptions made to derive the estimates presented in this chapter are difficult to validate. For reasons of transparency, details on the approaches and assumptions made in the GMAAR to derive the estimates are given in Annex X., with a summary given in the following sections.

Group 1: This group comprise sectors covered by the UNEP Toolkit (chlor-alkali industry, oil refining, large scale Au and non-ferrous metal production) and for which the Toolkit (UNEP, 2017) provides 'distribution factors' that proportionally 'distribute' total Hg releases between emissions to air and releases to water and land. We use these factors together with the most recent Global Mercury Assessment (GMA) atmospheric Hg emission inventory (Chapter 2) to calculate the corresponding magnitudes of releases to water. Sectors included in this first group are those included also in 2010 inventory.

Group 2: This group is comprised of sectors for which estimates were derived based on measured Hg concentrations reported in the literature for selected case studies and associated volumes of wastewater released and other relevant activity data, respectively. Following the approach recently used by Liu et al. (2016) to develop aquatic Hg release inventory for China, sectors considered important in terms of their relative contribution and included in this inventory, in addition to those from the first group, are: Hg releases associated with produced municipal wastewater and several industrial activities – wastewater from coal-fired power plants, coal washing and produced water generated during oil and

gas production. All sectors from the second group are new addition to the global inventory and have not been addressed in the 2010 inventory.

Group 3: This group covers Hg releases from wastes associated with the use of Hg-added products: batteries, measuring devices, lamps, electrical and electronic devices, dental applications, and other uses. Releases are produced using approach comparable to that applied to calculate emission to air (See section 2.2.2. of Chapter 2 and Annex 3 for details), adjusted to aquatic Hg fate. The model used considers regional patterns of consumption of Hg and Hg-containing products and initially distributes Hg in products to different pathways using distribution factors. Releases to water are then assumed for breakage during use, waste recycling and from waste landfills, using fate-specific release factor (see Annex X.6 for details). This is a new methodological approach, as releases from the use of Hg-added products in 2010 inventory were derived using the UNEP Toolkit distribution approach.

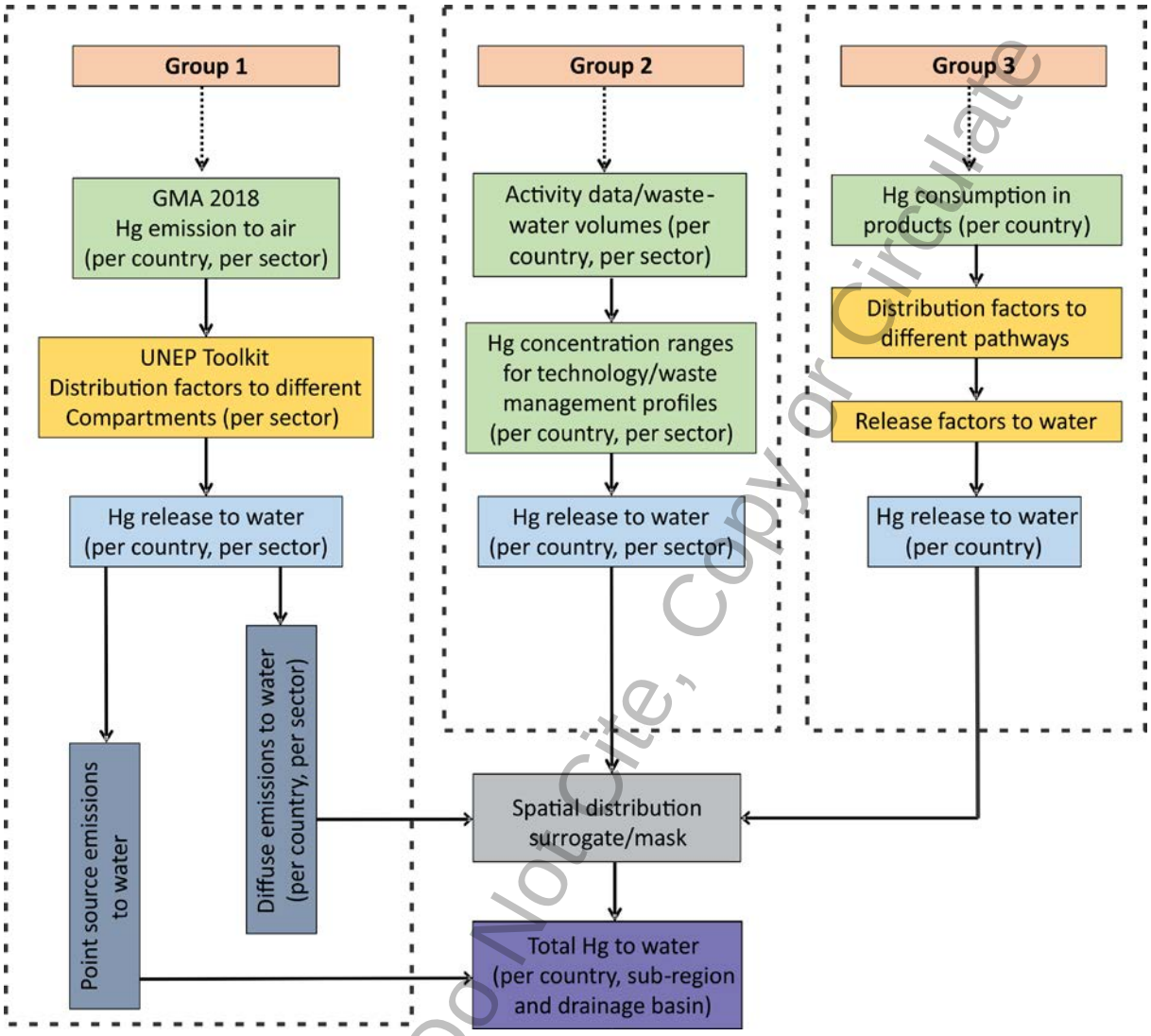

Figure 1. Methods for estimating releases

Initially, estimates of Hg releases for all sectors were made on the country level, as majority of input data used are country specific. Technology and waste-management profiles of individual country (cross ref.) were used for selection of Hg concentration ranges and other related activity data. Based on the country-level information, Hg release estimates were then summarised according to sub-continental regions, using the same regionalisation as that used for the air emission inventory.

In the next step, various methods were applied to geospatially distribute country scale releases, as described further in the Figure 1. Level of details of geospatial distribution vary from sector to sector, and depends mostly on distribution surrogate data availability. In case of Group 1 sectors, methods used

to geospatially distribute air emissions were applied also to the aquatic release estimates. The approach used is described previously in Wilson et al. (2006), AMAP/UNEP (2008, 2010) and Steenhuisen et al. (2015), and in summary assigns releases to point sources where possible, with the remainder being geospatially distributed according to distribution of appropriate surrogate parameter (see Section 2.3 and Annex X for details). In case of Group 2 and Group 3, several "distribution masks" were created for application to releases from different sectors: (i) population density mask for distribution of releases associated with municipal waste-water and use of Hg-added products; (ii) locations of coal-fired power plants (CFPPs) for distribution of Hg releases with associated wastewater; (iii) coal deposits mask for distribution of Hg releases from coal washing, and (iv) on-shore and off-shore oil fields mask for distribution of Hg releases during oil and gas production.

In the final step, in addition to sub-continental summary, Hg releases were summarised based on major drainage basins of the world (see Section 3.2). The above mentioned distribution masks were used along with the drainage basins mask to distribute country-level estimates for individual sectors into appropriate drainage basin.

5.2.2 Sectors and activities

5.2.2.1 Sectors and activities quantified in the inventory

Selection of the sectors and activities for the aquatic inventory is driven by previously established knowledge about their relative importance, while their categorisation depends mainly on the data and type of information available for individual sector/activity. To the extent possible, categorisation was kept comparable with that used for the air emission sectors. The release estimates in the new 2015 GMAAR inventory comprise the following release sectors:

- Production of non-ferrous metals (primary production of aluminium, copper, lead and zinc) (O1)
- Production of mercury metal (O2)
- Production of gold from large-scale mining (O3)
- Mercury releases from oil refining (E1)
- Production of gold from artisanal and small-scale gold mining (O4)
- Mercury releases from chlor-alkali industry (Hg cell technology) (W1)
- Mercury releases with municipal waste-water (W2)

- Mercury releases from coal-fired power plants (E2)
- Mercury releases from coal washing (E3)
- Mercury releases from Hg-added products (batteries, measuring devices, lamps, electrical and electronic devices, dental applications, and other uses) use and waste disposal (W3)
- Mercury releases during oil and gas extraction (E4)

In broader terms these sectors can be divided into three general categories: ore mining and processing sector (O), energy sector (E) and waste treatment and disposal (W). The first six items on the list are those included previously in the 2010 inventory. Among these the first four sectors are associated with by-product or unintentional Hg releases and latter two with intentional uses of Hg. Other items from the list are new addition to the 2015 inventory and comprise categories for which relative contribution of Hg releases to aquatic systems is considered to be significant, following mostly the example of Liu et al. (2016) and their release estimates for China.

5.2.2.2 Sectors and activities not quantified in the inventory

We recognise that there are additional sectors and anthropogenic activities, not taken into account in this inventory, but might be responsible for the delivery of additional Hg to local aquatic systems. For example, in the Hg release inventory from anthropogenic sources in China, releases from iron and steel industry, fabrication of textiles and apparel and printing industry were also considered, however estimated at less than 5% of total releases (Liu et al., 2016). Considering relative low importance of these sectors, especially in the light of the fact that there is no data available that would allow any reasonable global quantitative estimate, these sectors were not included in the 2015 inventory.

On the other hand, it should be pointed out that there are processes associated with some of the sectors covered in the inventory that might result in additional quantities of Hg released, however not accounted for in the current inventory due to lack of sufficient information to develop a global inventory. One such example is dental industry where Hg releases are only partly covered within the releases from Hg-added products sector, while there might be additional ones during production and preparation of Hg amalgams fillings. The same goes also for production stage of other Hg-added products (e.g. thermometers, lamps and batteries), as only releases associated with the use of these products are considered in this inventory. Similar, in the case of Hg releases from coal industry, large

quantities of water used during coal mining and transport, apart from those associated with coal washing, might release significant amounts of Hg.

5.2.3 Sources of data and information used in the inventory

Primary sources of data and information used in the production of the release inventory are described in Table 1. The following section briefly summarises data and information used to produce the estimates.

Table 1. Primary sources of activity and other related data used do derive release estimates

Release category	Activity data[a]	Distribution/release factors[b]	Hg content[c]	Other
Non-ferrous metal (Cu, Pb, Zn, Al, Hg, large-scale Au) production	GMA 2015 air emissions	UNEP, 2017a,b	-	
Chlor-alkali industry	GMA 2015 air emissions	UNEP, 2017a,b	-	
Oil refining	GMA 2015 air emissions	UNEP, 2017a,b	-	
Artisanal and small-scale gold mining	Artisanal Gold Council	Artisanal Gold Council/ UNEP Partnership on Reducing Mercury in ASGM	Artisanal Gold Council/ UNEP Partnership on Reducing Mercury in ASGM	
Municipal sewage	AQUASTAT, 2017	-	*To be added*	Sato et al., 2013 UNEP, 2006
Coal-fired power plants	Liu et al. (2016); GCPT, 2017;	-	Liu et al., 2016	Biesheuvel et al., 2016
Coal washing	Enerdata, 2016	UNEP, 2017b; Liu et al, 2016; ENM, 2016	Annex 6 and Hg in coal reported therein	Carbon Locker, 2017
Hg-added products use and waste disposal	P. Maxon, pers. Comm.	UNEP, 2017b; Lin et al., 2016	-	
Produced water during oil production	IOGP, 2016 BP, 2016	-	IPIECA, 2012 IKIMP, 2012 Gallup and Strong, 2008	Lujala et al., 2007

Group 1 sources: For release categories using UNEP Toolkit distribution factors (chlor-alkali industry, oil refining, large scale Au and non-ferrous metal production), respective air emissions developed in Chapter 2 of this report were used as input data to calculate corresponding releases to water. For the ASGM category, releases are discussed based on the amounts of Hg used in these activities and practices employed in individual country, as discussed in detail in Annex 2 of this report.

Group 2 sources*:* For estimation of Hg releases associated with municipal sewage, information on amounts of municipal wastewater generated and its treatment practices in individual countries were used. Amounts of municipal wastewater were obtained mostly from AQUASTAT, the FAO's global water

10237 information system, while waste-water treatment practices were obtained based on national data on
10238 waste-water generation, treatment, and use, as summarised by Sato et al. (2013). For countries with no
10239 data general regional averages were adopted from the UNEP report (UNEP, 2006). Ranges of Hg
10240 concentrations for untreated wastewater and water treated in treatment plants were selected based on
10241 ranges reported in literature, taking the waste management profile of individual country into account
10242 (see Annex X.1 for details).

10243 Releases associated with wastewater from coal-fired power plants were estimated based on amounts of
10244 waste-water generated per MWh of energy produced, as estimated from data presented by Liu et al.
10245 (2016). Hg concentration ranges applied were taken from the same source. Realized total energy output
10246 from CFPPs in individual country which was calculated from electricity generation capacities obtained
10247 from the Global Coal Plant Tracker database (GCPT, 2017) using country-specific capacity factors
10248 adopted from Biesheuvel et al. (2016).

10249 Global releases due to coal washing are estimated using information on production rates, Hg coal
10250 content, the Hg removal efficiency of coal washing and the coal washing rates. Activity levels of raw coal
10251 production for individual country were obtained from the global energy statistical yearbook (Enerdata,
10252 2016), information on type of coal produced from international energy statistics (EIA, 2017), Hg content
10253 of various coal types was selected based on ranges reported in scientific literature (see Annex 6), coal
10254 washing rates in major producing countries adopted from Energy News Monitor (ENM, 2016) and Hg
10255 removal efficiency from UNEP (2017) and Liu et al. (2016).

10256 Releases of Hg with water produced during oil and gas extraction are estimated based on global oil and
10257 gas production patterns, discharged produced water and Hg content in various oil and gas fields.
10258 Amounts of produced water discharged globally were estimated based on data from International
10259 Association of Oil and Gas Producers (IOGP, 2016) and BP Statistical Review of World Energy (BP, 2016),
10260 while ranges of associated Hg concentrations were selected considering regional differences in Hg
10261 content in oil fields throughout the world (IPIECA, 2012).

10262 **Group 3 sources:** For estimation of Hg releases associated with the use and disposal of Hg added
10263 products information consist of estimated Hg consumption in one year covering the product groups:
10264 batteries, measuring devices, lamps, electrical and electronic devices, dental applications, and other

uses (P. Maxon, 2017). The same distribution factors as in the case of air emissions were used to follow the fate of mercury through major pathways (see Annex 3 for details). Water specific release factors were selected and adjusted according to waste management profile of individual country based on factors from the Toolkit (UNEP, 2017) and Lin et al. (2016).

5.2.4 Relationship with independent inventories and approaches

In Figure 2 comparison of sectors for which releases to aquatic systems are being reported in various independent release inventories is shown schematically. Arrows indicate sectors comparable to various extent to GMAAR approach used in this study and which we use for comparisons with our estimates. In the following section, an overview of these independent inventories is given.

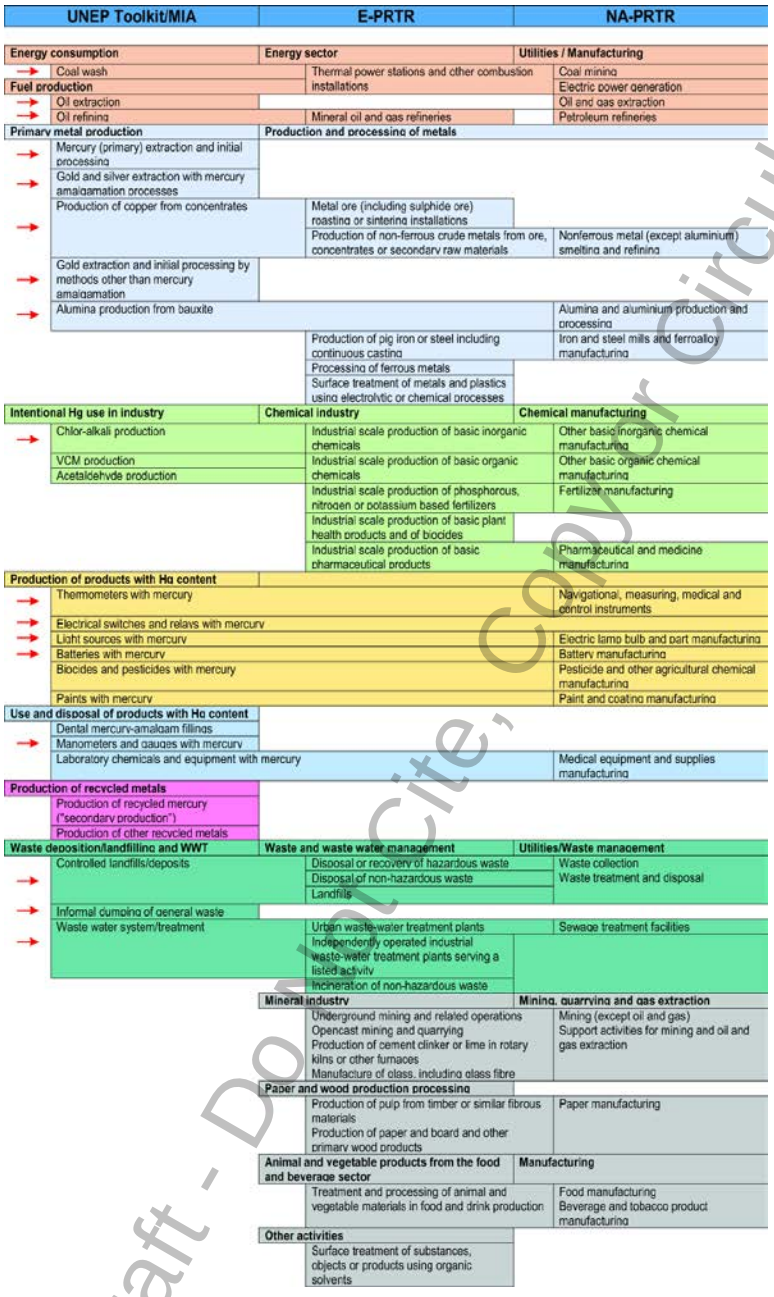

Figure 2. Comparison sectors used in various release inventories with arrows indicating sectors comparable (directly or indirectly) to GMA approach used in this study

For some countries independent inventories are available conducted as part of the Minamata Initial Assessments (MIAs) (ref.) and where UNEP Toolkit was used for identification and quantification of Hg releases.

The European Pollutant Release and Transfer Register (E-PRTR) is publically available Europe-wide register that provides key environmental data, including measurement of Hg releases to the air, water and soil as well as off-site transfers of waste, from by over 30,000 industrial facilities in European Union Member States and in Iceland, Liechtenstein, Norway, Serbia and Switzerland (UNEP, 2016). The following main sectors are covered in E-PRTR (http://prtr.ec.europa.eu) and data is available for 2007-2014 period: 1) energy sector, 2) production and processing of metals, 3) mineral industry, 4) chemical industry, 5) waste and wastewater management, 6) paper and wood production processing, 7) intensive livestock production and aquaculture, 8) animal and vegetable products from the food and brewery and 9) other activities. For each sector several sub-activities exist, however only those reporting Hg releases to water are shown in Figure 2. In case of E-PRTR it should be noted that reporting requirements are subject threshold which is set at the relatively high 1 kg Hg/yr.

NA-PRTR: Canada, Mexico, United States report data from 2006 to 2013 for states, provinces and territories on different levels (http://www.cec.org/) for different pollutant types including Hg within the North American Pollutant Release and Transfer Register (NA-PRTR). In the NA-PRTR inventory North American Industry Classification System (NAICS) is used, a system working on various levels of detail. In Figure 2, for the comparability reasons, sectors relevant for aquatic Hg releases from different NAICS levels are indicated. Similar as in the case of E-PRTR there is a threshold amount for reporting in NA-PRTR.

5.2.5 Regionalisation based on drainage basins

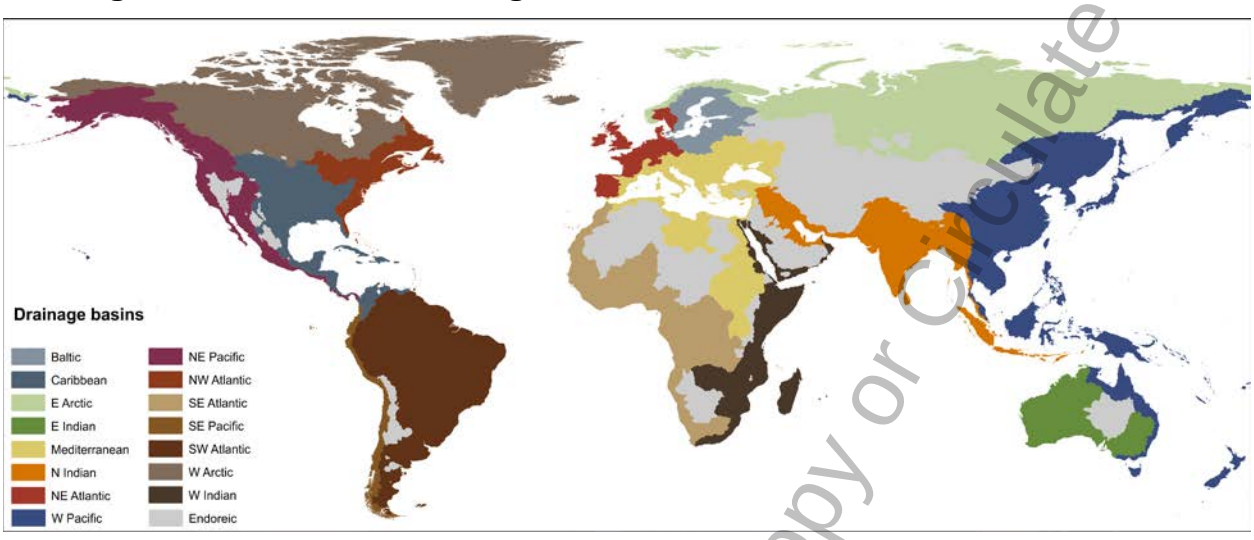

Figure 3. Drainage basins considered in the inventory (source: compiled by William Rankin (personal communication) based on USGS Hydro1k database (Garretson, SD, USA))

Additional regionalisation used to summarise inventory results is based on major global drainage basins map illustrated in Figure 3. The map comprises 15 basins draining to the principal oceans and seas of the world. An additional group of endorheic basins consists of several basins distributed in various parts of the world and that do not drain to the oceans. These basins used for the spatial distribution of Hg releases estimated in our inventory have quite different characteristics, e.g. in terms of land-use and population density. Important shares of crop land are present in NE Atlantic, N Indian, Caribbean and Mediterranean basins. The artificial surfaces have the highest shares in NE Atlantic and NW Atlantic basins, followed by Caribbean, Baltic and Mediterranean basins. On the other hand, drainage basins with the highest population density are N Indian, NE Atlantic and W Pacific.

5.2.6 Uncertainties and limitations

It should be pointed out that, given the global scope of this assessment, there are several limitations of this work and the estimates presented here are just that – the estimates. Numbers discussed in the following sections are derived using a number of different approaches and various assumptions, and the use of alternative approaches and assumptions might result in significantly different values. It was out of the scope of this work, however, to address these aspects into detail.

In order to provide some quantification of the uncertainties associated with the 2015 inventory, upper and lower range releases were produced for all sectors. For the sectors using the Toolkit approach, upper and lower range release estimates were calculated using the methodology used for emission inventory and described in Chapter 2 of this report. For the Group 2 and Group 3 sectors, upper and lower range releases were produced using the respective upper and lower ranges of Hg levels and associated activity data, respectively. Uncertainties related to the input data selected are further discussed for selected sectors in Section 3.4.

In addition to the above mentioned uncertainties, an additional limitation of this work is the possible double counting on one hand and the potential for underestimation of releases on the other. All sectors included in the inventory have a distinctive Hg sources and their pathways are clearly identified. The exception are releases associated with municipal waste-water which might contain a fraction of releases accounted for in the Hg-added products sector, releases resulting from breakage during use pathway to be specific. This latter pathway is however a minor share representing only 5% of releases from Hg-added products sector. As to the possible underestimation, a number of sectors and activities are identified in Section 2.2.2 that are not included in the current inventory, but might be important contributors to Hg releases on global scales. The current inventory of global anthropogenic Hg releases to aquatic systems is a work in progress, and an important step towards filling a major gap in inventories of anthropogenic Hg releases to the environment.

5.3 Estimating global anthropogenic mercury releases: Results

Given the specific nature of releases associated with artisanal and small scale gold mining (see section 3.3.6 for details), results for ASGM and non-ASGM sectors are discussed separately. In section 3.1 overall results are discussed considering releases summarised based on three general source categories (ore mining and processing, energy sector and waste treatment) and sub-regions. Section 3.2 presents inventory results spatially resolved according to major drainage basins of the world, while details for selected sectors are given in section 3.3, including discussions on trends where possible and the associated uncertainties.

Using the methods described above, the total estimated inventory of anthropogenic Hg releases from sources for which there was enough information to provide quantitative estimates, is 434 (x-y) t/y (ASGM not included).

5.3.1 Inventory results by region and sectors

Table 2 summarises the distribution of the estimates of global anthropogenic Hg releases to aquatic systems according to sub-continental regions. Table 3 presents the results per region on a per capita basis, for ASGM and other sectors.

Table 2. Global anthropogenic mercury releases to aquatic systems from different regions

Sub-continent	Releases[a] (range), t	%
Australia, New Zealand & Oceania	5.01 (x – y)	1.2
Central America and the Caribbean	19.9 (x – y)	4.6
CIS & other European countries	46.3 (x – y)	11
East and Southeast Asia	160 (x – y)	37
European Union	17.7 (x – y)	4.1
Middle Eastern States	14.9 (x – y)	3.4
North Africa	10.8 (x – y)	2.5
North America	22.3 (x – y)	5.1
South America	36.1 (x – y)	8.3
South Asia	54.2 (x – y)	12
Sub-Saharan Africa	46.7 (x – y)	11
Total	434 (x – y)	100

[a]Values rounded to three significant figures, ASGM not included

Table 3. Per capita anthropogenic mercury releases to aquatic systems in different regions

Sub-continent	Per capita releases from non-ASGM sectors, g	Per capita releases from ASGM [a], g
Australia, New Zealand & Oceania	0.16	0.00
Central America and the Caribbean	0.09	0.30
CIS & other European countries	0.14	0.03
East and Southeast Asia	0.07	0.19
European Union	0.04	0.00
Middle Eastern States	0.05	0.00
North Africa	0.06	0.00
North America	0.06	0.00
South America	0.09	0.95
South Asia	0.03	0.00
Sub-Saharan Africa	0.05	0.10
Global	0.06	0.14

[a]To both land and water

Figure 4 and Table 4 summarise the distribution of the estimates of global anthropogenic Hg releases to aquatic systems according to sector. Apart from combined releases to water and land resulting from ASGM activities, the majority of the global anthropogenic releases of Hg to aquatic systems are associated with the waste treatment sectors (52%), followed by energy sector (26%) and ore mining and processing group of sectors (22%). Overall, the new inventory is dominated by releases from two individual sectors, namely releases resulting from the use and disposal of Hg added products, and those associated with municipal wastewater. These two sectors alone contribute more than half (52%) of the total releases from all the sectors included. Other major release sectors include waste-water from coal fired power plants (13%), non-ferrous metals production (11%), coal washing (9.7) and production of gold from large-scale mining (9.4%).

The three newly added sectors (municipal wastewater, CFPPs and coal washing) are driving the relatively large difference between the 2010 and 2015 anthropogenic Hg release inventory (185 t/y in 2010 compared to 434 t/y in 2015). Here it should be noted that compilation of the global aquatic Hg inventory including identification of new sources is an ongoing activity, and as recognised in the 2010 inventory already, global releases are assumed to be underestimated due to the lack of information for some sources. In addition, there were some methodological changes incorporated in the 2015 inventory and as such both inventories cannot be directly compared. On the other hand, it must be pointed out that the three newly added sectors have the largest associated uncertainty among all included sectors. Methodological changes and uncertainties are further discussed in Section 3.3.

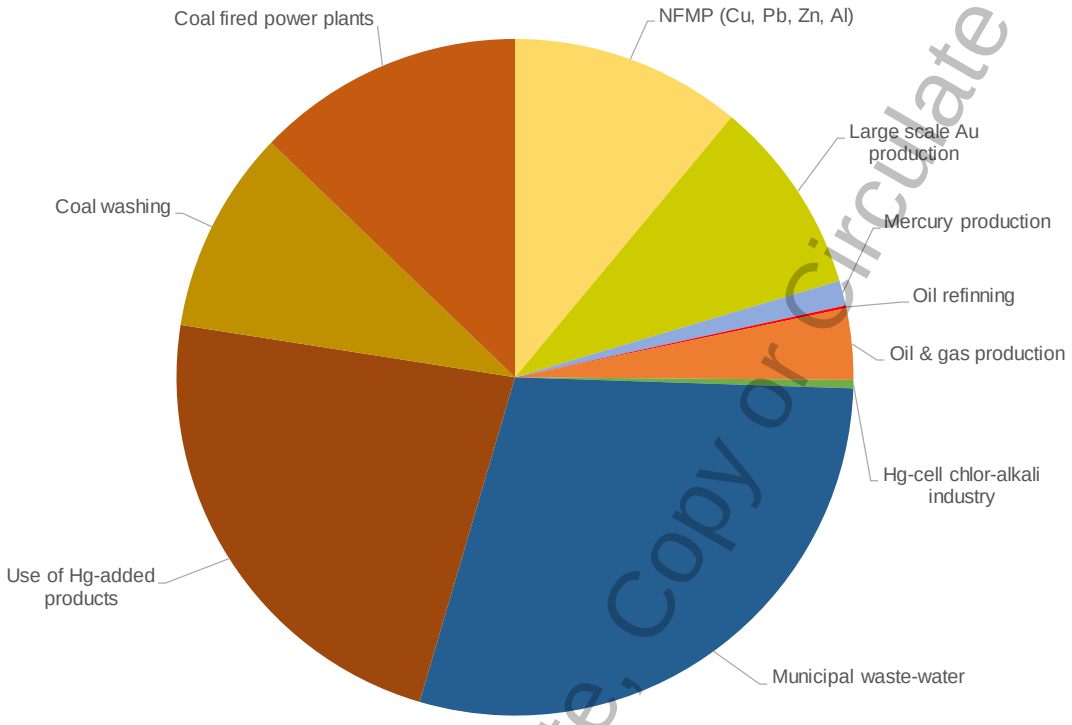

Figure 4. Proportions of global anthropogenic mercury releases to water in 2015 inventory from different sectors

Table 4. Global anthropogenic mercury releases to aquatic systems from different sectors

Sector	Releases (range), t[a]	%[b]
Production of non-ferrous metals (primary production of copper, lead, zinc and aluminium)	47.9 (x - y)	11
Production of mercury metal	5.18 (x - y)	1.2
Production of gold from large-scale mining	40.6 (x - y)	9.4
Mercury releases from oil refining	0.56 (x - y)	0.1
Mercury releases during oil and gas production	14.7 (x - y)	3.4
Mercury releases from chlor-alkali industry (Hg cell technology)	1.74 (x - y)	0.4
Mercury releases with municipal sewage	126 (42 - 210)	29
Mercury releases from coal-fired power plants	55.6 (12.3 - 123)	13
Mercury releases from coal washing	42 (23 - 65)	9.7
Mercury releases from Hg-added products use and waste disposal	99.4 (66.5 - 133)	23
Production of gold from artisanal and small-scale gold mining[c]	1011 (509 - 1513)	-
Total	434 (x – y)	

[a]Values rounded to three significant figures;, [b]ASGM not included;[c]Releases to both land and water

Figure 5 presents the 2015 inventory graphically by region and sector. It can be clearly seen from the illustration that relative contribution to the global anthropogenic Hg releases to water is by far the greatest in East and Southeast Asia. This is driven by large population and associated large industrial and other activities. As this region is a dominant source of Hg releases from all sectors, distribution of releases between sectors reflects the global one. On the other hand, relative contribution of Hg releases from different sectors varies a lot from region to region, clearly reflecting differences in technological and socio-economic status of the regions.

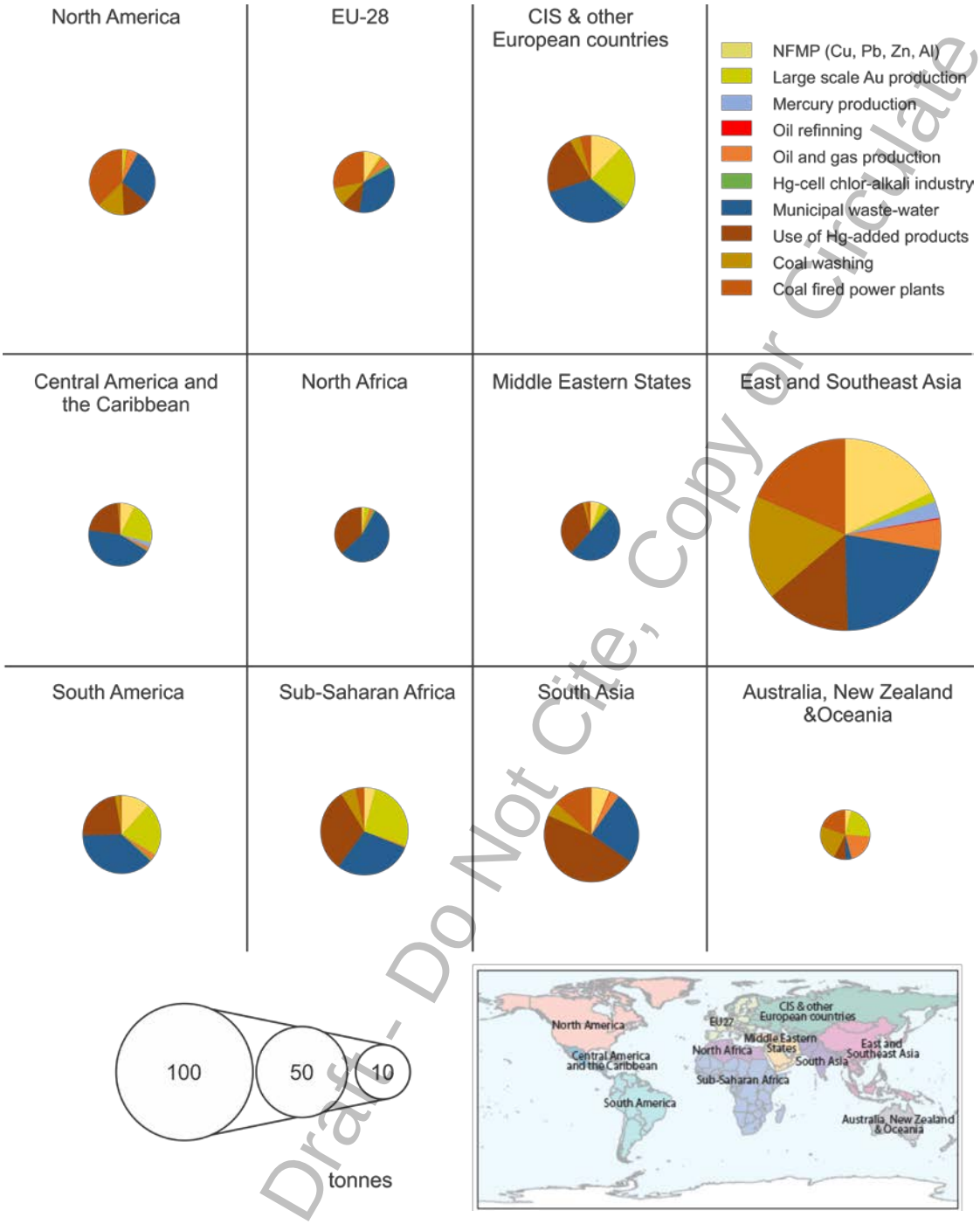

10389

10390 **Figure 5.** Regional pattern of global anthropogenic mercury releases to water in 2015 inventory from different sectors

10391 ### 5.3.2 Inventory results by drainage basin

10392 To be added

5.3.3 Discussion of results for selected sectors

The following sections discuss details on Hg releases associated with major release sectors. For the sectors included in both 2010 and 2015 inventory, trends in releases are also addressed, as well as differences in methods used to derive the estimates.

5.3.3.1 NFMP including Cu, Pb, Zn, Al, Hg and large scale Au production

The estimates included in the current inventory for releases from copper (Cu), lead (Pb), zinc (Zn), aluminium (Al), mercury (Hg), large scale gold (Au) production were all included previously in the 2010 inventory. Sum of releases from these sectors is comparable between the two inventories (92.5 vs. 88.5t/y), with around half of it resulting from large-scale gold production. It should be noted however that this latter sector has large associated uncertainties.

5.3.3.2 Municipal sewage

Releases from municipal sewage have not been addressed in the 2010 inventory. Estimates suggest that this sector is an important sector contributing significant amounts (29%) to the total global inventory. Given the input data and approach used for estimating Hg releases (details in Annex X.2), Hg releases from this sector are linked closely to water-use patterns and wastewater treatment practices in individual countries. Substantial part of municipal waste-water results from domestic water uses, but also from commercial and industrial effluents and storm water. While developed nations have very large per-capita water use and efficient wastewater treatment, people in developing countries use much less water, however with poorly developed wastewater collection and treatment systems (Sato et al., 2013). It is expected that with increases in population of developing nation's water demand and associated Hg releases will increase in these regions. On the other hand, it should be noted that global distribution and consumption of Hg containing products as one of the most important sources of Hg for this sector, is not uniform, and will largely depend on individual country's economy, with more products being consumed in developed parts of the world. Phase out of many products that contain Hg under the Minamata Convention is expected to result in decreases of Hg releases with municipal sewage, and so is the anticipated increased treatment of wastewater.

While Hg concentrations in both treated and untreated municipal waste-water are relatively well documented in the literature, Hg release estimates for this sector depend largely on data on global water use patterns, information that is considered as the least reliable and most inconsistent of all

water resources information (Gleick et al., 2014). The major limitations are lack of reporting standards, differences in approaches used to derive the information on water usages, and large inconsistencies in reporting years (Gleick et al., 2014). Another source of uncertainties lies in the fact that country-scale wastewater treatment levels (i.e. primary, secondary, and tertiary), practices that have significantly influence on effluent Hg concentrations, are mostly unknown. In our estimates, different Hg removal efficiencies for treated water were assigned to individual countries based on their waste management profile (cross ref).

5.3.3.3 Coal industry

Releases from coal industry have not been addressed in previous global inventories. In the 2015 inventory we consider two types of releases resulting from associated water use: Hg releases with wastewater from coal-fired power plants and those resulting from coal washing. Together both releases are estimated to contribute 23% to the global inventory. Both types of release estimates are considered preliminary and have large associated uncertainties. In the case of coal-fired power plants, this reflects the fact that information on actual profiles of installations - water use practices, treatment and wastewater generation - is missing for most of the world's CFPPs and so is information on Hg concentrations in respective effluents. In case of coal washing the major uncertainties are the result of assumptions that had to be made regarding coal washing rates, removal efficiencies and especially selected share of Hg reaching aquatic systems in individual countries. Estimates are therefore made based on gross generic assumptions as described in Annexes X.3 and X.4.

Coal-fired power plants. CFPPs are recognised as one of the major anthropogenic Hg emission sources. However, due to the lack of quantitative information, Hg releases to water from this sector were neglected in previous inventories. Large releases are the result of the fact that coal industry is by far the greatest water demanding anthropogenic activity in the world, and it was estimated that in 2013 CFPPs alone consumed 19 billion m^3 of freshwater globally (Cheng and Lammi, 2016). While the vast majority of this water is used for cooling, and is usually not contaminated with Hg, additional water uses such as pollution control can also generate large amounts of Hg contaminated wastewater. Here, an attempt was made to quantify Hg releases with this latter non-cooling water-use types.

Despite many uncertainties, there is now much more evidence based on both measured and estimated data about the significance of Hg releases from CFPPs. It is known that plants using wet scrubbers can

discharge up to tens of kg of Hg to local surface waters per year (EIP, 2016, E-PRTR, 2014). In addition to discharges to surface water, even larger amounts of Hg (up to hundreds kg per year) are dumped into ash ponds which are prone to leaks (EIP, 2016). In a recent aquatic release inventory for China, wastewater discharged from CFPPs, although in gradual decline in the last decade, is recognised as one of the most important anthropogenic sources of Hg (Liu et al., 2016). Similar, according to European Pollutant Release and Transfer Register (E-PRTR, 2017), Hg releases from thermal power stations and other combustion installations are the second largest source – second only to urban waste-water treatment plants. Global Hg releases from this sector using assumptions described in Annex X.3 are based on information available for China (Liu et al., 2016) and are estimated in the 12-123 t/y range. Alternative to this approach would be an estimate made based on simple global upscaling of ratio of anthropogenic Hg released to water and air for China for this sector which is approximately 1:4. This would result in a global release of 50-110 t/y, which is a range comparable to the first approach.

Coal washing. In addition to water used in CFPPs, large amounts of water are used during coal mining and washing. The latter is used to remove impurities and ash from the coal and results in the generation of a slurry of toxic material (Cheng and Lammi, 2016). Here, in the absence of detailed information, we use the approach similar to that of Liu et al. (2016) and make a preliminary estimate of likely magnitude of global Hg releases due to coal washing based on global coal production, coal Hg content, assumed Hg removal efficiencies, washing rates and environmental fate in individual countries (see Appendix X.4 for details). Given the fact that coal washing results in higher caloric value of coal and consequently a higher economic value, coal beneficiation is increasing throughout the world. Available information suggests that a higher share of the coal produced is treated in more developed countries but is also in increase in developing economies (Budge et al., 2000). Estimates available for China, the major coal producer in the world, indicate rapid increase of Hg releases from coal mining and washing with an annual average growth rate of 25% in the 2001-2012 period, making this sector the second largest anthropogenic source of aquatic Hg in China (Liu et al., 2016). Overall releases from this sector are largely dominated by releases from China (>60%), followed by other important coal producing countries such as United States, India, Australia and Indonesia. In addition to high uncertainty of the approach and sensitivity of all input information used to derive these estimates, it should be pointed out that these numbers are obtained based on very gross assumptions regarding environmental fate of Hg once washed from coal. Nevertheless, even larger quantities of Hg in the magnitude of tens of tonnes per year are assumed to

accumulate in the slurry ponds at coal washing sites globally, representing a great environmental hazard for local aquatic systems, as these ponds are often very prone to brakeage and leaking (Cheng and Lammi, 2016).

5.3.3.4 Oil industry

The 2015 inventory includes two types of releases associated with oil industry. Hg releases from oil refining were included previously in the 2010 inventory, while releases with produced water during crude oil and gas production is a newly added sector. Given the fact that in 2015 oil refineries processed similar amounts of crude as in 2010, and that the same method was used to estimate releases, differences between the two inventories are negligible. Both release types, refining and crude processing, together contribute approximately 3.5% of the total inventory. Of that a vast majority (96%) is attributed to produced water, and of which ~85% is occurring off-shore. Using the approach described in detail in Annex X.5, almost 70% of these releases are attributed to Asian countries due to large amounts of produced water and more mercury contained in these regions oil and gas fields. There might be additional releases from this industrial activity such as releases during separation and transportation of crude oil and gas not accounted for in this inventory.

5.3.3.5 Hg-added products – use and waste disposal

Hg-added products sector comprise of releases from the following product groups: batteries, measuring devices, lamps, electrical and electronic devices, dental applications, and other uses (see Annex 3 for details). In the 2010 inventory, releases for this sector were estimated based on Hg emission inventory by using the distribution factors from the UNEP Toolkit to calculate the corresponding magnitudes of releases to water. The 2015 inventory adopts the model used to estimate mercury emission from waste streams associated with intentional use sectors and considers releases for three main pathways of Hg-added products: breakage during use, waste recycling and waste landfilling (see details in Annex X.6). In addition to the new method used to derive the estimates, there is a change in the models input data. In the 2010 inventory part of the mercury from Hg-added products (approx. 30%) was considered as "retained in use" and is now included in the waste streams and consequently in emission and release pathways, respectively.

Our estimates suggest significant Hg releases due to usage and disposal of Hg added products (66-133 t/y), a vast majority (91%) being associated with uncontrolled landfilling of waste which is primarily

occurring in developing countries, followed by releases during breakage (5%) and recycling (4%). Due to environmental regulations and new technologies available, the use of Hg in products is in decline and so are environmental releases of Hg, especially in developed countries. Substitution of Hg-added products with non-Hg containing alternatives, however, is also becoming evident in developing countries. An exception are products without the adequate Hg-free alternatives such as lightning devices which are also excluded from the Minamata Convention.

It should be noted that these estimates depend largely on estimates of regional consumption of Hg-added products. While this information is available for developed countries, very little information is available on the real consumption patterns for Hg-added products in developing countries.

5.3.3.6 Artisanal and small-scale gold mining (ASGM)

Given the fact that there is still not enough information and knowledge to separate terrestrial releases between water and land, releases associated with artisanal and small-scale gold mining (ASGM) remain a "special" sector in the inventory. The detailed reasoning for this is given in 2010 inventory (AMAP/UNEP, 2013). In summary, Hg releases for this sector are based on amounts of Hg used in ASGM activities and the characteristics of the mining practices applied in individual countries. The methodological approach used differentiates between emissions to air and releases to both land and water (details including example calculation is given in Annex 2). At this point, it is not possible to directly determine what the proportion is of Hg associated with this later pathway that will enter hydrosphere. In addition to the direct losses occurring during ore amalgamation, large quantities of Hg are accumulating in soils and sediments surrounding ASGM sites over the time. This accumulated Hg has potential to be remobilised and enter aquatic systems, however with a time-lag usually unknown, depending largely on site-specific environmental conditions. It is estimated that ASGM releases to water and land in 2015 are 1011 t/y (range, 509-1513 t/y).

5.3.4 Comparison of estimates with national reported inventories and other sources

To be added

5.3.5 Inventory in the context of global Hg cycle

To be added

5.4 Conclusions

5.4.1 Key findings

- The 2015 global inventory of Hg releases from anthropogenic sources is more complete and reinforces the importance of these sources in the global context.
- Global releases of anthropogenic Hg to freshwater, excluding ASGM, based on revised estimates are 430 t/y, compared to 180 t/yr in the 2010 estimate.
- New sectors were added to this inventory and include releases with municipal wastewater, from coal washing, coal fired power plants and with produced water during oil and gas production. Uncertainties for these sources are large (+/- X%). Better information about coal washing practices and fate of Hg during various water uses in coal fired power plants are needed, in particular.
- While levels of Hg associated with individual sectors included in the inventory are relatively well established, all other supporting information (e.g. production rates, waste-water generation, treatment practices etc.) is much more unreliable and inconsistently reported, and drives the uncertainties of the estimates.

5.4.2 Future gaps and needs

- Reduction of uncertainties for all the sectors included in the inventory is needed by using more systematic and harmonised approaches in data collection.
- Not only information on Hg content must be improved, but especially information on related activity data needed to derive the estimates.
- Additional sectors and anthropogenic activities, not taken into account in this inventory, as discussed in detail in Section 2.2.2, should be included in future inventories. Although recognised as less relevant in the global context in this work, some of these sources might be significant contributors of Hg to local aquatic systems.
- Estimates in the 2015 inventory are made based on country-level information. Future work would benefit from inclusion of more detailed facility-level information to improve the spatial distribution component of this work. Along these lines, more detailed knowledge on differences in technologies used, waste treatment practices and Hg consumption patterns in individual countries should be incorporated.

- Harmonisation of methodological approaches for estimating the releases is needed, e.g. something along the lines of the UNEP Toolkit approach but focused on aquatic Hg releases.
- Although out of the scope of this chapter, lack of knowledge regarding the fate of Hg once released from the source was recognised as a limiting factor for placing inventory results in the context of the global Hg cycle. Future work should focus more on establishing relationships between catchments characteristics, sources within individual catchments and the Hg outflows. Nowadays, techniques like isotope tracer experiments and isotope ratio measurements of Hg are available to address this issues.

Annex X

Given the global nature of the inventory and general lack of data/information on aquatic Hg releases and associated information, assumptions had to be made to derive the estimated presented in this work. Often these assumptions are difficult to validate. For the transparency reasons details on the data/information and assumptions made within individual release category are given here.

X.1 Group 1 sectors

Group 1 sectors use UNEP Toolkit distribution factors from Table X.1 to calculate releases to water from the 2015 air emission inventory. Details for compiling data and derivation of air emissions are given in Chapter 2 and Appendixes 1-6.

Table X.1. UNEP Toolkit distribution factors and scaling factors for water/air distribution

Sector	UNEP Toolkit distribution factor		Scaling factor (water/air)
	to air	to water	
Chlor-alkali industry	0.1	0.01	0.1
Oil refining	0.25	0.01	0.04
Large scale Au	0.04	0.02	0.5
Non-ferrous metal production (Cu, Pb, Zn)	0.1	0.02	0.2
Non-ferrous metal production (Al)	0.15	0.1	0.67
Non-ferrous metal production (Hg)	0.25	0.06	0.24

X.2 Municipal wastewater

The 2015 inventory for Hg releases associated with municipal wastewater is based on information regarding volumes of municipal wastewater produced, wastewater treatment practices and reported Hg concentrations measured in wastewater before (influent) and after the treatment (effluent). Municipal wastewater is water that has been used for municipal use and is afterwards released back to the environment. Treatment of this released water mostly depends on prosperity of the country and consequently its capacities and number of wastewater treatment plants. Bulk of the information for individual countries was obtained from the AQUASTAT database of the Food and Agriculture Organisation of the United Nations (FAO). AQUASTAT reports amounts of municipal wastewater generated within urban areas. Since not all countries are reporting their amounts of municipal wastewater on regular yearly basis, the last available data for each country was used. For countries with no data available, waste-water was calculated based on assumed water use per person per day. Water use averages for individual continent were selected and assigned to the countries with missing data: 230 for Asia, 50 for Africa, 200 for Europe, 100 for Oceania and 100 l/person/day for Caribbean countries. Percentage of treated waste-water has been then assigned to each country. Treatment data are based on the numbers from Sato et al. (2013). For the countries with no specific values on treatment, general regional ratios from UNEPs state of the marine environment report were adopted (UNEP, 2006), assuming similarities within regions and between the neighbouring countries.

Magnitude of Hg releases from this sector will depend greatly on the amount of Hg products used, general waste handling practices and especially level of waste-water treatment - information lacking for most of the countries. In absence of such information, generic waste management profile of a country was used and different ranges of Hg concentrations applied for untreated wastewater and wastewater treated in treatment plants, to estimate releases for individual country. These estimates are based on an assumption that Hg concentrations in untreated wastewater are lower in more developed countries compared to those in developing nations, as seen from values reported in scientific literature. Further assumption is that Hg removal is more efficient in developed countries due to greater levels of waste-water treatment (Table X.2).

Table X.2 Ranges of Hg concentrations in untreated and treated sewage used to derive the estimates

Profile	Hg in untreated wastewater [ng/L]	Hg removal efficiency [%]	Hg in treated wastewater [ng/L]
1	100-500	95	5-25
2	300-1500	80	60-300
3	300-1500	70	90-450
4	300-1500	60	120-600
5	300-1500	50	150-750

X.3 Coal-fired power plants

The 2015 inventory for Hg releases with wastewater from coal-fired power plants uses a very coarse approach for a first preliminary estimate of global magnitudes associated with this sector. In the absence of more detailed country-specific information, the approach largely relies on information available for China and work carried out by Liu et al. (2016), by upscaling globally relationships between CFPPs electric capacities, amounts of wastewater produced and associated reported ranges of Hg concentrations reported in their work.

The method applied is based on an assumption that on average global water use patterns in CFPPs are similar to those in China, country that is the single largest user of coal-derived electricity in the world. This is of course a rough generalisation, however inevitable in order to perform harmonised global calculation approach.

Based on wastewater volumes reported by Lie et al. (2016) and total electricity generation capacity of CFPPs in China, wastewater generation was estimated at 0.25-0.5 m^3 per MWh of energy produced. For the purpose of this wastewater generation estimate, realized energy output from CFPPs was calculated using the capacity factor of 0.55 (Biesheuvel et al., 2016). In order to estimate generation of wastewater in each country of the world with CFPP, wastewater generation rate from China was then used along with the information on country-wide CFPPs total capacity based on information provided in Global Coal Plant Tracer database (GCPT, 2017). Capacity factors used for calculation of the amount of energy produced in individual country were adopted from Biesheuvel et al. (2016). Final amounts of Hg releases

per country were estimated using Hg concentrations in CFPPs generated wastewater in 5-25 mg/m^3 range (Liu et al., 2016 and references therein).

X.4 Coal washing

The 2015 inventory for Hg releases associated with coal washing is based on global coal production, coal Hg content, Hg removal efficiency and coal washing rates, following the approach of Liu et al. (2016).

Total coal production in 2015 for individual country was obtained from the Global Energy Statistical Yearbook 2016 (Enerdata, 2016). In the absence of detailed per-country information on amounts of different coal types, regional information on coal type produced (anthracite, metallurgical, bituminous, subbituminous and lignite) was obtained from International Energy Statistics available for the year 2014 (U.S. Energy Information Administration, 2017b). Regional ratios were then applied to individual country. For countries where information on Hg content in various Hg coals was available as summarised in Annex 6, country specific average Hg content was used, while for countries where this information is missing generic values were applied. Information on coal washing rates in individual countries is available for world's major coal producers only, China, United States, India and Australia, and varies in the 20-90% range. For the rest of the world we assume that higher percentages of coal produced are being washed in developed countries and assign the following washing rates using technology profiles (TP) of the country: TP1-80%, TP2-65%, TP3-50%, TP4-35% and TP5-20%. The Hg removal efficiency of coal washing is selected in 20-30% range (UNEP, 2017; Liu et al, 2016). It is further assumed that only part of Hg released during washing will reach local aquatic systems, the rest being deposited in slurry ponds. Using waste management profiles of individual country, following percentages for Hg reaching water courses were selected: WP1-20%, WP2-30%, WP3-40%, WP4-50% and WP5-60%.

X.5 Releases with produced water during oil and gas production

The 2015 inventory of Hg releases with produced water during oil and gas production is based on information on global oil and gas production patterns and knowledge about associated amounts of discharged produced water and Hg content in various oil and gas fields.

Initially, amounts of produced water discharged globally were estimated using amounts and knowledge regarding percentage of global coverage as reported for various regions of the world (Africa, Asia/Australasia, Europe, FSU, Middle East, North America and South & Central America) by the

International Association of Oil and Gas Producers (IOGP, 2016) for the target year 2015. Information on produced water discharged is available separately for onshore and offshore oil and gas production.

Total per region amounts were then used together with selected Hg concentration ranges to derive regional Hg releases. Publically available information on Hg concentration in produced water is very scarce. It is known, however, that there can be significant differences in Hg content in different oil and gas fields throughout the world. Limited data available indicate Hg levels in produced water can vary from less than 1 ppm (IKIMP, 2012) to tens of ppm in some of the oilfields in the gulf of Thailand (Gallup and Strong, 2008). In the absence of detailed information on Hg concentrations in produced water from oil and gas fields of the world, different Hg concentrations were assigned to different regions of the world, using the regional breakdown for crude oil Hg concentrations by IPIECA (2012) (Table X.3).

In the next step, regional releases divided to onshore and offshore share were proportionally downscaled to per country level, using information on oil and gas production in individual country as reported in BP Statistical Review of World Energy (BP, 2016) for the target year 2015. In the absence of detailed information on onshore and offshore production in individual country, PETRODATA, a spatially distributed dataset on global oil and gas fields (Lujala et al., 2007) was used to identify the countries with both or just one type of production.

Table X.3. Regional breakdown of mercury median crude oil concentrations and assigned produced waste-water Hg concentrations

Continent	Median crude oil concentrations [ppm]	Produced water concentrations [µg/l]
Africa	1	3.0
Middle East	1	3.0
Europe	1.2	3.5
North America	1.2	3.5
South America	1.4	4.0
Pacific and Indian	3	9.0

[a]IPIECA, 2012

X.6 Hg added products

In 2015 inventory mercury releases to water from Hg added products are produced using methodology comparable to that applied to estimate emissions to air (see Annex 3 for details). The approach uses regional patterns of consumption of Hg and Hg-containing products. Mercury releases at various points

in the life-cycle of these products are estimated using assumptions regarding rates of breakage, waste handling, and factors for releases to water. The input data consist of estimated Hg consumption in one year (2015) covering following product groups: batteries, measuring devices, lamps, electrical and electronic devices, dental applications, and other uses. These amounts are then distributed to four different initial pathways (safe storage, breakage and releases of Hg during use, paths to the waste stream, products remained in use) using distribution factors. Waste pathways are further differentiated among waste recycling, waste incineration and waste landfill. This latter pathway is further distributed between two levels of waste management, controlled and uncontrolled waste landfill. Within these pathways, releases to water are assumed for breakage/release during use, recycling and from waste landfills. Releases to water are then estimated by applying release factors (RF) according to Table X.4 to the distributed individual amounts of Hg. For releases resulting from breakage during use, waste recycling and controlled landfills, release factors are the same for assigned generic profiles of waste management. A differentiation is introduced for releases from uncontrolled landfills by using different release factors for individual profiles. Using this approach, estimates were made for individual countries, while global population density/distribution map was then used to spatially distribute and summarise the estimates according to major drainage basins of the world.

Table X.4. Release factors (fraction released) applied to distributed amounts of mercury in Hg-added products

Profile	Break/release during use	Waste recycling	Landfill	
			controlled	uncontrolled
1	0.1	0.05	0.0001	0.05
2	0.1	0.05	0.0001	0.10
3	0.1	0.05	0.0001	0.15
4	0.1	0.05	0.0001	0.20
5	0.1	0.05	0.0001	0.25

References:

AMAP, 2010. Updating Historical Global Inventories of Anthropogenic Mercury Emissions to Air. By: Wilson, S., J. Munthe, K. Sundseth, K. Kindbom, P. Maxson, J. Pacyna and F. Steenhuisen. AMAP Technical Report No. 3. Arctic Monitoring and Assessment Programme (AMAP), Oslo, Norway. 12 pp.

AMAP/UNEP, 2008. Technical Background Report to the Global Atmospheric Mercury Assessment. Arctic Monitoring and Assessment Programme / UNEP Chemicals Branch. 159 pp. Online at: www.chem.unep.ch/mercury/Atmospheric_Emissions/Technical_background_report.pdfAMAP/UNEP. Arctic Monitoring and Assessment Program: Oslo, Norway/UNEP Chemicals Branch: Geneva, Switzerland. Technical

10716 Background Report for the Global Mercury Assessment 2013, pp. vi–263.AQUASTAT, FAO, Produced Municipal
10717 Wastewater, 1985-2014.
10718 AQUASTAT, 2017. Available at http://www.fao.org/nr/water/aquastat/main/index.stm
10719 Biesheuvel et al. (2016), Modelling global water demand for coal based power generation, Methods
10720 and results report, Greenpeace.
10721 BP, 2016, Statistical Review of World Energy. Available at https://www.bp.com/content/dam/bp/pdf/energy-
10722 economics/statistical-review-2016/bp-statistical-review-of-world-energy-2016-full-report.pdf
10723 Budge et al., 2000. Review of worldwide status pf coal preparation technology, Available at:
10724 http://citeseerx.ist.psu.edu/viewdoc/download?doi=10.1.1.557.9262&rep=rep1&type=pdf
10725 Carbon Locker, 2017. http://www.carbonlocker.org
10726 Cheng, I., Lammi, H., 2016. The Great Water Grab. How the Coal Industry is Deepening the Global Water Crisis.
10727 Greenpeace.
10728 Coal preparation, 2011. (http://webarchives.gov.uk/+/http:/www.berr.gov.uk/files/file19296.pdf)
10729 Drainage Basins. William Rankin (personal communication) based on USGS Hydro1k database. Garretson, SD, USA.
10730 EIA, 2017, International Energy Statistics, 2017. US Energy Information Administration.
10731 https://www.eia.gov/beta/international/data/browser/#/?pa=3g000000000000000000000000000000000000
10732 180000000000000g&c=4100000002000060000000000000g0002000000000000000001&tl_id=1-
10733 A&vs=INTL.7-1-AFRC-TST.A&vo=0&v=H&start=1980&end=2014
10734 EIP, 2016. Toxic Wastewater from Coal Plants, Available at:
10735 https://www.eenews.net/assets/2016/08/11/document_gw_05.pdf
10736 Enerdata, 2016, Global Energy Statistical Yearbook 2016, https://yearbook.enerdata.net/coal-and-lignite-
10737 production.html
10738 ENM, 2016. Energy News Monitor | Volume XII; Issue 30, https://indiaenergyanalysis.wordpress.com/2016/01/08/coal-
10739 washing-global-perspective/
10740 E-PRTR, 2014, The European Pollutant Release and Transfer Register (E-PRTR), 2014. (http://prtr.ec.europa.eu)
10741 Gallup, D. L. & Strong, J. B. (2006). Removal of Mercury and Arsenic from Produced Water. In 13th Annual International
10742 Petroleum Environmental Conference. http://www.hgsolution.com.my/research/paper2.asp
10743 GCPT, 2017. Global Coal Plant Tracker, http://endcoal.org/global-coal-plant-tracker/
10744 Gleick et al., 2014, The World's Water Volume 8.
10745 IES, 2017. International Energy Statistics, 2015.
10746 (https://www.eia.gov/beta/international/data/browser/#/?pa=0000000000000000000000000000000000002&
10747 c=ruvvvvvfvtvnvv1urvvvvfvvvvvfvvvou20evvvvvvvvvvnvvuvo&ct=0&tl_id=5-A&vs=INTL.57-1-AFG-
10748 TBPD.A&vo=0&v=H&start=1980&end=2016)
10749 IKIMP, 2012. Mercury arising from oil and gas production in the United Kingdom and UK continental shelf. By: Lang, D., M.
10750 Gardner and J.Holmes. Integrating Knowledge to Inform Mercury Policy (IKIMP). University of Oxford. 38 pp.
10751 IOGP, 2016, Environmental performance indicators – 2015 data, International Association of Oil and Gas Producers.
10752 http://www.iogp.org/bookstore/product/environmental-performance-indicators-2015-data/
10753 IPIECA, 2012. Industry input to the UN global mercury treaty negotiations focus on oil and gas. By: Doll, B.E., B.M.
10754 Knickerbocker and E. Nucci. The global oil and gas industry association for environmental and social issues
10755 (IPIECA).
10756 Kamal, A.S.M., Goyer, K., Koottatep, T., Amin, A.T.M.N, 2008. Domestic wastewater management in South and Southeast
10757 Asia: the potential benefits of a decentralised approach. Urban Water Journal, 5, p. 345-354.
10758 Lin et al., 2016 , Material Flow for the Intentional Use of Mercury in China.Environ Sci Technol. 2016 Mar 1;50(5):2337-
10759 44. doi: 10.1021/acs.est.5b04998
10760 Liu, M.; Zhang, W.; Wang, X.; Chen, L.; Wang, H.; Luo, Y.; Zhang, H.; Shen, H.; Tong, Y.; Ou, L.; et al. Mercury Release to
10761 Aquatic Environments from Anthropogenic Sources in China from 2001 to 2012. Environ. Sci. Technol. 2016, 50,
10762 8169–8177.
10763 Lujala, Päivi; Jan Ketil Rød & Nadia Thieme, 2007. 'Fighting over Oil: Introducing A New Dataset', Conflict Management
10764 and Peace Science 24(3), 239-256.
10765 Sato, T., Qadir, M., Yamamoto, S., Endo, T., Zahoor, A., 2013. Global, regional, and country level need for data on
10766 wastewater generation, treatment, and use. Agricultural Water Management, 130, p. 1-13.
10767 Steenhuisen, F.; Wilson, S. Identifying and characterizing major emission point sources as a basis for geospatial
10768 distribution of mercury emissions inventories. Atmos. Environ. 2015, 112, 167–177
10769 UNEP, 2017a, Toolkit for Identification and Quantification of Mercury Sources, Guideline for Inventory Level 1, UNEP
10770 Chemicals Branch: Geneva, Switzerland.
10771 UNEP, 2017b. Toolkit for Identification and Quantification of Mercury Sources, Reference Report and Guideline for
10772 Inventory Level 2, UNEP Chemicals Branch: Geneva, Switzerland

10773 UNEP. The state of the marine environment - trends and processes, 43 pp., United Nations Environment Programme and
10774 the Global Programme of Action for the Protection of the Marine Environment from Land-based Activities (GPA)
10775 of the United Nations Environment Programme (UNEP), The Hague, Netherlands. 2006.UNEP, 2017
10776 Wilson, S., F. Steenhuisen, J.M. Pacyna and E.G. Pacyna, 2006. Mapping the spatial distribution of global anthropogenic
10777 mercury atmospheric emission inventories. Atmospheric Environment, 40: 4621-4632.

Note to reader

This draft version of Chapter 6 in the Technical Background Report to the Global Mercury Assessment 2018 is made available for review by national representatives and experts. The draft version contains material that will be further refined and elaborated after the review process. Specific items where the content of this draft chapter will be further improved and modified are:

1. All graphics will be redrawn to a common appearance from the originals presented here, with their sources cited in the captions.
2. References will be completed and presented in a uniform style.
3. Conclusions and main messages will be formulated

GMA 2018 Draft Chapter 6. Relationships between Trends in Atmospheric Hg and Hg in Aquatic Biota.

Peter Outridge, Robert Mason, Feiyue Wang, Lars-Eric Heimburger, Milena Horvat, Xinbin Feng

11027 ## Contents

11038

11039

6.1 Relationships between Trends in Atmospheric Hg and Hg in Aquatic Biota

The goal of the Minamata Convention is to reduce Hg emissions mainly from atmospheric sources (see Chapter 1.1), with the ultimate aim of reducing the exposure and harmful effects of Hg in wildlife and humans. However, the pathway between Hg´s release into the atmosphere and its eventual accumulation in wildlife and humans is biochemically and geochemically complex. Mercury is emitted into the air from most low- and high-temperature anthropogenic and natural sources primarily as gaseous elemental Hg (GEM; Hg^0). In the atmosphere, GEM is ultimately oxidized to Hg^{II} and part of this airborne inorganic Hg is deposited into aquatic environments, where it joins other inorganic Hg^{II} that is present as a result of waterborne releases from other natural and anthropogenic sources. A small fraction of the inorganic Hg pool in aquatic environments is converted by natural microbial processes into more toxic methylated forms - monomethyl Hg (MeHg), and (less commonly) dimethyl Hg (DMeHg), with MeHg being the form that is bioaccumulated and biomagnified within foodwebs.

The aquatic geochemistry stage of the global Hg cycle is therefore an important transformative step in the sequence between anthropogenic GEM emissions, the atmospheric deposition of inorganic Hg^{II}, and MeHg accumulation in foodwebs. A number of environmental and ecological factors (including redox condition, pH, organic carbon and nutrient concentrations, food web trophic structure, temperature, and light intensity) have a strong influence on the rates of MeHg production and degradation, as well as the rate of uptake of MeHg by aquatic biota. Together, the complexity of the atmospheric Hg cycle, the limits of our understanding of the methylation/demethylation cycle, and the number of influential factors affecting MeHg bioaccumulation, mean that there is considerable uncertainty about how closely changes in the emissions and deposition of Hg into the environment brought about by regulatory action will be tracked by changes of Hg in aquatic food webs.

This chapter describes recent advances in our developing understanding of the aquatic geochemistry of Hg, particularly focussing on the connectivity between atmospheric Hg and Hg levels in aquatic biota. The chapter is divided into two sections which address the following issues: (1) recent advances in understanding of methylation and demethylation in marine systems (6.1); and (2) observed relationships between the trends in atmospheric Hg emissions and deposition and in aquatic biota, and the reasons for dichotomies between those trends (6.2). These topics were chosen because they are of the greatest

11069 importance with respect to advances in aquatic Hg geochemistry since AMAP/UNEP (2013), and because
11070 of their relevance to predicting the efficacy of the Minamata Convention in ultimately reducing Hg
11071 exposure in humans and wildlife.

11072 **6.1.1 How has our understanding of the marine methylation and demethylation cycle**
11073 **evolved since GMA 2013?**

11074 The concentration of methylated Hg species (MeHg, DMeHg) in an aquatic water column represents the
11075 culminating effect of various processes that influence the methylation of ionic Hg (Hg^{II}) to MeHg and
11076 DMeHg, their demethylation, as well as transport from the location of their formation to the water
11077 column. Generally, Hg is methylated by bacterial processes in sediments and the water column of large
11078 water bodies, such as the ocean and large lakes, but not in the water column of most freshwater
11079 ecosystems. While methylated Hg can be produced by abiotic reactions and processes, its formation is
11080 thought to be primarily biotic and microbially-mediated (Paranjape and Hall 2017). In contrast,
11081 demethylation of these compounds is thought to be by both abiotic and biotic pathways, with DMeHg
11082 being volatile and more unstable in the environment than MeHg. Overall, therefore, the concentration
11083 of methylated Hg is the net result of many competing processes of formation, transport, and
11084 destruction.

11085 Methylated Hg compounds constitute a small fraction of the total Hg present in some environments
11086 (e.g. < 1% in air and typically <5% in marine sediments, but with somewhat higher relative
11087 concentrations in freshwater sediments and wetland soils; Paranjape and Hall 2017). However, these
11088 compounds can be a much larger fraction of the total Hg in the water column, and can exceed 20% of
11089 total Hg in the open ocean. Additionally, in some marine waters such as in the Arctic Ocean, DMeHg can
11090 be as abundant as MeHg (Lehnherr 2014). In biota, the fraction as MeHg increases as a function of
11091 trophic level, from ~20% of total Hg in seston to >90% in high trophic level biota. As MeHg is the more
11092 toxic form of Hg, and poses the primary exposure risk to humans and other top predators, it is of prime
11093 importance to understand the production and fate of these compounds.

11094 As discussed further below, due to the complexity of methylation and demethylation, it is not possible
11095 to generalise these processes into either global or regional MeHg budgets, although some progress is
11096 being made in this regard. Furthermore, given the complexities that control the *net* formation of MeHg
11097 in the environment, it is clear that while reducing total Hg emissions to the environment can be
11098 expected to ultimately reduce MeHg in biota in general and over time, more detailed predictions of the

effects of regulatory actions on Hg in biota in a specific ecosystem requires further understanding of the methylation/demethylation processes in the ecosystem in focus. This conclusion is further outlined in the sections below. The following text focuses on methylation/demethylation in marine systems, because of the predominance of MeHg from marine foodwebs as the main exposure route in many human populations around the world (see Chapter X in this Report).

6.1.1.1 Methylation in Coastal Waters

Key points: 1) sediments are not always the most important source of MeHg to the estuarine water column; 2) water column methylation occurs in coastal waters; and 3)the factors controlling methylation in coastal environments (e.g. nutrient and carbon loading, redox) are complex.

Much of the earlier work concerning Hg methylation in coastal waters highlighted in the previous Technical Report (AMAP/UNEP 2013) was focused on the factors controlling methylation in the sediments and the flux from sediments to the water column. Overall, the consensus view at that time was that for many environments, sediments were the major source of MeHg to coastal waters, although there were indications that this was not always the case and that inputs from terrestrial watershed and/or from ocean exchange were important in many ecosystems. Nevertheless, the consensus was that any new (*in situ*) production of MeHg within the estuarine and coastal environment was due to the production of MeHg in sediments.

In the last few years, however, a number of studies have challenged this notion, and suggested that MeHg accumulation in coastal/estuarine biota is not exclusively from sediment inputs. Firstly, Chen et al. (2014) found that the concentrations of MeHg in forage fish across multiple estuaries on the US east coast did not track with the MeHg content of the sediments, but with the water column concentration, even though these fish are considered to forage at the sediment-water interface. Conversely, in the same study MeHg in benthic worms did track the sediment MeHg concentrations. Mercury stable isotope analyses also tended to confirm that the sediment may not have been the most important source of MeHg to the organisms in these ecosystems (Kwon et al., 2014). Li et al. (2016) used Hg isotope analyses to demonstrate that the source of MeHg in biota in Lake Melville, a large subarctic fjord, was from pelagic production. Similarly, sulphur (S) isotope analyses of plankton from Long Island Sound (LIS) did not support the idea that the accumulated MeHg had a substantial sediment component (Gosnell et al., 2017).

However, Buckman et al. (2017) showed that within the Delaware estuary, these patterns were more complex and it was less easy to discern the importance of sediment inputs of MeHg compared to riverine inputs. Gosnell et al. (2016) showed that for the Delaware River, sediment could be an important MeHg source at certain times of the year, suggesting that sediment sources should not be completely ignored. Jonsson et al. (2017) showed that it is not just the MeHg loading that was important, but that changes in the concentration of dissolved organic carbon (DOC) can influence MeHg bioaccumulation (see also Balcom et al., 2015, and Gosnell et al., 2016). Comparison of water column and sediment MeHg concentrations show that in some ecosystems, such as the Hudson River, there is a reasonably strong relationship between dissolved water column MeHg and porewater MeHg, and between sediment and suspended particulate MeHg, but there are many ecosystems where there is little correlation.

One important factor, which has received less attention, is the degree to which the MeHg levels are influenced by demethylation of MeHg rather than by its formation. Many studies have assumed that demethylation is not a strong control on MeHg levels in coastal ecosystems but this assumption needs to be tested further. Overall, current literature suggests that there are no clear-cut trends across coastal ecosystems and that both internal and external sources of MeHg are likely important contributors of MeHg to the food chain.

Recent studies have reached contrasting conclusions on the role of nutrient inputs impacting methylation rates in sediments, and MeHg levels is coastal waters and biota. In mesocosm studies, Liem-Nguyen et al. (2016) showed that the addition of nutrients could impact Hg methylation in sediments, and that inorganic Hg input to the water column was more efficiently methylated than Hg injected into sediment, as found in earlier studies (Jonsson et al., 2014), suggesting that the bioavailability of inorganic Hg for methylation may change with time. Oxygen status of the water column is also an important factor in methylation rates, with the consensus being that increased eutrophication leading to oxygen depletion (hypoxia) in bottom waters results in increased MeHg production. A recent example of this process was provided by the modelling of Soerensen et al. (2016) which suggested that increased MeHg in Baltic Sea plankton was associated with increasing eutrophication. However, contrary examples have also been reported recently, with no increase in sediment MeHg levels in some coastal regions with bottom water hypoxia (Chakraborty et al., 2016; Liu et al., 2015). In LIS, in the more eutrophic regions where bottom waters are seasonally hypoxic, plankton had lower MeHg than those from more oligotrophic regions, which was the opposite of the expected pattern (Gosnell et al., 2017). Again, these

11159 results suggest that the interaction between eutrophication and MeHg levels in biota is complex, and
11160 likely to differ in different locations.

11161 Organic carbon (OC) is an additional important factor influencing both Hg methylation as well as MeHg
11162 retention in sediments. Mazrui et al. (2016), for example, found that the binding of Hg to DOC enhanced
11163 methylation compared to Hg bound to particulate (POC) and cinnabar. However, the origins and
11164 geochemical quality of the OC (terrestrial or marine) is at least as important as its quantity in terms of its
11165 effect on Hg bioavailability (Schartup et al., 2015b; Jonsson et al., 2012, 2017). Additionally, it has been
11166 shown in pure cultures and laboratory sediment studies that nanoparticulate Hg has higher
11167 bioavailability for methylation than microparticulate (Mazrui et al., 2016; Zhang et al., 2014). These
11168 studies reinforce the conclusions of prior studies (Schartup et al., 2013; 2014; Jonsson et al., 2012) that
11169 the factors controlling Hg methylation in sediments are extremely complex given the interactions
11170 between Hg (and MeHg) and sediment biogeochemistry (primarily, the levels of OC and reduced
11171 sulphur) which impact binding, bioavailability and sediment-water exchange. While speciation of the Hg
11172 is an important driver, desorption kinetics and microbial community activity are also important controls
11173 over the extent of Hg methylation in sediments.

11174 The weight of evidence for the importance of water column methylation in coastal waters has increased
11175 in recent years. A number of studies have followed up on earlier work in the Thau Lagoon, France
11176 (Monperrus et al., 2007), examining the potential for methylation of Hg within the water column of
11177 coastal environments. A number of other studies have now shown that there is the potential for
11178 methylation in the water column of estuaries and coastal waters, especially in locations of mixing and
11179 flocculation of particulate material (Schartup et al., 2015; Sharif et al., 2016; Ortiz et al., 2015). These
11180 studies point to the likely enhancement of methylation within aggregated particles where micro-anoxic
11181 conditions could exist, as demonstrated by the laboratory experiments of Ortiz et al. (2015). Overall,
11182 these studies do not suggest that Hg methylation is occurring through a different microbial biochemical
11183 pathway, but that it is occurring within the anoxic microzones within large particulates. Some of these
11184 studies have concluded that there is significant net methylation within the water column (Schartup et
11185 al., 2015; Ortiz et al., 2015) while in other cases, the extent of demethylation leads to a net decrease in
11186 MeHg (Sharif et al., 20016).

11187 In conclusion, there is not one specific source for the MeHg accumulating in biota in coastal systems,
11188 and the sources are likely to vary spatially and temporally. In examining, and understanding, the

dynamics of MeHg bioaccumulation in coastal environments it is necessary to examine both the potential external inputs (watershed and ocean inputs), and the internal production within the system (water column and sediment net Hg methylation). Furthermore, it is likely that their relative importance will change in the future due to climate and other human-caused alterations within these ecosystems.

6.1.1.2 Open Ocean Hg methylation

Like coastal seas, there is increasing evidence for active methylation in the oxygenated water column of open oceans. Early pioneering work by Mason and Fitzgerald (Mason et al. 1990) suggested the potential for high rates of *in situ* production of MeHg in the open ocean, however, the prevailing paradigm continued to favour a coastal sediment MeHg source with offshore transport to the open oceans. Since GMA 2013, additional studies have confirmed the suggestion that *in situ* MeHg formation takes place in open ocean waters (Monperrus et al. 2007, Cossa et al. 2009, Sunderland et al. 2009, Heimbürger et al. 2010, Cossa et al. 2011). There is now published evidence for water column methylation from almost all major ocean basins: the Atlantic Ocean (Bowman et al. 2015, Bratkič et al. 2016), Pacific Ocean (Hammerschmidt et al. 2012, Munson et al. 2015, Bowman et al. 2016, Kim et al. 2016), Arctic Ocean (Wang et al. 2012, Heimbürger et al. 2015), Southern Ocean (Gionfriddo et al. 2016), Mediterranean Sea (Cossa et al. 2012), Baltic Sea (Soerensen et al. 2016), and Black Sea (Rosati et al., GBC in review). No data has been published for the Indian Ocean thus far. Laboratory experiments confirm that net Hg methylation can occur in "marine snow" (settling organic particles), with similar rates compared to marine sediments (Ortiz et al. 2015). Furthermore, several papers point out open ocean methylation is required to balance the oceanic MeHg mass budget (Sunderland et al. 2009, Mason et al. 2012, Soerensen et al. 2016).

The relationships observed between MeHg concentrations and apparent oxygen utilization as well as organic carbon remineralization in the oceanic water column indicate that particulate organic matter remineralization controls the methylation of Hg by providing inorganic Hg as the substratum, and by stimulating the activity of methylating bacteria. A pioneering study explored for the first time the carbon isotope composition of the MeHg compound in tuna fish, and found similar $\delta^{13}C$ values to marine algal-derived organic matter, suggesting its role as the carbon substrate for Hg methylation (Masbou et al. 2015). Additional evidence comes from Hg isotopic analysis of marine biota. Fish that forage at different depths in the North Pacific Ocean show Hg isotope gradients that can only be explained if 60-80% of their MeHg is produced below the surface mixed layer and is not from a sediment source (Blum et al. 2013).

In general, the depth, shape and importance of the MeHg peak in ocean waters depend on physical forcing and biological productivity. Several independent studies found methylation hotspots at the density gradients of stratified systems (Wang et al. 2012, Heimbürger et al. 2015, Schartup et al. 2015, Soerensen et al. 2016). Two field studies (Baya et al. 2015, St. Pierre et al. 2015) and a modelling study (Soerensen et al. 2016) suggest important evasion of DMHg from the Arctic Ocean, where MeHg is produced at shallow depths (Heimbürger et al. 2015).

A major breakthrough has been made with the discovery of two key genes, hgcA and hgcB, that control anaerobic Hg methylation in sulphate-reducing bacteria (Parks et al. 2013). The hgcA and hgcB genes were found to be present in many anaerobic microorganisms. An analysis of publicly available microbial metagenomes found the hgcAB genes in nearly all anaerobic environments, but not in aerobic systems (Podar et al. 2015). A marine microaerophilic bacterium has been identified as a potential Hg methylator within sea ice, where anaerobic bacteria which are known to methylate Hg were absent (Gionfriddo et al. 2016). Surprisingly, laboratory experiments have not found a clear relationship between the expression level of the key genes and net MeHg production (Goni-Urriza et al. 2015).

6.2 How and why do Hg levels in aquatic biota respond to changes in atmospheric Hg?

As discussed, there are many processes that may affect the dissolved concentrations and biouptake of MeHg following its formation. Other factors and processes affect the transport and fate of inorganic Hg (GEM and ionic Hg^{II}) between their emission sources and aquatic environments (see earlier chapters of this GMA). The complexity of these processes raises the question of whether Hg emissions, especially those that are regulated under the Minamata Convention, are likely to result in immediate and proportional changes of Hg concentrations in aquatic food-chains. In this section, we review the evidence that atmospheric Hg and biotic Hg levels have changed synchronously in the recent past.

6.2.1 Does Hg in aquatic biota follow the trends in atmospheric Hg emissions and deposition?

Here a number of case studies which examined temporal trends of Hg in aquatic biota are compared against the trends of Hg in atmospheric concentrations and/or deposition fluxes in the same regions. These case studies come from North America, Europe, China and the Arctic; no other regions of the

world are represented in the literature, and are thus not discussed. First, we review the literature concerning the trends of atmospheric Hg from the three study regions.

Trends in Atmospheric Hg Emissions, Concentrations, and Wet Deposition

North America and Europe: North America and Europe are considered together here because their overall atmospheric Hg concentrations and deposition fluxes have trended together over the past few decades (Zhang et al., 2016). Measured near-surface gaseous elemental mercury (GEM) concentrations in North America and Europe have declined by 30–40% between 1990 and 2010 (Slemr et al., 2011; Cole et al., 2014), a pattern that has been matched by trends in wet deposition Hg fluxes (Prestbo et al., 2009; Cole et al., 2014). By contrast, global emission inventories for the same period have suggested flat or slightly increasing total Hg emissions, because declines in Hg emitted by the energy and other industrial sectors in North America and Europe were offset by rising coal-fired power generation in Asia and by emissions from a rapidly-growing global artisanal and small-scale gold mining (ASGM) sector (AMAP 2010; AMAP/UNEP 2013). Recently, however, Zhang et al. (2016) showed that the discrepancy between emission inventories and atmospheric measurements could be resolved mainly by accounting for the declining emissions from commercial Hg-containing products since 1990 which had not been previously counted in the inventories (Horowitz et al., 2014); additional corrections were made for shifts in the speciation of airborne Hg emissions related to air pollution control technology, and by reducing the putative importance of atmospheric Hg emissions from ASGM. Calculated atmospheric Hg concentrations and trends, based on GEOS-CHEM modelling of the revised emission inventories, then agreed within error with observations (Figure 6.1). In North America and Europe, the observed and modelled atmospheric GEM trends since 1990 were –1.5 and –2.0% per year, respectively, and the trends for Hg^{II} fluxes in wet deposition were –1.6 and –1.4% per year, respectively. The agreement between the new corrected emission history by Zhang et al. (2016) and empirical atmospheric data lends confidence that the modelled atmospheric trends presented by Zhang et al. (2016) conform to reality.

The Arctic: For the Arctic region (above 60°N), atmospheric GEM concentrations have also been declining, but at a markedly slower rate than elsewhere (see Figure 6.1). The observed and modelled trend regressions also disagreed more than in other regions, with observed GEM concentrations decreasing at –0.2±0.45% per year since 1994, and the modelled rate at –1.3±0.11% per year. There are no decade-long observational datasets of Hg trends in deposition available for the Arctic or sub-Arctic; existing depositional data are confined to 1-2 years of measurements only (e.g. Sanei et al., 2010).

China: China is the largest national emitter of atmospheric Hg worldwide (Fu et al., 2015b). In contrast to the global trend, anthropogenic Hg emissions in China increased rapidly from 1978 to as recently as 2007 at an average rate of ~5.5% per year, except for 1998-2000 when the emissions decreased due to the Asian financial crisis which led to a reduction in fuel consumption (Wu et al., 2016). Mercury emissions in China are reported to have plateaued around 2007 to 2010, and showed a declining trend in the past few years (Wu et al., 2016).

Available but limited data on atmospheric Hg concentrations in the past decade in China are in general agreement with this emissions trend. Direct measurements of GEM at Guiyang, an urban site in southwest China (Fu and Feng, 2015), revealed that annual mean GEM concentrations increased at a rate of ~2.5% per year between 2002 and 2010 (Fu and Feng, 2015); GEM concentrations also increased at Mt. Changbai, a remote site in north-eastern China, at about the same rate from 2009 to 2013 but then appeared to stabilize (Fu et al., 2015b, 2016; Fig. 6.2). Mercury passive sampling and plant biomonitoring on the Tibetan Plateau suggested that atmospheric Hg concentrations were stable during 2006 to 2009 and decreased during 2010 to 2015 (Tong et al., 2016).

For the purposes of this review, the reported trends in atmospheric Hg concentrations and wet deposition by Zhang et al. (2016) and Wu et al. (2016) are taken as the basis for our comparison with aquatic biota Hg trends over recent decades. The key test of agreement between atmospheric and biotic datasets will be whether the direction of trend (increasing, decreasing, or stable) is the same in both.

Biological Hg Trend Cases Studies

Major recent studies since GMA-2013 on biotic Hg trends over the last few decades are summarized in four case studies below. ***While biotic Hg trends often follow the concurrent pattern in atmospheric Hg concentrations, there is widespread evidence for non-matching trends between them, especially in the past decade.***

Case Study 1: Fish and Birds in Lakes and Coastal Waters of North America

In the Great Lakes, Blukacz-Richards et al. (2016) evaluated the temporal trends since the 1970s of Hg levels in eggs of a piscivorous bird (herring gull - *Larus argentatus*), in two piscivorous fish (trout - *Salvelinus namaycush*, and walleye - *Sander vitreus*), and in a planktivorous fish (rainbow smelt - *Osmerus mordax*). Lipid content in bird eggs and fish tissues, and length of fish, were used as covariates in temporal statistical models. The results present a mixed temporal pattern (Figure 6.3a), with declining biotic Hg trends in all species in the first few decades (up to about 1995–2000), which matched the

declining atmospheric Hg trend in North America (see Figure 6.1), but were followed by trend reversals in most (but not all) species at some sites. In the 2000s, Hg trend reversals occurred for herring gull eggs at two sites in Lake Erie and two sites in Lake Ontario, and for lake trout in Lake Superior and at a single station in Lake Ontario. Mercury levels in lake trout continued to slowly decline at all of the remaining stations, except for Lake Huron, where the levels remained stable. Similar trends were reported by Eagles-Smith et al. (2016) when examining over 96,000 fish muscle samples from 206 species in over 4,200 lakes in western Canada and the USA. They found a significant, rapid decline in length-adjusted tissue Hg concentrations during the 1970s (from 1969 to 1977), with no subsequent significant trend up to 2012. In both of these studies, ***the authors attributed the early decline in biotic Hg to regional declines in atmospheric Hg concentration and deposition. They suggested that the subsequent trend reversal, or lack of a significant trend, could be explained by shifts in trophic dynamics resulting from invasive species, and/or geochemical changes in Hg cycling and methylation rates possibly driven by climate change.***

A more complex temporal pattern in hundreds of small Ontario lakes was reported by Gandhi et al. (2014), who found a general decline in length-adjusted fish muscle Hg concentrations from the 1970s to 1990s for northern pike (*Esox lucius*), walleye and lake trout. This decline was followed by relatively small increases in some lakes starting about 1995–2000. The initial declines in the 1970s and 1980s were more rapid in most lakes than during the 1990s, and were more pronounced in northern Ontario lakes than in southern Ontario lakes at that time. In fact, northern Ontario boreal forest lakes displayed significant overall muscle Hg declines from 1974 up until 2012 for walleye and northern pike, but not for lake trout which were relatively constant over time. In contrast to the Great Lakes studies discussed above, Gandhi et al. (2014) found that southern Ontario lakes displayed non-significant changes between 1974–2012 in walleye, pike and lake trout. Furthermore, the recent increasing trends were also more pronounced in northern Ontario lakes than in southern Ontario lakes which were nearly constant or weakly increasing, and more so in northern pike and walleye than in lake trout.

Different patterns were, however, reported by Tang et al. (2013), which examined changes in muscle Hg in 5 piscivorous fish (walleye, northern pike lake trout, burbot (*Lota lota*), and smallmouth bass (*Micropterus dolomieu*) and 2 benthivorous species (lake whitefish (*Coregonus clupeaformis*) and white sucker (*Catostomus commersonii*)) from 873 Ontario lakes based on data collected from the Ontario Sport Fish Contaminant Monitoring Program. In contrast to the declining patterns in walleye and northern pike in northern Ontario lakes reported by Gandhi et al. (2014), no significant decreases over

recent decades were observed in any of the 7 species in this study; instead, mean concentrations were found to be slightly higher in 2005-2010 than in 1974-1981, and were significantly so in northern pike. The reason for the difference between these two studies is unknown.

Substantial reductions in muscle Hg were reported between 1972–1974 and 2011 in a marine fish species, the bluefish (*Pomatomus saltatrix*), caught off the northeast coast of the USA (Figure 6.3b). Although no data were available for the period 1974 to 1993, it is clear that a ~30–40% decline in bluefish Hg concentrations in New York and New Jersey waters occurred at some period between 1972–1974 and the mid-1990s (Cross et al., 2015). Subsequently, however, the New York regional data suggest no further change in fish Hg levels up to 2007.

Most of the above studies did not include stable C and N isotopic data, making it impossible to investigate whether changes in feeding behaviour (prey trophic level and feeding location) influenced the Hg trends. The value of including trophic dynamic information based on stable C and N isotopic data in the interpretation of Hg temporal trends was clearly demonstrated by Burgess et al. (2013) in a study of Hg in herring gull eggs on the eastern Canadian seaboard. Between 1972 and 2008, two sites displayed a trend of significantly declining egg Hg, which is consistent with the declining atmospheric Hg deposition occurring at that time (see Figure 6.1). However, when trophic level changes over time were factored into the analysis using $\delta^{15}N$ isotope data, it was found that the Hg declines were due to feeding behaviour shifts. $\delta^{15}N$ is a widely-used indictor of the trophic level of species' prey selection, and was highly correlated with egg Hg in the birds. ***The authors concluded that Hg in coastal waters in that region had remained relatively constant over the last few decades despite the reduction in airborne Hg fluxes.***

Case Study 2: Fish in Swedish Lakes

Åkerblom et al. (2014) assessed the Hg temporal trends in 15 species of fish (mainly northern pike, Eurasian perch (*Perca fluviatilis*), and Arctic char (*Salvelinus alpinus*)) during the past 50 years based on almost 45,000 observations from 2881 lakes throughout Sweden. To allow for trend analysis, individual Hg concentrations of fish from any species were normalized to a standard 1-kg pike in the same lake. The average Hg concentrations in such 1-kg pike equivalent fish were found to have increased during the 1970s and peaked at the end of the 1980s before decreasing sharply between 1990 and 1996. During the late1990s, Hg levels increased again and, after peaking by 2003, they appeared to have decreased up to present (Figure 6.4A). Overall Hg levels decreased approximately 1% per year since 1970,

corresponding to a decrease of about 30% over 40 years. ***This trend matches well with the general declining atmospheric Hg trend over Northern Europe*** (see Figure 6.1). Also of note is that fish Hg levels in "limed" lakes across Sweden were consistently higher than in the lakes that were never-limed (Åkerblom et al. 2014), pointing to a significant effect on fish Hg from pH or other indirect ecosystem effects caused by the recovery of the limed ecosystems. However, the mechanism responsible for this pattern was not investigated. The temporal trends in both limed and non-limed lakes were similar.

Further analysis of data from the latest decade (2003–2012; Figure 6.4B) revealed that while there was an overall significant decreasing trend in southwestern Sweden (up to 10% per year), the trends were weaker, mostly not significant, and in a few cases even increasing in northern Sweden. In one lake (Spjutsjön), fish Hg concentrations increased steeply at a rate of about 20% per year. ***The authors noted that the more prominent decrease in fish mercury in the south matches with a larger decrease in atmospheric Hg loads in the south compared to the north of Sweden, and attributed the significant increase in Spjutsjön to possible local anthropogenic sources of Hg.***

Case Study 3: Fish in Reservoirs: North America and Europe vs China

Some of the longest time series of aquatic Hg data exist for man-made reservoirs due to concerns about the effects of impoundment on Hg methylation rates and thus on fish Hg levels. Although these reservoirs are not natural habitats for aquatic life, they contain abundant fish and invertebrate communities, and support important recreational fisheries in some areas and large aquaculture operations in others.

Studies in North America and Europe have shown that following the impoundment, the large influx of flooded vegetation and organic matter in submerged soil stimulates microbial methylation of Hg, resulting in sharp increase in fish Hg due to biomagnification of methylmercury (St. Louis et al. 2004; Hall et al. 2005; Lucotte et al., 1999; Bodaly et al., 2007). Hg methylation rates and hence fish Hg levels typically decrease as the reservoir ages and the organic matter further decomposes (Bodaly et al., 2007). This was clearly demonstrated in a recent analysis of the temporal trends of Hg in a range of fish species from 883 reservoirs across western North America (Willacker et al. 2016). Temporal patterns (normalized for confounding variables such as species and body length) were clearly related to the time elapsed since reservoir impoundment, with maximum fish Hg concentrations being reached on average three years after the impoundment (Figure 6.5). Fish Hg levels thereafter declined relatively rapidly for 4–12 years, followed by a monotonic slow decline that last many decades. Because the reservoirs were

built at different dates over the last century and a half, it may be concluded that the fish Hg pattern is not related to changing atmospheric Hg deposition over the last few decades. Instead, water storage management is shown to be a key factor influencing this temporal pattern. Fish in reservoirs that experienced maximum drawdown during summer months (May–July) exhibited significantly (up to 11-fold) higher concentrations than fish in reservoirs in which drawdown occurred during other times of the year (Willacker et al., 2016).

Reservoirs in China, however, present a different story. Different from reservoirs in North America and Europe which are typically inhabited by native fish populations used for recreational purposes, reservoirs in much of China support important aquaculture activities with fish harvested for human consumption. The fish in Chinese reservoirs thus tend to grow faster and be harvested while young. Therefore, the Hg concentrations in fish from these reservoirs are typically low due to biodilution. Unfortunately, monitoring of fish Hg concentrations in most of the Chinese reservoirs only started recently, making it impossible to deduct long-term temporal trends. One exception to this is the reservoirs in the Wujiang Basin in southwest China, where extensive studies have been carried out in the past decade. Since these reservoirs vary greatly in their ages (time since their initial impoundment), an interesting evolution scheme in fish Hg concentrations starts to emerge when the data from all the reservoirs are pooled together.

The Wujiang (Wu River) is the largest tributary of the upper Changjiang (Yangtze River). Since the 1960s, numerous large cascade reservoirs have been or are being constructed in the Wujiang Basin, including Wujiangdu (built in 1979), Dongfeng (1994), Puding (1994), Yingzidu (2003), Suofengying (2003), Hongjiadu (2004), and Pengshui (2008) on the main stream, and Aha (1960), Baihua (1966), and Hongfeng (1966) on its tributaries (Figure 6.6). Although impoundment was found to have significantly increased fish Hg concentrations in a newly constructed reservoir (Pengshui) (Li et al., 2013), fish Hg concentrations in this and another newly constructed reservoir (Hongjiadu) (Yao et al., 2011) were much lower than those in newly built reservoirs in North America and Europe (Yao et al., 2011; Li et al., 2013). For the much older Baihua Reservoir, no statistically significant differences were observed in Hg concentrations in common carp (*Cyprinidae*) among the four sampling campaigns from 2003 to 2011, more than 40 years after the impoundment (Liu et al., 2012). In general, Hg concentrations in various fish species studied, including carnivorous, omnivorous, planktivorous, and herbivorous fish, are remarkably low in all these reservoirs regardless of the age of the reservoir (Yao et al., 2011; Li et al.,

2009; Yan et al. 2010; Liu et al. 2012; Li et al., 2013), often an order of magnitude lower than the World Health Organization (WHO) guideline of 0.5 μg/g (wet weight) (WHO, 1990).

While biodilution and simple (short) food web structures clearly contribute to the generally low fish Hg concentrations (Yao et al., 2011; Meng et al., 2010, 2016; Feng et al., 2009a, 2009b; Larssen, 2010; Liu et al., 2012; Yan et al., 2010), comparisons of fish Hg concentrations in reservoirs with different ages in the same basin reveal three distinct stages of evolution due to changes in the source and concentration of organic matter in the submerged soil/sediment as the reservoir ages and cage aquaculture activities increase (Figure 6.7). As much of the Wujiang Basin is located in a karst environment, the organic matter contents in the submersed soils (typical range: 1.9 – 4.1%) are much lower than those in submersed soil (typically 30 – 50%) from the boreal forest or wetlands in North America and Europe (Yao et al., 2011; St. Louis et al. 2004; Hall et al. 2005; Lucotte et al. 1999). In addition, the water was lightly alkaline in most of the reservoir water as the result of the karstic geology of the Wujiang River, which could restrain the Hg methylation (Meng et al., 2010; Yao et al., 2011). Primary productivity in the newly constructed reservoirs in the Wujiang Basin is also low (oligotrophic–mesotrophic) due to the absence of cage aquaculture fishing (Yao et al., 2011; Meng et al., 2010, 2016), and thus autochthonous contribution to organic matter is also very limited (Jiang 2005; Yao et al., 2011). Therefore, in contrast to their counterparts in Europe and North America, the newly constructed reservoirs in the Wujiang Basin are not active sites of net Hg methylation due to the low organic carbon content in the submersed soils and/or low primary productivity (Yao et al., 2011; Meng et al., 2010). Consequently, the newly constructed reservoirs, such as Suofengying, Hongjiadu, and Yingzidu in the Wujiang River, are not a net source of MeHg and instead represent a net sink (Guo, 2008) (Figure 6.7a).

As these reservoirs become more productive (mesotrophic to eutrophic) with time, the organic matter content in the sediment increased due to continuous increases in autochthonous productivity due to the cage aquaculture activities. This would tend to promote in-situ Hg methylation, and as such reservoirs at this stage (e.g., Dongfeng and Puding) have transited from a net MeHg sink to MeHg source (Guo, 2008; Feng et al., 2009a,b; Zhang et al., 2009) (Figure 6.7B).Over the long-term evolution of the reservoir, primary productivity continues to increase and the reservoir will eventually become eutrophic. Phytoplankton-derived organic matter, and the fish feed and faeces, become significant sources of organic matter input to the surface sediments, as shown in Wujingdu (Meng et al., 2010, 2016; Zhang et al., 2009; Feng et al., 2009a). The increased oxygen consumption during fresh organic matter degradation causes progressively more anoxic conditions at the sediment-water interface (Meng et al.,

2010, 2016), which promotes microbial Hg methylation processes (Figure 6.7C), as shown in Wujingdu (Guo, 2008) where both the surface sediment and the hypolimnetic water are sites of net MeHg production (Meng et al., 2010, 2016; Feng et al., 2009a). Thus, in contrast to fish in North American reservoirs, and in spite of the relatively high atmospheric Hg loading across much of China, fish Hg levels in Chinese impoundments reflect within-impoundment processes, especially organic matter loadings to sediments, water/soil quality, food web structure, and biodilution, rather than atmospheric inputs.

Case Study 4: The Arctic

Rigét et al. (2011) summarized all available temporal Hg datasets on Arctic biota up to about 2009, and found that some species in some locations had shown significant increases over recent decades, whereas others with closely adjacent or overlapping distributions exhibited non- significant changes. Most of the increasing biotic Hg trends occurred in marine species in the North American and west Greenland sector of the Arctic, whereas declining trends were mostly observed in east Greenland and European Arctic biota. This regional dichotomy is clearly seen in the hair of polar bears (*Urus maritimus*), and has been suggested to be due to increased emissions from Asia entering the western Arctic coincident with decreasing emissions from North America and Europe in the eastern Arctic (Dietz et al., 2006).

A few additional studies have been published since then. Rigét et al. (2012) analysed temporal trends of Hg in livers of ringed seals collected from the early 1980s to 2010 from Greenland. Increasing levels of Hg were found in ringed seals in two out of three Greenlandic seal populations (Central East and Northwest Greenland), rising at a rate of 10.3% per year and 2% per year, respectively. In addition to age and trophic positions, the study showed that the Atlantic Oscillation Index, a parameter related to climate change, was positively associated with Hg concentrations in seals although the specific mechanism involved was not clear.

By analysing Hg in the teeth of polar bear from Svalbard in the Norwegian Arctic, Aubail et al. (2012) reported a decreasing trend in Hg concentrations over the period 1964–2003 (Fig. 6.8A). Since no temporal changes were found in tooth $\delta^{15}N$ and $\delta^{13}C$, they concluded that the decrease of Hg was not due to changes in trophic dynamics; instead, it was more likely due to a lower environmental Hg exposure in the region. McKinney et al. (2017) also reported a significant declining trend in hair Hg of the southern Beaufort Sea (SBS) polar bear population, at an average rate of -13% per year, between 2004 and 2011. This dataset differs from the general west-east pattern in Arctic biota Hg trends noted

above. However, only males in the SBS area exhibited significant decreases; females from the same area showed no significant trend. Mercury levels in the bears' main prey (ringed seal) also did not change up to 2007 (Gaden et al., 2009), which argues against changes in Hg inputs or the biogeochemical Hg cycle as contributing to the decline. Analyses of body condition and diet led to the conclusion that the bears' Hg trend was due to changing foraging patterns over time and not to alteration in environmental Hg levels (McKinney et al., 2017).

Braune et al. (2014) reported the temporal trend of Hg in thick-billed murre (*Uria lomvia*) eggs from Coats Island, northern Hudson Bay, and Prince Leopold Island in Lancaster Sound, Nunvut. Although there was no significant change in Hg concentrations in murre eggs from Coats Island from 1993 to 2013, $\delta^{15}N$ values for the eggs were found to be decreasingly significantly, suggesting a decline in trophic position for the bird due to the switch of its diet from Arctic cod to capelin. After adjusting egg Hg concentrations for the decline in trophic position, time trends in Hg concentrations at Coats Island changed from non-significant to significantly increasing. In contrast, at Prince Leopold Island, after adjustment for trophic position the egg Hg time trends changed from nonsignificant to significantly decreasing over the same period. These results suggest that in addition to trophic change in diet, there may have been other geographic factors at play that influenced Hg concentrations at the base of the marine food web, such as differences in Hg deposition, or in Hg bioavailability related to climate change.

Subsequently, Braune et al. (2016) updated the Hg trends in High Arctic seabird eggs at Prince Leopold Island to 2014 for five species: thick-billed murres, northern fulmars (*Fulmarus glacialis*), black-legged kittiwakes (*Rissa tridactyla*), black guillemots (*Cepphus grylle*), and glaucous gull (*Larus hyperboreus*). The first three species' eggs had been collected from the Island as early as 1975, while the guillemots and gulls were sampled from 1993 to 2013. Egg Hg trends were adjusted for possible shifts in tropic position of the birds using $\delta^{15}N$ data. Adjusted Hg concentrations in eggs of murres, fulmars and kittiwakes increased from 1975 to the 1990s, followed by a plateauing or slight decline of levels from the 1990s to 2014 (Figure 6.8B). However, the kittiwake trend was strongly influenced by the 1975 samples; when these were excluded, kittiwake eggs actually displayed a significant decreasing trend from 1976 to 2013. Trends in the eggs of murres, fulmars, kittiwakes, and guillemots had negative slopes between 1993 and 2013. The pattern in glaucous gull eggs was unique: decreasing by 50% from 1993 to 2003 before starting to increase again.

Braune et al. (2016) concluded that the general increasing trends in egg Hg during the 1970s and 1980s were consistent with atmospheric Hg increases over the Arctic *during that period.* They noted that the migratory habits of the five bird species, which overwinter in different southern regions away from Lancaster Sound, complicated interpretation of the reasons for the temporal trends. Environmental Hg changes in their wintering areas could have been different to those in the Arctic. Interpretation is also complicated by significant differences in the findings from glacier archives of atmospheric Hg on the western and eastern edges of the North American Arctic. Greenland glacial snow/firn (Faïn et al., 2009) showed a monotonic decline in atmospheric GEM concentrations during the 1970s and 1980s, following peak levels in the 1950s to 1960s. Glacial snow and ice core reconstructions of atmospheric Hg deposition from Mt. Logan (Yukon) showed increases in deposition through the 1990s, which could be an indication of increasing trans-Pacific contamination from Asia (Beal et al., 2015). Overall, these data, especially the declining GEM trend on Greenland through the 1970s and 1980s, are inconsistent with Braune et al.'s (2016) conclusions. However, the flat or slightly declining egg Hg data from about 1990 onwards is consistent with the recent remodelling of atmospheric GEM in the Arctic (see Fig. 6.1). Zheng (2015), on the other hand, reported that 20th century total Hg accumulation in a Greenland ice core was relatively constant until it increased during the 1970s to 2000s, a pattern similar to those in most of the bird species but not in agreement with the Zhang et al. (2016) modelling. Thus, uncertainty about the actual trends in Arctic atmospheric Hg deposition is a limiting factor in assessing agreement between environmental and biological Hg trends in this region.

In Great Slave Lake in the western Canadian Arctic, temporal trends of Hg in lake trout, burbot, and northern pike were monitored irregularly between the late 1980s or early 1990s and 2012 (Evans et al., 2013; Fig. 6.8C). Muscle Hg data were adjusted for fish length, but not for trophic shifts over time. Mercury concentrations generally increased over time in lake trout and burbot, but not in northern pike, with considerable inter-annual variation. These increasing or flat patterns are inconsistent with atmospheric GEM concentrations and wet deposition fluxes that were declining at the time (see Figure 6.1), and with the Mt. Logan atmospheric deposition record of Beal et al. (2015). Statistical analysis of climate factors suggested that varying annual mean air temperatures, and particularly cold season temperatures, were related to the fish Hg patterns although a precise mechanism linking temperature to fish Hg could not be elucidated (Evans et al., 2013).

6.2.2. What Causes Decoupling between Aquatic Biota and Atmospheric Hg Trends?

In contrast to the recent decadal datasets described above, the available century-scale biotic Hg trends (from the Arctic; Dietz et al., 2009) generally matched remote glacial ice core archives of atmospheric Hg deposition and GEM concentrations (Zheng, 2015; Beal et al., 2015; Kang et al., 2016). In both cases, starting about the late-19th century, shortly after major anthropogenic uses and emissions of Hg became more common, Hg concentrations in the atmosphere and in aquatic biota increased steadily up to about the 1970s to 80s. Subsequently, as atmospheric and biological monitoring became more widespread and frequent, it became increasingly apparent that decoupling between the aquatic biotic and atmospheric Hg trends has been occurring in some areas and in some species within specific areas, especially in the past decade. Fundamentally, this decoupling can be generally attributed to the exceptional sensitivity of the Hg biogeochemical cycling to changes in climatic (e.g., temperature, light, hydrology), geochemical (e.g., pH, redox status, complexing ligands), biological (e.g., feeding behaviour of an organism) and ecological (e.g., organic carbon flux, microbial processes, and food web structure and dynamics) conditions (Table 6.1). Some of the major processes that trigger changes in these conditions and thus the decoupling between biotic and environmental Hg include:

Landscape changes: Major changes in landscape, such as flooding, damming, and deforestation, not only increase Hg flux from the terrestrial system to the aquatic system, but more importantly they change the organic carbon flux and redox conditions that directly control the Hg methylation process and mobilize Hg stored in soil organic matter This process is clearly demonstrated by the construction of reservoirs where biotic Hg concentrations are almost exclusively controlled by organic carbon dynamics and bear no relationship with Hg trends in the atmosphere (see Case Study 3).

Ecosystem changes: As methylmercury biomagnifies in the food web (i.e., methylmercury concentration increases from prey to predator), any changes in ecosystem structure, function and dynamics would result in major changes in Hg concentrations within the ecosystem. Processes such as acidification (Case Study 2) and eutrophication (see Case Study 3) affect not only methylmercury production by altering Hg speciation and bioavailability, but also Hg food-chain transfer and thus biotic Hg concentrations by altering species composition, biomass and growth rates (e.g., Clayton et al., 2013; Jardin et al., 2013). Aquaculture, overfishing, and invasion of non-native species can change not only the nutrient status of an aquatic ecosystem, but also change directly the structure, function, and dynamics of food webs, and thus could result in major changes in biotic Hg.

Climate change: On the global scale, climate change is the most prevalent contributor to the decoupling between biotic and environmental Hg. The impact of climate change on biotic Hg is perhaps most profoundly felt in the Arctic, where rapid climate warming has resulted in dramatic changes in many biogeochemical and ecological processes that drive Hg cycling (Wang et al., 2010; Stern et al., 2012). For instance, the rapid decline in the aerial coverage and thickness of Arctic sea ice and the replacement of multi-year sea ice with first-year ice have been shown to influence Hg distribution and transport across the ocean–sea ice–atmosphere interface, alter Hg methylation and demethylation rates, promote changes in primary productivity, and shift food web structures (bottom-up processes). In addition, changes in animal social behaviour associated with changing sea-ice regimes can affect dietary exposure to Hg (top-down processes) (Stern et al. 2012). As shown in Case Study 4, thick-billed murre from Coats Island in northern Hudson Bay has been shown to have moved down in its trophic position in the food web, presumably due to feeding increasingly on capelin instead of Arctic cod (Braune et al., 2014). However, the population's egg Hg concentrations did not change significantly from 1993 to 2013; thus, to explain this stable trend the availability of methylmercury in the environment and efficiency of Hg food web transfer must have increased. It has also been suggested that climate warming may cause a shift in energy flow from benthic to pelagic food webs as aquatic productivity increases in High Arctic lakes. Since zooplankton species such as Daphnia contain higher methylmercury than benthic organisms, this shift could increase Hg transfer in the food web (Chetelat and Amyot, 2008). The impact of climate change on biotic Hg has also been observed in lower latitude regions (e.g., Pinkney et al., 2014).

6.2.3. What are the implications for the Minamata Convention?

Recent reports about widespread biotic Hg trends not following the atmospheric Hg trends is not discouraging news when it comes to implementation of the Minamata Convention. The fact that the effectiveness of Hg emission control is expected to be followed by long delays before an ensuing reduction is seen in food-web Hg levels makes it all the more pressing to control and reduce mercury emissions as early as possible (Wang et al. 2010).

Wang et al. (2010) and Wang and Zhang (2013) proposed that the decoupling between biotic and environmental Hg is an indication that an aquatic ecosystem has entered a new "paradigm" in which the key controls on Hg bioaccumulation have switched from being "emissions-driven" to "processes-driven" (Figure 6.9). This switch occurs because the level of Hg in an aquatic ecosystem is determined not only by Hg influx (natural or anthropogenic) to the system, but also by the processes in the ecosystem that control the recycling, speciation, bioavailability, methylation and biological uptake of Hg. As the

accumulated mass of Hg in a water body becomes large enough relative to the emission-driven loading rate, the internal biogeochemical processes that control its permanent removal (e.g., burial), re-emission, or uptake into the biosphere would increasingly become the determining steps in bioaccumulation.

The changing relationship over time between atmospheric Hg concentrations or deposition, and biotic Hg, is shown in Figure 6.9. During the Holocene, when Hg emissions were at their natural level, the flux of Hg to the aquatic system was generally low, and so were its biotic concentrations (Phase I – "Holocene background"). At the onset of the Anthropocene in the 19th century, however, as industrialization resulted in a sharp increase in anthropogenic Hg emissions, aquatic biota Hg concentrations responded rapidly due to increasing Hg deposition, exposure and uptake of Hg from a small but growing environmental Hg inventory (Phase II – "Emissions-driven"). Once an aquatic ecosystem has accumulated sufficient Hg, additional increases in Hg influx become secondary to the amount that has been stored in the system accumulated by years of loading ("legacy" Hg). Bioaccumulation then draws predominantly on this "legacy" Hg, which is operated on by the internal biogeochemical processes (Phase III –"Internal Processes-driven"). Throughout all these three phases, biogeochemical processes (shown as sine-wave ''noise" in Figure 6.9) determines the transport of Hg from the abiotic part of the ecosystem to biota, but it is in Phase III that these processes emerge to create a variability that is large enough to obscure the external Hg emission trends, and hence the mismatch between biotic and atmospheric Hg trends (Wang et al., 2010).

In the context of the Minamata Convention to control Hg emissions, a new phase, Phase IV, can be envisioned (see Figure 6.9). As anthropogenic Hg emissions decrease, atmospheric Hg concentrations will decrease and eventually stabilize at a new steady state. However, recycling of the large quantities of legacy anthropogenic Hg presently contained in the world's oceans and soils, and revolatilization between oceans, soils and the atmosphere, means that atmospheric and aquatic Hg concentrations are likely to decrease much more slowly than changes in current emissions (see Chapter 1.2). While biotic Hg concentrations are also projected to decrease over the long term, the current phase of "processes-driven" bioaccumulation dictates that it will take much longer to establish a new steady-state in biotic Hg. The biotic Hg concentrations at the new steady-state are also likely to remain above the Holocene background levels. In the shorter term, however, aquatic biotic Hg concentrations, especially in marine ecosystems, are likely to continue to increase despite recent emission controls (Sunderland and Selin,

2013). Biota in smaller waterbodies such as lakes and coastal marine systems with restricted water mass turnover are more likely to respond relatively rapidly to emissions controls.

Examples of this long and "bumpy" recovery in biotic Hg can be found following the impoundment of a river, or following "de-acidification" of a lake. As shown in Case Study 2, fish Hg in reservoirs decreases a few years after the impoundment, but remains above the pre-impoundment level even after more than a century (see Figure 6.5). In the 1970s, liming was applied to many Swedish lakes that were acidified due to atmospheric acid deposition to help restore the lake ecosystem. Following the liming, fish Hg in those lakes declined 10-20% by the 1990s (Meili, 1995) and continued to decline to the present day (Åkerblom et al., 2014). Yet, more than 30 years after the liming, fish Hg concentrations in these lakes remained considerably higher (twice as high on average) than those in lakes that were not impacted by acidification (and not subjected to liming) (Åkerblom et al., 2014) (see Figure 6.4a).

Therefore, as anthropogenic Hg emissions are being placed under control due to the Minamata Convention, research and management emphasis should focus on the fate and effect of legacy Hg that is already stored in environmental reservoirs, and on the factors and processes that affect the recovery time of biotic Hg. Given the long and bumpy recovery road ahead, effective remediation and adaptation strategies are needed to assist the local communities that facing Hg contamination in their ecosystems and food sources.

11659 **Table 6.1** Unique properties of mercury and implications for its biogeochemistry (Wang and Zhang, 2013)

Property	Implications
Redox between Hg(0) and Hg(II)	Sensitive to changes in pe and pH; Sensitive to photochemical and microbial processes.
High vapor pressure of Hg(0)	Sensitive to changes in temperature; Long range atmospheric transport; A global problem needing global solutions.
Hg^{2+} ions being one of the softest Lewis acids	Strong affinity to ligands (e.g., reduced sulphides, halogens); Sensitive to changes in organic carbon.
Methylation is primarily microbial, with MeHg being the most bioavailable and toxic	Sensitive to changes in organic carbon, nutrients, redox and microbial processes; Direct source control of MeHg difficult.
MeHg biomagnifies in the food chain	Sensitive to changes in food web structure and dynamics.

11660

11661

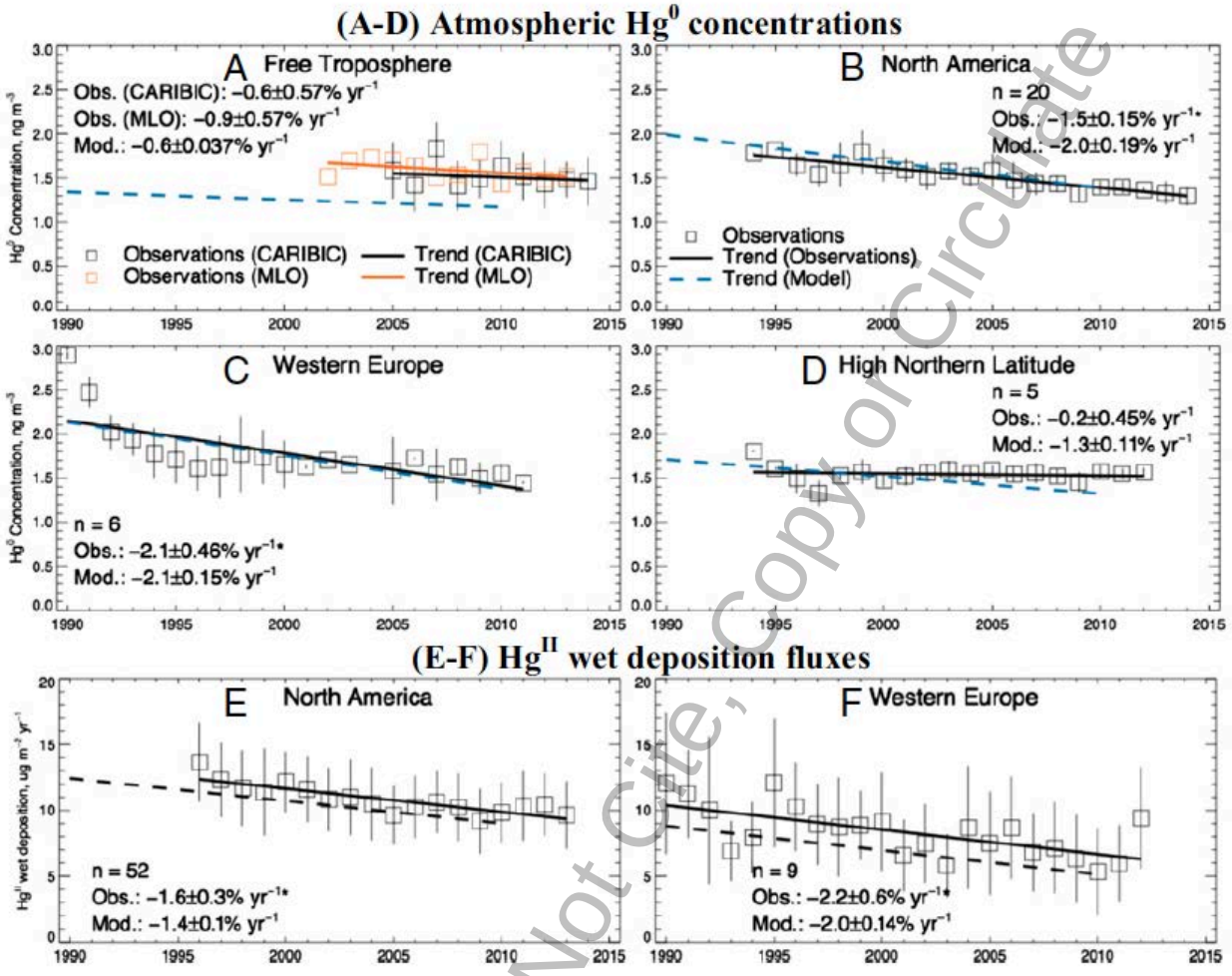

Figure 6.1. Observed and modelled trends for 1990 to 2013 in atmospheric Hg(0) concentrations (**A-D**) and Hg (II) wet deposition fluxes (**E** and **F**) in different regions of the northern hemisphere.Observations for individual years are shown as squares with linear regression as solid line. The dashed line is the trend from the GEOS-CHEMsimulation using the revised anthropogenic emissions inventory for 1990 and 2010. The data are averaged regionally across for the free troposphere (**A**), North America (**B**and **E**), Western Europe (**C** and **F**), and high northern latitude regions (**D**) (vertical bars show the SDs).Regression coefficients (slope ± SE) and number of sites (**n**) are given (**Insets**). From Zhang et al. (2016)

N.B., All captions will be recast, and figures redrawn by UNEP copy editors and graphic designers.

11674

11675

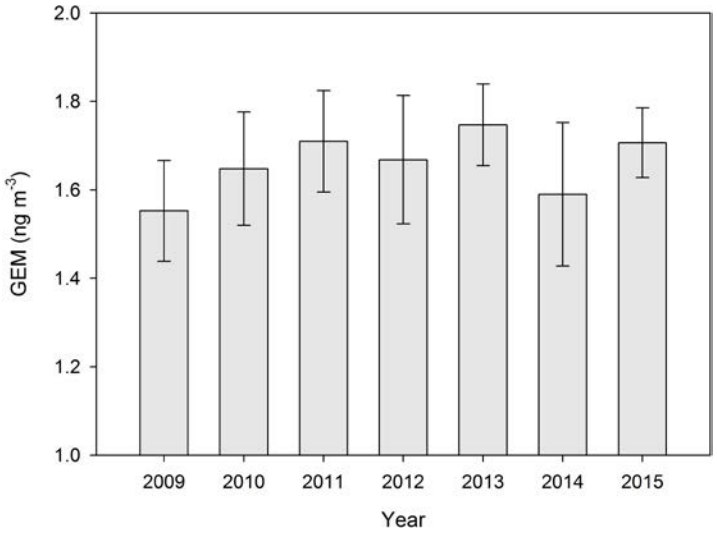

11676

11677

11678 **Figure 6.2**. Annual mean gaseous elemental mercury concentrations measured at Mt. Changbai in

11679 northeastern China (Fu et al. 2015b)

11680 A

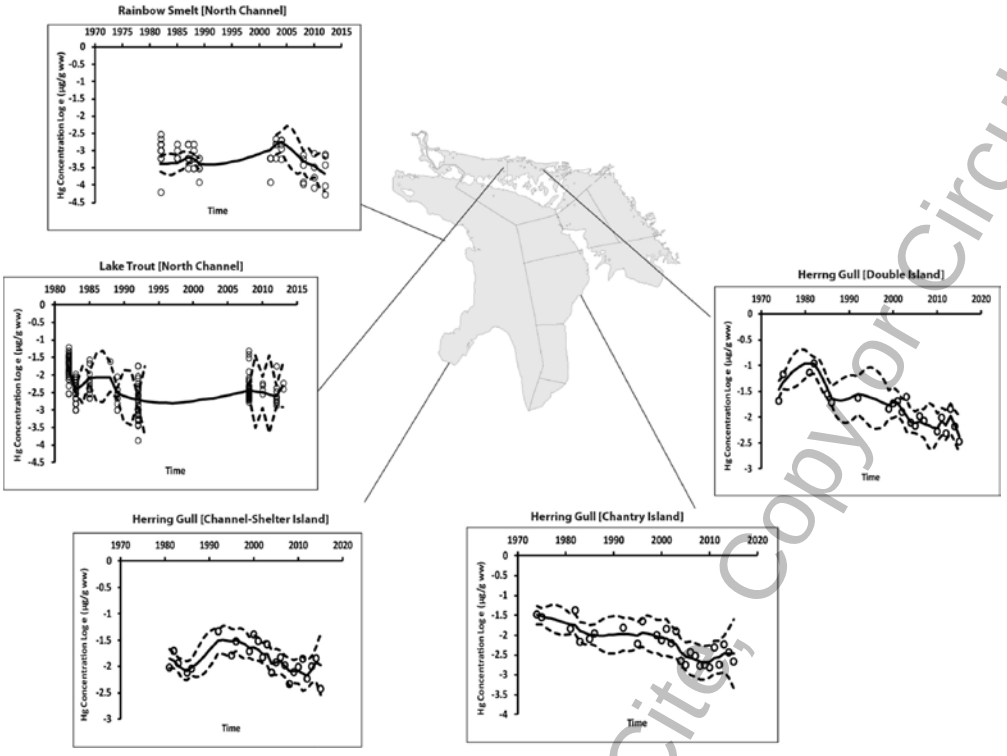

11681

11682

11683 B

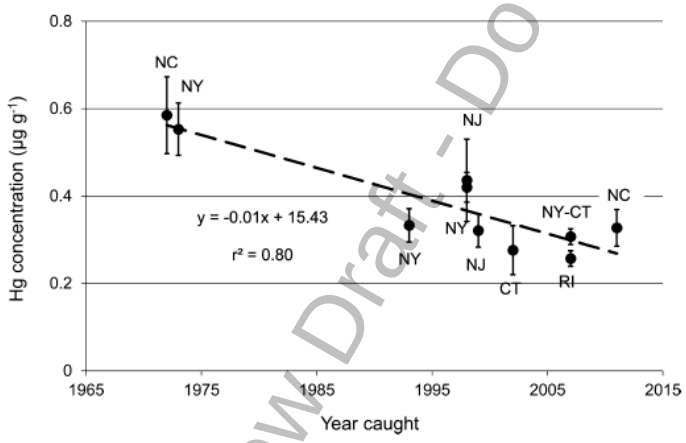

11684

11685 Figure 6.3. Mercury trends in fish and waterfowl of North America. A) Hg concentrations (Ln-

11686 transformed mg/g wet weight for Herring Gulls, Lake Trout and Rainbow Smelt) in Lake Huron. The

11687 solid and dashed lines correspond to the median and the 95% credible intervals of the predicted mercury
11688 concentrations (Blukacz-Richards et al. 2016). B) Mean and two SEM of the estimated mercury
11689 concentrations for bluefish from 1972 to 2011 (Cross et al. (2015). NC = North Carolina; NY = New
11690 York; NJ = New Jersey; CT = Connecticutt; RI = Rhode Island.

11691

11692 NOTE TO GRAPHICS: draw a basemap of North America and then show each of these (and perhaps
11693 others cited in the text) as an inset

11694

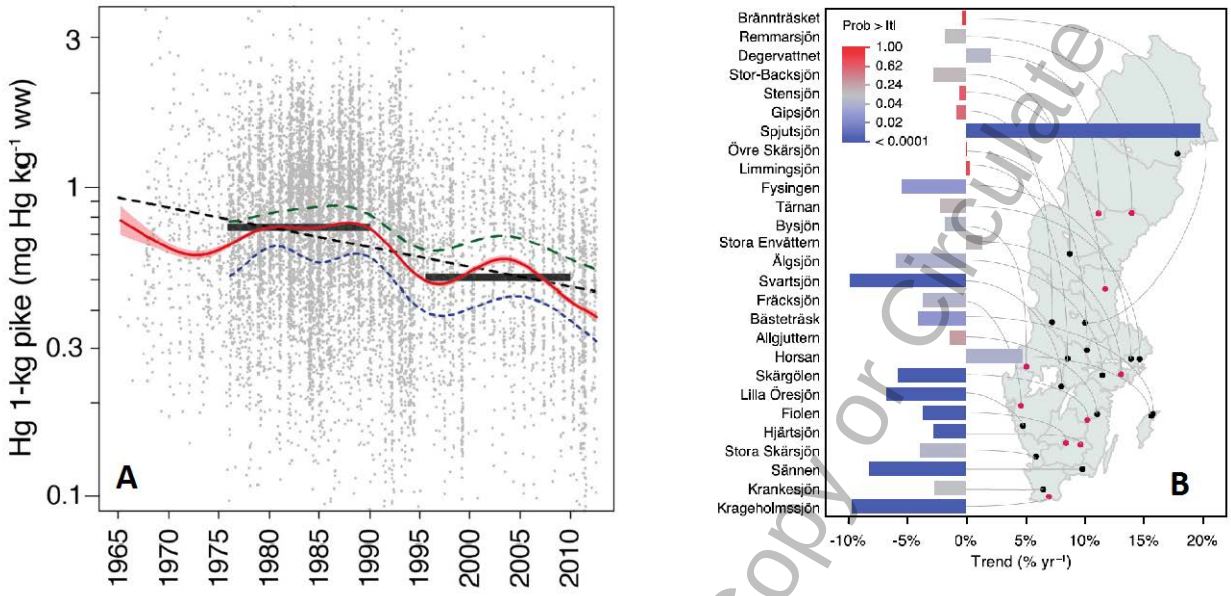

11695

11696

11697 **Figure 6.4.** Total Hg concentrations in Swedish fish 1965–2012. A) Normalized (1-kg pike) Hg
11698 concentrations of 10,176 catches; each point represents the mean from a single date and site. A linear
11699 regression model (black dashed line) and a generalized additive model (GAM; red line ± SE) were
11700 applied to all data to visualize temporal patterns. The parallel dashed lines are separate GAMs fitted either
11701 to limed lakes (upper green dashed line) or to never-limed lakes (lower blue dashed line). The black step
11702 lines indicate the geometric mean Hg concentrations between 1976–1990 (0.74 mg kg^{-1} ww) and1996–
11703 2010 (0.52 mg kg^{-1} ww). B) Recent trends of total ww Hg concentrations in medium-sized perch (total
11704 length 140–220 mm) from 27 national monitoring lakes during the period 2003 (red dots) or
11705 2005/2006/2007 (black dots) to 2012. Trends were estimated by linear regression on log-transformed Hg
11706 concentration normalized site specifically for fish age and body length. The bar colour represents the
11707 probability of individual trends being equal to zero (t test). Blue bars highly significant, red bars not
11708 significant. From Åkerblom et al. (2014).

11709

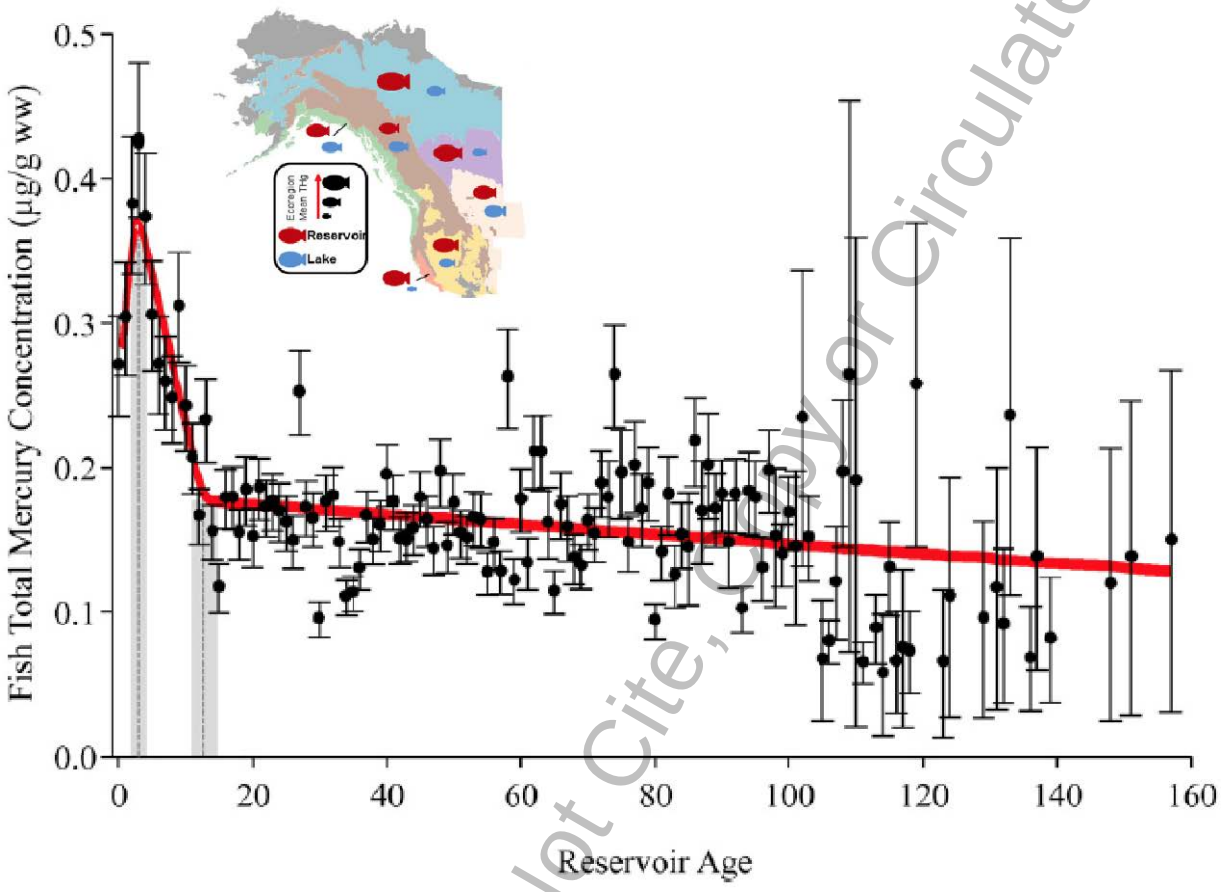

Figure 6.5. Fish tissue Hg trends from reservoirs across western North America. The data show least squares mean total mercury concentrations (µg/g ww±standard error) in size-standardized fish. Least squares mean account for the effects of ecoregion, waterbody, species, and sampling year. Vertical grey dashed lines and shaded regions indicate estimated breakpoints (±standard error) from segmented linear regression (solid line) on fish mercury concentration when accounting for the effects of ecoregion, waterbody, species, and sampling year. (From Willacker et al 2016). NOTE TO GRAPHICS: REMOVE RED LINE DURIGN REDRAW.

11722

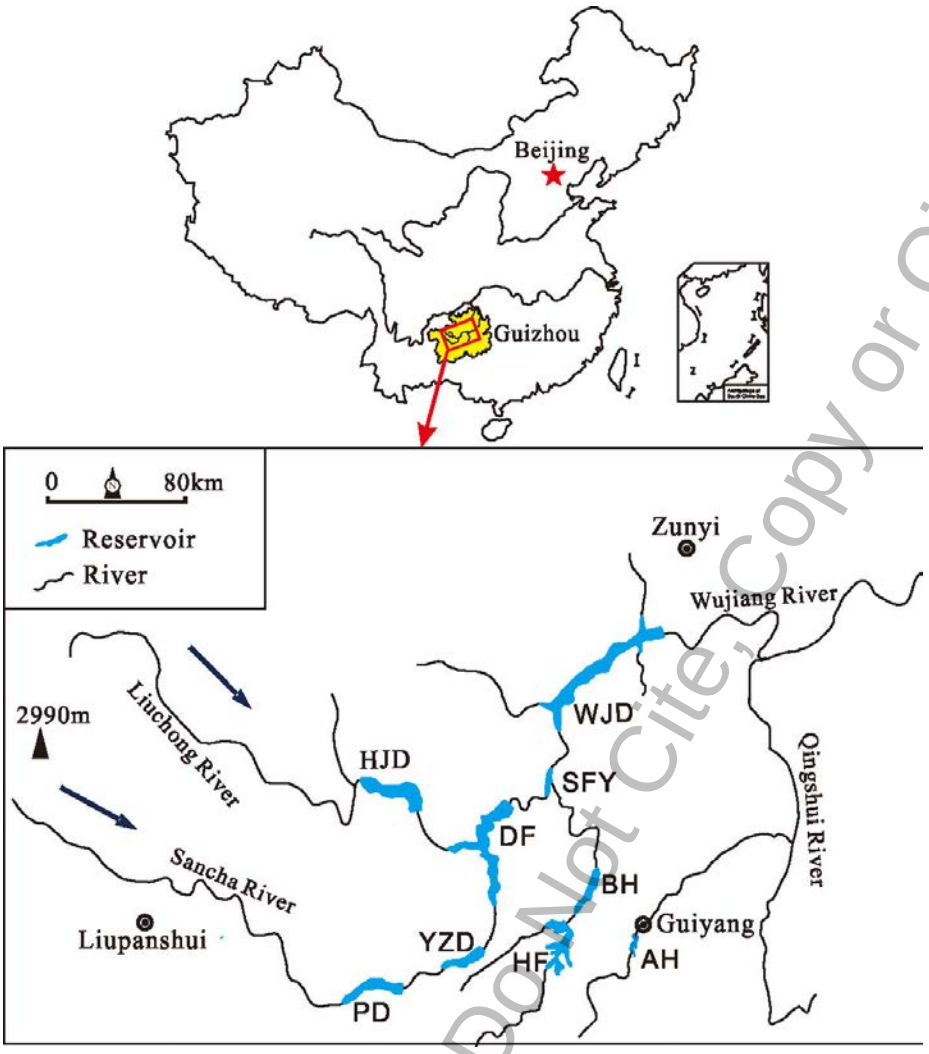

11723

11724

11725 Figure 6.6. Reservoirs along the Wujiang River

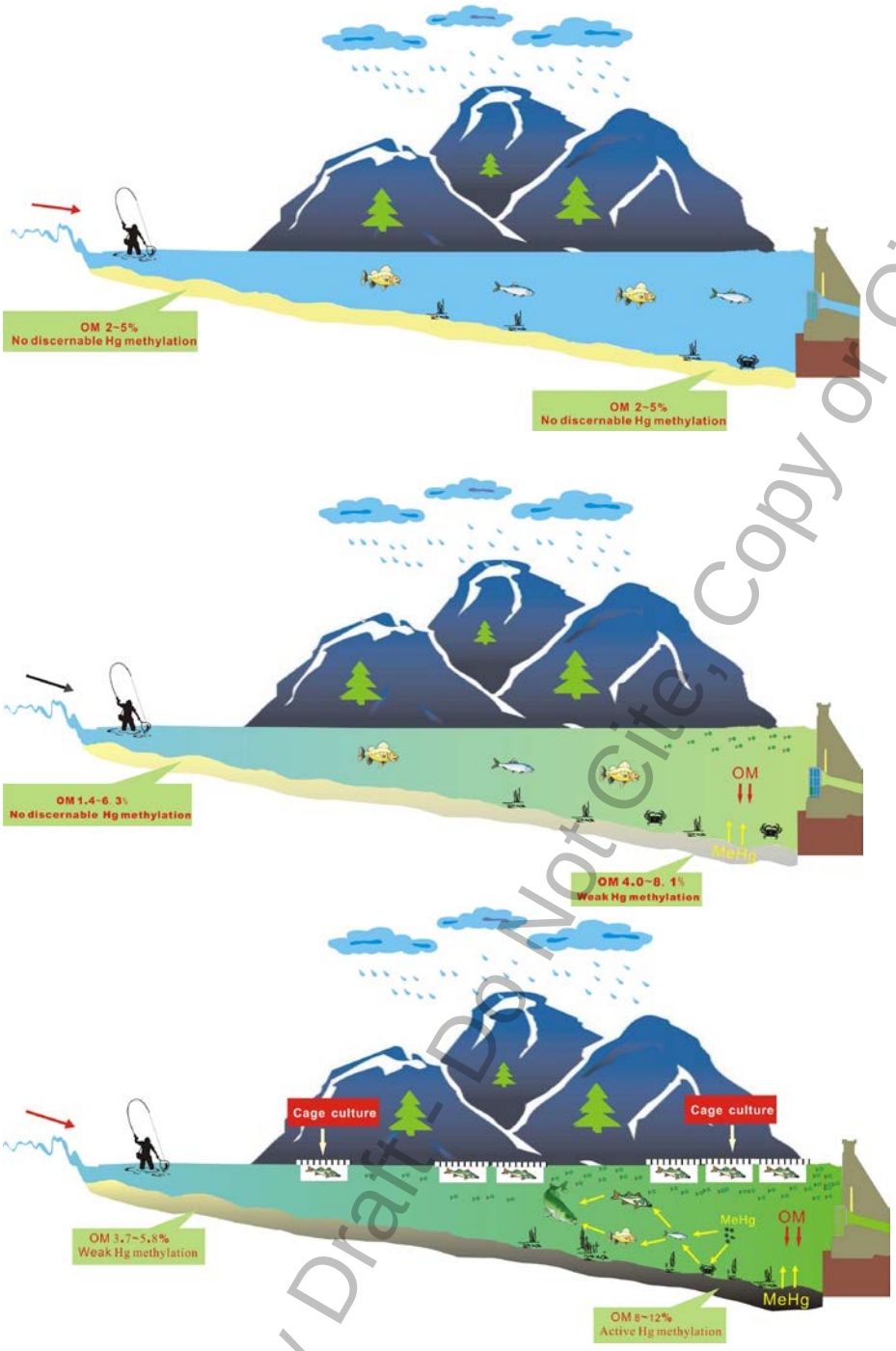

11726

11727

11728

11729 Figure 6.7. Conceptual models of the Hg cycling in A) primary, B) intermediate, and C) advanced

11730 evolutionary stage reservoirs in the Wujiang River Basin, Southwest China

11731 A

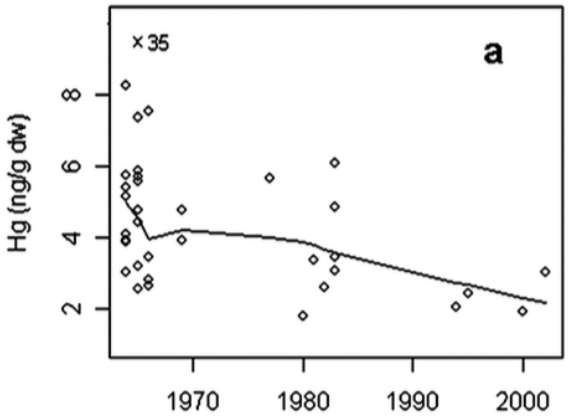

11732

11733 B

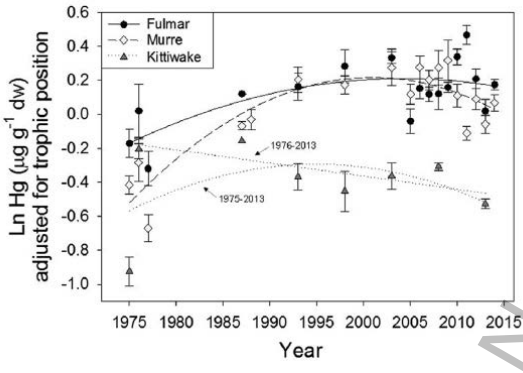

11734

11735 C

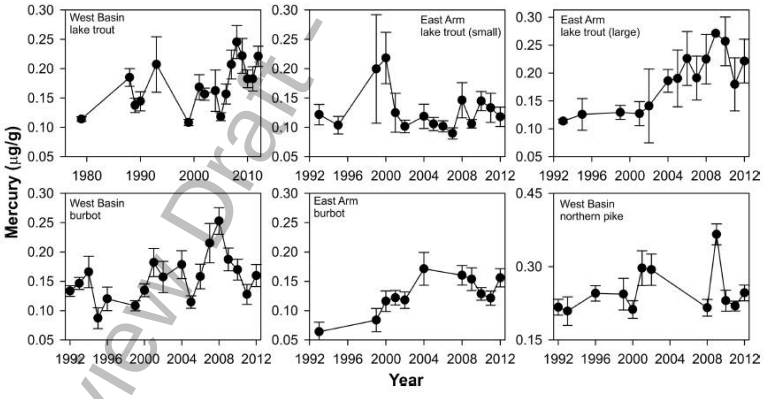

11736

11737 Figure 6.8. Mercury trends in the Arctic. A) Year vs. dental Hg concentrations (ng/g dw) in polar bears
11738 from Svalbard, aged from 3 to 10 years. Smoothing lines (robust, locally weighted scatter plot smoothing
11739 system based on the LOWESS algorithm) represent the fitted non-linear trend of the values. From Aubail
11740 et al. (2012). B) Annual mean Hg concentrations (ug/g dry weight; ln-transformed) adjusted for trophic
11741 position in eggs of thick-billed murres, northern fulmars, and black-legged kittiwakes from 1975 to 2014.
11742 from Braune et al. (2016). C) Hg concentrations in burbot and lake trout collected from the West basin
11743 and east Arm of Great Slave Lake. from Evans et al. (2013). NOTE TO GRAPHICS: draw a basemap of
11744 the Arctic and then show each of these (and perhaps others cited in the text) as an inset

11745

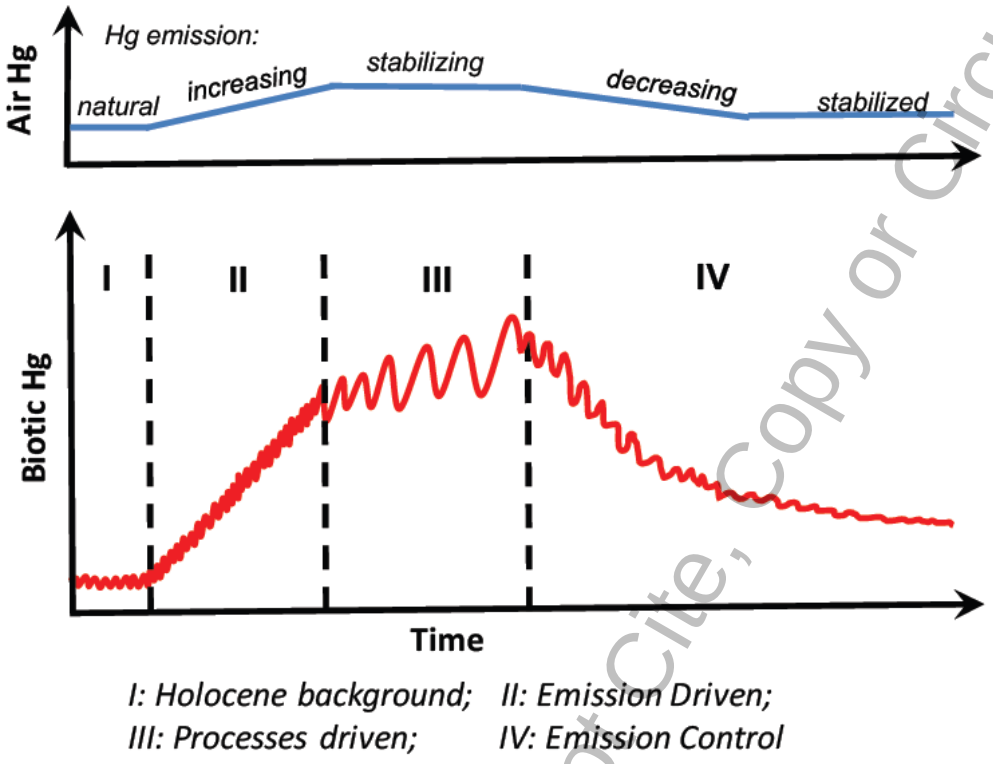

Figure 6.9. General stages in the principal drivers of mercury bioaccumulation (bottom panel), following increasing and decreasing trends in anthropogenic emissions (top panel). Modified from Wang et al. (2010).

6.3 References

Åkerblom S, Bignert A, Meili M, Sonesten L, Sundbom M. 2014. Half a century of changing mercury levels in Swedish freshwater fish. Ambio. 43 Suppl 1:91-103. doi: 10.1007/s13280-014-0564-1.

AMAP (2010) Updating Historical Global Inventories of Anthropogenic Mercury Emissions to Air. AMAP Technical Report No. 3 (Arctic Monitoring and Assessment Programme, Olso).

Aubail A., Dietz R., Rigét F., Sonne C., WiigØ, and Caurant F. 2012. Temporal trend of mercury in polar bears (*Ursus maritimus*) from Svalbard using teeth as a biomonitoring tissue. J. Environ. Monit. 14, 56–63.

Balcom, P.H., Schartup, A.T., Mason, R.P., Chen, C.Y. Sources of water column methylmercury across multiple estuaries in the Northeast U.S. (2015) Marine Chemistry, 177, pp. 721-730.

Baya, P. A., M. Gosselin, I. Lehnherr, V. L. St Louis and H. Hintelmann (2015). "Determination of monomethylmercury and dimethylmercury in the arctic marine boundary layer." Environ Sci Technol49(1): 223-232.

Beal SA, Osterberg EC, Zdanowicz CM, Fisher DA. 2015. Ice core perspective on mercury pollution during the past 600 years. Environ. Sci. Technol. 49, 7641−7647, doi: 10.1021/acs.est.5b01033.

Blukacz-Richards EA, Visha A, Graham ML, McGoldrick DL, de Solla SR, Moore DJ, and Arhond GB. 2017. Mercury levels in herring gulls and fish: 42 years of spatio-temporal trends in the Great Lakes. Chemosphere 172: 476-487.

Bowman, K. L., C. R. Hammerschmidt, C. H. Lamborg and G. Swarr (2015). "Mercury in the North Atlantic Ocean: The U.S. GEOTRACES zonal and meridional sections." Deep Sea Research Part II: Topical Studies in Oceanography116: 251-261.

Bowman, K. L., C. R. Hammerschmidt, C. H. Lamborg, G. J. Swarr and A. M. Agather (2016). "Distribution of mercury species across a zonal section of the eastern tropical South Pacific Ocean (U.S. GEOTRACES GP16)." Marine Chemistry186: 156-166.

Bratkič, A., M. Vahčič, J. Kotnik, K. Obu Vazner, E. Begu, E. M. S. Woodward and M. Horvat (2016). "Mercury presence and speciation in the South Atlantic Ocean along the 40°S transect." Global Biogeochemical Cycles: n/a-n/a.

Braune B.M., Gaston A.J., and Mallory M.L. 2016. Temporal trends of mercury in eggs of five sympatrically breedingseabird species in the Canadian Arctic. Environ. Pollut. 214, 124–131.

Braune B.M., Gaston A.J., Hobson K.A., Gilchrist H.G., and Mallory M.L. 2014. Changes in food web structure alter trends of mercury uptake at two seabird colonies in the Canadian Arctic. Environ. Sci. Technol. 48, 13246–13252.

Burgess, N.M., Bond, A.L., Hebert, C.E., Neugebauer, E., Champoux, L., 2013. Mercury trends in Herring Gull (*Larus argentatus*) eggs from Atlantic Canada, 1972-2008: temporal change or dietary shift? Environ. Pollut. 172, 216-222.

Chakraborty, P., Mason, R.P., Jayachandran, S., Vudamala, K., Armoury, K., Sarkar, A., Chakraborty, S., Bardhan, P., Naik, R. Effects of bottom water oxygen concentrations on mercury distribution and speciation in sediments below the oxygen minimum zone of the Arabian Sea. (2016) Marine Chemistry, 186, pp. 24-32.

Chen, C.Y., Borsuk, M.E., Bugge, D.M., Hollweg, T., Balcom, P.H., Ward, D.M., Williams, J., Mason, R.P. Benthic and pelagic pathways of methylmercury bioaccumulation in estuarine food webs of the Northeast United States. (2014). PLoS ONE, 9 (2), art. no. e89305.

Cole A, et al. (2014) A survey of mercury in air and precipitation across Canada: Patterns and trends. Atmosphere 5(3):635–668.

Cossa, D., M. Harmelin-Vivien, C. Mellon-Duval, V. Loizeau, B. Averty, S. Crochet, L. Chou and J. F. Cadiou (2012). "Influences of Bioavailability, Trophic Position, and Growth on Methylmercury in Hakes (Merluccius merluccius) from Northwestern Mediterranean and Northeastern Atlantic." Environmental Science & Technology46(9): 4885-4893.

Cross FA, Evans DW, and Barber RT. 2015. Decadal Declines of Mercury in Adult Bluefish (1972−2011) from the Mid-Atlantic Coast of the U.S.A. Environ. Sci. Technol. 49: 9064−9072.

Dietz, R.; Riget, F.; Born, E. W.; Sonne, C.; Grandjean, P.; Kirkegaard, M.; Olsen, M. T.; Asmund, G.; Renzoni, A.; Baagoe, H.; Andreasen, C. 2006. Trends in mercury in hair of greenlandic polar bears (Ursus maritimus) during 1892−2001. Environ. Sci. Technol. 40: 1120−1125.

Drevnick, P. E., C. H. Lamborg and M. J. Horgan (2015). "Increase in mercury in Pacific yellowfin tuna." Environmental Toxicology and Chemistry: n/a-n/a.

Driscoll, C.T., C.Y. Chen, C.R. Hammerschmidt, R.P. Mason, C.C. Gilmour, E.M. Sunderland, B.K. Greenfield, K.L. Buckman and C.H. Lamborg. Nutrient supply and mercury dynamics in marine ecosystems: A conceptual model. (2012) *Environmental Research***119**: 118-131.

Eagles-Smith CA, Ackerman JT, Willacker JJ, Tate MT, Lutz MA, Fleck JA, Stewart AR, Wiener JG, Evers DC, Lepak JM, Davis JA, Pritz CF. 2016. Spatial and temporal patterns of mercury concentrations in freshwater fish across the Western United States and Canada. Science of the Total Environment 568: 1171–1184.

Evans M, Muir D, Brua RB, Keating J, Wang X. 2013. Mercury Trends in Predatory Fish in Great Slave Lake: The Influence of Temperature and Other Climate Drivers. Environ. Sci. Technol. 47, 12793−12801.

Faïn, X.; Ferrari, C. P.; Dommergue, A.; Albert, M. R.; Battle, M.; Severinghaus, J.; Arnaud, L.; Barnola, J.-M.; Cairns, W.; Barbante, C.; et al. 2009. Polar firn air reveals large-scale impact of anthropogenic mercury emissions during the 1970s. Proc. Natl. Acad. Sci. U.S.A. 106: 16114−16119.

Feng XB, Jiang HM, Qiu GL, Yan HY, Li GH, Li ZG. 2009a. Geochemical processes of mercury in Wujiangdu and Dongfeng reservoirs, Guizhou, China. Environ Pollut 157: 2970-2984.

Feng XB, Jiang HM, Qiu GL, Yan HY, Li GH, Li ZG. 2009b. Mercury mass balance study in Wujiangdu and Dongfeng Reservoirs, Guizhou, China. Environ Pollut 157: 2594-2603.

Fitzgerald WF, Mason RP. 1997. Biogeochemical cycling of mercury in the marine environment. In Sigel A, Sigel H, eds, Metal Ions in Biological Systems, Vol 34-Mercury and its Effect on Environment and Biology. Marcel Dekker, New York, NY, USA.

Fu XW, Feng XB. 2015. Variations of atmospheric total gaseous mercury concentrations for the sampling campaigns of 2001/2002 and 2009/2010 and implications of changes in regional emissions of atmospheric mercury, Bull Miner Petr Geochem, in press (in Chinese, with English abstract), 2015.

Fu XW, Zhang H, Lin CJ, Feng XB, Zhou LX, Fang SX. 2015a. Correlation slopes of GEM/CO, GEM/CO2, and GEM/CH4 and estimated mercury emissions in China, South Asia, the Indochinese Peninsula, and Central Asia derived from observations in northwestern and southwestern China, Atmos. Chem. Phys. 15: 1013-1028.

Fu XW, Zhang H, Yu B, Wang X, Lin CJ, Feng XB. 2015b. Observations of atmospheric mercury in China: a critical review. Atmos. Chem. Phys. 15: 9455-9476.

Fu XW, Zhu W, Zhang H, Sommar J, Yu B, Yang X, Wang X, Lin CJ, and Feng XB. 2016. Depletion of atmospheric gaseous elemental mercury by plant uptake at Mt. Changbai, Northeast China. Atmos. Chem. Phys. 16: 12861-12873.

11843 Gaden, A.; Ferguson, S. H.; Harwood, L.; Melling, H.; Stern, G. 2009. A. Mercury trends in ringed seals
11844 (*Phoca hispida*) from the western Canadian Arctic since 1973: Associations with length of ice-
11845 free season. Environ. Sci. Technol. 43: 3646−3651.
11846 Gandhi, N., Tang, Rex W.K., Bhavsar, Satyendra P., Arhonditsis, George B., 2014. Fish mercury levels
11847 appear to be increasing lately: a report from 40 years of monitoring in the Province of Ontario,
11848 Canada. Environ. Sci. Technol. 48, 5404-5414.
11849 Gionfriddo, C. M., M. T. Tate, R. R. Wick, M. B. Schultz, A. Zemla, M. P. Thelen, R. Schofield, D. P.
11850 Krabbenhoft, K. E. Holt and J. W. Moreau (2016). "Microbial mercury methylation in Antarctic
11851 sea ice." Nat Microbiol1(10): 16127.
11852 Goni-Urriza, M., Y. Corsellis, L. Lanceleur, E. Tessier, J. Gury, M. Monperrus and R. Guyoneaud (2015).
11853 "Relationships between bacterial energetic metabolism, mercury methylation potential, and
11854 hgcA/hgcB gene expression in Desulfovibrio dechloroacetivorans BerOc1." Environ Sci Pollut Res
11855 Int.
11856 Gosnell, K. J. and R. P. Mason (2015). "Mercury and methylmercury incidence and bioaccumulation in
11857 plankton from the central Pacific Ocean." Marine Chemistry177, Part 5: 772-780.
11858 Gosnell, K., Balcom, P., Ortiz, V., DiMento, B., Schartup, A., Greene, R., Mason, R. 2016. Seasonal cycling
11859 and transport of mercury and methylmercury in the turbidity maximum of the Delaware
11860 Estuary. Aquatic Geochemistry, 22 (4), pp. 313-336.
11861 Gosnell, K.J., Balcom, P.H., Tobias, C.T., Gilhooly III, W.P., Mason, R.P. 2017. Spatial and temporal trophic
11862 transfer dynamics of mercury and methylmercury into zooplankton and phytoplankton of Long
11863 Island Sound. *Limnol. Oceanogr.*, DOI: 10.1002/lno.10490.pdf
11864 Gregoire, D. S. and A. J. Poulain (2016). "A physiological role for HgII during phototrophic growth."
11865 Nature Geosci9(2): 121-125.
11866 Guo YN. 2008. Input and output fluxes of mercury in different evolutive reservoirs in Wujiang River
11867 Basin. Ph.D. diss. Graduate School of the Chin. Acad. of Sci., Beijing. (In Chinese, with English
11868 abstract)
11869 Hall BD, St. Louis VL, Rolfhus KR, Bodaly RA, Beaty KG, Paterson M. 2005. The impact of reservoir
11870 creation on the biogeochemical cycling of methyl and total mercury in boreal upland forests.
11871 Ecosystems 8: 248-266.
11872 Hammerschmidt, C. R. and K. L. Bowman (2012). "Vertical methylmercury distribution in the subtropical
11873 North Pacific Ocean." Marine Chemistry132–133(0): 77-82.
11874 Heimbürger, L.-E., J. E. Sonke, D. Cossa, D. Point, C. Lagane, L. Laffont, B. T. Galfond, M. Nicolaus, B. Rabe
11875 and M. R. van der Loeff (2015). "Shallow methylmercury production in the marginal sea ice zone
11876 of the central Arctic Ocean." Sci. Rep.5.
11877 Horowitz HM, Jacob DJ, Amos HM, Streets DG, Sunderland EM (2014) Historical Mercury releases from
11878 commercial products: Global environmental implications. Environ Sci Technol 48(17):10242–
11879 10250.
11880 Jaffe D, Prestbo E, Swartzendruber P, Weiss-Penzias P, Kato S, Takami A, Hatakeyama S, and Kajii Y.
11881 2005. Export of atmospheric mercury from Asia. Atmos. Environ. 39: 3029-3038.
11882 Jiang HM. 2005. Effects of hydroelectric reservoir on the biogeochemical cycle of mercury in the Wujiang
11883 River. Ph.D. diss. Graduate School of the Chin. Acad. of Sci., Beijing. (In Chinese, with English
11884 abstract)
11885 Jonsson, S., A. Andersson, M.B. Nilsson, U. Skyllberg, E. Lundberg, J.K. Schaefer, S.Å., E. Björn.
11886 Terrestrial discharges mediate trophic shifts and enhance methylmercury accumulation in
11887 estuarine biota. Science Advances (2017) 3, e1601239.

11888 Jonsson, S., Skyllberg, U., Nilsson, M.B., Lundberg, E., Andersson, A., Björn, E. Differentiated availability
11889 of geochemical mercury pools controls methylmercury levels in estuarine sediment and biota.
11890 (2014) Nature Communications, 5, art. no. 4624.
11891 Jonsson, S., Skyllberg, U., Nilsson, M.B., Westlund, P.-O., Shchukarev, A., Lundberg, E., Björn, E. Mercury
11892 methylation rates for geochemically relevant HgII species in sediments. (2012) Environmental
11893 Science and Technology, 46 (21), pp. 11653-11659.
11894 Kim, H., A. L. Soerensen, J. Hur, L.-E. Heimbürger, D. Hahm, T. S. Rhee, S. Noh and S. Han (2016).
11895 "Methylmercury Mass Budgets and Distribution Characteristics in the Western Pacific Ocean."
11896 Environmental Science & Technology.
11897 Kwon, S.Y., Blum, J.D., Chen, C.Y., Meattey, D.E., Mason, R.P. Mercury isotope study of sources and
11898 exposure pathways of methylmercury in estuarine food webs in the northeastern U.S. (2014)
11899 Environmental Science and Technology, 48 (17), pp. 10089-10097.
11900 Larssen T. 2010. Mercury in Chinese reservoirs. Environ Pollut 158: 24-25.
11901 Lee, C.-S., M. E. Lutcavage, E. Chandler, D. J. Madigan, R. M. Cerrato and N. S. Fisher (2016). "Declining
11902 Mercury Concentrations in Bluefin Tuna Reflect Reduced Emissions to the North Atlantic
11903 Ocean." Environmental Science & Technology.
11904 Lehnherr I. 2014. Methylmercury biogeochemistry: a review with special reference to Arctic aquatic
11905 ecosystems. Environ. Rev. 22: 229–243. doi.org/10.1139/er-2013-0059.
11906 Li SX, Zhou LF, Wang HJ, Liang YG, Hu JX, Chang JB. 2009. Feeding habits and habitats preferences
11907 affecting mercury bioaccumulation in 37 subtropical fish species from Wujiang River, China.
11908 Ecotoxicology. 18: 204-210
11909 Li SX, Zhou LF, Wang HJ, Xiong MH, Yang Z, Hu JX, Liang YG, Chang JB. 2013. Short-term impact of
11910 reservoir impoundment on the patterns of mercury distribution in a subtropical aquatic
11911 ecosystem, Wujiang River, southwest China. Environ SciPollut Res 20: 4396-4404.
11912 Li, M., Schartup, A.T., Valberg, A.P., Ewald, J.D., Krabbenhoft, D.P., Yin, R., Balcom, P.H., Sunderland,
11913 E.M. Environmental Origins of Methylmercury Accumulated in Subarctic Estuarine Fish Indicated
11914 by Mercury Stable Isotopes (2016) Environmental Science and Technology, 50 (21), pp. 11559-
11915 11568.
11916 Liang S, Xu M, Liu Z, Suh S, Zhang TZ. 2013. Socioeconomic Drivers of Mercury Emissions in China from
11917 1992 to 2007, Environ. Sci. Technol. 47: 3234-3240.
11918 Liem-Nguyen, V., Jonsson, S., Skyllberg, U., Nilsson, M.B., Andersson, A., Lundberg, E., Björn, E. Effects of
11919 nutrient loading and mercury chemical speciation on the formation and degradation of
11920 methylmercury in estuarine sediment. (2016) Environmental Science and Technology, 50 (13),
11921 pp. 6983-6990.
11922 Lindberg S, Bullock R, Ebinghaus R, Engstrom D, Feng XB, Fitzgerald W, Pirrone N, Prestbo E, Seigneur, C.:
11923 A synthesis of progress and uncertainties in attributing the sources of mercury in deposition.
11924 Ambio. 36, 19-32, 2007.
11925 Liu B, Yan HY, Wang CP, Li QH, Guedron S, Spangenberg JE, Feng XB, Dominik J. 2012. Insights into low
11926 fish mercury bioaccumulation in a mercury-contaminated reservoir, Guizhou, China. Environ.
11927 Pollut. 160: 109-117.
11928 Liu, B., Schaider, L.A., Mason, R.P., Shine, J.P., Rabalais, N.N., Senn, D.B. Controls on methylmercury
11929 accumulation in northern Gulf of Mexico sediments. (2015) Estuarine, Coastal and Shelf Science,
11930 159, pp. 50-59.
11931 Lucotte M, Schetagne R, Therien N, Langlois C, Tremblay A. 1999. Mercury in the biogeochemical cycle:
11932 Natural environments and hydroelectric. Springer, Berlin, Germany.

11933 Mason, R. P., A. L. Choi, W. F. Fitzgerald, C. R. Hammerschmidt, C. H. Lamborg, A. L. Soerensen and E. M.
11934 Sunderland (2012). "Mercury biogeochemical cycling in the ocean and policy implications."
11935 Environmental Research119(0): 101-117.
11936 Mazrui, N. M., S. Jonsson and R.P. Mason. Enhanced availability of mercury bound to organic matter for
11937 methylation in marine sediments. (2016) *Geochimica et Cosmochimica Acta,* **194**: 153-162.
11938 McKinney MA, Atwood TC, Pedro S, Peacock E. 2017. Ecological change drives a decline in mercury
11939 concentrations in Southern Beaufort Sea polar bears. Environ. Sci. Technol.
11940 Doi:10.1021/acs.et.7b00812.
11941 Meng B, Feng XB, Chen CX, Qiu GL, Sommar J, Guo YN, Wan Q. 2010. Influence of eutrophication on the
11942 distribution of total mercury and methylmercury in hydroelectric reservoirs. J Environ Qual 39:
11943 1624-1635.
11944 Meng B, Feng XB, Qiu GL, Li ZG, Yao H, Shang LH, Yan HY. 2016. The impacts of organic matter on the
11945 distribution and methylation of mercury in a hydroelectric reservoir in Wujiang River, Southwest
11946 China. Environ Toxic Chem 35: 191-199.
11947 Monperrus, M., E. Tessier, D. Amouroux, A. Leynaert, P. Huonnic, O.F.X. Donard. Mercury methylation,
11948 demethylation and reduction rates in coastal and marine surface waters of the Mediterranean
11949 Sea. (2007) Mar. Chem.
11950 Munson, K. M., C. H. Lamborg, G. J. Swarr and M. A. Saito (2015). "Mercury species concentrations and
11951 fluxes in the Central Tropical Pacific Ocean." Global Biogeochemical Cycles29(5): 656-676.
11952 Muntean M, et al. (2014) Trend analysis from 1970 to 2008 and model evaluation of EDGARv4 global
11953 gridded anthropogenic mercury emissions. Sci Total Environ 494–495:337–350.
11954 Ortiz, V.L., Mason, R.P., Ward, J.E. An examination of the factors influencing mercury and
11955 methylmercury particulate distributions, methylation and demethylation rates in laboratory-
11956 generated marine snow. (2015) Marine Chemistry, 177, pp. 753-762.
11957 Paranjape AR, and Hall BD. 2017. Recent advances in the study of mercury methylation in aquatic
11958 systems . FACETS 2: 85–119. doi: 10.1139/facets-2016-0027.
11959 Parks, J. M., A. Johs, M. Podar, R. Bridou, R. A. Hurt, S. D. Smith, S. J. Tomanicek, Y. Qian, S. D. Brown, C.
11960 C. Brandt, A. V. Palumbo, J. C. Smith, J. D. Wall, D. A. Elias and L. Liang (2013). "The Genetic Basis
11961 for Bacterial Mercury Methylation." Science.
11962 Podar, M., C. C. Gilmour, C. C. Brandt, A. Soren, S. D. Brown, B. R. Crable, A. V. Palumbo, A. C.
11963 Somenahally and D. A. Elias (2015). "Global prevalence and distribution of genes and
11964 microorganisms involved in mercury methylation." Science Advances1(9).
11965 Prestbo EM, Gay DA (2009) Wet deposition of mercury in the US and Canada, 1996-2005: Results and
11966 analysis of the NADP mercury deposition network (MDN). Atmos Environ 43(27):4223–4233.
11967 Rigét F., Dietz R., and Hobson K.A. 2012. Temporal trends of mercury in Greenland ringed seal
11968 populations in a warming climate. J. Environ. Monit. 14, 3249–3256.
11969 Rigét, F.; Braune, B.; Bignert, A.; Wilson, S.; Aars, J.; Born, E.; Dam, M.; Dietz, R.; Evans, M.; Evans, T.;
11970 Gamberg, M.; Gantner, N.; Green, N.; Gunnlaugsdóttir, H.; Kannan, K.; Letcher, R.; Muir, D.;
11971 Roach, P.; Sonne, C.; Stern, G.; Wiig, O. 2011. Temporal trends of Hg in Arctic biota, an update.
11972 Sci. Total Environ. 409: 3520−3526.
11973 Sanei H, Outridge PM, Goodarzi F, Wang F, Armstrong D, Warren K, and Fishback L. 2010. Wet deposition
11974 mercury fluxes in the Canadian sub-Arctic and southern Alberta, measured using an automated
11975 precipitation collector adapted to cold regions. **Atmospheric Environment** 44: 1672-1681.
11976 Schartup, A.T., Balcom, P.H., Mason, R.P. Sediment-porewater partitioning, total sulfur, and
11977 methylmercury production in estuaries. (2014) Environmental Science and Technology, 48 (2),
11978 pp. 954-960.

11979 Schartup, A.T., Balcom, P.H., Soerensen, A.L., Gosnell, K.J., Calder, R.S.D., Mason, R.P., Sunderland, E.M.,
11980 St. Louis, V.L. Freshwater discharges drive high levels of methylmercury in Arctic marine biota.
11981 (2015) Proceedings of the National Academy of Sciences of the United States of America, 112
11982 (38), pp. 11789-11794.
11983 Schartup, A.T., Mason, R.P., Balcom, P.H., Hollweg, T.A., Chen, C.Y. Methylmercury production in
11984 estuarine sediments: Role of organic matter. (2013) Environmental Science and Technology, 47
11985 (2), pp. 695-700.
11986 Schartup, A.T., U. Ndu, R.P. Mason, and E.M. Sunderland. Contrasting effects of marine and terrestrially
11987 derived dissolved organic matter on mercury speciation and bioavailability in seawater. (2015b)
11988 *Environ. Sci. Technol.,***49** (10): 5965-5972; DOI: 10.1021/es506274x.
11989 Sharif, A., Monperrus, M., Tessier, E., Bouchet, S., Pinaly, H., Rodriguez-Gonzalez, P., Maron, P.,
11990 Amouroux, D. Fate of mercury species in the coastal plume of the Adour River estuary (Bay of
11991 Biscay, SW France). (2014) Science of the Total Environment, 496, pp. 701-713.
11992 Slemr F, Brunke EG, Ebinghaus R, Kuss J (2011) Worldwide trend of atmospheric mercury since 1995.
11993 Atmos Chem Phys 11: 4779–4787.
11994 Slemr F., Angot H., Dommergue A., Magand O., Barret M., Weigelt A., Ebinghaus R., Brunke E.-G.,
11995 Pfaffhuber K., Edwards G., Howard D., Powell J., Keywood M., and Wang F. 2015. Comparison of
11996 mercury concentrations measured at several sites in the Southern Hemisphere. Atmos. Chem.
11997 Phys. 15: 3125-3133.
11998 Soerensen AL, et al. (2012) Multi-decadal decline of mercury in the North Atlantic atmosphere explained
11999 by changing subsurface seawater concentrations. Geophys Res Lett 39(21):L21810.
12000 Soerensen, A. L., D. J. Jacob, A. T. Schartup, J. A. Fisher, I. Lehnherr, V. L. St. Louis, L.-E. Heimbürger, J. E.
12001 Sonke, D. P. Krabbenhoft and E. M. Sunderland (2016). "A mass budget for mercury and
12002 methylmercury in the Arctic Ocean." Global Biogeochemical Cycles30:
12003 doi:10.1002/2015GB005280.
12004 Soerensen, A.L., A.T. Schartup, E. Gustafsson, B.G. Gustafsson, E. Underman and E. Bjorn. Eutrophication
12005 increases phytoplankton methylmercury concentrations in a coastal sea – A Baltic Sea case
12006 study. (2016)Environ. Sci. Technol., DOI: 10.1021/acs.est.6b02717.
12007 St. Louis VL, Rudd JWM, Kelly CA, Bodaly RAD, Paterson MJ, Beaty KG, Hesslein RH, Heyes A, Majewsk
12008 AR. 2004. The rise and fall of mercury methylation in an experimental reservoir. Environ Sci
12009 Technol 38: 1348-1358.
12010 St. Pierre, K., V. L. St.Louis, J. Kirk, I. Lehnherr, S. Wang and C. La Farge (2015). "The importance of open
12011 marine waters to the enrichment of total mercury and monomethylmercury in lichens in the
12012 Canadian High Arctic." Environmental Science & Technology.
12013 Stern GA, Macdonald RW, Outridge PM, Wilson S, Cole A, Chetelat J, Hintelmann H, Loseto LL, Steffen A,
12014 Wang F, and Zdanowicz C. 2012. How does climate change affect Arctic mercury? **Science of the**
12015 **Total Environment** 414: 22-42.
12016 Streets DG, Hao JM, Wu Y, Jiang JK, Chan M, Tian HZ, Feng XB. 2005. Anthropogenic mercury emissions
12017 in China. Atmos. Environ. 39: 7789-7806.
12018 Tang, R. W. K.; Johnston, T. A.; Gunn, J. M.; Bhavsar, S. P. 2013. Temporal Changes in Mercury
12019 Concentrations of Large-Bodied Fishes in the Boreal Shield Ecoregion of Northern Ontario,
12020 Canada. Sci. Total Environ. 444: 409−416.
12021 Tong YD, Yin XF, Lin HM, Buduo, Danzeng, Wang HH, Deng CY, Chen L, Li JL, Zhang W, Schauer JJ, Kang
12022 SC, Zhang GS, Bu XG, Wang XJ, Zhang QG. 2016. Recent Decline of Atmospheric Mercury
12023 Recorded by Androsace tapete on the Tibetan Plateau, Environ. Sci. Technol. 50: 13224-13231.

12024 United States Environmental Protection Agency (USEPA). 2010. Guidance for Implementing the January
12025 2001 Methylmercury Water Quality Criterion. EPA 823-R-10-001
12026 Visha, A., Gandhi, N., Bhavsar, S.P., Arhonditsis, G.B., 2015. A Bayesian assessment of the mercury and
12027 PCB temporal trends in lake trout (*Salvelinus namaycush*) and walleye (*Sander vitreus*) from lake
12028 Ontario, Ontario, Canada. Ecotoxicol. Environ. Saf. 117, 174-186.
12029 Wang F. and Zhang J. 2013. Mercury contamination in aquatic ecosystems under a changing
12030 environment: Implications for the Three Gorges Reservoir. *Chin. Sci. Bull.* 58, 141-149
12031 Wang F., Macdonald R.W., Stern G.A., and Outridge P.M. 2010. When noise becomes the signal:
12032 Chemical contamination of aquatic ecosystems under a changing climate. *Mar. Pollut. Bull.* 60.
12033 1633-1635.
12034 Wang X, Lin CJ, Yuan W, Sommar J, Zhu W, Feng XB. 2016. Emission-dominated gas exchange of
12035 elemental mercury vapor over natural surfaces in China. Atmos. Chem. Phys. 16: 11125-11143.
12036 Wang, F., R. W. Macdonald, D. A. Armstrong and G. A. Stern (2012). "Total and Methylated Mercury in
12037 the Beaufort Sea: The Role of Local and Recent Organic Remineralization." Environmental
12038 Science & Technology46(21): 11821-11828.
12039 Willacker JJ, Eagles-Smith CA, Lutz MA, Tate MT, Lepak JM, and Ackerma JT. 2016. Reservoirs and water
12040 management influence fish mercury concentrations in the western United States and Canada.
12041 Science of the Total Environment 568: 739–748.
12042 World Health Organization (WHO). 1990. Environmental health criteria 101: Methylmercury,
12043 International Programme of Chemical Safety. International Programme of Chemical Safety,
12044 Geneva.
12045 Wu QR, Wang SX, Li GL, Liang S, Lin CJ, Wang YF, Cai SY, Liu KY, Hao JM. 2016. Temporal Trend and
12046 Spatial Distribution of Speciated Atmospheric Mercury Emissions in China During 1978-2014.
12047 Environ. Sci. Technol. 50: 13428-13435.
12048 Wu Y, Streets DG, Wang SX, Hao JM. 2010. Uncertainties in estimating mercury emissions from coal-
12049 fired power plants in China. Atmos. Chem. Phys. 10: 2937-2946.
12050 Wu Y, Wang SX, Streets DG, Hao JM, Chan M, Jiang JK. 2006. Trends in anthropogenic mercury emissions
12051 in China from 1995 to 2003. Environ. Sci. Technol. 40: 5312-5318.
12052 Yan HY, Rustadbakken A, Yao H, Larssen T, Feng XB, Liu B, Shang LH, Haugen, TO. 2010. Total mercury in
12053 wild fish in Guizhou reservoirs, China. J. Environ. Sci. 22: 1129-1136.
12054 Yao H, Feng XB, Guo YN, Yan HY, Fu XW, Li ZG, Meng B. 2011. Mercury and methylmercury
12055 concentrations in 2 newly constructed reservoirs in the Wujiang River, Guizhou, China. Environ
12056 ToxicolChem 30: 530-537.
12057 Zhang JF, Feng XB, Yan HY, Guo YN, Yao H, Meng B, Liu K. 2009. Seasonal distributions of mercury
12058 species and their relationship to some physicochemical factors in Puding Reservoir, Guizhou,
12059 China. Sci. Total Environ. 408: 122-129.
12060 Zhang L, Wang SX, Wang L, Wu Y, Duan L, Wu QR, Wang FY, Yang M, Yang H, Hao J. M, Liu X. 2015.
12061 Updated Emission Inventories for Speciated Atmospheric Mercury from Anthropogenic Sources
12062 in China, Environ. Sci. Technol. 49: 3185-3194.
12063 Zhang Y, Jacob D, Horowitz HM, Chen L, Amos HM, Krabbenhoft DP, Slemr F, St. Louis VL, and
12064 Sunderland EM. 2016. Observed decrease in atmospheric mercury explained by global decrease
12065 in anthropogenic emissions. Proc. Nat. Acad. Sci., doi: 10.1073/pnas.1516312113.
12066 Zhang, T., K.H. Kucharzyk, B. Kim, M.A. Deshusses and H. Hsu-Kim. Net methylation of mercury in
12067 estuarine sediment mesocosms amended with dissolved, nanoparticulate and microparticulate
12068 mercuric sulfide. (2014) Environ. Sci. Technol. 48, 9133-9141.

12069 Zheng, J. 2015. Archives of total mercury reconstructed with ice and snow from Greenland and the
12070 Canadian High Arctic. Sci. Total Environ. 509–510: 133–144.
12071

12072

Note to reader

This draft version of Chapter 7 in the Technical Background Report to the Global Mercury Assessment 2018 is made available for review by national representatives and experts. The draft version contains material that will be further refined and elaborated after the review process. Specific items where the content of this draft chapter will be further improved and modified are:

1. Quality of all graphics (Maps, Figures, Tables) will be improved prior to publication.
2. Content of all graphics (Figures, Tables) will be double-checked, updated, and refined prior to publication.
3. Table 2 and 3 will be further updated over the next couple of months.

GMA 2018 Draft. Chapter 7 Mercury concentrations in biota. David Evers, Staffan Åkerblom, David Buck, Dominique Bally, Nil Basu, Nathalie Bodin, Paco Bustamante, John Chetelat, Monica Costa, Rune Dietz, Paul Drevnick, Collin Eagles-Smith, José Lailson, Diego Henrique Costa Pereira, Frank Riget, Carlos Rodriguez Brianza, Elsie Sunderland, Akinori Takeuchi, Eleuterio Umpiérrez, Simon Wilson, Younghee Kim (UNEP Fate & Transport Partnership Group, Biota Subgroup Technical Expert Team)

13022 # Contents

13048

13049

Chapter 7 Mercury concentrations in biota

7.1 Introduction

7.1.1 Principal sources and pathways of methylmercury availability to biota

Mercury (Hg) globally enters ecosystems through the air (e.g., emissions from coal-fired power plants and incinerators) or water (e.g., both inactive and active chlor-alkali facilities and landfills) (Pacyna et al. 2016, Kocman et al. 2017, Streets et al. 2017). Inorganic Hg emitted from natural or anthropogenic sources becomes toxic in the environment when it is converted to methylmercury (MeHg), by sulphur-reducing bacteria and other microbes (Gilmour et al. 2013). Certain ecosystem conditions (such as those found in wetlands) can encourage the production and bioavailability of MeHg in the environment. Bacteria often produce more MeHg when moderate amounts of sulphate and low oxygen (anoxic) conditions are present to provide optimal conditions for the metabolic processes of the bacteria (Hsu-Kim et al. 2013). Mercury also readily binds to dissolved organic carbon (DOC), so areas with high DOC levels may generate MeHg more readily (depending on the type of DOC) (Schartup et al. 2015), as will areas that have acidified conditions (Wyn et al. 2009).

These factors are important in assessing ecosystems sensitive to both Hg input and methylation potential. The complex chemical conversions and cycling of Hg make it particularly challenging to predict from air, water and sediment to levels of potential concern in upper trophic level fish and wildlife (Gustin et al. 2016, Sunderland et al. 2016). In other words, in areas where Hg deposition is low, effects on biota may be disproportionately high if conditions are conducive to MeHg production and biomagnification. A robust example is in southern Nova Scotia's Kejimkujik National Park of Canada, where Hg deposition levels are low, but concentrations in fish and birds tissue are above ecological health thresholds (Burgess and Hobson 2006; Burgess and Meyer 2008) and trends in fish MeHg concentrations continue to increase (Wyn et al. 2010).

Mercury is a potent neurotoxin that can cause physiological, neurologic, behavioural, reproductive, and survival harm to fish and wildlife (Scheuhammer et al. 2011). It readily biomagnifies, resulting in increasing concentrations of MeHg in the ecosystem as it moves from water and sediment, to phytoplankton and plants, aquatic insects, spiders, fish and wildlife. Once MeHg is taken up at the base of the food web it can efficiently biomagnify. As a result, top predators in a food web, such as fish, birds and mammals that prey on items that are themselves at relatively high trophic status, may have

concentrations of MeHg in their tissues that are many orders of magnitude higher than the concentrations found in the water (often > 10^6 to 10^7 higher). Generally, each trophic change in the foodweb accounts for an order of magnitude of increase in MeHg concentrations, with the largest magnification occurring between water and phytoplankton in aquatic systems (Lee and Fisher, 2016).

Mercury exposure has been well documented in fish and wildlife around the world, including areas with both point sources of contamination and remote from such sources (i.e., >100 miles) across North America (Evers et al. 2005, Kamman et al. 2005, Monson et al. 2011, Evers et al. 2011, Ackerman et al. 2016, Eagles-Smith et al. 2016, Jackson et al. 2016), Europe (Nguetseng et al. 2015), Asia (Abeysinghe et al. 2017) and representing ocean basins (Carravieri et al. 2014, Drevnick et al. 2015, 2017; Lee et al. 2016, Bodin et al. 2017). Numerous studies, particularly recent ones, document adverse impacts such as reduced reproductive success, behavioural change (e.g., reduced time incubating), and neurological problems (e.g., ataxia) (Depew et al. 2012a,b; Dietz et al. 2013, Ackerman et al. 2016, Whitney and Cristol 2017, Evers 2017). Based on these and other in *situ* studies, the biomagnification and bioaccumulation of MeHg is shown to adversely affect the reproductive success of many fish and wildlife populations, representing multiple foraging guilds across many habitats and geographic areas of the world.

Building on recent and compelling evidence, wildlife species vary in their sensitivity to MeHg toxicity (potentially based on foraging guilds and phylogeny) (Heinz et al. 2009). Passeriforms (i.e., songbirds) for example, appear to be highly sensitive to the toxicity of MeHg when compared to other orders of birds. Evidence to date indicates songbirds are more sensitive to MeHg toxicity on hatching and fledging success when compared to piscivores. Understanding MeHg in foodweb pathways and the ability of MeHg to adversely impact upper trophic level wildlife is critical for developing comprehensive assessments and monitoring efforts.

In the end, identifying the proper fish and wildlife bioindicators for Hg biomonitoring are varied and complex. They differ according to the geographic area, timescale of interest, conservation concern, and whether the overall goal is for ecological or human health.

7.1.2 Existing Biotic Mercury Concentrations

There is an extensive list of published Hg data for biota and there are many biomonitoring programs in place around the world, particularly in high-income countries (e.g., U.S., Canada, across several European countries, and Japan) that generally track temporal-spatial patterns of environmental Hg (with

an emphasis on fish). Existing biomonitoring programs were identified by a recent UNEP review (UNEP 2016). Existing data within the peer-reviewed literature define the many case studies that include Hg in taxa identified in Article 19 of the Minamata Convention. Those data can be summarized with an emphasis on fish (both teleosts and elasmobranchs), sea turtles, birds and marine mammals.

7.1.3 Spatiotemporal trends of methylmercury in the environment:

Based on existing data from the literature and the many well-established biomonitoring programmes, global and regional patterns are identified herein. One of the longest standing and perhaps most influential programs in connecting Hg exposure in the environment to the foods that human communities depend on is by the Arctic Monitoring and Assessment Programme (AMAP 2011). This regional program uses relatively standardized methodologies across a large geographic area, using multiple taxa (e.g., fish, birds, and marine mammals), and incorporates other variables (e.g., other contaminants). AMAP has established the bets regional template for effectively monitoring MeHg availability in the environment that can be used concurrently for ecological and human health,

7.1.4 Bioindicators useful for monitoring and assessing risk

Organisms that are at greatest risk for developing elevated MeHg body burdens are defined and grouped at relevant taxonomic resolutions. The emphasis is on biota that may pose concern for human health purposes in marine (e.g., tuna) or freshwater (e.g., bass and walleye) ecosystems, for temporal timelines of interest (e.g., short-term timeframes should use young individuals with relatively low trophic level species vs. long-term timeframes should use older individuals at high trophic levels), for spatial gradients of local to regional to global interests (e.g., for the latter, wide-ranging species such as swordfish are key), or for conservation purposes (e.g., wildlife that are rare or are well-established as at threat from Hg – such as albatrosses and loons).

7.2 Objectives

The overall goal of this chapter is to provide an overview about exposure to biota from environmental loads of Hg. The objectives of our analyses are to characterize:

1. Coverage of existing biotic Hg concentrations and biomonitoring programs;
2. Spatial gradients in Hg exposure, with an emphasis on identifying biological Hg hotspots;
3. Temporal trends of biotic Hg exposure;

4. Identification of bioindicators, with an emphasis on vulnerable taxa because of high exposures and susceptibility/sensitivity to toxic effects;
5. Linkages between Hg sources and targeted bioindicators;
6. Critical knowledge gaps.

7.3 Approach

7.3.1 Identification of existing data

A systematic literature search was used with an emphasis on long-term, standardized and broadly geographic monitoring efforts, as well as on biota identified in Article 19, with a special emphasis on (1) organisms used for human consumption and (2) species at greatest risk to adverse impacts (particularly at population levels). Only peer-reviewed publications were used and are archived in BRI's Global Biotic Mercury Synthesis (GBMS) database (Evers et al. 2016a).

This chapter aims to present data from peer-reviewed studies for which there can be reasonable confidence about the accuracy and precision of analytical results as well as about the comparability of the results over time. Studies were selected based on an adequately described study method that generally included the following parameters:

- Adequate description of the characteristics of the organism sampled, including species, size, location, date, and tissue analysed;
- Method of sample collection that met scientific standards;
- Large sample sizes (e.g., >100 for an area) or small sample sizes (<20) from areas poorly represented;
- An appropriate analytical method was used for measurement of Hg (or MeHg) in terms of limit of quantification, accuracy, and precision;
- Appropriate statistical methods were used for reporting results.

Consideration was given to selecting lower quality studies if the data were necessary to fill gaps for geographical distributions of biotic Hg exposure.

7.3.2 Explanation of preferred tissue types

This review focuses on tissues with well-established methods of measurement and interpretation and for which there is a reasonably large body of data. There are many available matrices and the choice of a tissue depends on monitoring interests and outcomes. Often the most useful tissues that can be

collected in the field are non-lethal. Samples that can be analysed to assess total or MeHg exposure are commonly from the following tissues (i.e., matrix) types (Table 1).

Table 1. Major biota groupings and tissues commonly analysed for Hg.

Biota Group	Matrix	% MeHg	Sample prep type*	Analyses type
Fish	Muscle fillet	>95%	ww or dw	THg
	Muscle Biopsy	>95%	dw (because greater possibility of moisture loss)	THg
	Blood	>95%	Ww	THg
Sea Turtles	Scales	>95%	Fw	THg
	Eggs	>95%	Dw	THg
Birds	Blood	>95%	Ww	THg
	Feather	>95%	Fw	THg
	Eggs	>95%	Dw	THg
	Liver/kidney	40-80%	Dw	MeHg
Marine mammals	Skin	>95%	Dw	THg
	Muscle	>95%	Dw	THg
	Liver/kidney	40-80%	Dw	MeHg
	Brain	>90%	Dw	THg

*Reported as wet weight (ww), dry weight (dw) or fresh weight (fw) analyses.

7.3.3 Identification of Hg biomonitoring programs

The identification of Hg biomonitoring programs was conducted under a formal request by the Interim Secretariat at a global level. Responses were compiled (UNEP 2016) and provide the best record of existing local, regional and global abiotic and biotic Hg monitoring programs.

7.4 Results

7.4.1 Existing biotic Hg data from peer-reviewed studies

Biotic Hg concentrations for targeted taxa (based on Article 19 of the Minamata Convention) were collected from over 700 peer-reviewed scientific publications that represent approximately 152,000 individuals at 1,675unique locations in 98 countries. It is believed that this is a relatively exhaustive literature review for field Hg concentrations in elasmobranchs, sea turtles, and marine mammals. The literature review is less exhaustive for teleost fish (both marine and freshwater) and birds.

Elasmobranchs(i.e., sharks, skates and rays) were represented in 11 Orders by 9,024 individuals at 294 distinct locations. Marine teleost fish were represented in 20 Orders by 30,483 individuals at 1785 distinct locations. A total of 73 distinct locations were found with Hg concentrations in one of three

tissue types of 1,259 individual sea turtles. Marine birds were represented in 9 Orders by 9,485 individuals at 619 distinct locations, while marine mammals were placed in 4 groups and represent 6,491 individuals at 558 locations (Table 2).

Table 2. Mercury concentrations (ug/g or ppm of total Hg for selected fish, sea turtle, birds and marine mammals at the taxonomic level of Order (or other groupings for marine mammals). Biota are arranged by major group, then mean Hg concentrations from high to low.

Common Name		Order	Sites (n)	Individuals (n)	Mean	SD	Min	Max
SHARKS, SKATES, AND RAYS		***CHONDRICHTHYES***	***Muscle (ww)***					
Chimaeras		Chimaeriformes	2	161	3.13	0.27	0.73	3.14
Cow sharks		Hexanchiformes	5	37	2.56	0.85	0.92	2.99
Electric rays		Torpediniformes	6	44	1.66	1.06	0.12	2.42
Dogfishes		Squaliformes	20	647	1.48	2.16	0.09	9.66
Mackerel sharks		Lamniformes	25	308	1.43	1.15	0.01	5.42
Ground sharks		Carcharhiniformes	183	7364	1.08	0.83	0.00	18.29
Carpet sharks		Orectolobiformes	4	44	0.96	0.29	0.05	1.05
Angel Sharks		Squatiniformes	3	98	0.40	0.07	0.03	0.48
Stingrays		Myliobatiformes	29	200	0.26	0.21	0.02	0.83
Guitarfishes		Rhinobatiformes	11	59	0.22	0.28	0.03	2.05
Skates and Rays		Rajiformes	6	62	0.15	0.09	0.02	0.30
MARINE FISH		***TELEOSTEI***	***Muscle (ww)***					
Roughy		Beryciformes	16	60	0.56	0.37	0.03	1.28
Perch-like fishes		Perciformes	1217	21225	0.39	0.49	0.00	10.52
Eels		Anguilliformes	12	207	0.37	0.12	0.05	0.56
Tarpons		Elopiformes	12	268	0.36	0.22	0.03	0.72
Flatfishes, Flounders, Soles		Pleuronectiformes	84	1701	0.32	0.30	0.00	0.88
Toadfish		Batrachoidiformes	6	117	0.30	0.14	0.03	0.37
Bonefishes		Albuliformes	5	42	0.28	0.19	0.10	0.53
Catfishes		Siluriformes	50	475	0.23	0.19	0.01	0.96
Minnows, Suckers		Cypriniformes	7	96	0.13	0.07	0.01	0.19
Silversides		Atheriniformes	10	641	0.12	0.07	0.03	0.51
Scorpion fishes, Sculpins		Scorpaeniformes	49	801	0.11	0.09	0.00	0.37

Cods, Hakes, Haddocks		Gadiformes	55	1207	0.11	0.14	0.01	0.74
Anglerfishes		Lophiiformes	4	43	0.10	0.03	0.01	0.12
Puffers, Triggerfishes, Leatherjackets		Tetraodontiformes	9	52	0.09	0.06	0.02	0.15
Mullets		Mugiliformes	80	992	0.08	0.11	0.00	0.40
Needlefishes		Beloniformes	7	54	0.07	0.03	0.02	0.11
Herrings, Sardinesm Anchovies		Clupeiformes	120	1973	0.06	0.15	0.00	3.40
Aulopiforms, Lizardfishes		Aulopiformes	14	66	0.06	0.08	0.01	0.36
Salmons		Salmoniformes	20	376	0.05	0.04	0.01	0.13
Smelts		Osmeriformes	8	87	0.03	0.02	0.00	0.05
REPTILES		***REPTILIA***	***Scutes (fw)***					
Sea turtles		Testunides	13	193	0.33	0.21	0.00	0.94
			Blood (ww)					
Sea turtles		Testunides	26	780	0.02	0.03	0.00	0.20
			Muscle (ww)					
Sea turtles		Testunides	34	286	0.14	0.15	0.00	0.39
BIRDS		***AVES***	***Body Feathers (fw)***					
Hawks, Eagles, Vultures		Accipitriformes	9	122	16.77	3.74	1.05	17.80
Albatrosses, Petrels, Shearwaters		Procellariiformes	124	3191	11.87	10.34	0.25	37.80
Rails and Cranes		Gruiformes	1	126	9.04		9.04	9.04
Cormorants		Suliformes	10	71	3.78	2.26	0.25	6.48
Gulls, Terns, Other Shorebirds		Charadriiformes	82	1216	2.43	2.25	0.18	11.66
Penguins		Sphenisciformes	51	1127	1.26	1.26	0.02	5.90
Waterfowl		Anseriformes	3	42	1.16	0.51	0.83	1.69
Tropicbirds		Phaethontiformes	1	31	0.84		0.84	0.84
			Blood (ww)					
Albatrosses, Petrels, Shearwaters		Procellariiformes	102	1398	6.23	16.34	0.03	209.37
Gulls, Terns, Other Shorebirds		Charadriiformes	146	887	1.95	5.33	0.03	36.52
Cormorants		Suliformes	37	574	1.38	1.89	0.19	17.14
Loons		Gaviiformes	37	2129	1.25	0.63	0.00	3.60
Hawks, Eagles, Vultures		Accipitriformes	28	86	0.74	1.05	0.00	7.40
Waterfowl		Anseriformes	13	82	0.56	1.41	0.01	4.68
Rails and Cranes		Gruiformes	2	82	0.46	0.30	0.01	0.56
Penguins		Sphenisciformes	31	372	0.41	0.27	0.02	0.84

Tropicbirds		Phaethontiformes	2	49	0.24	0.06	0.18	0.27
			Eggs (ww)					
Loons		Gaviiformes	8	544	1.22	0.65	0.00	1.63
Albatrosses, Petrels, Shearwaters		Procellariiformes	18	269	0.47	0.29	0.12	1.18
Pelecans, Ibises, Herons		Pelecaniformes	38	315	0.40	0.24	0.03	1.90
Cormorants		Suliformes	12	244	0.30	0.10	0.13	1.07
Gulls, Terns, Other Shorebirds		Charadriiformes	200	1825	0.28	0.26	0.00	1.71
Waterfowl		Anseriformes	10	132	0.26	0.15	0.07	0.43
Hawks, Eagles, Vultures		Accipitriformes	31	190	0.08	0.03	0.02	0.15
Grebes		Podicipediformes	8	130	0.07	0.03	0.04	0.13
Penguins		Sphenisciformes	2	33	0.04	0.01	0.04	0.05
Falcons		Falconiformes	11	124	0.04	0.02	0.02	0.08
MARINE MAMMALS		***MAMMALIA***	***Muscle (ww)***					
Toothed Whales		Cetacea: Odontoceti	401	4027	2.61	4.77	0.08	93.52
Seals and Walruses		Carnivora: Odobenidae, Otariidae, Phocidae	128	1969	0.39	0.35	0.00	3.22
Baleen Whale		Cetacea: Mysticeti	28	531	0.09	0.08	0.02	0.74
Polar Bears		Carnivora: *Ursus maritimus*	5	77	0.08	0.05	0.06	0.24

7.4.2 Existing biomonitoring programs

The existing biomonitoring programs for Hg that are operated by various governments and other entities are identified within many national networks, including initiatives in the EU (Norway, Sweden, Spain, UK, Poland), Canada, United States, Japan, Republic of Korea, Colombia and Brazil, and global or regional networks (UNEP 2016). The Arctic is best monitored through AMAP (AMAP 2011) with valuable subsets from Canada's National Contaminants Program (NCP) and the ARCTOX program based in Europe for tracking Hg in seabirds. There are many programs in the temperate regions of the U.S. (e.g., the U.S. Environmental Protection Agency's seafood Hg monitoring program and NOAA's mussel Hg watch program) and Europe and Japan. In tropical countries, there are fewer national or regional long-term initiatives. Oceanic Hg monitoring efforts are many and can be found in the peer-reviewed literature and are summarized by GBMS (Figure 1; Evers et al. 2016).

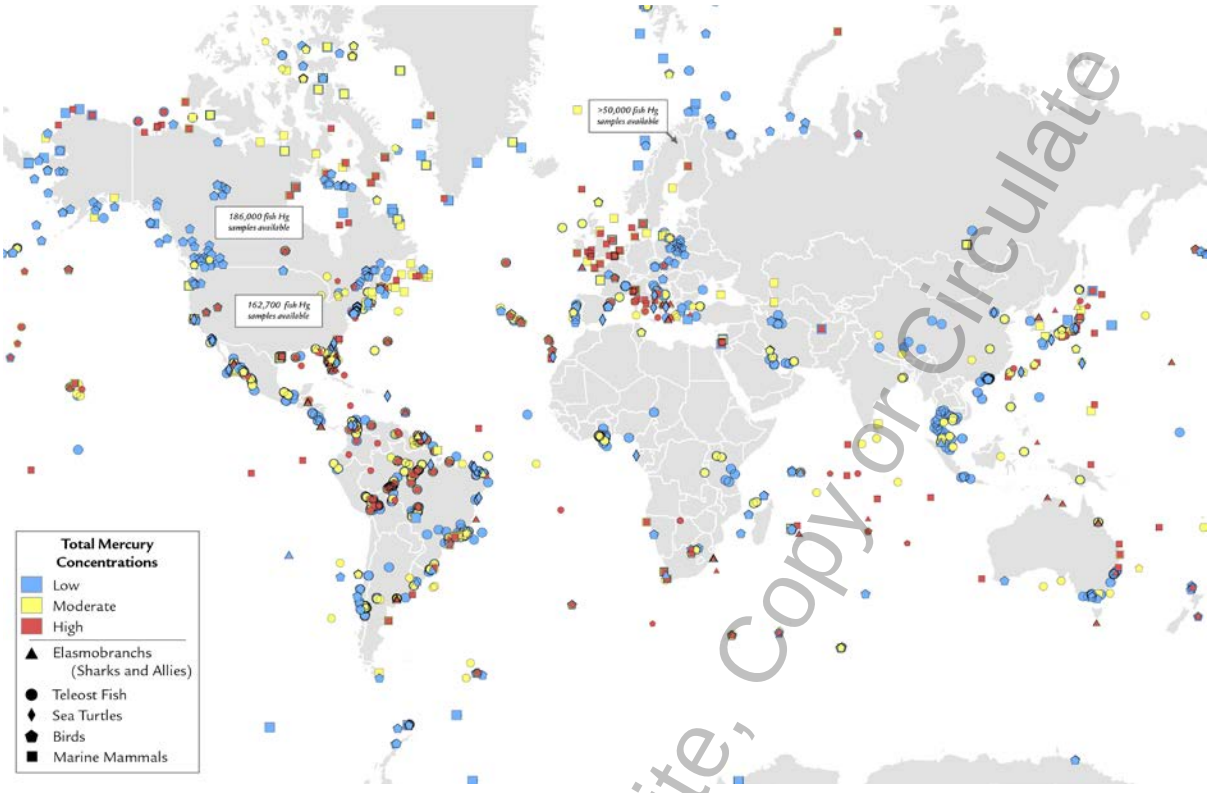

Figure 1. Distribution of four major taxa and their total Hg concentrations in three risk categories. Risk categories by major taxa and tissue type are: (1) Teleost and Elasmobranch fish muscle tissue (ppm, ww), <0.3=low, 0.3-1.0=moderate, >1.0= high; (2) Sea Turtle Blood (ppm, ww) – all tissues were deemed low exposure; (3) Bird Feathers (ppm, fw), <10=low, 10-20=moderate, >20=high; Adult Bird Blood (ppm, ww), <1.0=low, 1.0-3.0=moderate, >3.0=high; Eggs (ppm, ww), <0.5=low, 0.5-1.0=moderate, >1.0=high; Marine Mammal muscle (ppm, ww), <0.3=low, 0.3-1.0=moderate, >1.0=high.

7.5 Discussion

7.5.1 Selection of best bioindicators

The choice of target bioindicators depends on the question and circumstances. The initial choice of a human health vs. an ecological health endpoint is important and can be often combined if properly selected. Biota that have been identified to best fit these two categories are well described and should be categorized within biomes and associated aquatic ecosystems (Table 3). The taxa of greatest interest for the Minamata Convention include fish, sea turtles, birds and marine mammals – and, because of the extensive scientific published literature the exposure of Hg in biota from around the world provides confidence in properly selecting species of interest (Evers et al. 2016b).

Table 3. Potential choices of known bioindicators for ecological and human health as grouped by major terrestrial biomes and their associated aquatic ecosystems (Adapted from Evers et al. 2016b).

Target Terrestrial Biomes	Associated Aquatic Ecosystems	Ecological Health Bioindicators				Human and Ecological Health Bioindicators		
		Freshwater and Marine Fish	***Freshwater Birds***	***Marine Birds***	***Marine Mammals & Sea Turtles***	***Freshwater Fish***	***Marine Fish***	***Marine Mammals***
Arctic Tundra	Arctic Ocean and associated estuaries, lakes, rivers	Sticklebacks[1] (freshwater); Arctic Cod[2] Sculpin[3] (marine)	Loons[4,5]	Fulmars[6] Murres[6]	Polar Bears[7] Seals[8]	Arctic Char[9] Arctic Grayling[10]	Halibut[11] Cod[11]	Beluga[2, 12] Narwhal[2, 12] Ringed Seal[57], Hooded Seal[8]
Boreal Forest and Taiga	North Pacific and Atlantic Oceans and associated estuaries, lakes, rivers	Perch[13] (freshwater); Mummichogs [14] (marine)	Loons[15] Eagles[16] Osprey[17] Songbirds[18] (Warblers, Flycatchers, Blackbirds)	Osprey[19] Petrels[20,] Albatrosses[50, 51] Herring Gulls[58]	Mink[21,22] Otter[21,22] Seals[23]	Catfish[11] Pike[10] Sauger[10] Walleye[10]	Flounder[11] Snapper[11] Tuna[11]	Pilot Whale[24]
Temperate Broadleaf and Mixed Forest	North Pacific and Atlantic Oceans, Mediterranean and Caribbean Seas, and associated estuaries, lakes rivers	Perch[13] (freshwater); Mummichogs [14] Rockfish[11] Sticklebacks[25] (marine)	Loons[4] Grebes[5,26] Egrets[27] Herons[27] Osprey[17] Terns[26] Songbirds[18] (Warblers, Flycatchers, Wrens, Blackbirds, Sparrows) Herring Gulls[59]	Cormorants[28] Osprey[5,19] Terns[26,28], skuas[49]	Otter[21,22] Sea Turtles[29, 52] Seals[23], toothed whales[53,54]	Bass[10,30,31] Bream[11] Mullet[11] Walleye[31]	Barracuda[11] Mackerel[11] Mullet[11] Scabbard-fish[11] Sharks[11,32] Swordfish[11, 45] Tuna[11,32]	
Tropical Rainforest	South Pacific and South Atlantic and Indian Oceans and associated estuaries, lakes, rivers	Catfish[23] Piranha[34] Snook[11] (freshwater); Bay Snook[11,34] (marine)	Egrets[27] Herons[27] Kingfishers[35] Songbirds[36] (Wrens, Thrushes, Flycatchers)	Albatrosses[37,38] Noddy[39, 47] Shearwaters[39] Terns[39, 47]Tropicbirds[39], Frigatebirds[4], penguins[48]	Otter[40] Sea Turtles[29] Seals[41], toothed whales[55,56]	Catfish[11] Snakehead[11]	Barracuda[11] Grouper[42] Sharks[43,44,46] Snapper[11] Swordfish[46] Tuna[46]	

[1]Kenney et al. 2014, [2]AMAP 2011, [3]Riget et al. 2007, [4]Evers et al. 2014, [5]Jackson et al. 2016, [6]Braune 2007, [7]Rush et al. 2008, [8]Dietz et al. 2013, [9]Gantner et al. 2010, [10]Eagles-Smith et al. 2016, [11]Evers et al. 2016a, [12]Wagemann, and Kozlowska 2005, [13]Wiener et al. 2012, [14]Weis and Kahn 1990, [15]Evers et al. 2011, [16]Bowerman et al. 1994, [17]Odsjo et al. 2004, [18]Jackson et al. 2015, [19]Wiemeyer et al. 1988, [20]Goodale et al. 2008, [21]Yates et al. 2005, [22]Klenavic et al. 2008, [23]Brookens et al. 2008, [24]Dam and Bloch 2000, [25]Eagles-Smith and Ackerman 2009, [26]Ackerman et al. 2016, [27]Frederick et al. 2002, [28]Braune 1987, [29]Day et al. 2005, [30]Kamman et al. 2005, [31]Monson et al. 2011, [32]Cai et al. 2007, [33]Bastos et al. 2015, [34]Mol et al. 2001, [35]Lane et al. 2011, [36]Townsend et al. 2013, [37]Finkelstein et al. 2006, [38]Burger and Gochfeld 2000, [39]Kojadinovic et al. 2007, [40]Fonseca et al. 2005, [41]Marcovecchio et al. 1994, [42]Evers et al. 2009, [43]Kiszka et al. 2015, [44]Maz-Courrau et al. 2012, [45]Storelli and Marcotrigiano 2001, [46]Bodin et al. 2017, [47]Sebastiano et al. 2017, [48]Carravieri et al. 2016, [49]Carravieri et al. 2017, [50]Bustamante et al. 2016, [51]Anderson et al. 2010, [52]Maffucci et al. 2005, 53 Correa et al. 2013, 54 Aubail et al. 2013, 55 Bustamante et al. 2003, 56 Garrigue et al. 2016, [57]Brown et al. 2016, [58]Burgess et al. 2013, [59]Weseloh et al. 2011

7.5.1.1 Human health bioindicators

There are many communities that partly depend on wild animals for subsistence, including marine fish (e.g., tuna and billfish around the world), freshwater fish (e.g., bass and pike in temperate lakes; catfish and tigerfish in tropical rivers), and marine mammals (cetaceans and pinnipeds in the Arctic). Depicting patterns of dietary MeHg uptake in humans are illustrated for marine fish at a global level (e.g., tuna, Figure 1) and in Small Island Developing States at a local level (e.g., Seychelles Study, Figure 2). Freshwater lakes and rivers have many examples of elevated fish Hg concentrations around the world, especially in temperate regions (e.g., Scandinavia) and in the tropics (e.g., South America). In the Arctic, fish and marine mammals are regularly taken by subsistence communities as important protein sources for a large portion of the population as well described by the Arctic Monitoring Assessment Program (AMAP 2011).

Global Oceans – Case Study: Tuna species are one of the most important global sources of marine fish. Total FAO commercial harvests are nearly 3.5 million tonnes per year – although this may not include all fisheries properly and harvests could be higher (Pauly and Zeller 2016). Muscle Hg concentrations and commercial harvest vary widely by species (Figure 2). The smallest tuna species (e.g., skipjack tuna and yellowfin tuna) have average Hg concentrations under the U.S. EPA advisory level of 0.30 ppm (ww), while the largest species (e.g., Pacific and Atlantic bluefin tunas) have the highest average Hg concentrations. Even these patterns can vary though by size class within species and ocean basis origin. For example, while yellowfin tuna tends to have lower average muscle Hg concentrations than seven of the nine tuna species with known Hg body burdens (Figure 2), individuals over 70kg are recommended to be avoided because of higher risks from Hg contamination (Bosch et al. 2016). Yellowfin and bigeye tuna Hg concentrations grouped by major ocean basin indicates that the eastern and northern areas of the Pacific Ocean have significantly higher Hg concentrations than other ocean basins (Ferriss et al. 2011, Nicklisch et al. 2017) – an area where there are increasing tuna Hg concentrations recorded over the past decade (Drevnick et al. 2015, Drevnick and Brooks 2017) and modelled for several decades thereafter (Sunderland et al. 2009). When considering the size of tuna and its origin another factor to consider is that processed tuna (e.g., canned) tends to be lower than fresh tuna in their Hg concentrations (Garcia et al. 2016).

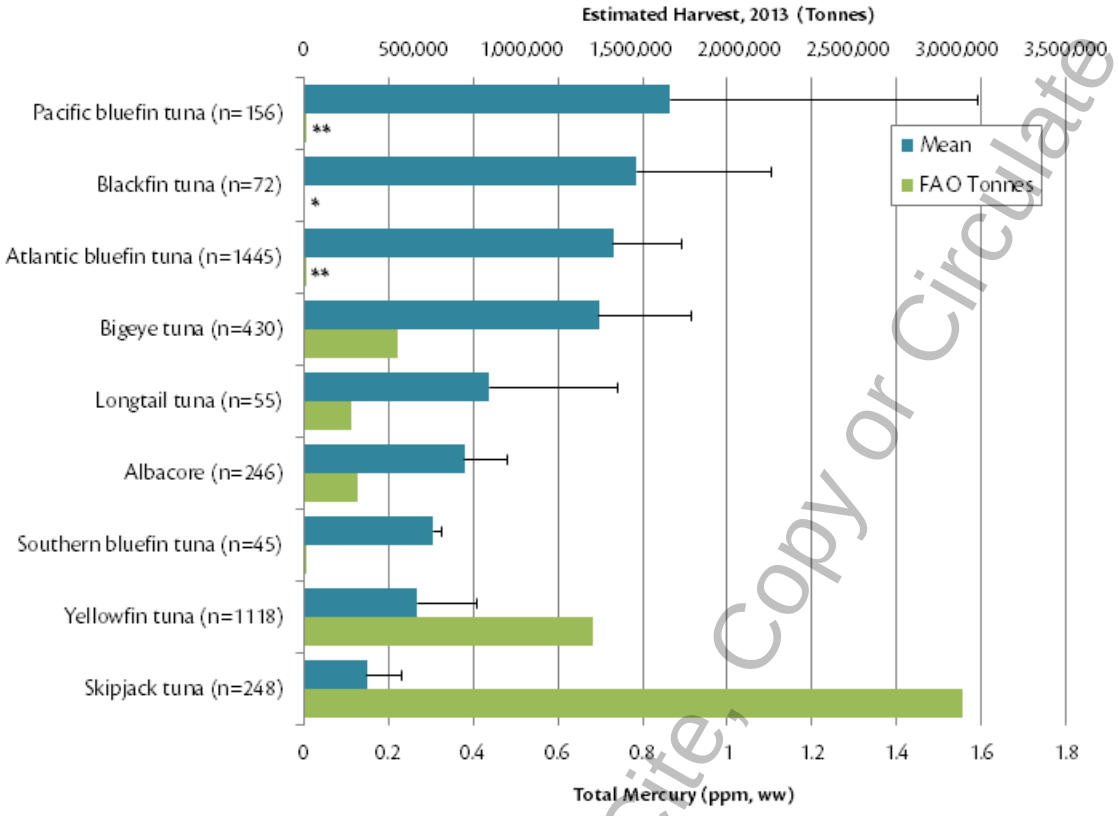

Figure 2. Average total Hg concentrations (ppm, ww) in muscle tissue of six tuna species compared with the FAO harvests estimates (in tonnes) and tuna with harvests of 10-15,000 tonnes are depicted with ** and tuna with harvest of <5,000 tonnes are depicted with *.

Small Island Developing States - Seychelles Case Study: Large pelagic species such as billfishes are one of the more appropriate bioindicators for developing and understanding broad spatial gradients of Hg contamination in the world's oceans. Mercury body burdens in billfish, such as marlin (Drevnick and Brooks 2017, Vega-Sanchez et al. 2017) and swordfish (Mendez et al. 2001, Branco et al. 2007), are some of the highest known for marine teleost fish (Table 1; Rodrigues and Amorim 2016). In swordfish, Hg body burdens vary according to major ocean basin with a tendency for the northern hemisphere having more elevated Hg concentrations than the southern hemisphere ocean basins (Figure 3; 0.83 +/- 0.42 ppm in the North and 0.38 +/- 0.34 in the South). In addition to their high trophic level and relatively long lifespan, swordfish have important commercial value and are an important income source for many Small Island Developing States (SIDS). In the Indian Ocean, 27,000 tonnes of swordfish have been harvested annually during 2006-2013 (including 270 tonnes caught by local semi-industrial fishing fleets in the Seychelles Exclusive Economic Zone-EZZ) and are mainly exported as whole fish to the

European Union (EU) (SFA 2016). The Seychelles Fisheries Authority (SFA) recently reported total Hg concentrations of 0.7±0.4 ppm (ww) measured in Seychelles swordfish edible muscle, with Hg levels increasing with fish size (Hollanda et al., in prep).

The Seychelles, as other SIDS (such as Sri Lanka; Jinadasa et al. 2014), are required to determine the muscle total Hg concentrations of swordfish and other large fish species, when exporting to the European Union (EU) – which requires fish imports to have <1.0 ppm (ww) in tissue edible for humans. Fish that are over this advisory level by the EU are not permitted (i.e., large-sized specimens with the highest commercial value) and either remain within the Seychelles or are exported to other countries for less value, which have a significant adverse economic cost on the Seychelles fishing industry and the overall country. The Seychelles semi-industrial fishing fleet is thus trying to switch from swordfish to tuna, as tuna species within the EZZ generally have Hg concentrations < 0.5 ppm (ww) (Bodin et al., 2017). This recent fishing development however may not be a long-term solution to cover the economic lost with swordfish because of the declining status of tuna populations in the Indian Ocean (e.g., yellowfin tuna: overexploited; bigeye tuna: fully exploited; IOTC 2016)

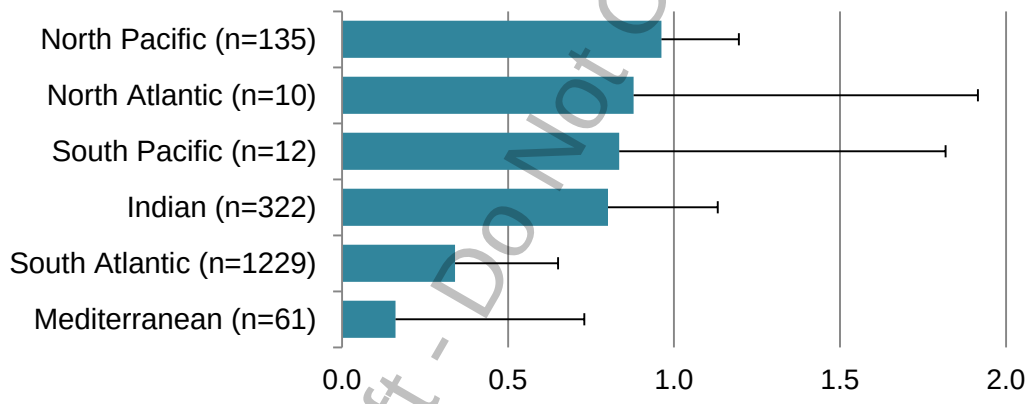

Figure 3. Average total Hg concentrations (ppm, ww) in muscle tissue of one billfish species, the swordfish, in six ocean basins.

Temperate Lakes - Scandinavian Case Study: Freshwater fish across the Fennoscandian shield have been sampled over 50 years in more than 3,000 lakes and streams. Studies on temporal trends over the recent half decade show trends of decreasing Hg concentrations in freshwater fish. Mercury levels in the southern part of the region (55°N–64°N (S)) are generally higher relative those found in the north (64°N–70°N (N)). Fennoscandian fish Hg data (ww in the muscle tissue) covers important fish species for

recreational fishing with perch (*Perca fluviatilis*) (S: 0.31 ± 0.27 ppm (n=20,276), N: 0.23 ± 0.18 ppm (n=2,326)), pike (*Esox lucius*) (S: 0.69 ± 0.36 ppm (n=24,849),N: 0.56 ± 0.36 ppm (n=3,360)), and Arctic char (*Salvelinus alpinus*) (S: 0.46 ± 0.31ppm (284), N: 0.09 ± 0.04 ppm (514)) having a tendency for higher Hg body burdens in the southern vs. the northern part of Scandinavia.

Tropical rivers - South American Case Study: The major river basins of South America, including the Magdalena, Orinoco, Amazon and La Plata, support a large freshwater fishery, providing livelihoods for small-scale artisanal fisherman as well as major commercial enterprises (Barletta et al. 2010). In the interior, more remote areas of South America, *ribeirinho* communities are highly dependent on freshwater resources for their subsistence and for communities with high fish consumption, the risk of exposure to Hg and MeHg can also be high (Oliveira et al. 1010). Extensive research over several decades in the Amazon Basin has repeatedly identified the linkage between a diet high in fish consumption, particularly piscivorous and omnivorous species, with elevated concentrations of Hg in human biomarkers such as hair (Bidone et al. 1997; Lebel et al. 1997; Castillhos et al. 1998; Boischio and Henshel 2000; Bastos et al. 2006; Faial et al. 2015).

The GBMS database for South America contains over 170 peer-reviewed publications on fish Hg concentrations from more than 240 sites within 100 different waterbodies. From these published sources, more than 27,000 individual fish from more than 240 genera are represented. Mean Hg concentrations range from below detection limit to 4.4 ppm (ww). The most commonly sampled taxa include species within the *Hoplias* (tigerfishes), *Serrasalmus* (piranhas), *Pseudoplatystoma* (sorubim catfishes), *Cichla* (neotropical cichlids) and *Odontesthes* (silversides) genera. Data from the South American GBMS database highlight areas of extensive freshwater sampling (e.g., Madeira and Tapajos rivers of Brazil) as well as areas where extensive data gaps exist (e.g., the countries of Paraguay and Guyana).

From these data, biological Hg hotspots of concern for ecological and human health start to emerge (Figure 1). Much of the research on Hg in environmental and human Hg exposure has been conducted in areas impacted by ASGM. For effective long-term biomonitoring, and the establishment of regional baselines of Hg concentrations, future monitoring may also need to be conducted in areas where currently little or no information is available (e.g., Paraguay and Guyana).

Arctic – AMAP Case Study: The Arctic Monitoring Assessment Programme (AMAP) regularly fosters international collaboration and compiles measurements of Hg levels in arctic biota, including shellfish,

freshwater and marine fish, seabirds, marine and terrestrial mammals and people. Temporal trends from 83 long time-series for Hg in biota monitored at 60 sites around the Arctic establish one of the best standardized, long-term biomonitoring efforts for Hg in the world (AMAP 2011). There is a need for a concerted international effort to reduce Hg levels in the Arctic environment, because of (1) long-range atmospheric transport of Hg from distance source regions including increasing emissions in east Asia that total approximately 100 tons of Hg to the Arctic, (2) changing climate of warmer and longer ice-free seasons potentially promoting the production of MeHg, (3) the release of Hg stored over the previous millennia in permafrost, soils, sediments and glaciers, and (4) the close association of native communities of people reliant on biota that are often upper trophic level species with elevated Hg body burdens (AMAP 2011, Dietz et al. 2013, Scheuhammer et al. 2015). Studies indicate that there has been a ten-fold increase in Hg levels in birds and marine mammals over the past 150 years with an average annual rate of increase of 1-4% (AMAP 2011). More recently over the last 30 years, temporal trends of MeHg bioaccumulation in Arctic fish and wildlife have been inconsistent, with Hg concentrations increasing in some cases but declining elsewhere depending on the species and location (Riget et al. 2011). Therefore, continued Hg biomonitoring is paramount to track the shifting Hg emissions and deposition and thereafter the bioavailability of MeHg in the foodweb across the Arctic region and protecting indigenous communities from contamination, especially in the eastern Canadian Arctic and Greenland (AMAP 2011) and in consideration that global climate changes are creating further uncertainty (Mckinney et al. 2015).

7.5.1.2 Ecological health bioindicators

There are many species of fish and wildlife that are at risk to the adverse impacts of Hg on their physiology, behaviour and reproductive success (Dietz et al. 2013, Scheuhammer et al. 2015, Ackerman et al. 2016, Evers 2017, Whitney and Cristol 2017). Some species are considered high profile and are listed by IUCN on their Red List, or listed as threatened or endangered by the United States.

The selection of the proper suite of bioindicators depends on the question. Taxa suitability may vary according to ecosystem interests (e.g., at habitat or biome levels of relevance), spatial gradient resolution (e.g., local, regional or global), temporal timelines (e.g., short- or long-term), human or ecological health interests, endpoints of importance (e.g., reproductive impairment), known adverse thresholds (e.g., by tissue and taxa using endpoints of interest), sampling availability (e.g., simple or challenging), and sampling outcome (e.g., non-lethal or lethal). A provisional slate of some potential bioindicators for evaluating and monitoring environmental Hg loads for ecological health purposes can

be grouped in four target biomes and their associated waterbodies and by major taxa of interest (Table 3; Evers et al. 2016b).

Sharks – Case Study: Many elasmobranchs (sharks, skates and rays) are well above the human health advisory levels set by the World Health Organization (1.0 ppm, ww; Table 1). Species within the mackerel and ground sharks generally have elevated Hg body burdens (de Pinho et al. 2010, de Carvalho et al. 2014, Teffer et al. 2014, Matulik et al. 2017) and are of particular concern because of their high conservation status and that they are often used for food in some places (e.g., Central America). Although human health standards are well-established for the consumption of fish based on their Hg concentrations, the potential adverse impacts of MeHg on organisms, like sharks, are not well understood. Chronic dietary MeHg uptake of 0.2 ppm (ww) in freshwater fish had effects on reproduction and other subclinical endpoints (Depew et al. 2012). While most sharks are well over this threshold level and many shark populations are experiencing declines, it is challenging to link MeHg toxicity to significant adverse effects. Of the 14 shark genera with published muscle Hg concentrations, average levels exceed 1.0 ppm (ww) in 71% of the genera.

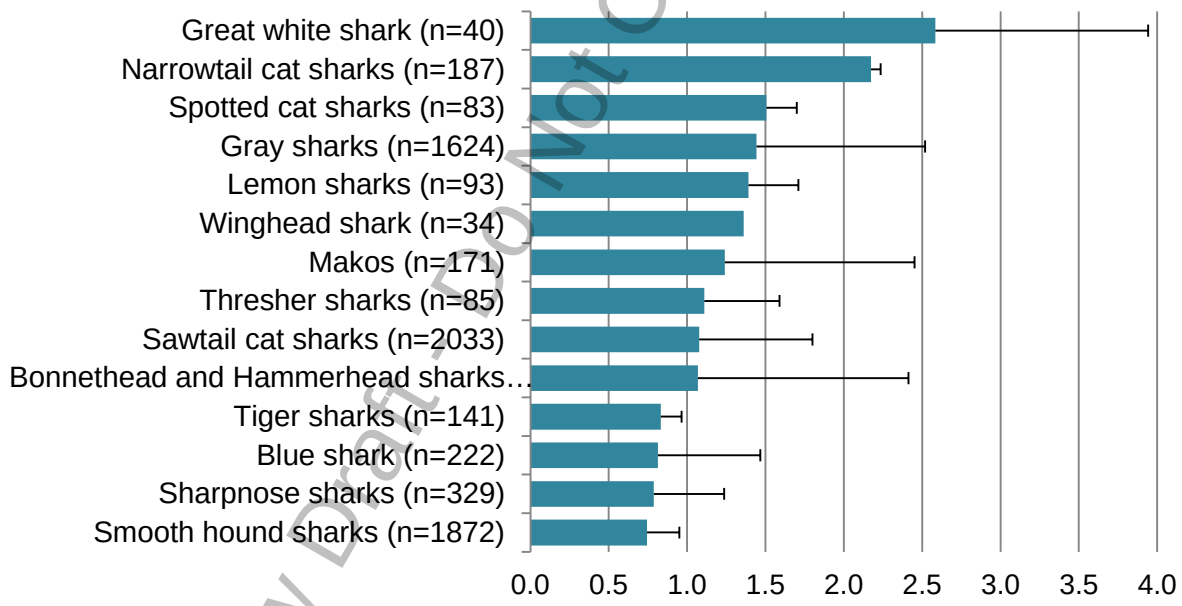

Figure 4. Average total Hg concentrations (ppm, ww) in muscle tissue of sharks by genus from the Orders of Mackerel and Ground Sharks.

Seabirds – Case Study: Marine Birds Case Study: Most seabirds are situated high in the food web, so they experience the biomagnification process and thus are highly exposed to MeHg (Monteiro and

13379 Furness 1995). Because of their feeding ecologies and specific features (e.g., breeding sequence,
13380 molting, foraging ranges, migration patterns), seabirds generally have elevated body burden of Hg which
13381 can reduce their reproductive capacity and impact their demography (Tartu et al. 2013, Goutte et al.
13382 2014ab). To date, a large number of studies have focused on seabirds from tropical to polar regions and
13383 from coastal to oceanic zones, covering most of the world's oceans (Table 1; Elliott and Eliott 2013). On
13384 a global scale, seabirds show a wide range of Hg concentrations regardless of the tissue examined
13385 (feathers, blood, eggs) with broad spatial differences as well as variation according to the phylogeny. For
13386 instance, penguins have the lowest Hg concentrations in eggs, blood and feathers (with the exception of
13387 tropicbirds in feathers), whereas Procellariiforms (e.g., petrels, shearwaters and albatrosses) generally
13388 had the highest ones (Table 1). Procellariiforms are the best studied group and they display a wide range
13389 of tissue Hg concentrations which reflect some phylogenetic differences. Seabirds within the family
13390 Diomedea (i.e., albatrosses) have the highest Hg concentrations among all seabirds (Muihead and
13391 Furness 1988; Stewart et al. 1999; Anderson et al. 2010).

13392 The most important factor for predicting seabird Hg exposure, and therefore risk, is their foraging
13393 ecology. Because seabirds feed on a wide range of habitats, from the littoral zones to the oceanic
13394 environment (e.g., benthic and pelagic), they reflect Hg contamination from different parts of the
13395 ecosystems both horizontally (e.g., coastal, benthic and oceanic food webs) and vertically (i.e. epipelagic
13396 and mesopelagic food webs). Therefore, the study of a group of seabirds with contrasting ecologies from
13397 the same region allows determination of MeHg availability for multiple marine zones and therefore a
13398 more holistic view (Ochoa-Ocuña et al., 2002). As an example, crustacean-feeding seabirds have lower
13399 Hg exposure than cephalopod- and fish-feeders (Carravieri et al. 2014) and epipelagic seabirds have
13400 lower Hg exposure than those relying on mesopelagic prey (Ochoa-Ocuña et al., 2002). Therefore,
13401 seabirds of the highest trophic levels with high Hg intakes (such as albatrosses or skuas), can suffer the
13402 effects of MeHg toxicity that are associated with potential long-term declines in their populations
13403 (Goutte et al. 2014a, b).

13404 In storm petrels from the northern hemisphere they have 10 times higher concentrations in the feathers
13405 than those from the southern hemisphere (14.1 ± 3.9 vs 1.6 ± 1.4 ppm, respectively). Such a difference is
13406 not found for albatrosses between hemispheres, but these patterns should be explored further and
13407 should be based on seabirds sharing not only close phylogeny but similar trophic ecology.

13408 Seabirds permit Hg monitoring across large geographical scales and variations within the same species
13409 over longitudinal (e.g., brown noddy) or latitudinal scales (e.g. skuas). The differences of Hg
13410 contamination recorded in seabird tissues does reveal both differences of major ocean basin
13411 contamination and latitudinal gradients of contamination for a single basin.

13412

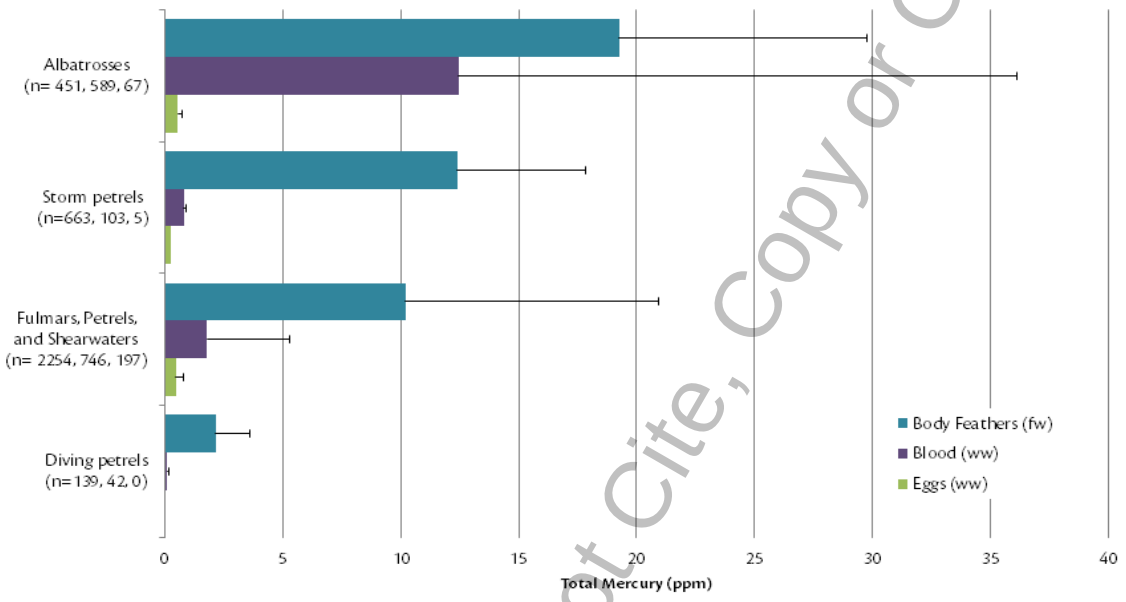

13413

13414 Figure 5. Average total Hg concentrations (ppm) in three tissues (fw in feathers, ww in blood and eggs) of seabird
13415 families within the Order Procellariformes.

13416 Loons/Divers – Case Study: Species within the Order Gaviiformes (loons or divers) are piscivores that breeding on
13417 freshwater ponds and lakes in temperate and Arctic areas of the Northern Hemisphere. The larger loon species
13418 (Common Loon, *Gavia immer*, and Yellow-billed Loon, *Gavia adamsii*) are obligate piscivores and in response, have
13419 some of the highest average Hg body burdens of birds in the world (Table 2). In the winter, all loon species
13420 migrate to marine ecosystems (with parts of some populations overwintering on freshwater lakes). Loons have
13421 been used as bioindicators of MeHg availability in both their breeding and wintering areas for several decades
13422 (Evers et al. 1998, 2008, 2011a, 2014; Jackson et al. 2016). In Canada, the Common Loon and its prey are being
13423 used to evaluate the success of national regulatory standards to reduce Hg emissions to the landscape
13424 (Scheuhammer et al. 2016). The effects of Hg on loon reproductive success are now well established (Evers et al.
13425 2011, Depew et al. 2012b) and are used as benchmarks for evaluating ecological concern.

Landbirds – Case Study: Many species of invertivorous birds (e.g., herein landbirds) are at high risk to Hg exposure. Avian invertivores often have higher body burdens of Hg within an ecosystem versus avian piscivores (Evers et al. 2005) and may have higher sensitivity to MeHg adversely impacting their rates of reproductive success (Heinz et al. 2009, Jackson et al. 2011a). There are now an increasing number of studies that have characterized Hg exposure in one group of landbirds, songbirds (Order Passeriformes); and, within the group of songbirds, certain species and breeding habitats are at higher risk than others. Generally gleaning and flycatching songbirds that breed in wetland habitats (Edmonds et al. 2010, Jackson et al. 2011b, Lane et al. 2011, Jackson et al. 2015, Ackerman et al. 2016), including rice fields (Abeysinghe et al. 2017), are at highest risk to Hg exposure, especially species that forage on predaceous arthropods such as spiders (Cristol et al. 2008). Songbird species where most of their annual life cycle is within wetland-oriented ecosystems and that migrate long-distances (e.g., neotropical migrants or palearctic migrants) may be at greatest risk to chronic Hg exposure adversely impacting reproductive success and ultimately population viability.

Marine Mammals – Case Study: Toothed whales and some pinnipeds (or seals) are the marine mammal taxa of greatest concern for human and ecological health purposes, with high concentrations of Hg recorded in brain tissue with associated signs of neurochemical effects (Table 1, Dietz et al. 2013). Many subsistence communities, mostly in the Arctic, depend on the harvest of species such as the narwhal, beluga, pilot whales, and ringed seals (Table 3). Although the effect levels in marine mammals is little understood (Desforges et al. 2016), a study on bottle-nosed dolphins found lesions were created in the liver at 61 ppm (ww) and are being used by scientists as a good benchmark for assessing ecological concern (Dietz et al. 2013). While liver tissue generally has a small percentage of MeHg and is challenging to relate to muscle tissue (which is a more relevant tissue to relate for human health purposes, Table 1), most species of toothed whales have average muscle tissue Hg concentrations well above 1.0 ppm (ww) (which generally has >95% MeHg content).

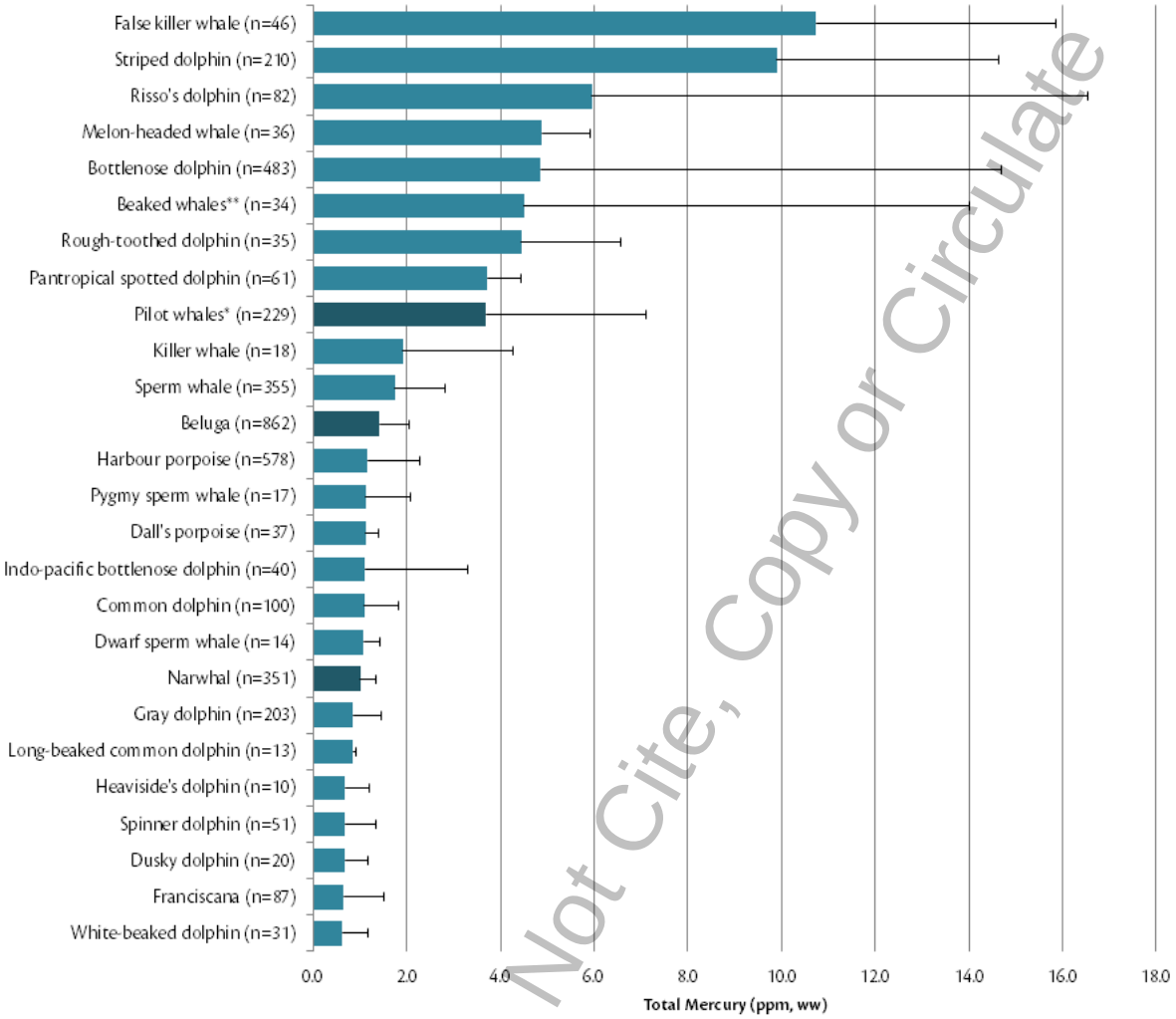

13450

13451 Figure 6. Average total Hg concentrations (ppm, ww) in muscle tissue of toothed whales by species (except beaked
13452 whales were combined under the family, Hyperoodontidae, and the two species of pilot whales were grouped).

13453 Therefore, toothed whales appear to be one of the most vulnerable groups of marine mammals with
13454 mean Hg concentrations (2.61 ppm, ww; Table 1) well above the WHO human health advisory level
13455 (which is most relevant with beluga and pilot whales, because of the dependence of certain Arctic
13456 human communities on them) and several species over 4.0 ppm (ww) (Figure 6). Various species of
13457 porpoises and dolphins (Aubail et al. 2013, Correa et al. 2013), as well as beaked whales (which
13458 specialize in foraging on deep water cephalopods) generally have elevated Hg body burdens (Figure 6;
13459 Bustamante et al. 2003, Garrigue et al. 2016).

7.5.2 Overarching global patterns

The compilation of existing biotic Hg data is an important approach to understand broad spatial gradients and temporal patterns. Models based on existing data and scientific findings are useful for extending observations in space and time. Recent global modelling efforts show 55% of global Hg(II) deposition occurs over the tropical oceans (Horowitz et al., 2017). Ocean cruise observations also show high MeHg concentrations in seawater in equatorial upwelling regions of the ocean (Mason and Fitzgerald, 1993).

In freshwater ecosystems, large contaminated sites are expected to be a main driver of variability in freshwater biota concentrations. One recent effort to characterize global aquatic Hg releases to inland ecosystems is therefore especially important for understanding the spatial distribution of these locations (Kocman et al., 2017). One major driver of such spatial patterns is the location of artisanal and small-scale gold mining (ASGM) activities in developing countries (Figure 7).

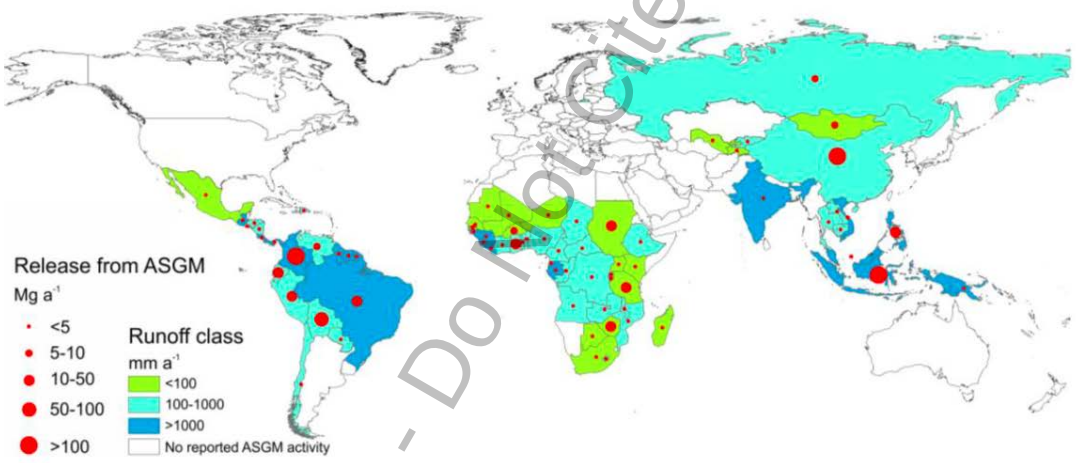

Figure 7. Global release of Hg from ASGM activities.

7.5.2.1 Spatial Gradients

The availability of MeHg to high trophic level organisms is not uniform across the world. Some ecosystems are more sensitive to Hg input than others (Driscoll et al. 2007) and it is these areas where biological Hg hotspots can form and are especially pronounced in higher trophic level organisms (Evers et al. 2007). Such areas are generally associated with wetlands and can be particularly pronounced in ecosystems with water chemistry variables such as low pH, moderate to high dissolved organic carbon

concentrations, and low to moderate primary productivity. Fluctuating water levels can have a particularly important contribution in generating higher methylation rates and increases in MeHg bioavailability; and, may happen at daily (e.g., estuaries), monthly (artificial reservoirs), or ever seasonal (transition to wet season in the tropics) timeframes. Therefore, the determination of areas that may be elevated with MeHg availability does not have a linear relationship of the deposition or release of Hg into the environment. As an example, some of the lowest air Hg deposition levels in North American are in Kejimkujik National Park in Nova Scotia, Canada, yet the biotic MeHg exposure is some of the highest in North America for fish and loons (Evers et al. 1998, Wyn et al. 2010). The identification of potential biological Hg hotspots can be made through the collection of existing biotic data (Evers et al. 2011) and modelling ecosystem sensitivity.

7.5.2.2 Temporal Trends

New models simulating the deposition of Hg from anthropogenic emissions at global scales indicate a decrease of up to 50% in the Northern Hemisphere and up to 35% in the Southern Hemisphere (Pacyna et al. 2016). While tracking Hg emissions, deposition and releases are important tools for understanding patterns of environmental Hg loads, but the relationship between modelled (or measured) deposition and concentrations biota is poorly understood. Trends in Hg concentrations are thought to differ among ocean basins because anthropogenic emissions have strongly declined in North America and Europe, leading to large declines in atmospheric concentrations, especially in the Atlantic Ocean (Zhang et al., 2016). Lee and Fisher (2016) postulated that this may also explain observed declines in Atlantic Bluefin tuna Hg concentrations between 2004 and 2012 in the North Atlantic Ocean.

By contrast, both atmospheric emissions and freshwater discharges of Hg have been growing on the Asian continent leading to increased Hg pollution in the North Pacific Ocean (Streets et al., 2009; Sunderland et al., 2009, Zhang et al. 2015). Temporal data on fisheries in the North Pacific are more limited but some researchers have suggested there is evidence for increases in tuna Hg concentrations over the past several decades (Drevnick et al., 2015) which is further supported in an additional analyses of bigeye tuna for the same area (Drevnick and Brooks 2017).

As an example of the importance of generating baselines and how factors, such as climate change, are key can be found in Canada. Total Hg levels in aquatic birds and fish communities have been monitored across the Canadian Great Lakes by Environment and Climate Change Canada for the past 42 years (1974–2015) at 22 stations (Blukacz-Richards et al. 2017). For the first three decades, Hg levels in gull

eggs and fish declined at all stations. In the 2000s, trend reversals were apparent for many stations and in most of the Great Lakes, although the specific taxa responsible varied. While strong trophic interactions among birds and fish is apparent, there also appears to be the strong likelihood of a trophic decoupling in some areas, which indicates the importance of not only long-term Hg biomonitoring efforts, but study designs that include other parameters that could be influenced by climate change (Pinkney et al. 2015).

7.5.3 Biomonitoring programs

Outside of the AMAP program (featured earlier in this chapter), an analysis of the geographical coverage of Hg biomonitoring networks reveals a general lack of national initiatives around the world. Per information gathered as part of the UNEP review of biomonitoring programs, there are no such national activities being undertaken in Africa and Australia (UNEP 2016). Most Asian countries are minimally involved with national initiatives to monitor Hg levels in biota, with notable exceptions of Japan and the Republic of Korea where more extensive programs exist.

In North America, Canada's Northern Contaminants Program is an example of an integrated initiative for Hg monitoring throughout Canada's vast Arctic territory (NCP 2017). Since its establishment in 1991, the program has focused on the measurement of contaminants (including Hg) in fish and wildlife that are traditional foods of northern Indigenous peoples. Monitoring and research funded by the program generates science on abiotic processes, spatial and temporal trends of MeHg bioaccumulation in biota, and human exposure to Hg from wild foods. One of the strengths of the program is the interdisciplinary approach taken to assess and monitor risks of Hg to ecological and human health through the participation of Indigenous organizations, environmental scientists, and human health professionals.

In addition to the AMAP program, there is an additional example of an international collaboration called ARCTOX, a program where seabird blood and feather samples have been collected over 54 Arctic sites and on a total of 14 seabird species (although not every species are sampled at each site). Samples are currently being collected or planned across Arctic countries, including U.S., Canada, Greenland, Scandinavia, and Russia.

Meanwhile, the hundreds of local studies, which are reflected within the GBMS database, are conducted by the global scientific community and together provide a comprehensive and geographically balanced global data platform about existing biotic Hg concentrations (Table 1). Based on the GBMS database, some of the countries with the highest fish consumption are poorly covered by biomonitoring efforts

(e.g., Western and Central Africa [except Ghana] and many parts of Asia). Additional efforts are therefore needed to develop and implement projects to fill geographic and ecosystem gaps. Although national efforts can be keystones for regional biomonitoring networks, local scientific studies can make a significant and welcome contribution toward better identifying where, what and when to conducting biomonitoring.

To provide sustainable and long-term biomonitoring capacity in key regions around the world (e.g., Arctic, tropical areas associated with ASGM, and SIDS), the focus should be placed on expanding and stabilizing existing national initiatives. Moreover, it is crucial to foster international collaboration and coordination among national projects to create harmonized regional approaches, and to strive, where possible, to integrate biomonitoring activities into an interdisciplinary framework to assess ecological and human health risk that can be stitched together to represent regional and eventually global spatiotemporal patterns.

7.5.4 Linkages between Hg source types and biota

Linkages between major Hg source types and biota can now be accomplished with confidence through the use of Hg isotopes (Blum et al. 2014, Kwon et al. 2014). Mercury isotopes can separate the origin of Hg from coal burning facilities, chlor-alkali facilities, gold mining, and other source types. Separation of current major Hg source types from existing contaminated sites are of interest to identify how they may influence human and ecological health as characterized through bioindicators for purposes related to the Minamata Convention (Evers et al. 2016b).

7.6 Summary of Findings

In summary, the careful selection and use of bioindicators that closely match objectives of the interested parties can be a cost-effective and time efficient way to track human and ecological health from the anthropogenic loading of Hg onto the water and landscape at a global level (Evers et al. 2016b). The methods for biomonitoring and the interpretation of the tissues sampled are generally well-described for our target taxa. The extensive knowledge of Hg exposure in a wide range of fish and wildlife that are available in the peer-reviewed literature and now in the GBMS database provide a platform for best selecting the proper species or guild and to know what taxa can provide the upper levels of MeHg dietary uptake within a certain biome or waterbody. Biomonitoring should build from existing programs, which are generally found within developed countries at local, national and

sometimes regional levels. Global pilot projects based on existing networks with local organizations and governmental agencies have been tested for fish (Buck et al. Submitted) and humans (Trasande et al. 2016) and biomonitoring approaches in temperate marine ecosystems are well described (Evers et al. 2008). Generating a more global approach that can stitch together the existing biomonitoring programs and identify the ecosystem, taxa, or geographic gaps can be completed within a structured plan. Once country needs and interests of the Minamata Convention are determined at the Conference of Parties, it is feasible to generate a biomonitoring approach that will assist in evaluating the effectiveness of parts of the treaty.

7.7 Critical Knowledge Gaps

By identifying critical knowledge gaps and adopting quantitative and replicable approaches a harmonized biomonitoring effort can be developed for all countries to use. One potential approach is to create a technical toolkit (i.e., spreadsheet of multiple data layers) that can quantify where, when, how and what to monitor for tracking environmental Hg loads, their changes over time, and potential impacts to human and ecological health. An Expert Group, compilation of existing data, and the development of a biomonitoring toolkit would provide: (1) a group of scientists and policymakers who can serve as advisors to the Conference of Parties, (2) a standardized and comprehensive database made available to Parties; (3) a peer-reviewed scientific platform of biomonitoring information (existing and new) that can be translated for policy purposes; and (4) a demonstrated model for training local field biologists and lab technicians that will ultimately build regional capacity and independence.

Iterative efforts to link realistic and applied biomonitoring efforts at local levels with science groups dedicated toward assisting the Conference of Parties of the Minamata Convention will help keep pace with the many emerging scientific findings that may fill existing information gaps that will be key for global policymaking.

7.8 References

Abeysinghe KS, Qiu G, Goodale E, Anderson CW, Bishop K, Evers DC, Goodale MW, Hintelmann H, Liu S, Mammides C, Quan RC. 2017. Mercury flow through an Asian rice-based food web. Environmental Pollution. 229:219-228.

Ackerman JT, CA Eagles-Smith, MP Herzog, CA Hartman, SH Peterson, DC Evers, AK Jackson, JE Elliott, SS Vander Pol, and CE Bryan. 2016. Avian mercury exposure and toxicological risk across western North America: A synthesis. Science of the Total Environment 568:749-769.

AMAP, 2011. AMAP Assessment 2011: Mercury in the Arctic. AMAP, Oslo. 2011.

and D. Perry. 2011. Mercury in breeding saltmarsh sparrows (*Ammodramus caudacutus*). Ecotoxicology 20:1984-1991.

Anderson, O.R.J., Phillips, R.A., Shore, R.F., McGill, R.A.R., McDonald, R.A., Bearhop, S. 2010. Element patterns in albatrosses and petrels: influence of trophic position, foraging range, and prey type. Environ. Pollut. 158:98–107.

Aubail, A., Méndez-Fernandez, P., Bustamante, P., Churlaud, C., Ferreira, M., Vingada, J.V. and Caurant, F., 2013. Use of skin and blubber tissues of small cetaceans to assess the trace element content of internal organs. Marine Pollution Bulletin 76:158-169.

Barletta, M, AJ Jaureguizar, C Baigun, NF Fontoura, AA Agostinho, VMF Almeida-Val, AL Val, RA Torres, LF Jimenes-Segura, T Giarrizzo, NN Fabre, VS Batista, C Lasso, DC Taphorn, MF Costa, PT Chaves, JP Vieira, MFM Correa. 2010. Fish and aquatic conservation in South America: a continental overview with emphasis on neotropical systems. Journal of Fish Biology 76:2118-2176.

Bastos, WR, JG Dórea, JV Bernardi, LC Lauthartte, MH Mussy, LD Lacerda, and O Malm. 2015. Mercury in fish of the Madeira River (temporal and spatial assessment), Brazilian Amazon. Environmental Research 140:191-197.

Bastos, WR, JPO Gomes, RC Oliveira, R Almeida, EL Nascimento, JVE Bernardi, LD de Lacerda, EG da Silveira, WC Pfeiffer. 2006. Mercury in the environment and riverside population in the Madeira River basin, Amazon, Brazil. Science of the Total Environment 368:344-351.

Bidone ED, ZC Casilhos, TM Cid de Souza, LD Lacerda. 1997. Fish contamination and human exposure to mercury in the Tapajoas River Basin, Para State, Amazon, Brazil: a screening approach. Bulletin of Environmental Contamination and Toxicology 59:194-201.

Blukacz-Richards EA, Visha A, Graham ML, McGoldrick DL, de Solla SR, Moore DJ, Arhonditsis GB. 2017. Mercury levels in herring gulls and fish: 42 years of spatio-temporal trends in the Great Lakes. Chemosphere 172:476-487.

Blum, J.D., Sherman, L.S. and Johnson, M.W. 2014. Mercury isotopes in earth and environmental sciences. Annual Review of Earth and Planetary Sciences 42:249-269.

Bodin, N., Lesperance, D., Albert, R., Hollanda, S., Michaud, P., Degroote, M., Churlaud, C. and Bustamante, P. 2017. Trace elements in oceanic pelagic communities in the western Indian Ocean. Chemosphere 174:354-362.

Boischio, AAP and D Henshel. 2000. Fish consumption, fish lore, and mercury pollution – risk communication for the Madeira River people. Environmental Research Section A 84:108-126.

Bosch AC, O'Neill B, Sigge GO, Kerwath SE, Hoffman LC. 2016. Mercury accumulation in Yellowfin tuna (*Thunnus albacares*) with regards to muscle type, muscle position and fish size. Food chemistry 190:351-356.

Bowerman IV, WW, ED Evans, JP Giesy and S Postupalsky. 1994. Using feathers to assess risk of mercury and selenium to bald eagle reproduction in the Great Lakes region. Archives of Environmental Contamination and Toxicology 27:294-298.

Branco, V., Vale, C., Canário, J. and dos Santos, M.N., 2007. Mercury and selenium in blue shark (*Prionace glauca*, L. 1758) and swordfish (*Xiphias gladius*, L. 1758) from two areas of the Atlantic Ocean. Environmental Pollution 150:373-380.

Braune BM. 1987. Comparison of total mercury levels in relation to diet and molt for nine species of marine birds. Archives of Environmental Contamination and Toxicology 16:217-224.

Braune, BM. 2007. Temporal trends of organochlorines and mercury in seabird eggs from the Canadian Arctic, 1975–2003. Environmental Pollution 148:599-613.

Brookens TJ, TM O'Hara, RJ Taylor, GR Bratton, and JT Harvey. 2008. Total mercury body burden in Pacific harbor seal, *Phoca vitulina richardii*, pups from central California. Marine Pollution Bulletin 56:27-41.

Brown, T.M., Fisk, A.T., Wang, X., Ferguson, S.H., Young, B.G., Reimer, K.J. and Muir, D.C. 2016. Mercury and cadmium in ringed seals in the Canadian Arctic: Influence of location and diet. Science of the Total Environment 545:503-511.

Buck, DG, DC Evers, E Adams, J DiGangi, B Beeler, J Samanek, J Petrlik, MA Turnquist, O Speranskaya, K Reagan. A rapid assessment of biological mercury hotspots at the global scale. Science of the Total Environment, In Review.

Burger, J. and Gochfeld, M. 2000. Metal levels in feathers of 12 species of seabirds from Midway Atoll in the northern Pacific Ocean. Science of the Total Environment 257:37-52.

Burgess, N.M., Bond, A.L., Hebert, C.E., Neugebauer, E. and Champoux, L. 2013. Mercury trends in herring gull (Larus argentatus) eggs from Atlantic Canada, 1972–2008: temporal change or dietary shift? Environmental Pollution 172:216-222.

Bustamante P, Garrigue C, Breau L, Caurant F, Dabin W, Greaves J, Dodémont R. 2003. Trace elements in two odontocetes species (*Kogia breviceps* and *Globicephala macrorhynchus*) stranded in New Caledonia (South Pacific). Environmental Pollution 124:263–271.

13650 Bustamante, P., Carravieri, A., Goutte, A., Barbraud, C., Delord, K., Chastel, O., Weimerskirch, H. and Cherel, Y., 2016. High
13651 feather mercury concentrations in the wandering albatross are related to sex, breeding status and trophic ecology
13652 with no demographic consequences. Environmental Research 144:1-10.
13653 Cai, Y, JR Rooker, GA Gill and JP Turner. 2007. Bioaccumulation of mercury in pelagic fishes from the northern Gulf of Mexico.
13654 Canadian Journal of Fisheries and Aquatic Sciences 64:458-469.
13655 Carravieri A, Cherel Y, Blévin P, Brault-Favrou M, Chastel O, Bustamante P. 2014. Mercury exposure in a large subantarctic avian
13656 community. Environmental Pollution 190C:51-57.
13657 Carravieri, A., Cherel, Y., Brault-Favrou, M., Churlaud, C., Peluhet, L., Labadie, P., Budzinski, H., Chastel, O. and Bustamante, P.,
13658 2017. From Antarctica to the subtropics: Contrasted geographical concentrations of selenium, mercury, and
13659 persistent organic pollutants in skua chicks (*Catharacta* spp.). Environmental Pollution 228:464-473.
13660 Carravieri, A., Cherel, Y., Jaeger, A., Churlaud, C. and Bustamante, P. 2016. Penguins as bioindicators of mercury contamination
13661 in the southern Indian Ocean: geographical and temporal trends. Environmental Pollution 213:195-205.
13662 Castilhos, ZC, ED Bidone, LD Lacerda. 1998. Increase of the background human exposure to mercury through fish consumption
13663 due to gold mining at the Tapajos River region, Para State, Amazon. Bulletin of Environmental Contamination and
13664 Toxicology 61:202-209.
13665 Correa, L., Castellini, J.M., Wells, R.S. and O'Hara, T. 2013. Distribution of mercury and selenium in blood compartments of
13666 bottlenose dolphins (*Tursiops truncatus*) from Sarasota Bay, Florida. Environmental Toxicology and Chemistry
13667 32:2441-2448.
13668 Costa, M., W. Landing, H. Kehrig, M. Barletta, C. Holmes, P. Barrocas, D.C. Evers, D. Buck, A. Vasconcellos, S. Hacon, J. Moreia,
13669 and O. Malm. 2012. Mercury in tropical and sub-tropical coastal environments. Environmental Research 119: 88-100.
13670 Cristol, D.A., Brasso, R.L., Condon, A.M., Fovargue, R.E., Friedman, S.L., Hallinger, K.K., Monroe, A.P. and White, A.E., 2008. The
13671 movement of aquatic mercury through terrestrial food webs. Science 320:335-335.
13672 Dam, M and D Bloch. 2000. Screening of mercury and persistent organochlorine pollutants in long-finned pilot whale
13673 (*Globicephala melas*) in the Faroe Islands. Marine Pollution Bulletin 40:1090-1099.
13674 Day RD, SJ Christopher, PR Becker, and DW Whitaker. 2005. Monitoring mercury in the loggerhead sea turtle, *Caretta caretta*.
13675 Environmental Science and Technology 39:437-446.
13676 de Carvalho, G.G.A., Degaspari, I.A.M., Branco, V., Canário, J., de Amorim, A.F., Kennedy, V.H. and Ferreira, J.R., 2014.
13677 Assessment of total and organic mercury levels in blue sharks (*Prionace glauca*) from the south and southeastern
13678 Brazilian coast. Biological Trace Element Research 159:128-134.
13679 de Pinho, A.P., Guimarães, J.R.D., Martins, A.S., Costa, P.A.S., Olavo, G. and Valentin, J., 2002. Total mercury in muscle tissue of
13680 five shark species from Brazilian offshore waters: effects of feeding habit, sex, and length. Environmental Research
13681 89:250-258.
13682 Depew, D.C., Basu, N., Burgess, N.M., Campbell, L.M., Devlin, E.W., Drevnick, P.E., Hammerschmidt, C.R., Murphy, C.A.,
13683 Sandheinrich, M.B. and Wiener, J.G. 2012a. Toxicity of dietary methylmercury to fish: derivation of ecologically
13684 meaningful threshold concentrations. Environmental Toxicology and Chemistry 31:1536-1547.
13685 Depew, D.C., Basu, N., Burgess, N.M., Campbell, L.M., Evers, D.C., Grasman, K.A. and Scheuhammer, A.M., 2012b. Derivation of
13686 screening benchmarks for dietary methylmercury exposure for the common loon (*Gavia immer*): rationale for use in
13687 ecological risk assessment. Environmental Toxicology and Chemistry 31:2399-2407.
13688 Desforges, J.P.W., Sonne, C., Levin, M., Siebert, U., De Guise, S. and Dietz, R., 2016. Immunotoxic effects of environmental
13689 pollutants in marine mammals. Environment International 86:126-139.
13690 Dietz, R., Sonne, C., Basu, N., Braune, B., O'Hara, T., Letcher, R.J., Scheuhammer, T., Andersen, M., Andreasen, C., Andriashek, D.
13691 and Asmund, G., 2013. What are the toxicological effects of mercury in Arctic biota? Science of the Total Environment
13692 443:775-790.
13693 Drevnick PE, Lamborg CH, Horgan MJ. 2015. Increase in mercury in Pacific yellowfin tuna. Environmental Toxicology and
13694 Chemistry 34:931-934.
13695 Drevnick, P. E., and Brooks, B. A. 2017. Mercury in tunas and blue marlin in the North Pacific Ocean. Environmental Toxicology
13696 and Chemistry 36:1365-1374.
13697 Driscoll, C.T., R.P. Mason, H.M. Chan, D.J. Jacob, and N. Pirrone. 2013. Mercury as a global pollutant: sources, pathways, and
13698 effects. Environmental Science and Technology 47:4967-4983.
13699 Driscoll, C.T., Y.J. Han, C.Y. Chen, D.C. Evers, K.F. Lambert, T.M. Holsen, N.C. Kamman, and R. Munson. 2007. Mercury
13700 contamination in remote forest and aquatic ecosystems in the northeastern U.S.: Sources, transformations and
13701 management options. Bioscience 57:17-28.
13702 Eagles-Smith C.A., J.T. Ackerman, J.J. Willacker, M.T. Tate, M.A. Lutz, J.A. Fleck, A.R. Stewart, J.G. Wiener, D.C. Evers, J.M. Lepak,
13703 and J.A. Davis. 2016. Spatial and temporal patterns of mercury concentrations in freshwater fish across the Western
13704 United States and Canada. Science of The Total Environment 568:1171-1184.
13705 Eagles-Smith, CA. and JT Ackerman. 2009. Rapid changes in small fish mercury concentrations in estuarine wetlands:
13706 Implications for wildlife risk and monitoring programs. Environmental Science and Technology 43:8658-8664.
13707 Ecotoxicology 20:1487-1499.

Ecotoxicology of mercury in fish and wildlife: Recent advances. Pp.223-238 in M. Bank (ed.). Mercury in the Environment: Pattern and Process, University of California Press, Berkeley, CA.
Edmonds, S.T., D.C. Evers, N.J. O'Driscoll, C. Mettke-Hoffman, L. Powell, D. Cristol, A.J.
Elliott, J. E.; Elliott, K. H. 2013. Tracking marine pollution. Science 340, 556−558.
Evers D.C., J.G. Wiener, N. Basu, R.A. Bodaly, H.A. Morrison, K.A. Williams. 2011a. Mercury in the
Evers, D.C. 2017. The Effects of Methylmercury on Wildlife: A Comprehensive Review and Approach for Interpretation. Encyclopedia of the Anthropocene. Elsevier.
Evers, D.C., D.G. Buck, A.K. Dalton, and S.M. Johnson. 2016a. Understanding spatial patterns for biomonitoring needs of the Minamata Convention on mercury. Biodiversity Research Institute Science Communications Series 2016-02. Portland, Maine, USA. 20pp.
Evers, D.C., K.A. Williams, M. W. Meyer, A.M. Scheuhammer, N. Schoch, A.T. Gilbert, L. Siegel, R. J. Taylor, R. Poppenga, C.R. Perkins. 2011b. Spatial gradients of methylmercury for breeding common loons in the Laurentian Great Lakes region. Ecotoxicology 20:1609-1625.
Evers, D.C., Kaplan, J.D., Meyer, M.W., Reaman, P.S., Major, A., Burgess, N., and Braselton, W.E. 1998. Bioavailability of environmental mercury measured in Common Loon feathers and blood across North American. Environmental Toxicology and Chemistry 17:173-183.
Evers, D.C., Keane, S.E., Basu, N. and Buck, D. 2016b. Evaluating the effectiveness of the Minamata Convention on Mercury: Principles and recommendations for next steps. Science of the Total Environment 569:888-903.
Evers, D.C., N. Burgess, L Champoux, B. Hoskins, A. Major, W. Goodale, R. Taylor, R. Poppenga, and T. Daigle. 2005. Patterns and interpretation of mercury exposure in freshwater avian communities in northeastern North America. Ecotoxicology 14:193-222.
Evers, D.C., Y.J. Han, C.T. Driscoll, N.C. Kamman, M.W. Goodale, K.F. Lambert, T.M. Holsen, C.Y. Chen, T.A. Clair, and T. Butler. 2007. Identification and Evaluation of Biological Hotspots of Mercury in the Northeastern U.S. and Eastern Canada. Bioscience 57:29-43.
Evers, DC, JA Schmutz, N Basu, CR DeSorbo, JS Fair, CG Osborne, J Paruk, M Perkin, K Regan, BD Uher-Koch and KG Wright. 2014. Mercury exposure and risk in Yellow-billed Loons breeding in Alaska and Canada. Waterbirds 37:147-159.
Evers, DC, RP Mason, NC Kamman, CY Chen, AL Bogomolni, DH Taylor, CR Hammerschmidt, SH Jones, NM Burgess, K Munney and KC Parsons. 2008. An integrated mercury monitoring program for temperate estuarine and marine ecosystems on the North American Atlantic Coast. EcoHealth 5:426-441.
Evers, DC, RT Graham, P Perkins, R Michener, and T Divoll. 2009. Mercury concentrations in the goliath grouper of Belize: an anthropogenic stressor of concern. Endangered Species Research 7:249-256.
Faial, K, R Deus, S Deus, R Neves, I Jesus, E Santos, CN Alves, D Brasil. 2015. Mercury levels assessment in hair of riverside inhabitants of the Tapajos River, Para State, Amazon, Brazil: fish consumption as a possible route of exposure. Journal of Trace Elements in Medicine and Biology 30:66-76.
Ferriss BE, Essington TE. 2011. Regional patterns in mercury and selenium concentrations of yellowfin tuna (*Thunnus albacares*) and bigeye tuna (*Thunnus obesus*) in the Pacific Ocean. Canadian Journal of Fisheries and Aquatic Sciences 68:2046-2056.
Finkelstein, M, BS Keitt, DA Croll, B Tershy, WM Jarman, S Rodriguez-Pastor, DJ Anderson, PR Sievert and DR Smith. 2006. Albatross species demonstrate regional differences in North Pacific marine contamination. Ecological Applications 16:678-686.
Fonseca, FRD, O Malm, O and HF Waldemarin. 2005. Mercury levels in tissues of Giant otters (*Pteronura brasiliensis*) from the Rio Negro, Pantanal, Brazil. Environmental Research 98:368-371.
Frederick, PC, MG Spalding and R Dusek. 2002. Wading birds as bioindicators of mercury contamination in Florida, USA: Annual and geographic variation. Environmental Toxicology and Chemistry 21:163-167.
Furness R.W., Camphuysen K.C.J. 1997. Seabirds as monitors of the marine environment. ICES Journal of Marine Science 54:726–737.
Gantner, N, M Power, D Iqaluk, M Meili, H Borg, M Sundbom, KR Solomon, G Lawson and DC Muir. 2010. Mercury concentrations in landlocked Arctic char (*Salvelinus alpinus*) from the Canadian Arctic. Part I: insights from trophic relationships in 18 lakes. Environmental Toxicology and Chemistry 29:621-632.
García MÁ, Núñez R, Alonso J, Melgar MJ. 2016. Total mercury in fresh and processed tuna marketed in Galicia (NW Spain) in relation to dietary exposure. Environmental Science and Pollution Research 23:24960-24969.
Garrigue C, Oremus M, Dodémont R, Bustamante P, Kwiatek O, Libeau G, Lockyer C, Vivier JC, Dalebout ML. 2016. A mass stranding of seven Longman's beaked whales (*Indopacetus pacificus*) in New Caledonia, South Pacific. Marine Mammal Science 32:884–910.
Gilmour, CC, M Podar, AL Bullock, AM Graham, SD Brown, A.C. Somenhally, A. Johs, R.A. Hurt Jr., K.L. Bailey, D.A. Elias. 2013. Mercury methylation by novel microorganisms from new environments. Environmental Science and Technology 47:11810-11820

13765 Goodale MW, DC Evers, SE Mierzykowski, AL Bond, NM Burgess, CI Otorowski, LJ Welch, CS Hall, JC Ellis, RB Allen, AW Diamond,
13766 SW Kress, and RJ Taylor. 2008. Marine foraging birds as bioindicators of mercury in the Gulf of Maine. EcoHealth
13767 5:409-425.
13768 Goutte A, Barbraud C, Meillère A, Carravieri A, Bustamante P, Labadie P, Budzinski H, Delord K, Cherel Y, Weimeskirch H,
13769 Chastel O. 2014. Demographic consequences of heavy metals and persistent organic pollutants in a vulnerable long-
13770 lived bird, the wandering albatross. Proceedings of the Royal Society B 281:20133313.
13771 Goutte A, Bustamante P, Barbraud C, Delord K, Weimeskirch H, Chastel O. 2014. Demographic responses to mercury exposure
13772 in two closely-related Antarctic top predators. Ecology 95:1075-1086.
13773 Great Lakes region – Bioaccumulation, spatial and temporal patterns, ecological risks, and policy.
13774 Gustin, M., D.C. Evers, M. Bank, C.R. Hammerschmidt, A. Pierce, N. Basu, J. Blum, P. Bustamante, C. Chen, C.T. Driscoll, M.
13775 Horvat, D. Jaffe, J. Pacyna, N. Pirrone, and N. Selin. 2016. Importance of integration and implementation of emerging
13776 and future mercury research into the Minamata Convention. Environmental Science and Technology 50:2767-2770.
13777 Heinz GH, Hoffman DJ, Klimstra JD, Stebbins KR, Kondrad SL, Erwin CA. 2009. Species differences in the sensitivity of avian
13778 embryos to methylmercury. Archives of Environmental Contamination and Toxicology 56:129-38.
13779 Hollanda SJ, Bustamante P, Churlaud C, Bodin N (in prep). Trace metal concentrations in swordfish caught in the Republic of
13780 Seychelles exclusive economic zone. The Science of the Total Environment, in prep.
13781 Horowitz, HM, DJ Jacob, Y Zhang, TS Dibble, F Slemr, HM Amos, JA Schmidt, ES Corbitt, EA Marais, EM Sunderland. 2017. A new
13782 mechanism for atmospheric mercury redox chemistry: Implications for the global mercury budget. Atmospheric
13783 Chemistry and Physics 17:6353-6371.
13784 Hsu-Kim, H, KH Kucharzyk, T Zhang, MA Deshusses. 2013. Mechanisms regulating mercury bioavailability for methylating
13785 microorganisms in the aquatic environment: a critical review. Environmental Science and Technology 47:2441-2456
13786 IOTC (2016) Report of the 19th Session of the IOTC Scientific Committee. IOTC, Seychelles, 1-5 December 2016.
13787 Jackson, A., D.C. Evers, C. Eagles-Smith, J. Ackerman, J. Willacker, J. Elliot, S.S. Vander Pol, and C.E. Bryan. 2016. Mercury risk to
13788 avian piscivores across the western United States and Canada. Science of the Total Environment
13789 doi:10.1016/j.scitotenv.2016.02.197.
13790 Jackson, A., D.C. Evers, E. Adams, C. Eagles-Smith, C. Osborne, O. Lane, S. Edmonds, T. Tear, D. Cristol, A. Sauer, and N.
13791 O'Driscoll. 2015. Mercury exposure in songbirds of eastern North America across habitats and guilds. Ecotoxicology
13792 24:453-467.
13793 Jackson, A.K., D.C. Evers, M.A. Etterson, A.M. Condon, S.B. Folsom, J. Detweiler, J. Schmerfeld, and D.A. Cristol. 2011. Mercury
13794 exposure affects the reproductive success of free-living terrestrial songbird, the Carolina wren (*Thryothorus*
13795 *ludovicianus*). Auk 128:759-769.
13796 Jackson, A.K., D.C. Evers, S.B. Folsom, A.M. Condon, J. Diener, L.F. Goodrick, A.J. McGann, J.
13797 Jinadasa, B.K.K.K., Edirisinghe, E.M.R.K.B. and Wickramasinghe, I., 2014. Total mercury, cadmium and lead levels in main export
13798 fish of Sri Lanka. Food Additives and Contaminants: Part B, 7:309-314.
13799 Kamman, N.C., Burgess, N.M., Driscoll, C.T., Simonin, H.A., Goodale, W., Linehan, J., Estabrook, R., Hutcheson, M., Major, A.,
13800 Scheuhammer, A.M. and Scruton, D.A. 2005. Mercury in freshwater fish of northeast North America–a geographic
13801 perspective based on fish tissue monitoring databases. Ecotoxicology 14:163-180.
13802 Kenney, L.A., Eagles-Smith, C.A., Ackerman, J.T. and von Hippel, F.A. 2014. Temporal variation in fish mercury concentrations
13803 within lakes from the western Aleutian archipelago, Alaska. PloS One 9(7):102244.
13804 Kiszka, JJ, A Aubail, NE Hussey, MR Heithaus, F Caurant and P Bustamante. 2015. Plasticity of trophic interactions among sharks
13805 from the oceanic south-western Indian Ocean revealed by stable isotope and mercury analyses. Deep Sea Research
13806 Part I: Oceanographic Research Papers 96:49-58.
13807 Klenavic, K, L Champoux, PY Daoust, RD Evans and HE Evans. 2008. Mercury concentrations in wild mink (*Mustela vison*) and
13808 river otters (*Lontra canadensis*) collected from eastern and Atlantic Canada: relationship to age and parasitism.
13809 Environmental Pollution 156:359-366.
13810 Kocman, D, SJ Wilson, HM Amos, KH Telmer, F Steenhuisen, EM Sunderland, RP Mason, P Outridge, M Horvat. 2017. Toward an
13811 Assessment of the Global Inventory of Present-Day Mercury Releases to Freshwater Environments. International
13812 Journal of Environmental Research and Public Health 14:138
13813 Kojadinovic, J, P Bustamante, C Churlaud, RP Cosson and M Le Corre. 2007. Mercury in seabird feathers: Insight on dietary
13814 habits and evidence for exposure levels in the western Indian Ocean. Science of the Total Environment 384:194-204.
13815 Kwon, S.Y., Blum, J.D., Chen, C.Y., Meattey, D.E. and Mason, R.P. 2014. Mercury isotope study of sources and exposure
13816 pathways of methylmercury in estuarine food webs in the Northeastern US. Environmental Science and Technology
13817 48:10089-10097.
13818 Lane, O.P., K.M. O'Brien, D.C. Evers, T.P. Hodgman, A. Major, N. Pau, M.J. Ducey, R. Taylor,
13819 Lebel, J, M Roulet, D Mergler, M Lucotte, F. Larribe. 1997. Fish diet and mercury exposure in a riparian Amazonian population.
13820 Water, Air and Soil Pollution 97:31-44.
13821 Lee CS and NS Fisher, 2016. Methylmercury uptake by diverse marine phytoplankton. Limnology and Oceanography 61:1626-
13822 1639.

13823 Lee CS, Lutcavage ME, Chandler E, Madigan DJ, Cerrato RM, Fisher NS. 2016. Declining mercury concentrations in bluefin tuna
13824 reflect reduced emissions to the North Atlantic Ocean. Environmental Science and Technology 50:12825-12830.
13825 Maffucci F, Caurant F, Bustamante P, Bentivegna F. 2005. Trace element (Cd, Cu, Hg, Se, Zn) accumulation and tissue
13826 distribution in loggerhead turtles (*Caretta caretta*) from the Western Mediterranean Sea (southern Italy).
13827 Chemosphere 58:535–542.
13828 Marcovecchio, JE, MS Gerpe, RO Bastida, DH Rodríguez and SG Morón. 1994. Environmental contamination and marine
13829 mammals in coastal waters from Argentina: an overview. Science of the Total Environment 154:141-151.
13830 Mason, RP and WF Fitzgerald. 1993. The distribution and biogeochemical cycling of mercury in the equatorial Pacific Ocean.
13831 Deep Sea Research Part I: Oceanographic Research Papers 40:1897-1924
13832 Matulik, A.G., Kerstetter, D.W., Hammerschlag, N., Divoll, T., Hammerschmidt, C.R. and Evers, D.C. 2017. Bioaccumulation and
13833 biomagnification of mercury and methylmercury in four sympatric coastal sharks in a protected subtropical lagoon.
13834 Marine Pollution Bulletin 116:357-364.
13835 Maz-Courrau A, C López-Vera, F Galvan-Magaña, O Escobar-Sánchez, R Rosíles-Martínez, and A Sanjuán-Muñoz. 2012.
13836 Bioaccumulation and biomagnification of total mercury in four exploited shark species in the Baja California
13837 Peninsula, Mexico. Bulletin of Environmental Contamination and Toxicology 88:129-134.
13838 McGann, J.W. Armiger, O. Lane, D.F. Tessler, and P. Newell. 2010. Geographic and seasonal variation in mercury exposure of
13839 the declining Rusty Blackbird. Condor 112:789-799.
13840 Mckinney, M.A., Pedro, S., Dietz, R., Sonne, C., Fisk, A.T., Roy, D., Jenssen, B.M. and Letcher, R.J., 2015. A review of ecological
13841 impacts of global climate change on persistent organic pollutant and mercury pathways and exposures in arctic
13842 marine ecosystems. Current Zoology 61:617-628.
13843 Mendez, E., Giudice, H., Pereira, A., Inocente, G. and Medina, D., 2001. Total mercury content—fish weight relationship in
13844 swordfish (*Xiphias gladius*) caught in the southwest Atlantic Ocean. Journal of Food Composition and Analysis 14:453-
13845 460.
13846 Mol JH, JS Ramlal, C Lietar, and M Verloo. 2001. Mercury contamination in freshwater, estuarine, and marine fishes in relation
13847 to small-scale gold mining in Suriname, South America. Environmental Research 86:183-197.
13848 Monson, B.A., Staples, D.F., Bhavsar, S.P., Holsen, T.M., Schrank, C.S., Moses, S.K., McGoldrick, D.J., Backus, S.M. and Williams,
13849 K.A., 2011. Spatiotemporal trends of mercury in walleye and largemouth bass from the Laurentian Great Lakes region.
13850 Ecotoxicology 20:1555-1567.
13851 Monteiro, L. R.; Furness, R. W. 1995. Seabirds as monitors of mercury in the marine environment. Water, Air, Soil Pollution
13852 80:851–870.
13853 NCP 2017. Northern Contaminants Program (NCP). Indigenous and Northern Affairs, Government of Canada.
13854 http://www.science.gc.ca/eic/site/063.nsf/eng/h_7A463DBA.html.
13855 Nguetseng, R., Fliedner, A., Knopf, B., Lebreton, B., Quack, M. and Rüdel, H. 2015. Retrospective monitoring of mercury in fish
13856 from selected European freshwater and estuary sites. Chemosphere 134:427-434.
13857 Nicklisch, S.C., Bonito, L.T., Sandin, S. and Hamdoun, A. 2017. Mercury levels of yellowfin tuna (*Thunnus albacares)* are
13858 associated with capture location. Environmental Pollution 229:87-93.
13859 Ochoa-Acuña H, Sepulveda MS, Gross TS. 2002. Mercury in feathers from Chilean birds: Influence of location, feeding strategy
13860 and taxonomic affiliation. Marine Pollution Bulletin 44:340–349.
13861 Odsjö, T, A Roos and AG Johnels. 2004. The Tail Feathers of Osprey Nestlings (*Pandion haliaetus* L.) as Indicators of Change in
13862 Mercury Load in the Environment of Southern Sweden (1969-1998): Case Study with a Note on the Simultaneous
13863 Intake of Selenium. AMBIO: A Journal of the Human Environment 33:133-137.
13864 Oliveira, RC, JG Dorea, JVE Bernardi, WR Bastos, R Almeida, AG Manzatto. 2010. Fish consumption by traditional subsistence
13865 villagers of the Rio Madeira (Amazon): impact on hair mercury. Annals of Human Biology 37: 629-642.
13866 Pacyna JM, Travnikov O, De Simone F, Hedgecock IM, Sundseth K, Pacyna EG, Steenhuisen F, Pirrone N, Munthe J, Kindbom K.
13867 2016. Current and future levels of mercury atmospheric pollution on a global scale. Atmospheric Chemistry and
13868 Physics 16(19):12495.
13869 Pauly, D. and Zeller, D. 2016. Catch reconstructions reveal that global marine fisheries catches are higher than reported and
13870 declining. Nature Communications 7:10244.
13871 Pinkney, A.E., C.T. Driscoll, D.C. Evers, M.J. Hooper, J. Horan, J.W. Jones, R.S. Lazarus, H.G. Marshall, A. Milliken, B.A. Rattner, J.
13872 Schmerfeld, and D.W. Sparling. 2015. Interactions between climate change, contaminants, nutrients, and ecosystems
13873 in the North Atlantic Landscape Conservation Cooperative. Integrated Environmental Assessment and Management
13874 DOI 10.1002/ieam.1612.
13875 Rigét F, R Dietz, EW Born, C Sonne, and KA Hobson. 2007. Temporal trends of mercury in marine biota of west and northwest
13876 Greenland. Marine Pollution Bulletin 54:72-80.
13877 Rigét, F., Braune, B., Bignert, A., Wilson, S., Aars, J., Born, E., Dam, M., Dietz, R., Evans, M., Evans, T. and Gamberg, M., 2011.
13878 Temporal trends of Hg in Arctic biota, an update. Science of the Total Environment, 409:3520-3526.
13879 Rodrigues, T., and Amorim, A. F. 2016. Review and analysis of mercury levels in blue marlin (Makaira nigricans, Lacepède 1802)
13880 and swordfish (*Xiphias gladius*, Linnaeus 1758). bioRxiv doi: https://doi.org/10.1101/043893.

13881 Rush, SA, K Borgå, R Dietz, EW Born, C Sonne, T Evans, DCG Muir, RJ Letcher, RJ Norstrom and AT Fisk. 2008. Geographic
13882 distribution of selected elements in the livers of polar bears from Greenland, Canada and the United States.
13883 Environmental Pollution 153:618-626.
13884 Schartup, AT, U Ndu, PH Balcom, RP Mason, EM Sunderland. 2015. Contrasting effects of marine and terrestrially derived
13885 dissolved organic matter on mercury speciation and bioavailability in seawater. Environmental Science and
13886 Technology 49:5965-5972
13887 Scheuhammer, A. M., S. I. Lord, M. Wayland, N. M. Burgess, L. Champoux, and J. E. Elliott. 2016. Major correlates of mercury in
13888 small fish and common loons (*Gavia immer*) across four large study areas in Canada. Environmental Pollution
13889 210:361-370.
13890 Scheuhammer, A., Braune, B., Chan, H.M., Frouin, H., Krey, A., Letcher, R., Loseto, L., Noël, M., Ostertag, S., Ross, P. and
13891 Wayland, M., 2015. Recent progress on our understanding of the biological effects of mercury in fish and wildlife in
13892 the Canadian Arctic. Science of the Total Environment 509:91-103.
13893 Scheuhammer, A.M., N. Basu, D.C. Evers, G.H. Heinz, M.B. Sandheinrich, and M.S. Bank. 2011.
13894 Schmerfeld, D.A. Cristol. 2011. Mercury exposure in terrestrial birds far downstream of an historical point source.
13895 Environmental Pollution 159:3302-3308.
13896 SFA (2016) Fisheries statistical report, year 2015. Seychelles Fishing Authority, Victoria, Seychelles
13897 Storelli MM and GO Marcotrigiano. 2001. Total mercury levels in muscle tissue of swordfish (*Xiphias gladius*) and bluefin tuna
13898 (*Thunnus thynnus*) from the Mediterranean Sea (Italy). Journal of Food Protection 64:1058-1061.
13899 Streets, DG, HM Horowitz, DJ Jacob, Z Lu, L Levin, AFH Ter Schure, EM Sunderland. 2017. Total Mercury Released to the
13900 Environment by Human Activities. Environmental Science & Technology 51:5969-5977
13901 Streets, DG, Q Zhang, Y Wu. 2009. Projections of global mercury emissions in 2050. Environmental Science and Technology
13902 43:2983-2988.
13903 Sunderland EM, Krabbenhoft DP, Moreau JW, Strode SA, Landing WM. 2009. Mercury sources, distribution, and bioavailability
13904 in the North Pacific Ocean: Insights from data and models. Global Biogeochemical Cycles 23(2).
13905 Sunderland, EM, CT Driscoll Jr, JK Hammitt, P Grandjean, JS Evans, JD Blum, CY Chen, DC Evers, DA Jaffe, RP Mason, S Goho, W
13906 Jacobs. 2016. Benefits of regulating hazardous air pollutants from coal and oil-fired utilities in the United States.
13907 Environmental Science and Technology 50:2117-2120.
13908 Tartu S, Goutte A, Bustamante P, Angelier F, Moe B, Clément-Chastel C, Bech C, Gabrielsen GW, Bustness JO, Chastel O. 2013.
13909 To breed or not to breed: endocrine response to mercury contamination by an arctic seabird. Biology Letters
13910 9(4):20130317.
13911 Teffer, A.K., Staudinger, M.D., Taylor, D.L. and Juanes, F. 2014. Trophic influences on mercury accumulation in top pelagic
13912 predators from offshore New England waters of the northwest Atlantic Ocean. Marine Environmental Research
13913 101:124-134.
13914 Townsend JM, CC Rimmer, CT Driscoll, KP McFarland, and E Inigo-Elias. 2013. Mercury concentrations in tropical resident and
13915 migrant songbirds on Hispaniola. Ecotoxicology 22:86-93.
13916 Trasande L, J DiGangi, DC Evers, P Jindrich, DG Buck, J Samanek, B Beeler, MA Turnquist, and K Regan. 2016. Economic
13917 implications of mercury exposure in the context of the global mercury treaty: hair mercury levels and estimated lost
13918 economic productivity in selected developing countries. Journal of Environmental Management 183:229-235.
13919 UNEP. 2016. UNEP Global Review of Mercury Monitoring Networks. United Nations Environment, Geneva, Switzerland.
13920 Vega-Sánchez B, Ortega-García S, Ruelas-Inzunza J, Frías-Espericueta M, Escobar-Sánchez O, Guzmán-Rendón J. 2017. Mercury
13921 in the Blue Marlin (*Makaira nigricans*) from the Southern Gulf of California: Tissue Distribution and Inter-Annual
13922 Variation (2005–2012). Bulletin of Environmental Contamination and Toxicology 98:156-61.
13923 Wagemann, R and H Kozlowska. 2005. Mercury distribution in the skin of beluga (*Delphinapterus leucas*) and narwhal
13924 (*Monodon monoceros*) from the Canadian Arctic and mercury burdens and excretion by moulting. Science of the Total
13925 Environment 351:333-343.
13926 Weis JS and AA Khan. 1990. Effects of mercury on the feeding behavior of the mummichog, *Fundulus heteroclitus* from a
13927 polluted habitat. Marine Environmental Research 30:243-249.
13928 Weseloh, D.C., Moore, D.J., Hebert, C.E., de Solla, S.R., Braune, B.M. and McGoldrick, D.J. 2011. Current concentrations and
13929 spatial and temporal trends in mercury in Great Lakes Herring Gull eggs, 1974–2009. Ecotoxicology 20:1644-1658.
13930 Whitney, M.C. and D.A. Cristol. 2017. Impacts of Sublethal Mercury Exposure on Birds: A Detailed Review. Reviews of
13931 Environmental Contamination and Toxicology, DOI 10.1007/398_2017_4.
13932 Wiemeyer, SN, CM Bunck and AJ Krynitsky. 1988. Organochlorine pesticides, polychlorinated biphenyls, and mercury in osprey
13933 eggs—1970–79—and their relationships to shell thinning and productivity. Archives of Environmental Contamination
13934 and Toxicology 17:767-787.
13935 Wiener, JG, MB Sandheinrich, SP Bhavsar, JR Bohr, DC Evers, BA Monson and CS Schrank. 2012. Toxicological significance of
13936 mercury in yellow perch in the Laurentian Great Lakes region. Environmental Pollution 161:350-357.
13937 Wyn, B, KA Kidd, NM Burgess, RA Curry. 2009. Mercury biomagnification in the food webs of acidic lakes in Kejimkujik National
13938 Park and National Historic Site, Nova Scotia. Canadian Journal of Fisheries and Aquatic Sciences 66:1532-1545

13939 Wyn, B., Kidd, K.A., Burgess, N.M., Curry, R.A. and Munkittrick, K.R., 2010. Increasing mercury in yellow perch at a hotspot in
13940 Atlantic Canada, Kejimkujik National Park. Environmental Science and Technology, 44:9176-9181.
13941 Y Zhang, DJ Jacob, S Dutkiewicz, HM Amos, MS Long, EM Sunderland. 2015. Biogeochemical drivers of the fate of riverine
13942 mercury discharged to the global and Arctic oceans. Global Biogeochemical Cycles 29:854-864
13943 Yates, DE, DT Mayack, K Munney, DC Evers, A Major, T Kaur, and RJ Taylor. 2005. Mercury levels in mink (*Mustela vison*) and
13944 river otter (*Lontra canadensis*) from northeastern North America. Ecotoxicology 14:263-274.
13945 Zhang, Y, DJ Jacob, HM Horowitz, L Chen, HM Amos, DP Krabbenhoft, F. Slemr, VL St Louis, EM Sunderland. 2016. Observed
13946 decrease in atmospheric mercury explained by global decline in anthropogenic emissions. Proceedings of the National
13947 Academy of Sciences 113: 526-531.
13948

13949

Note to reader

This draft version of Chapter 8 in the Technical Background Report to the Global Mercury Assessment 2018 is made available for review by national representatives and experts. The draft version contains material that will be further refined and elaborated after the review process. Specific items where the content of this draft chapter will be further improved and modified are:

1. Quality of all graphics (Figures, Tables) will be improved prior to publication.
2. Content of all graphics (Figures, Tables) will be double-checked, updated, and refined prior to publication.
3. The report's section on "Vulnerable Populations" is in preliminary draft form. It has not been reviewed yet by all authors. It will be updated after reviews have been received.
4. The report "Summary Section" is in preliminary draft form. It has not been reviewed yet by all authors. It will be updated after reviews have been received.
5. Table in Appendix #3 (Birth Cohort studies) will be further updated and cleaned-up.
6. Linkages will be made to the "Biotic Indicators" chapter once we have co-reviewed the two pieces.
7. We welcome comments and suggestions!!!

GMA Draft for review. Chapter 8 Mercury levels and trends in human populations worldwide. Nil Basu, Joanna Tempowski, David Evers, Milena Horvat, Pál Weihe, Irina Zastenskaya, Carla Achcar (WHO coordinated working group)

14028 # Table of Contents

14045

14046

Chapter 8 Mercury levels and trends in human populations worldwide

8.1 Background

8.1.1 Health effects of mercury

Mercury (Hg) is a pollutant of global concern principally due to its adverse effects towards human health. Mercury is also found in a number of items of great public health benefit such as seafood, dental amalgams, and vaccines. The current state of knowledge concerning Hg's human health impacts has been reviewed by Ha et al. (2017) and Karagas et al. (2012), and extends upon solid background papers by WHO/UNEP/IOMC (2008), Mergler et al. (2007), Clarkson and Magos (2006), the U.S. CDC's ATSDR (1999), and the U.S. EPA (1997). In brief, all individuals worldwide are exposed to some amount of Hg, and the possibility of exposure-related adverse health effects is dependent upon a range of factors (e.g., chemical form, concentration, duration, life stage). It is widely agreed that developing organs are the most sensitive to the toxic effects of Hg. Mercury has been documented to impair a range of physiological systems with the nervous, renal, and cardiovascular systems being most susceptible. Exposures to elemental Hg (Hg^0) may affect the nervous system with key symptoms including tremors, emotional lability, neuromuscular changes, and polyneuropathies. Exposures to inorganic Hg compounds may affect the kidneys. Exposures to methylmercury (MeHg) have received the most attention largely due to notorious poisoning events in Japan and Iraq which showed exposures to relatively high levels to be associated with adverse neurodevelopmental outcomes. This work has expanded over recent decades, and there is a growing body of evidence to illustrate that chronic exposures to relatively low-level MeHg exposures can be associated with a range of adverse health outcomes.

8.1.2 Mercury exposure assessment

Detailed reviews concerning the conduct and approaches of Hg exposure assessment have been reviewed by WHO/UNEP/IOMC (2008) and the U.S. EPA (1997). Mercury is a naturally occurring element that can enter the ecosystem via natural or anthropogenic-mediated process. Three major chemical forms of Hg relevant to human exposures are found in the environment: elemental Hg (Hg^0), inorganic Hg compounds (Hg^{2+}), and organic methylmercury (MeHg). The source, environmental fate, exposure, and toxicity of these different Hg forms vary.

14075 Mercury has unique physical and chemical properties that have rendered it attractive for use in a range
14076 of industrial and medical applications. Major sources of elemental and inorganic Hg exposure to humans
14077 include occupational use (e.g. in artisanal and small-scale gold mining (ASGM) and dentistry), the use of
14078 products containing Hg (e.g. dental amalgams, skin-lightening creams, traditional medicines,
14079 thermometers, compact fluorescence lamps), and as a result of environmental pollution (e.g., fish and
14080 rice from contaminated ecosystems). Some notable examples are highlighted (Figure 1).

14081 Mercury released into the environment may be converted to organic MeHg, which bioaccumulates and
14082 biomagnifies through the food chain, particularly in aquatic systems. For many communities worldwide,
14083 consumption of fish, shellfish and marine mammals that are contaminated with MeHg is arguably the
14084 most important source of exposure with key examples highlighted in Figure 1.

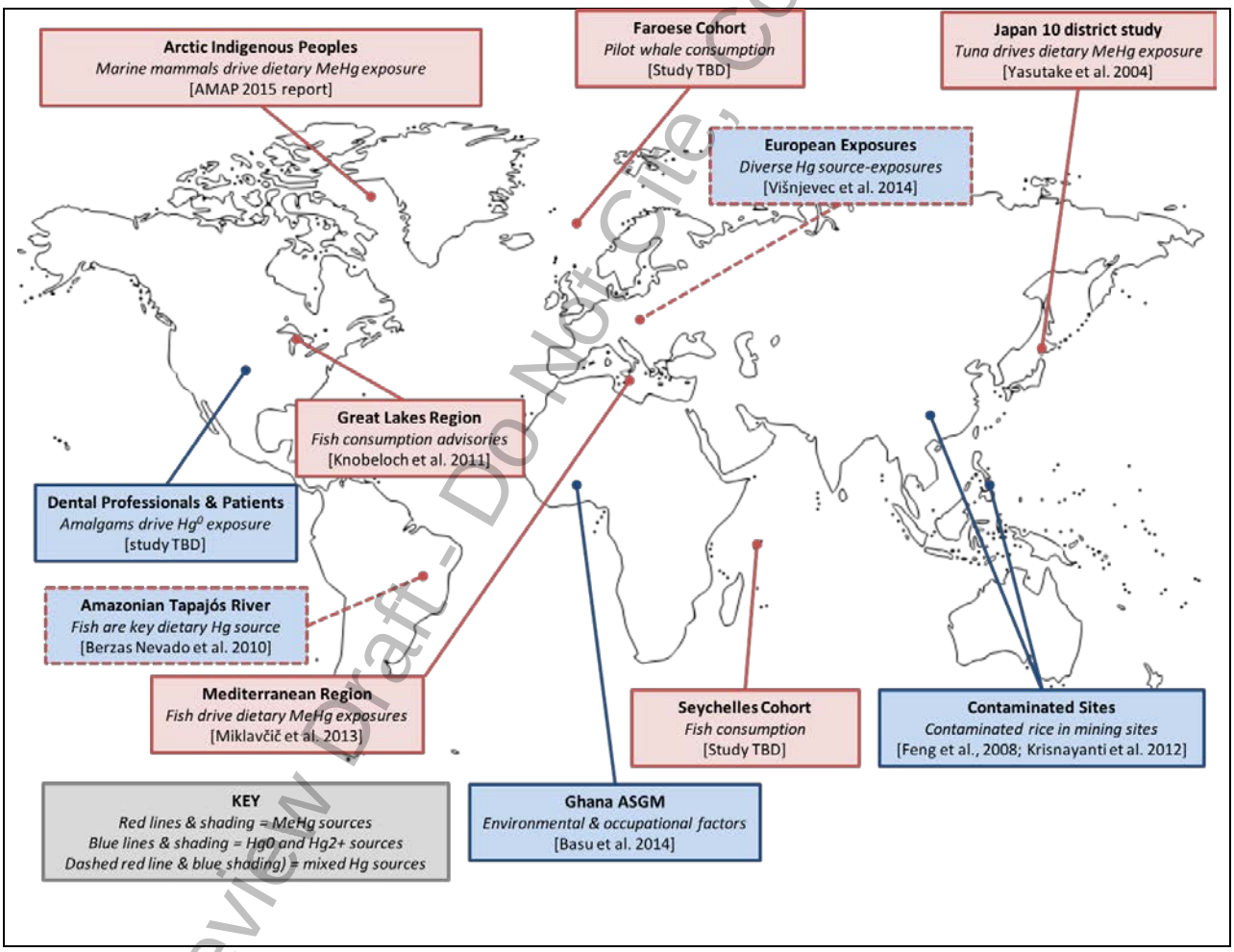

Figure 1. Selected studies across the world depicting strong and representative evidence of mercury source-exposure relationships.

8.1.3 Biomarkers of mercury exposure

Human exposure to Hg is estimated by the use of human tissues that serve as biomarkers (WHO/UNEP/IOMC, 2008). This report focuses on biomarkers of Hg exposure for which there are well-validated methods of measurement and interpretation and for which there is a reasonably large body of knowledge. Within the scientific community there are four established biomarkers of Hg exposure - hair (for MeHg), urine (for inorganic Hg), whole blood (mostly MeHg but can contain inorganic Hg), and cord blood (to gauge developmental exposures). Blood measurements indicate recent exposures (~1-2 months) and speciation measures can deepen understanding of potential sources, though blood collection, storage, and transport poses certain logistical and financial barriers. Hair and urine samples are particularly suitable as they provide information on the two main forms of Hg, and their collection is relatively non-invasive, requires no specialized training, and is cost-effective (e.g., sampling and analyses can likely be achieved for <$50 USD/measure). Further, hair grows at approximately 1 cm per month and thus Hg measurements can be tracked over time. Each biomarker can provide pertinent exposure information on the type of Hg (organic vs. inorganic) and timeline of exposure (acute or chronic). When multiple biomarker measures are taken from a given individual, and also combined with surveys, a deeper exposure assessment may be performed.

To maximize the use of Hg biomarker data, it is sometimes necessary to convert across biomarker types and there are two conventions to be noted. First, the Joint Food and Agriculture Organization (FAO) and World Health Organization (WHO) Expert Committee on Food Additives (JECFA 2004) established a MeHg hair-to-blood ratio of 250 that is now commonly used by the research community. Second, cord blood levels are on average 70% higher than maternal blood as discussed by Stern and Smith (2003). While we use these two biomarker ratios in the current report, we acknowledge on-going debate in the literature concerning the validity of these approaches particularly in consideration of heterogeneity across individuals with respect to influential factors such as sex, age, and ethnicity (Stern and Smith, 2003; Bartell et al., 2000). Nonetheless, biomarker conversions facilitate comparability across studies, and have been effective at helping derive large, regional biomonitoring assessments and maps (e.g., Europe, Miklavcic et al., 2014; Arctic, AMAP 2015) that are effective communication tools. In addition, to make judgements from biomarker measures it is necessary to have reference guidelines and as such we briefly summarise key propositions by stakeholder organizations (Appendix 1 and 2). For the purposes of this report we have adapted the colour scale used by Miklavcic et al. (2014) in their European assessment of Hg exposure (Appendix 3).

8.2 Objective

The overall goal of this chapter is to provide an overview about worldwide human exposures to Hg as reflected by concentrations in biomarker samples. The specific objectives of this study are to outline:

- whether exposures have changed over time in specific populations;
- geographical variations in exposure;
- exposures in vulnerable groups because of high exposures and susceptibility to toxic effects;
- exposure biomarker data with respect to guideline values;
- links between Hg sources and biomarker levels; and
- key knowledge gaps.

8.3 Method

8.3.1 Identification of studies

An international advisory group of scientific experts (i.e., report authors) on Hg exposure was convened to guide the work. The group decided to focus this initial global assessment on three study population types:

A-National human biomonitoring programs. These programs are usually sponsored and/or run by official government agencies and provide high quality data. A list of such programs was compiled by UN Environment (UNEP 2016), and augmented by report authors.

B-Longitudinal birth cohort studies. These studies are usually well designed and most pertinent for establishing exposure-outcome relationships. They tend to provide high quality exposure data for vulnerable groups (pregnant women, newborns, and children), and these data can be used to explore geographic differences, temporal trends, and characterize Hg source-exposure-biomarker relationships.

C-Cross-sectional studies on vulnerable populations. While many vulnerable populations exist, here we focused on two broad groups: a) populations exposed to inorganic Hg from point sources (i.e., artisanal and small-scale gold miners (ASGM) and community members; people living and working in former Hg contaminated sites); and populations exposed to organic Hg from dietary sources (i.e., Indigenous Peoples; recreational or subsistence fishers; pregnant women and foetuses).

8.3.2 Search strategy

A systematic search of the peer-reviewed scientific literature was performed in three databases (PubMed, SCOPUS, Web of Science). The search strategy included the following two Boolean search phrases: #1 – "mercury OR methylmercury OR (methyl AND mercury) OR MeHg"; and #2 - "blood OR hair OR urine". In addition to the systematic search, we considered grey literature and polled key scholars identified by report authors. There were no language restrictions as the committee was willing to devote resources to having pertinent foreign language papers properly translated. When a study was reported upon in multiple articles, we chose the article with the most complete dataset to serve as a representative piece.

Scientific papers were reviewed through a two-stage process: First, the title and abstract fields were searched to ascertain relevancy; and second, the full text was reviewed on papers that were deemed relevant. In brief, national biomonitoring studies (Study Type A) were identified through the 2016 UN Environment survey, authors' knowledge, and an electronic search. All national biomonitoring programs that measured Hg in hair, blood, urine, or cord blood were included (i.e., no exclusion criteria were applied). Longitudinal birth cohort studies (Study Type B) were identified through the 2016 UN Environment survey, authors' knowledge, and an electronic search. Similar to national biomonitoring studies, we did not apply any exclusion criteria except that these studies needed to: A) include at least two discrete sampling periods, one of which needed to be a biomarker measured during pregnancy or birth; and B) measure a health outcome in the newborn during some later lifestage. Vulnerable population group studies (Study Type C) were selectively identified (i.e., most illustrative works) through bibliographic searches.

8.3.3 Data analyses

For all studies, we extracted data on population characteristics (age, lifestage, sex, city/country/region location), Hg exposure measurements (sample size, Hg biomarker and speciation information, quality control measures), and measures of central tendencies (geometric mean, median) and high-end (90th or 95th percentile or maximum) biomarkers. To compare across the biomarker types, we normalized datasets to blood THg equivalents using the conventions mentioned earlier. To further interpret the results, we compared the values against the aforementioned reference guidelines (Appendix 1) and used a colour scale to visually represent the findings (Appendix 3).

8.4 Results

8.4.1 National Biomonitoring Studies

We obtained national data from seven countries (Belgium, Canada, Czech Republic, Germany, Republic of Korea, Sweden, USA), of which three surveys were designed to be nationally representative (Canada, Republic of Korea, USA). The other surveys were included here as they were either legally mandated or government-run to yield actionable information. The total sample population of these surveys was 97,696 people from which 150,929 biomarker measurements of Hg exposure were extracted. The survey data were compared with a particular focus on the following factors: country, lifestage, sex, sampling year(s), and biomarker type.

Table 1. Summary of National Biomonitoring programs that measure mercury

Country	Survey	Lead Organization	Year Started	# Cycles; Frequency	Size /Cycle	Age; Sex	Biomarkers
Canada	CHMS	Statistics Canada	2007	4; every 2 yrs	~5,000	3-79; both	Blood, urine
Germany	GerES	Umwelt Bundesamt	1985	5; variable	~5,000	3-69; both	Blood, urine
Sweden	Riksmaten	Swedish National Food Agency	1990	2; variable	~300	18-80; both	Blood
Korea	KoNEHS	Korean Ministry of Environment	2005	3; every 2 yrs	~5,000	3-19+; both	Blood, urine
USA	NHANES	Centers for Disease Control and Prevention	1960	6; every 2 yrs	~8,000	1-70+; both	Blood, urine
Czech Republic	CZ-HBM	National Institute of Public Health	1994	16; ~every yr	~400	8-64; both	Blood, urine, hair
Belgium	FLEHS	Vlaanderen Departement Omgeving	2002	2; every 2 yrs	~5,000	1-65; both	Hair

Table 2. Count of individuals and mercury biomarker measures from the National Biomonitoring programs.

	Demographics					Mercury Measures				
Country	**Total Sample Size**	**Children**	**Adults**	**Males**	**Females**	**Total # Measures**	**Blood (THg)**	**Blood (MeHg)**	**Urine**	**Hair**
Canada	**17,210**	6,983[1]	10,227[2]	8,418	8,792	**29,099**	16,927	1,032	11,140	
Germany	**10,520**	2,466	8,054			**16,757**	6,237		10,520	
Sweden	**297**			128	145	**297**	297			
Korea	**14,688**	2,346	12,342			**14,688**	14,688			
USA	**46,974**	19,086[3]	27,888[4]	23,292	23,682	**75,778**	46,974	13,016	15,788	
Czech Republic	**7,542**	3,623	3,919			**13,845**	4,700		6,459	2,686
Belgium	**465**	210	255		255	**465**				465
Totals	**97,696**					**150,929**				

Across the national biomonitoring programs the majority of participants had blood Hg levels that fell below 5 ug/L. Blood Hg levels were consistently highest in Korea versus the other countries. Blood Hg levels in adults were approximately 2.1-fold higher than in children, and this varied across lifestage. For example, median blood Hg levels in Canadians from the CHMS increased with age as follows: 0.24 μg/L for 6-11 yr olds, 0.28 μg/L for 12-19 yr olds, 0.76 μg/L for 20-39 yr olds, 1.1 μg/L for 40-59 yr olds, and 0.96 μg/L for 60-79 yr olds. Similar trends were observed in the U.S. and Korean datasets.

Urine Hg levels were consistent across the countries from which data were obtained, with a majority of the values falling under 3 μg/L. Like blood, urine Hg levels were higher in adults than in children.

[1] includes study participants ages 3-19
[2] includes study participants ages 20-79
[3] includes study participants ages 1-19
[4] includes study participants ages 20+

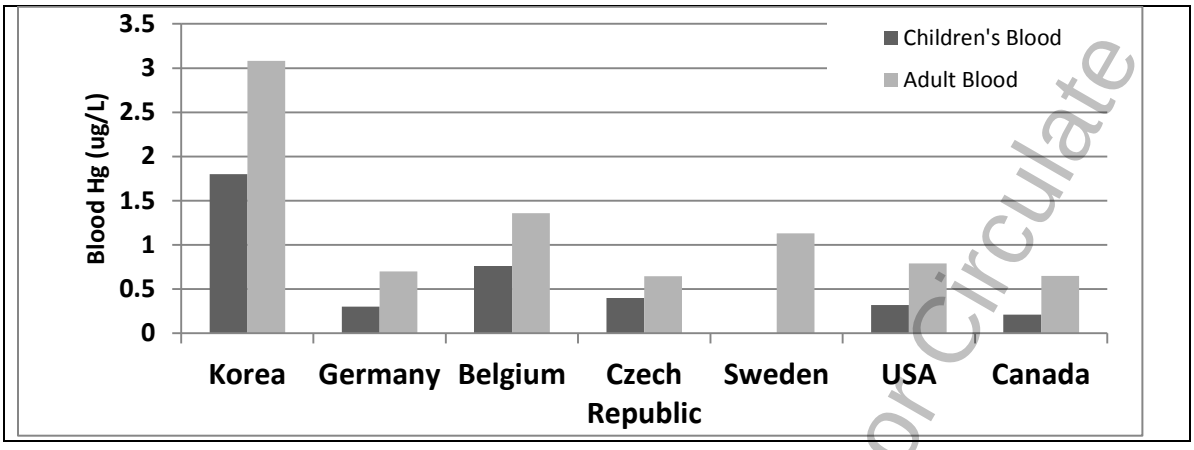

Figure 2. Comparison of median whole blood total Hg (μg/L) measurements across children (<19 years) and adults from national biomonitoring datasets between the years 2003-2014.

14195

TABLE 3. Cross-sectional comparison of whole blood total mercury measurement (μg/L) in adults and children via national biomonitoring data. Males and females are grouped together.

		Korea	Germany	USA	Canada	Belgium	Czech Republic	Sweden
	Survey Name	KHANES (Adults), KorEHS-C (Children)	GerES-3 (Adults), GerES-2 (Children)	NHANES	CHMS Cycle 2	FLEHS2	CZ-HBM	Riksmaten
Adults	Year	2011	1998	2011-2012	2009-2011	2007-2011	2015	2010-2011
	Age	19+	18-69	20+	20-39	18-42	18-64	18-80
	Sample Size	2014	3973	5030	1313	255	302	297
	Whole Blood Hg (50%)	3.08 (GM)	0.70	0.79	0.65	1.36	0.65	1.13
	Whole Blood Hg (95%)	??	2.40	5.02	5.20	3.44	2.50	3.45
Children	Year	2012-2014	2003-2006	2011-2012	2009-2011	2007-2011	2008	
	Age	3-18	3-14	6-11	6-11	14-16	8-10	
	Sample Size	2346	1240	1048	961	210	198	
	Whole Blood Hg (50%)	1.80	0.30	0.32	0.21	0.76	0.40	
	Whole Blood Hg (95%)	3.68	1.00	1.40	2.00	1.88	1.40	

14196

14197

TABLE 4. Cross-sectional comparison of urinary total mercury measurement (μg/L) in adults and children via national biomonitoring data. Males and females are grouped together.

		Germany	USA	Canada	Czech Republic
Adults	Year	1998	2011-2012	2012-2013	2009
	Age	18-69	20+	20-39	18-64
	Sample Size	4052	1716	1048	373
	Urine Hg (50%)	0.40	0.34	0.20	0.80
	Urine Hg (95%)	3.00	1.93	1.10	5.30
Children	Year	2003-2006	2011-2012	2012-2013	2008
	Age	3-14	6-11	6-11	8-10
	Sample Size	1734	401	1010	318
	Urine Hg (50%)	<0.1 [LOD is 0.1]	.22	<LOD	0.2[5]
	Urine Hg (95%)	0.5	1.37	.93	1.1

14198

14199 Temporal changes in Hg exposure were evaluated by reviewing national datasets in which there were 2
14200 or more comparable sampling periods. For blood Hg, datasets from four countries were reviewed and in
14201 general they showed declining exposures. For example, combining the work from USA, Canada, and the
14202 Czech Republic into a linear regression model showed annual decreases in blood Hg of approximately
14203 0.026 μg/L or 2.25% (i.e., over 10 years this would be a decrease of 0.26 μg/L or ~22.5%) with median
14204 blood Hg levels levelling around 0.75 μg/L (Figure 3A). For urinary Hg, similar over-time decreases can
14205 be observed particularly when examining the US NHANES dataset as the Hg levels in the latest dataset is
14206 approximately 50% lower than it was 10 years earlier (Figure 3B). The urinary Hg values now in the US
14207 are similar to Canada and hover around 0.2 μg/L.

14208

[5] creatinine corrected

14209

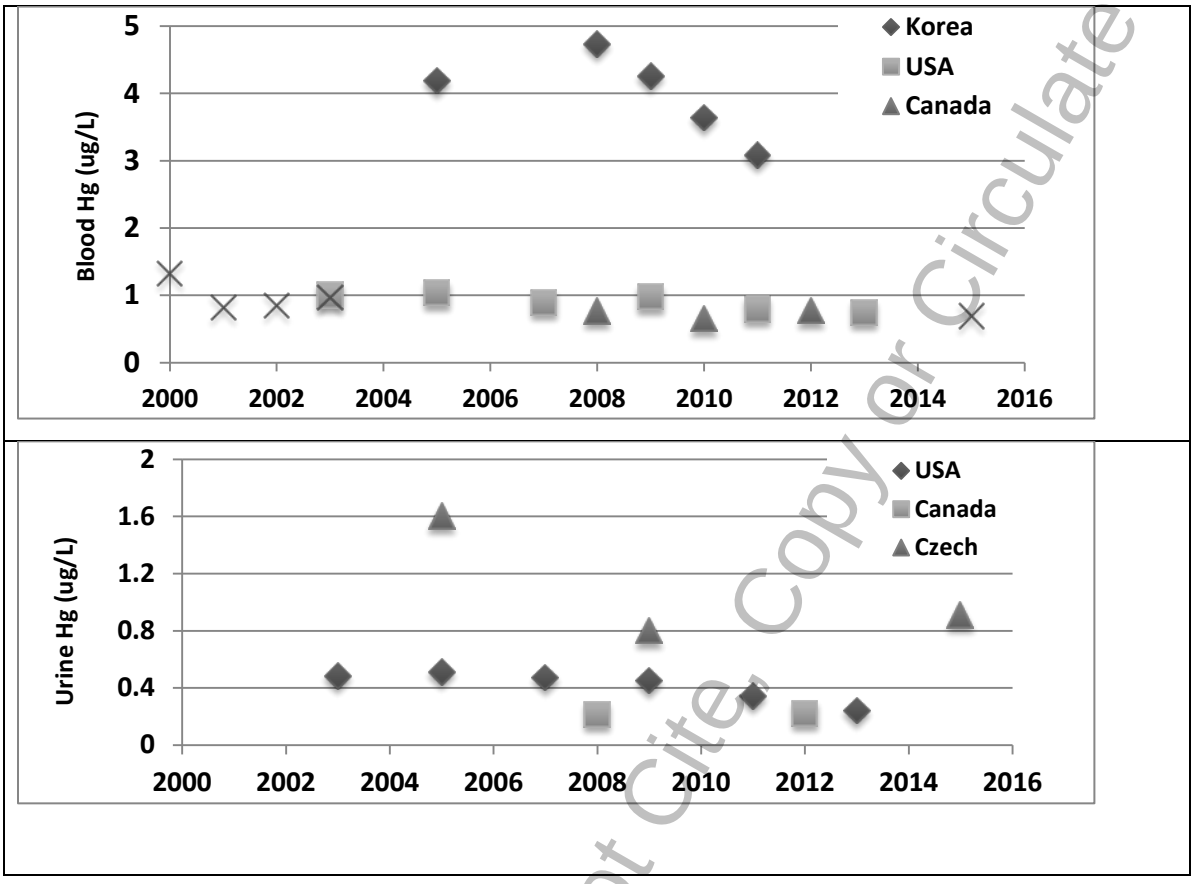

Figure 3. Temporal trends of adult A) whole blood and B) urinary total Hg (μg/L; median values) measurements across the national biomonitoring studies in which data was available from 2+ comparable sampling periods.

14210 **8.4.2 Longitudinal birth cohorts**

14211 We found 26 birth cohort studies in which at least there was one Hg exposure measurement during
14212 pregnancy or birth, as well as a follow-up time period in which an outcome measurement was taken
14213 (Appendix 4). The total sample population of these birth cohort studies was 19,940 mother-child pairs
14214 from which 42,750 biomarker measurements were taken. Of these birth cohort studies, 16 (62%)
14215 measured Hg in cord blood, 9 (35%) measured Hg in maternal blood during pregnancy, and 14 (54%)
14216 measured Hg in maternal hair, and these are summarized in Figures 4 and 5.

14217 From this dataset, there are some noteworthy observations: A) groups consuming large amounts of
14218 seafood (Seychelles, Spanish) and/or marine mammals (e.g., Faroe Islands, Inuit) have the highest Hg
14219 cord blood values, which often exceed 10 μg/L; B) cord blood Hg levels range between 5 and 10 μg/L
14220 across several Mediterranean populations, are approximately 5 μg/L in Asia, and generally less than 5

14221 µg/L across communities in North America and Europe (excluding Indigenous Peoples and
14222 Mediterranean); and C) exposures in the Faroe Islands have dropped nearly five-fold from ~1987 to
14223 ~2008 (whole blood Hg from 22.3 to 4.6 µg/L), and in the Seychelles approximately two-fold from ~1989
14224 to ~2008 (hair Hg from 5.9 to 2.9 µg/g);

Figure 4. **Cord blood mercury measurements (µg/L) across the birth cohort studies.**

[aside, graphics quality and content will be improved]

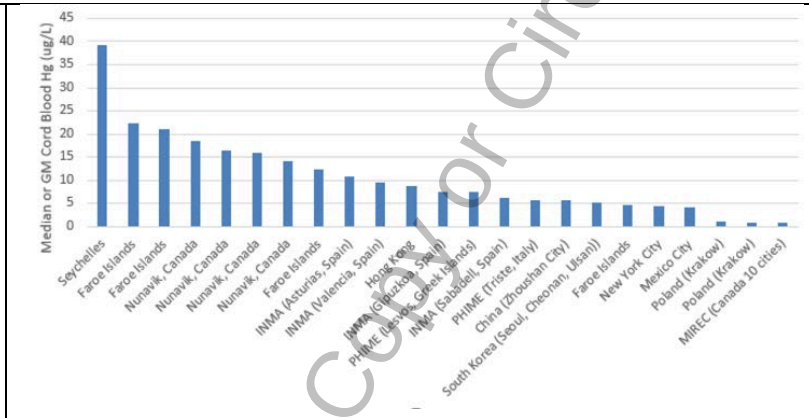

14225

Figure 5. **Maternal A) blood (ug/L) and B) hair (µg/g) mercury values across the birth cohort studies. [aside, graphics quality and content will be improved]**

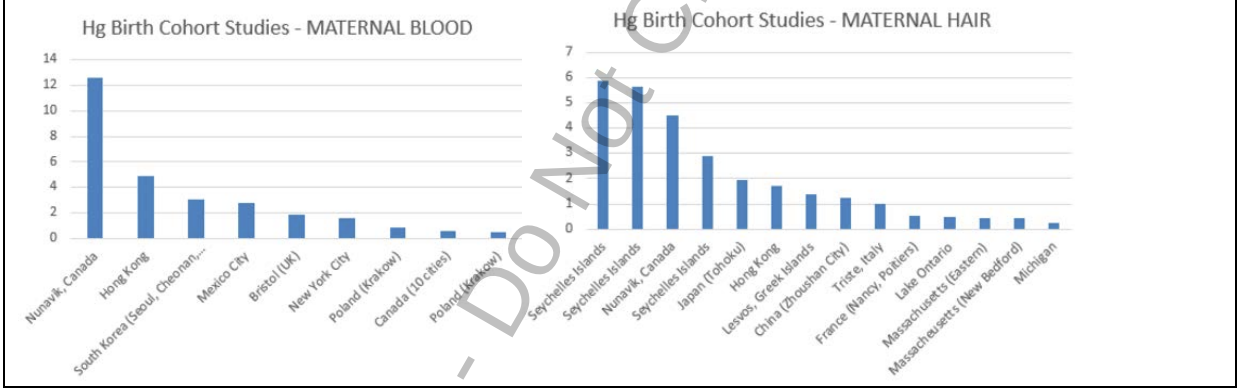

14226
14227 In these birth cohort studies a range of health outcomes were measured in the newborn, infant, toddler,
14228 or child, including for example, birth weight, motor function, and intelligence (see reviews by Ha et al.
14229 2017, Karagas et al. 2012). Here, we flag the cohorts in which a Hg-associated adverse health outcome
14230 was observed, and in doing so we see that these span a range of exposures and are not restricted to
14231 highly exposed groups or particular regions (Figure 6).

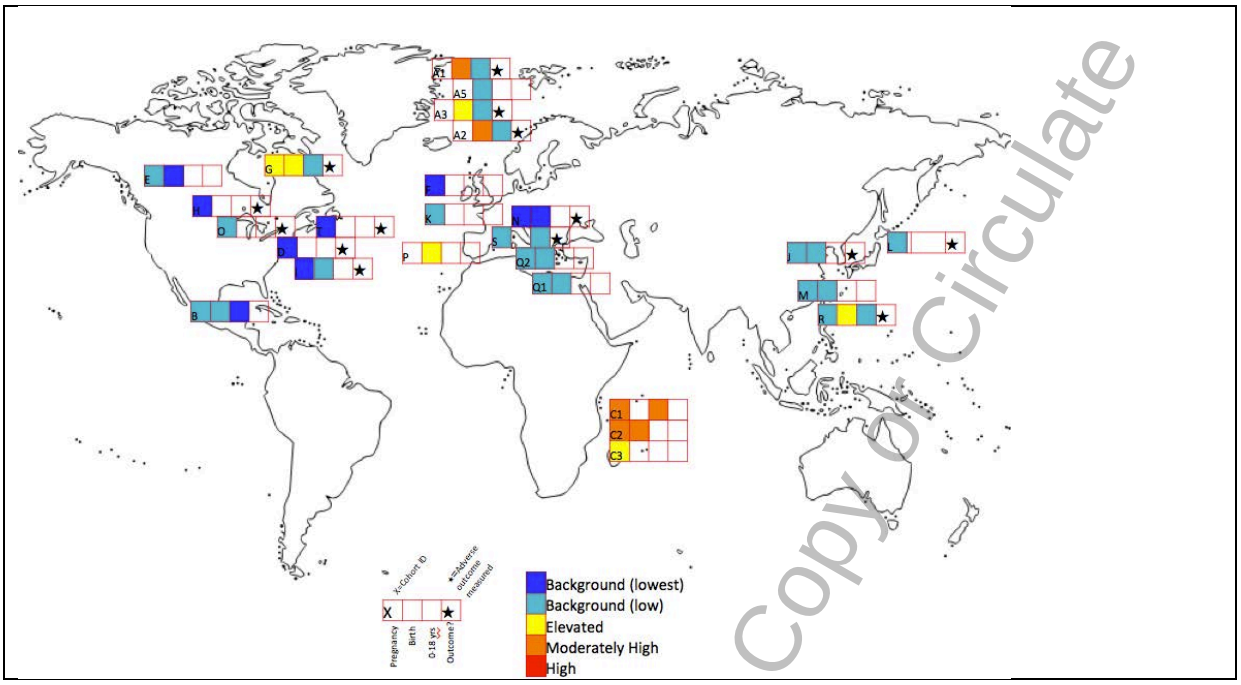

Figure 6. Map outlining the locations of the selected mercury birth cohort studies. Data represents 26 cohort studies and 42,750 Hg biomarker measures. The first three boxes refer to mercury measures taken during pregnancy, at birth, and up until age 18 according to the colour scale (see Appendix 3; cohort ID is indicated in the first box via a letter). If the final box has a star, then a Hg-associated adverse outcome was reported in that cohort.

8.4.3 Vulnerable populations

*** this Section is in EARLY DRAFT phase. It has not been reviewed by all team members. It will be updated following the review ***

From the bibliometric search and group discussions, a selection of exemplary and representative papers was identified and discussed here to showcase the current state of knowledge mercury exposure in notable vulnerable groups. In general we prioritized conclusions from high-quality review papers. Some of these examples were captured in Figure 1.

Pregnant women and foetuses. MeHg-contaminated seafood poses particular risk-benefit dilemmas (Mahaffey et al. 2011). Sheehan et al. (2014) conducted a systematic review of Hg exposure biomarkers in these populations worldwide (164 studies from 43 countries) and drew some meaningful conclusions: 1) exposures are highest amongst riverine gold mining communities (median hair Hg 5.4 μg/g; n=10,152 participants) and Arctic Indigenous Peoples (median hair Hg 2.1 μg/g; n=5,935 participants); 2) coastal Pacific regions of Asia have higher median hair Hg levels (1.3 μg/g; n=14,704 participants) than

Mediterranean (0.7 μg/g; n=6,536), Atlantic (0.4 μg/g; n=9,675), as well as inland populations (0.4 μg/g; n=10,745)

Indigenous Peoples. Groups in the Arctic are exposed to some of the highest MeHg levels globally largely due to their reliance on marine mammals and seafood as culturally important food staples. The 2015 AMAP Human Health Report reviewed several human biomonitoring programs across the circumpolar region. As an example, in Canada as part of the International Polar Year study the geometric mean of whole blood Hg across 4 study regions ranged from 2.8 to 12 μg/L, with individual values ranging from 0.1 to 240 μg/L. Beyond the Arctic region, there are studies from several other communities documenting elevated exposures in Indigenous Populations (e.g., selected examples to be listed here) especially since fish are a vital component of the culture of these communities. For example, Cisneros-Montemayor et al. (2016) compiled data from over 1,900 coastal Indigenous groups (27 million people from 87 countries) to show that per capita seafood consumption in these communities is 15-times higher than in non-Indigenous groups.

Artisanal and small-scale gold mining (ASGM). ASGM is rapidly growing worldwide with upwards of 15 million miners estimated to be directly involved in the sector and potentially 100 million people living in ASGM communities (World Health Organization, 2016; United Nations, 2012). There are a number of public health concerns in ASGM communities (Basu et al., 2015; World Health Organization, 2016) as well as a growing number of human biomonitoring studies (reviewed by Gibb and O'Leary, 2014). A noteworthy meta-analysis of 1,245 miners from across Indonesia, Philippines, Tanzania, Zimbabwe, and Mongolia reporting median urine Hg values of 3.6 μg/L (95th percentile 119 μg/L) with upward values in excess of 1,000 μg/L, and median blood Hg levels in 1,121 miners being 5.1 μg/L (95th percentile 38.2 μg/L) (Baeuml et al., 2011).

8.5 Summary of findings

*** this Summary is in EARLY DRAFT phase. It has not been reviewed by all team members. It will be updated following the review ***

The current assessment documents great variability in Hg exposures worldwide. All people are exposed to some amount of Hg. Individuals in select background populations worldwide have blood Hg levels that generally fall under 5 μg/L and urine Hg levels that fall under 3 μg/L, and corresponding levels in

hair and cord blood may be determined using the ratios outlined in Appendix 1. There are a number of notable groups with relatively high Hg exposures. Elevated exposures to Hg in key populations of concern for which there exist a relatively robust dataset include Arctic Indigenous Peoples who consume fish and marine mammals, coastal and/or small-island communities who are avid seafood consumers, and individuals who either work or reside amongst ASGM sites.

Despite a relatively large dataset to work from (e.g., here we had 150,929 and 42,750 biomarker measurements from national biomonitoring programs and birth cohort studies, respectively) there remain outstanding questions. Foremost is that there exist a number of countries and geographic regions for which data is completely lacking. There are several other groups of potential concern (e.g., individuals living in Hg contaminated sites; consumers of rice from contaminated sites; users of skin-lightening creams) but relatively little data to draw firm conclusions. In addition to focusing on vulnerable groups due to elevated exposures to Hg, there remain concerns about Hg susceptibility during certain lifestages (e.g., pregnancy and infancy), the range of physiological systems targeted (Karagas et al., 2012), the complex interactions between Hg and other chemical and non-chemical stressors particularly in the context of global change drivers (Eagles-Smith et al., 2017), and the increasing acceptance that genetic differences in sub-populations can influence exposure biomarkers and exposure-outcome relationships (Basu et al., 2014).

There are also success stories to be noted. Through our review identified studies that showed that steps to reduce Hg exposure may be effective. First, the approximately two-fold reduction in urinary Hg levels measured over the past decade across the U.S. has been linked with the phase-down on the use of dental amalgam (Figure 3B). Similar trends have been observed elsewhere, such as in German children (Link et al., 2007) and dental professionals (Goodrich et al., 2016). Second, across Arctic circumpolar regions Hg exposures are elevated though over the past two decades these have dropped likely as a result of local dietary advisories and changing consumption patterns. According to AMAP (2015) these decreases may be a sign that risk management efforts are having a beneficial effect, but that there remain concerns about changing consumption patterns and how this may affect culture and spirituality, recreational opportunities, and human nutrition. In other jurisdictions, there have been cases of decreased Hg exposures as a result of dietary consumption advisories (e.g., Kirk et al., 2017; Knobeloch et al., 2011), and we also note that decreases have also been observed in both the Faroe Islands and the Seychelles (Figure 6). Third, within the ASGM sector there is increasing interest in assessing the efficacy

of interventions in terms of reducing exposures. Calys-Tagoe et al. (2017) found that urinary Hg levels are significantly lower in workers from licensed ASGM sites versus unlicensed ones in Ghana.

8.6 References

AMAP 2015. AMAP Assessment 2015: Human Health in the Arctic. Arctic Monitoring and Assessment Programme (AMAP), Oslo, Norway. vii + 165 pp.

Baeuml J, Bose-O'Reilly S, Matteucci Gothe R, Lettmeier B, Roider G, Drasch G, et al. 2011. Human biomonitoring data from mercury exposed miners in six artisanal small-scale gold mining areas in Asia and Africa. Minerals 1:122–143.

Bartell SM, Ponce RA, Sanga RN, Faustman EM. 2000. Human variability in mercury toxicokinetics and steady state biomarker ratios. Environ Res. 84(2):127-32.

Basu N, Goodrich JM, Head J. 2014. Ecogenetics of mercury: from genetic polymorphisms and epigenetics to risk assessment and decision-making. Environ Toxicol Chem. 33(6):1248-58.

Basu N, Clarke E, Green A, Calys-Tagoe B, Chan L, Dzodzomenyo M, Fobil J, Long RN, Neitzel RL, Obiri S, Odei E, Ovadje L, Quansah R, Rajaee M, Wilson ML. 2015. Integrated assessment of artisanal and small-scale gold mining in Ghana--part 1: human health review. Int J Environ Res Public Health. 12(5):5143-76.

Calys-Tagoe, B., Basu, N., Clarke, E., Robins, T. 2017. Mercury exposure biomarkers differ between licensed and un-licensed ASGM miners in Tarkwa, Ghana. Presented at the 13th International Conference on Mercury as a Global Pollutant, July 16-21, Rhode Island, USA.

Cisneros-Montemayor AM, Pauly D, Weatherdon LV, Ota Y. 2016. A Global Estimate of Seafood Consumption by Coastal Indigenous Peoples. PLoS One. 5;11(12):e0166681.

Clarkson TW, Magos L. 2006. The toxicology of mercury and its chemical compounds. Crit Rev Toxicol. 36(8):609-62.

Eagles-Smith, C., Silbergeld, E., Basu, N., Bustamante, P., Diaz-Barriga, F., Hopkins, W., Kidd, K., Nyland, J. 2017. A synthesis of how global change drivers modulate mercury exposure, bioaccumulation, and adverse outcomes in wildlife and humans. Ambio. In Preparation. [ICMGP2017 Plenary Panel]

Gibb H, O'Leary KG. 2014. Mercury exposure and health impacts among individuals in the artisanal and small-scale gold mining community: a comprehensive review. Environ Health Perspect. 122(7):667-72.

Goodrich JM, Chou HN, Gruninger SE, Franzblau A, Basu N. Exposures of dental professionals to elemental mercury and methylmercury. 2016. J Expo Sci Environ Epidemiol. 26(1):78-85.

Ha E, Basu N, Bose-O'Reilly S, Dórea JG, McSorley E, Sakamoto M, Chan HM. 2017. Current progress on understanding the impact of mercury on human health. Environ Res. 152:419-433.

JECFA. 2004. Evaluation of Certain Food Additives and Contaminants Sixty-first Report of the Joint FAO/WHO Expert Committee on Food Additives 922, World Health Organization, Geneva (WHO Technical Report Series)

Karagas MR, Choi AL, Oken E, Horvat M, Schoeny R, Kamai E, Cowell W, Grandjean P, Korrick S. 2012. Evidence on the human health effects of low-level methylmercury exposure. Environ Health Perspect. 120(6):799-806.

Kirk LE, Jørgensen JS, Nielsen F, Grandjean P. 2017. Public health benefits of hair-mercury analysis and dietary advice in lowering methylmercury exposure in pregnant women. Scand J Public Health. 45(4):444-451.

Knobeloch, L., Tomasallo, C., Anderson, H. 2011. Biomonitoring as an intervention against methylmercury exposure. Public Health Reports. 126: 568-574.

Link B, Gabrio T, Piechotowski I, Zöllner I, Schwenk M. 2007. Baden-Wuerttemberg Environmental Health Survey (BW-EHS) from 1996 to 2003: toxic metals in blood and urine of children. Int J Hyg Environ Health. 210(3-4):357-71.

Mahaffey KR, Sunderland EM, Chan HM, Choi AL, Grandjean P, Mariën K, Oken E, Sakamoto M, Schoeny R, Weihe P, Yan CH, Yasutake A. 2011. Balancing the benefits of n-3 polyunsaturated fatty acids and the risks of methylmercury exposure from fish consumption. Nutr Rev. 69(9):493-508.

Mergler D, Anderson HA, Chan LH, Mahaffey KR, Murray M, Sakamoto M, Stern AH. 2007. Panel on Health Risks and Toxicological Effects of Methylmercury. Methylmercury exposure and health effects in humans: a worldwide concern. Ambio. 36(1):3-11.

Miklavcic, A, Kocman D, Horvat M. 2014. Human mercury exposure and effects in Europe. Environ Toxicol Chem. 33(6):1259-70.

Sheehan MC, Burke TA, Navas-Acien A, Breysse PN, McGready J, Fox MA. 2014. Global methylmercury exposure from seafood consumption and risk of developmental neurotoxicity: a systematic review. Bull World Health Organ. 92(4):254-269F.

Stern AH, Smith AE. 2003. An assessment of the cord blood:maternal blood methylmercury ratio: implications for risk assessment. Environ Health Perspect. 111(12):1465-70.

ATSDR 1999. Toxicological Profile for Mercury. Agency for Toxic Substances and Disease Registry. U.S. Centres for Disease Control, Atlanta, Georgia.

US EPA 1997. Mercury Study Report to Congress. https://www.epa.gov/mercury/mercury-study-report-congress

World Health Organization (2016). *Environmental and occupational health hazards associated with artisanal and small-scale gold mining*. WHO Document Production Services, Geneva, Switzerland.

UNEP 2016. Global Review of Mercury Monitoring Networks. United Nations Environment. Geneva (http://www.mercuryconvention.org/Portals/11/documents/2016%20call%20for%20submissions/UNEP%20-%20Global%20Review%20of%20Mercury%20Monitoring%20Networks_Final.pdf)

WHO/UNEP/IOMC . 2008. Guidance for identifying populations at risk from mercury exposure. http://www.who.int/foodsafety/publications/chem/mercuryexposure.pdf

14378 # Appendices

14379

APPENDIX 1. Reference Values for Mercury Biomarkers. Italicized values are estimated based on biomarker conversions indicated in the text.				
	Whole Blood	**Hair**	**Cord Blood**	**Urine**
NAS/NRC BMDL (concerning women of child-bearing age)	*3.5 ug/L*	1 ug/g	5.8 ug/L	
Qualitative conclusions by expert panel (Karagas) on "High" Levels	>12 ug/L	>4 ug/g	>20 ug/L	
Health Canada (Legrand Paper)	8 ug/L (pregnant women); 100ug/L for "general" men/women	*2 ug/g* *25 ug/g*	*13.6 ug/L* *and* *170 ug/L*	
German HBM-1[6] [no risk, background]	5	*1.25 ug/g*	*8.5 ug/L*	7
German HBM-2 [increased risk for adverse outcome]	15	*3.75 ug/g*	*25.5ug/L*	25
World Health Organization (WHO). Recommended Health-Based Limits in Occupational Exposure to Heavy Metals; WHO: Geneva, Switzerland, 1980.		<0.5 ug/g (non fish consumers); 1-2 ug/g (low and moderate fish consumers); >10 ug/g (frequent consumers)		50 ug/l
The ACGIH (2007) https://www.osha.gov/dts/osta/otm/otm_ii/pdfs/otmii_chpt2_appb.pdf				35 µg/g of creatinine.
Florida Health Department[7]	<10 ug/L (background); 50 and above (clinical effects)	*<2.5 (background); 12.5 and above (clinical effects)*		<40ug/L (no clinical effects); 40-60 (medium); 60+ (high)

[6] https://www.umweltbundesamt.de/sites/default/files/medien/355/bilder/dateien/hbm-werte_engl_stand_2017_02_06.pdf

[7] http://www.floridahealth.gov/environmental-health/mercury-spills/mercury-poisoning/_documents/guidelines-for-mercury.pdf [document HG05-2009]

14380
14381
14382

APPENDIX 2. Reference Values for Mercury Intake.				
		Inorganic Hg	**MeHg**	**REF**
European Food Safety Authority[8] (CONTAM panel), 2012	Tolerable Weekly Intake;	4 ug/kg bw for Inorganic Hg	1.3 ug/kg/bw for MeHg	
Joint FAO/WHO Expert Committee on Food Additives (JECFA), 2010	Tolerable Weekly Intake;	Similar to EFSA Above	1.6 ug/kg bw for MeHg	
U.S. EPA Reference Dose	Daily Intake	0.3 ug/kg/d mercuric chloride	0.1 ug/kg/d for MeHg	
U.S. EPA Reference Dose	Weekly Intake	0.3 ug/kg/d mercuric chloride	0.7 ug/kg/d for MeHg	
Canada (adopted 1997)	Weekly Intake		1.4 ug/kg wk for MeHg	WHO Doc Ref 6,7
Japan (adopted 2005)	Weekly Intake		2 ug/kg wk for MeHg	WHO Doc Ref 8
Netherlands	Weekly Intake		0.7 ug/kg/d for MeHg	WHO Doc ref 9

14383
14384

[8] http://www.efsa.europa.eu/en/press/news/121220

14385
14386
14387

Appendix 3. Colour scale related to mercury biomarker values. Adapted from Mikalavcic et al. with minor modifications.				
	Hair (ug/g)	**Whole Blood (ug/L)**	**Cord Blood (ug/L)**	**Urine (ug/L)**
Background-non seafood consumers [BLUE]	<0.5	<2	<3.4	<1
Background-seafood consumers [Turquoise]	0.5-2	2-8	3.4-13.6	1-3
Elevated [yellow]	2-5	8-20	13.6-34	3-10
Moderately High [orange]	5-10	20-40	34-68	10-50
High [red]	>10	>40	>68	>50

14388
14389

Appendix 4. Summary of birth cohort studies that were included in the current report. [NOTE this will be updated with new studies and cleaned accordingly prior to publication]

				LIFESTAGE EXPOSURES							
Cohort-ID	Cohort-Name	n	Yr	Pregnancy	Birth	Infant (0-1	Toddler (1	Child (3-11	Adolescen	Adult (18+	Outcome?
H	POUCH (Michigan)	1024	1998	0.92							★
N	Poland	313	2002	0.83	1.09						★
E	MIREC	1673	2008	2.24	0.802						
D	VIVA	135	2002	1.8							★
T	Massacheusetts	421	1993	1.8							★
F	ALSPAC	4131	1991	1.86							
O	Oswego	212		2							★
K	EDEN	665	2003	2.08							
I	World Trade Center	280	2001	1.6	4.44						★
S	Italy	128	2001	3.2				2.16			★
B	ELEMENT	348	1994	2.8	4.1			1.37			
J	MOCEH (Korea)	797	2006	3.1	5.2						★
A5	Faroe Islands	500	2008		4.6						
Q1	PHIME-Italy	573		4	5.6						
M	Zhoushan	406	2004	4.98	5.58						
Q2	PHIME-Greece	281		5.6	7.5						
R	Hong Kong	1057	2000	4.92	8.8			2.62			★
L	Tohoku	498	2001	7.8							★
P	INMA	1883	2004		8.2						
C3	Seychelles		2008	11.68							
A3	Faroe Islands	475	1999		12.4			2.6			★
G	Nunavik Child Development	130	1994	12.6	15.9			5.9			★
A2	Faroe Islands	182	1995		21			3.2			★
A1	Faroe Islands	1022	1987		22.3			8.4	4.1		★
C1	Seychelles	779	1989	23.6		26.4	19.2	25.2	32.4	27.3	
C2	Seychelles		2001	22.5	39.3						